

BIOMASS DEPOLYMERIZATION USING BIPHASIC CO₂-H₂O MIXTURES

A Dissertation

Presented to the Faculty of the Graduate School
of Cornell University

in Partial Fulfillment of the Requirements for the Degree of
Doctor of Philosophy

by

Jeremy Scott Luterbacher

August 2012

© 2012 Jeremy Scott Luterbacher

ALL RIGHTS RESERVED

BIOMASS DEPOLYMERIZATION USING BIPHASIC CO₂-H₂O MIXTURES

Jeremy Scott Luterbacher, Ph.D.

Cornell University 2012

Sustainably producing concentrated solutions of carbohydrates is a key bottleneck in the conversion of lignocellulosic biomass to biofuels or bioproducts. Most pretreatment and enzymatic hydrolysis processes used for biomass depolymerization are run at low-solid concentration (<10 wt%) and use chemical catalysts, while high-solids enzymatic hydrolysis reactions are almost always performed with air-dried pretreatment mixtures. Biphasic H₂O-CO₂ mixtures are an interesting alternate medium for high-solids (up to 40 wt%) pretreatment. Initial studies were done in a small (25 ml) unstirred reactor using a single temperature stage. More recently, two-temperature stage pretreatment was introduced and optimized in a larger 1 L stirred reactor to take advantage of the biomass depolymerization temperature dependent reaction sequence. Optimally pretreated substrates were then used as feedstock in high-solids (30 wt%) enzymatic hydrolysis reactions that gave glucose yields above 80% for both switchgrass and hardwood after 48 hours of hydrolysis. Therefore, without additional chemical catalysts or any drying, two-temperature stage H₂O-CO₂ pretreatment coupled with high-solids enzymatic hydrolysis can produce monosaccharide solutions of 185 g/L and 148 g/L for mixed hardwood and switchgrass, respectively. This suggests that H₂O-CO₂ pretreatment is an attractive alternative to chemically catalyzed processes such as dilute acid pretreatment.

Parallel to these studies, efforts were undertaken to better understand the

relationship between the effects of pretreatment and the enzymatic depolymerization mechanisms of cellulosic substrates. A fluorescence confocal microscopy method was developed for observing and measuring the binding and reaction of cellulase cocktails and their substrates in situ. The Spezyme CP cellulase cocktail was supplemented with a small fraction of fluorescently labeled *Trichoderma Reesei* Cel7A, which served as a reporter to track cellulase binding onto the internal physical structure of bacterial microcrystalline cellulose. A kinetic model was constructed using the variation in fluorescence intensity of the substrate and the bound enzyme over time and was successfully used to predict reaction yields in solution. Building on this result a reaction and diffusion model was developed to model the enzymatic hydrolysis of pretreated biomass. This model was shown to be able to predict the well-known relationship between accessible surface area in biomass and initial enzymatic hydrolysis rates. The development of this theoretical framework that accurately describes the key relations between pretreatment and enzymatic hydrolysis could be the first step in developing tools that could lead to the rational design of pretreatment technologies.

BIOGRAPHICAL SKETCH

Jeremy Scott Luterbacher was born on July 14th 1984 in Geneva, Switzerland. After graduating from the Gymnase Cantonal de Nyon in 2002, he pursued studies in chemistry and chemical engineering at l'École Polytechnique Fédérale de Lausanne, receiving a bachelor's degree in 2005. He obtained a master's degree in chemical engineering from the same institution in 2007, performing the research for his master's thesis at the Massachusetts Institute of Technology in Cambridge, MA.

Jeremy then decided to pursue a PhD at Cornell University in the newly established Biofuels Research Laboratory under the supervision of his principal advisor Professor Larry Walker and Professor Jeff Tester, who had advised him at MIT. Professor Jean-Yves Parlange was added to his committee a year later. On his way to obtaining his PhD degree, he earned a second Master's degree in Chemical Engineering in 2010. His work was recognized by the Austin Hooey Award for outstanding PhD research in 2011.

In the coming months, he will join Professor James Dumesic's research group at the University of Wisconsin Madison as a postdoctoral fellow for a two-year stay. After that, he will likely pursue a career in academia and is currently considering several tenure-track faculty appointments.

Parallel to his academic pursuits Jeremy has been a fencing competitor and teacher for almost 20 years. He was a member of the Swiss Cadet and Junior National Teams competing in several world cup meets. He was ranked number one junior in Switzerland in 2003-2004 and number 6 senior in 2005-2006. He

was a fencing instructor at the University of Lausanne from 2001 to 2006 and an assistant coach for the women's varsity team at Cornell since 2007. While fencing at Cornell, he met the captain of the women's varsity team, Celia Smith, who turned out to be the love of his life. They will marry in August 2012.

To my mother and father.

ACKNOWLEDGEMENTS

My PhD years will be remembered as fun and enriching times and I primarily have Larry Walker, my principal PhD advisor, to thank for that. During the last five years, he was an unbelievably kind advisor who always enjoyed peppering scientific discussions with good humor, life lessons or his thoughts on Finger Lakes wine. Perhaps more importantly, he has taken upon himself to worry about funding my research, leaving me free to think about scientific problems, which was undoubtedly more fun. As Larry likes to remind my fellow researchers and me, “research is a human endeavor” and I was incredibly lucky to have such a caring and thoughtful advisor during the last five years.

Jeff Tester welcomed me at MIT during my master’s and guided me toward Cornell for my PhD, where he joined me a year later. He played an active advising role during my PhD and provided many wonderful memories of grueling multi-day bike trips around the finger lakes. I have his guidance to thank for being where I am today.

My third committee member, Jean-Yves Parlange greatly influenced my thinking on transport, thermodynamics and mathematics through his wonderful courses but also during our subsequent discussions in the hall or in his office. He was always eager to stop and chat about scientific or non-scientific subjects and it has been a pleasure interacting with him over the last few years.

I was fortunate to take advantage of a great amount of knowledge already available within the Walker and Tester research group. At the start of my PhD, Deborah Sills was a great lab mentor and a good friend. She taught me how

to run pretreatment and enzymatic hydrolysis experiments and Sarah Munro taught me how to use the HPLC. Towards the end of my PhD, José Moran-Mirabal taught me how to use a fluorescence confocal microscope during a very productive and congenial collaboration. Michael Johnson helped greatly expand my knowledge of high pressure systems. I had great pleasure in interacting with my remaining Walker group colleagues: Ben, Marie, Dong and Hnin. They were instrumental in making sure my PhD was filled with more good days than bad. I could always count on my fellow chemical engineering friends, Jason Boock, Nate Hansen, Anthony Altieri, Ed Kish and Ananth Kaushik to help me out during my first year courses, blow off some steam and have a good time in Ithaca. In addition, I benefited from interesting scientific conversations with Jason and Anthony, which often formed the basis for research ideas.

Most importantly, I have had a loving and supportive family that has made my life what it is today. I was fortunate to find in Celia, my soon-to-be wife, an amazingly funny, thoughtful and interesting companion who always found time to look over my scientific manuscripts. A bad day would have been a lot worse without her around. My father always spent time with me as a child pointing out interesting mathematical and scientific facts, which undoubtedly sparked the interest that made PhD research possible. My mother always believed in me (even when I was a weird kid), encouraged me and took the time to talk with me for hours about my life and my choices. Nothing makes me quite as sad as not being able to share this accomplishment with her. They were both always so proud and interested in me that it would have been difficult not to get a PhD. Mom and Dad, thank you for everything and more... This Thesis is dedicated to the two of you.

TABLE OF CONTENTS

Biographical Sketch	iii
Dedication	v
Acknowledgements	vi
Table of Contents	viii
List of Tables	xii
List of Figures	xiii
1 Introduction: Biomass as a source of fuel	1
1.1 Gasification	5
1.2 Lignocellulosic biomass liquefaction.	6
1.3 Conversion of high-lipid biomass to bio-oil and biodiesel.	7
1.4 Biomass conversion through depolymerization and sugar conversion.	8
2 Biomass depolymerization	10
2.1 Cellulose depolymerization	11
2.1.1 Cellulose depolymerization in pure water	13
2.1.2 Acid catalyzed cellulose depolymerization	16
2.1.3 Base catalyzed cellulose depolymerization	21
2.1.4 Enzyme catalyzed cellulose depolymerization	21
2.2 Hemicellulose	32
2.2.1 Hemicellulose depolymerization in pure water	33
2.2.2 Acid catalyzed hemicellulose depolymerization	37
2.2.3 Base catalyzed hemicellulose depolymerization	40
2.2.4 Enzyme catalyzed hemicellulose depolymerization	43
2.3 Lignin	45
2.3.1 Lignin deconstruction in pure water	47
2.3.2 Acid catalyzed lignin deconstruction	48
2.3.3 Base catalyzed lignin deconstruction	50
2.3.4 Biological lignin deconstruction	51
2.4 Pretreatment and Enzymatic Saccharrification	53
2.4.1 Biomass pretreatment provides accessibility for cellulases	54
2.4.2 Challenges facing current pretreatment technologies	56
2.4.3 Leading pretreatment technologies	59
2.4.4 Conclusions	66
3 Objectives	69
3.1 Objective 1: Sustainably and economically producing concentrated solutions of monosaccharrides from biomass	69
3.2 Objective 2: Developing a modeling framework for understanding the relationship between pretreatment and enzymatic hydrolysis and forming a basis for the rational design of these conversion processes	71

4	High-solids biphasic CO₂-H₂O biomass pretreatment	73
4.1	Introduction	73
4.2	Materials and methods	75
4.2.1	Biomass: species and analysis	75
4.2.2	Pretreatment	76
4.2.3	Enzymatic hydrolysis	78
4.2.4	Liquid analysis	80
4.3	Results	80
4.3.1	Yield	80
4.3.2	Hardwood pretreatment	81
4.3.3	Switchgrass pretreatment and saccharification	85
4.3.4	Mixed perennial grasses pretreatment and saccharification	87
4.4	Discussion	89
4.4.1	Effect of solids content	89
4.4.2	Effect of biomass species	91
4.4.3	Comparison with leading pretreatment technologies	91
4.5	Conclusions	92
5	Two-temperature stage biphasic CO₂-H₂O pretreatment of lignocellulosic biomass at high solid loadings	94
5.1	Introduction	94
5.2	Materials and Methods	96
5.2.1	Biomass: species and analysis	96
5.2.2	Pretreatment	97
5.2.3	Enzymatic hydrolysis	99
5.2.4	Yield calculations	99
5.3	Results and Discussion	101
5.3.1	Single temperature stage results: effect of mixing and particle size	101
5.3.2	Two-temperature stage results	106
5.3.3	Tradeoff between Glucose and Hemicellulose sugar yields	109
5.3.4	Comparison to other pretreatment processes	111
5.4	Conclusions and outlook	112
6	Producing concentrated solutions of monosaccharides using biphasic CO₂-H₂O mixtures	114
6.1	Introduction	114
6.2	Material and Methods	118
6.2.1	Biomass: species and analysis	118
6.2.2	Two-temperature stage biphasic CO ₂ -H ₂ O pretreatment	119
6.2.3	High-solids enzymatic hydrolysis	120
6.2.4	Liquid analysis and yield calculations	123
6.3	Results and Discussion	123
6.3.1	Optimal pretreatment results	123

6.3.2	High-solids enzymatic hydrolysis	126
6.3.3	Solid content effect	130
6.3.4	Comparison to other pretreatment and high-solids enzymatic hydrolysis processes	134
6.3.5	Process overview	138
6.4	Conclusions	141
7	Observing and modeling BMCC degradation by commercial cellulase cocktails with fluorescently labeled <i>Trichoderma reesei</i> Cel7A through confocal microscopy	143
7.1	Introduction	143
7.2	Materials and Methods	145
7.2.1	Cellulase preparation	145
7.2.2	Microscopy sample preparation	146
7.2.3	Confocal microscopy imaging	147
7.2.4	Image processing	148
7.2.5	Bulk experiments	149
7.2.6	Model development	150
7.2.7	Instantaneous binding model	154
7.3	Results and discussion	156
7.3.1	Cellulose and cellulase imaging	156
7.3.2	Irreversible and reversible binding models	158
7.3.3	Instantaneous binding models	161
7.3.4	Model validation	163
7.4	Conclusions	163
8	A pore-hindered diffusion and reaction model can help explain the importance of pore size distribution in enzymatic hydrolysis of biomass	166
8.1	Introduction	166
8.2	Methods	168
8.2.1	Model	168
8.3	Results and discussion	176
8.3.1	Proposed model	176
8.3.2	Effect of neglecting diffusion	180
8.3.3	Predictive variant	182
8.4	Conclusions	185
9	Conclusions	186
9.1	Summary of work	186
9.1.1	Can biphasic mixtures of CO ₂ and water be used to successfully produce concentrated solutions of monosaccharides from biomass?	186

9.1.2	Can modeling help better understand the relationship between biomass pretreatment and enzymatic hydrolysis and provide a basis for the rational design of biomass depolymerization processes?	188
9.2	Outlook and future research	190
A	Appendix for Chapter 4	193
A.1	Thermodynamic equilibrium of the CO ₂ -H ₂ O system	193
A.2	Heating curves	194
A.3	Water-saturated supercritical CO ₂ pretreatment	195
B	Appendix for Chapter 5	196
B.1	Mixing impeller	196
B.2	Heating curves	196
B.3	Additional optimization of two-temperature stage CO ₂ -H ₂ O pretreatment	197
B.3.1	Mixed Hardwood pretreatment	197
B.3.2	Switchgrass pretreatment	199
C	Appendix for Chapter 6	202
C.1	High-solids enzymatic hydrolysis reaction system	202
C.2	Characterization of sampling error	203
D	Appendix for Chapter 7	205
D.1	Hydrolytic activity of fluorescently labeled Cel7A	205
D.2	Correcting for photobleaching	206
D.3	Model development	208
D.3.1	Irreversible binding model	208
D.3.2	Reversible model	211
D.3.3	Instantaneous binding model	215
D.4	Parameter estimation	218
D.5	Effect of substrate preparation	219
D.6	Imaging at high enzyme concentrations	220
D.7	Variations of enzyme concentration within the supernatant	221
E	Appendix for Chapter 8	223
E.1	Dataset	223
E.2	Particle geometry and lignin binding assumptions	223
E.3	Computational methods	226
E.3.1	Numerical solver	226
E.3.2	Parameter estimation	227
E.4	Neglecting diffusion	228
	Bibliography	230

LIST OF TABLES

2.1	Glucose degradation products in hydrothermal media	14
2.2	List of symbols and their associated description	19
2.3	Xylose degradation products in hydrothermal media	34
2.4	Kinetic parameters obtained in various studies for xylan depoly- merization in acidic conditions	41
2.5	Lignin degradation products in hydrothermal media	48
2.6	Parameters and monosaccharride yields for leading Corn stover pretreatment technologies	67
2.7	Parameters and monosaccharride yields for leading Poplar (hardwood) pretreatment technologies	68
4.1	Results of biomass analyses	77
4.2	Batch reactor yields	88
6.1	Results of biomass analyses	125
7.1	List of symbols and their associated description	151
7.2	Fitting results for the reversible and irreversible models	158
7.3	Fitting results for the instantaneous model	163
8.1	List of symbols and their associated source	170
8.2	Parameter estimation results for the reaction and diffusion model	177
D.1	List of symbols and their associated description	209
E.1	Dataset used for the enzymatic hydrolysis reaction-diffusion model	224

LIST OF FIGURES

1.1	Effects of biofuel implementation on car fuel usage, land allocation and CO ₂ sequestration.	4
1.2	Biomass conversion using sugar as an intermediate.	9
2.1	Cellulose composition and structure.	12
2.2	Acid and base catalyzed mechanism of cellobiose hydrolysis . .	13
2.3	Overlay of the Arrhenius plots of cellulose depolymerization and glucose degradation	16
2.4	Glucose yields during acid catalyzed cellulose depolymerization	20
2.5	Depiction of cellulose depolymerization by cellulase mixtures . .	25
2.6	Structure of the repeating unit of Vetiver grass leaf hemicellulose.	32
2.7	Xylan depolymerization model	35
2.8	Xylose, xylo-oligomers, xylose and furfural concentration as a function of time in hydrothermally (175°C) pretreated wood . . .	38
2.9	Xylose yields during acid catalyzed xylan depolymerization . . .	42
2.10	Cellulolytic and hemicellulose side-chain attacking enzymes and their points of attack on hemicellulose	44
2.11	The three basic molecular subunits of lignin.	45
2.12	A simplified reaction network for lignin in water close to the critical point.	49
2.13	Relationship between initial rates of cellulose hydrolysis and available surface area to cellulases.	55
2.14	Diagram of pretreatment's effect on biomass	56
4.1	Diagram of the batch pretreatment apparatus	79
4.2	Batch reactor yields for 40 wt% solids mixed hardwood as a function of residence time and temperature	83
4.3	Batch reactor yields for 40 wt% solids mixed hardwood as a function of residence time and temperature	85
4.4	Batch reactor yields for 40 wt% solids switchgrass as a function of residence time and temperature	86
4.5	Batch reactor yields for 40 wt% solids mixed perennial grasses as a function of residence time and temperature	89
5.1	Stirred pretreatment reactor schematic	98
5.2	Yields for single-temperature stage pretreatment of hardwood . .	102
5.3	Yields for single-temperature stage pretreatment of switchgrass .	105
5.4	Yields for two-temperature stage pretreatment of hardwood . . .	107
5.5	Yields for two-temperature stage pretreatment of switchgrass . .	109
5.6	Total molar sugar yields (Y_T) for two-temperature stage pretreatment	110
6.1	High-solids biomass conversion setup	120

6.2	High-solids yields for optimally two-temperature stage pre-treated mixed hardwood	127
6.3	Effect of doubling the enzyme content and of pH control on mixed hardwood conversion yields	128
6.4	High-solids yields for optimally two-temperature stage pre-treated switchgrass	130
6.5	Effect of doubling the enzyme content and of pH control on switchgrass conversion yields	131
6.6	Mixed hardwood enzymatic hydrolysis yields as a function of solid content	132
6.7	Switchgrass enzymatic hydrolysis yields as a function of solid content	134
6.8	Comparison of glucose yields obtained with different pretreatment technologies in different studies	136
6.9	Overall H ₂ O-CO ₂ pretreatment and saccharification mass balance	139
7.1	Imaging chamber setup	147
7.2	Illustration of the image processing method	149
7.3	Confocal fluorescence imaging of BMCC during degradation . .	157
7.4	Data fitting to the reversible and irreversible binding model . . .	159
7.5	Data fitting to the instantaneous binding model	162
7.6	Irreversible and reversible binding model validation	164
7.7	Instantaneous binding model validation	164
8.1	Enzymatic hydrolysis reaction-diffusion modeling geometry . .	169
8.2	Proposed cellulase reaction mechanism in an accessible biomass pore	172
8.3	Reaction-diffusion mass balance results as a function of time and radius	178
8.4	Comparison between reaction-diffusion modeling and experimental results	180
8.5	Effect of the particle radius and diffusion on enzymatic hydrolysis yields	182
8.6	Estimation of the fraction of accessible cellulose from the fraction of accessible pores	183
8.7	Comparison between experimental results and two sets of predictive modeling results	184
A.1	Isobaric phase equilibrium data (100 and 200 bar) for the CO ₂ -H ₂ O biphasic system	193
A.2	Batch reactor heating curves	194
A.3	Chromatogram overlay for enzymatically hydrolyzed pretreated and non-pretreated hardwood.	195
B.1	Pictures of the custom-machined biomass impeller.	196

B.2	Temperature and pressure profiles during two-temperature stage pretreatment	198
B.3	Additional yields for two-temperature stage pretreatment of hardwood	199
B.4	Additional yields for two-temperature stage pretreatment of switchgrass	201
C.1	Custom-built high-solids enzymatic hydrolysis reaction system .	202
C.2	Characterization of sampling error	204
D.1	Hydrolytic activity of fluorescently labeled Cel7A	205
D.2	Bleaching of DTAF labeled BMCC	206
D.3	Bleaching of AF647 labeled Cel7A	207
D.4	Effect of BMCC drying and BSA blocking buffer	220
D.5	BMCC degradation imaging at high enzyme concentration	221
D.6	Fraction of initial absorbance at 280 nm as a function of reaction time in the presence of BMCC	222
E.1	Fluorescence images of two-temperature stage biphasic CO ₂ -H ₂ O pretreated hardwood	225
E.2	Close-up of fluorescence images of two-temperature stage biphasic CO ₂ -H ₂ O pretreated hardwood	226
E.3	Comparison between experimental results and those predicted by the simplified model (neglecting diffusion)	229

CHAPTER 1

INTRODUCTION: BIOMASS AS A SOURCE OF FUEL

Earth's predominant source of energy is, and always has been, sunlight. Living organisms take advantage of this resource through photosynthesis, which allows them to capture solar energy. By using solar input to convert water and carbon dioxide to carbohydrates and other complex organic compounds, plants create energy-rich substances from molecules that have no heating value. The energetic conversion efficiency of photosynthesis is only of about 1 to 2% [1]. Furthermore, since plants cannot convert all solar radiation, their actual energy fixation on land is only of about 0.24% according Lieth & Whittaker [2]. Nevertheless, the amount of energy produced through photosynthesis on the continents alone is still greater than human energy use. Indeed, Lieth and Whittaker find that the annual terrestrial growth is of about 118×10^9 dry tons per year [2], which corresponds to (assuming 16.3 gigajoules per dry ton for biomass [1]) almost 2000 exajoules per year. In comparison, human primary energy use is about 480 Exajoules a year or roughly one quarter of the energy produced by biomass growth [3]. If one accounts for marine biomass, which is more difficult to harvest, earth's annual biomass production becomes 173×10^9 dry tons per year [2] or almost six times more than human primary energy usage.

Terrestrial biomass was naturally humans' main source of energy until the industrial revolution. However, three limiting factors led to the gradual replacement of biomass by fossil fuels as well as electrical generation technologies:

Low energy density. Since terrestrial biomass is primarily formed of carbohydrate polymers, it has a high oxygen content (30-45% [1]) and is therefore limited by the amount of heat it can generate through further oxida-

tion during combustion. Biomass has an energy density that is about 2.6 times lower than that of oil, which contains virtually no oxygen. A lower energy density makes its transportation and/or use as a transportation fuel less efficient.

Structure. Like all living organisms, biomass's natural structure is rigid and cannot be pumped. This makes its transport and transfer more complicated. In addition, solids when combusted suffer mass transfer limitations, which produce particulates and lead to inefficiency.

Moisture content. When harvested, terrestrial biomass can have moisture contents between 2 and 75% [1] (and close to 100% for marine biomass). To get this material to combustion temperatures, all the water must be evaporated, which can require a large amount of energy compared to that contained in the biomass itself.

In contrast, fossil fuels suffer from fewer or none of these limitations. Coal, oil and liquid (pressurized) natural gas all have higher energy densities than biomass, virtually no moisture content and, in the case of oil and natural gas, can be transported and distributed using pipelines. Initially, fossil fuels were produced through photosynthesis and were similar to today's biomass. However, through a series of slow biological and geological processes on the timescale of 10-100 million years [1], their oxygen was removed and they were converted to dense solids, liquids or gases. It is therefore important to distinguish biomass, which is considered to have been alive within the last 50-100 years, from fossil fuels, which have not been alive for millions of years.

Recently, fears of an approaching fossil resource depletion and concerns of the increased environmental and economic burdens of fossil fuel extraction have

led the world to look for more sustainable energy sources. Indeed, fossil fuels are a limited resource, since their regeneration time far exceeds that of a human generation. In addition, they consist of a large amount sequestered carbon, which, if fully released into the atmosphere, could lead to a dramatic increase in global temperatures because of the greenhouse gas effect [4]. In addition, the localized nature of fossil fuel resources create economic disparities and political instabilities.

Fuel produced from biomass (biofuels) can serve as a uniformly distributed and sustainable alternative to fossil fuels. The uptake of carbon dioxide during plant growth, which compensates for emissions released during the fuel's use, can help alleviate the environmental impact of energy use. Sheehan et al.[5] demonstrate that, even when accounting for fossil fuel use in the entire biofuel's life cycle, a reduction of 80% fossil fuel use can be obtained (see part 1 of Figure 1.1). In addition, if the appropriate global policy initiatives are taken, biofuels can be part of an effort of reforestation and sequestration of carbon in soils. Mellilo et al. [6, 7] present two land use options for biofuels and their effect on the global carbon balance. The deforestation option only considers conversion costs when allocating land, while the intensification scenario limits conversion of unmanaged land based on previous regional conversion rates. The effects of both scenarios are shown in part 2 of Figure 1.1. While the authors warn of possible losses in biodiversity for both alternatives, the comparison between the two scenarios demonstrates that, by fertilizing previously moderately fertile land for biofuel production, carbon sequestration in soils can increase rather than decrease.

Of course, biofuels are not necessarily the silver bullet for solving the energy

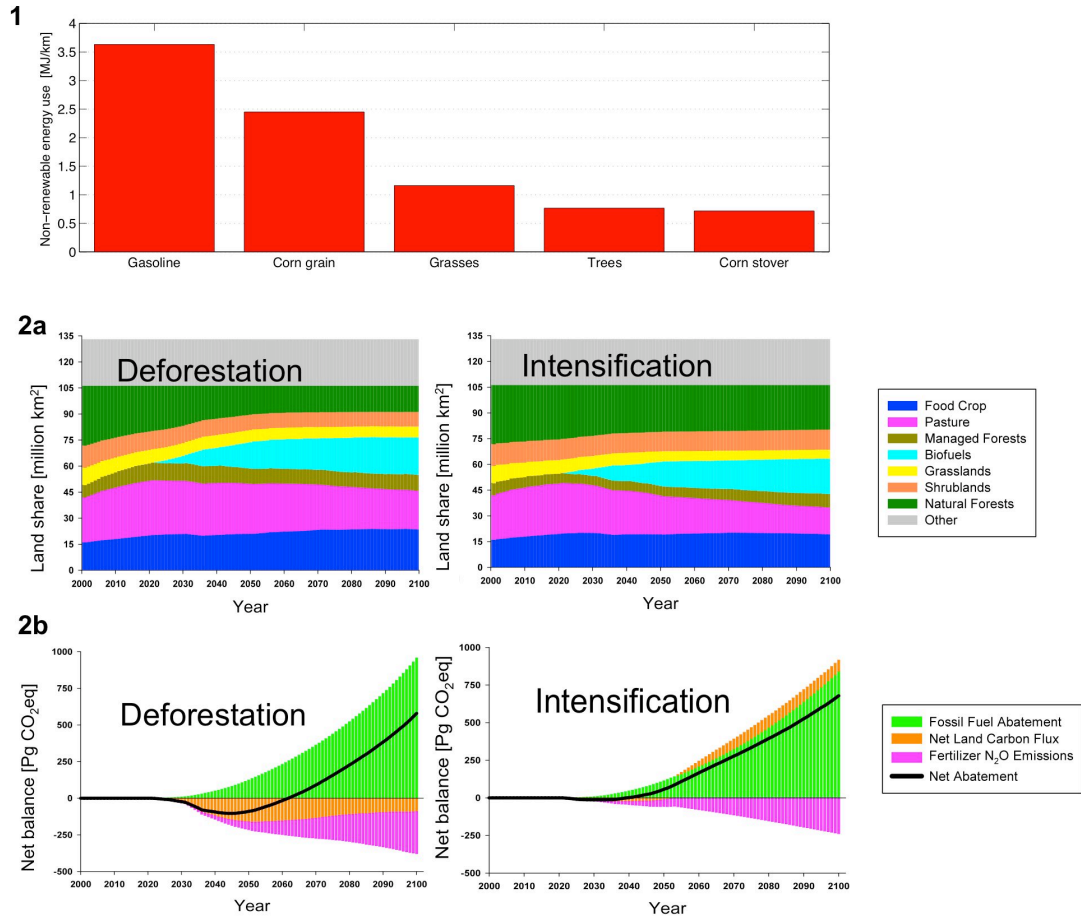


Fig. 1.1: Effects of biofuel implementation on car fuel usage, land allocation and CO₂ sequestration. Part 1 shows the decrease of fossil fuel usage in cars as a result of biofuel use (based on data from Sheehan et al. [5]). Part 2 (modified from Melillo et al. [6]) shows the effect of two alternative global policies on land allocation (part a) and CO₂ sequestration (part b). The deforestation option only considers conversion costs when allocating land, while the intensification scenario limits conversion of unmanaged land based on previous regional conversion rates.

paradigm. Important improvements in renewable and nuclear electricity production, combined with improvements in battery or fuel cell technology could end the need for carbon-based fuels even in the transportation sector. However, as the petroleum reserves disappear, the chemical industry will need a new source for carbon-based raw materials, for which biomass seems like the most obvious candidate.

Producing a higher quality fuel from biomass involves removing some or all of its oxygen while converting it to a liquid or a gas. Oxygen leaves biomass in the form of CO_2 or H_2O and these molecules have to be separated from the fuel at the tail end of the conversion process. Strategies for converting biomass can be categorized into four different process families that are detailed below.

1.1 Gasification

Processes seeking to convert biomass to gases using high temperatures and, in some cases, catalysts are considered to be thermochemical gasification. They have the advantage of being able to almost completely convert any type of biomass. Conventional gasification (i.e. when biomass is in the presence of gases) can convert biomass to syngas (CO and H_2), a gas containing hydrogen and CO_2 or a gas containing methane and CO_2 depending on the temperatures (ranging from 600 to 1500°C) and catalysts present [8, 9]. Through an additional methanation step, the gas can be converted to methane and CO_2 [10]. Alternatively, hydrothermal gasification (i.e. gasification in high-temperature liquid water) can convert biomass to methane at temperatures between 400 and 500°C with the help of catalysts; or to hydrogen at temperatures above 500°C with or

without the help of non-metal catalysts [11, 12, 13]. Finally, the Fisher-Tropsch process can catalytically convert syngas to liquid alkanes [14, 15], and fermentation can be used to convert syngas to ethanol [16]. Thus, gasification can be a first step toward producing liquid fuels from biomass.

Wet biomass can be biologically gasified to a mixture containing roughly 50%vol each of CO₂ and CH₄. This process takes place in anaerobic conditions at temperatures between 35 and 55°C [1]. It can convert almost any fraction of biomass except for lignin, which represents about 20-30 wt% of most terrestrial biomass [17]. It is especially effective for very wet and partially degraded feedstocks such as animal or human waste.

1.2 Lignocellulosic biomass liquefaction.

Biomass can be thermally decomposed and liquefied by gas-phase pyrolysis or through treatment in a hydrothermal environment. In general, hydrothermal liquefaction occurs between 280 and 380°C while gas phase pyrolysis generally occurs around 500°C with residence times in seconds [18, 13]. Depending on the conditions and feedstocks, a vast array of products are obtained. These products have in common that they generally form a viscous crude-oil-like replacement contain less oxygen (10-20% vs. 30-50%) and thus higher heating value (30 to 36 MJ/kg vs 10-20 MJ/kg) than untreated biomass [13]. However, their oxygen content is still much higher than petroleum (which is typically less than 1%). In addition, about 20% of the energy density of the products are generally found in the form of soluble organics [19]. These soluble organics are difficult to be used as a fuel since they are dissolved in water. The high oxygen content and

low energy density of the bio-crude make these products difficultly usable as direct replacement without significant upgrading [18].

1.3 Conversion of high-lipid biomass to bio-oil and biodiesel.

High-lipid biomass can be converted to biodiesel. Indeed, some lipids, specifically those with fatty acids, have long hydrocarbon chains that are similar in length to those found in the alkanes that form transportation fuels. The main difference of a carboxyl group at the end of the chain which is itself linked to a glycerol backbone [13]. Once the oil is extracted from the biomass (generally through pressing), this linkage can be cleaved through transesterification. Transesterification is the reaction of fat or glyceride with an alcohol to form an ester and a glycerol [20]. Typical feedstocks that can be converted are vegetable oils, animal fats, or high-lipid algae [21, 20]. Glycerol removal and decarboxylation can be achieved in a hot pressurized water or “hydrothermal” environment above 300°C, producing long alkane molecules. This can be done “in situ”, i.e. while the fat is still part of the biomass structure. Such processes have been used to produce a “bio-crude” from turkey processing wastes [13] and high lipid algae [22]. The drawback of such technologies, in addition to the conversion processes still being under development, is the mass production of high lipids from biomass, which is less straightforward than growing herbaceous or woody biomass. Vegetable oils suffer from food vs. fuel issues and their mass production can be energetically and environmentally intensive [20]. Micro-algae is an interesting feedstock because it is not used as a source of food and it can, theoretically, reach much more important mass yields per growth area than conventional terrestrial biomass [23]. However, much more research

is needed before this can be achieved on an industrial scale.

1.4 Biomass conversion through depolymerization and sugar conversion.

Lignocellulosic biomass is constituted of about 50 to 70% sugars. Cellulose and hemicellulose are polymers of 6-carbon and mostly 5-carbon sugars, respectively, and are two of the main constituents of the majority of terrestrial biomass. Monosaccharides, once produced from biomass, can be converted to a range of products through fermentation such as fuels or other specialty chemicals. In addition, recent discoveries have proven that sugars can be converted to liquid alkanes [24, 25, 26], hydrogen [27] or dimethyl-furan [28]. This conversion route is represented in Figure 1.2. Though challenges remain for sugar conversion technologies, the main bottleneck for all these processes is still the efficient depolymerization of biomass to monosaccharides [29, 30].

The focus of the work presented in this thesis is to develop new strategies for biomass depolymerization that could offer more efficient and sustainable options compared to current leading technologies. Concurrently, the study of these new strategies will improve the understanding of biomass depolymerization processes. The precise objectives of this PhD work are defined and described in Chapter 3. The following chapter (Chapter 2) provides an overview of the current understanding of biomass depolymerization and the leading technologies that are used.

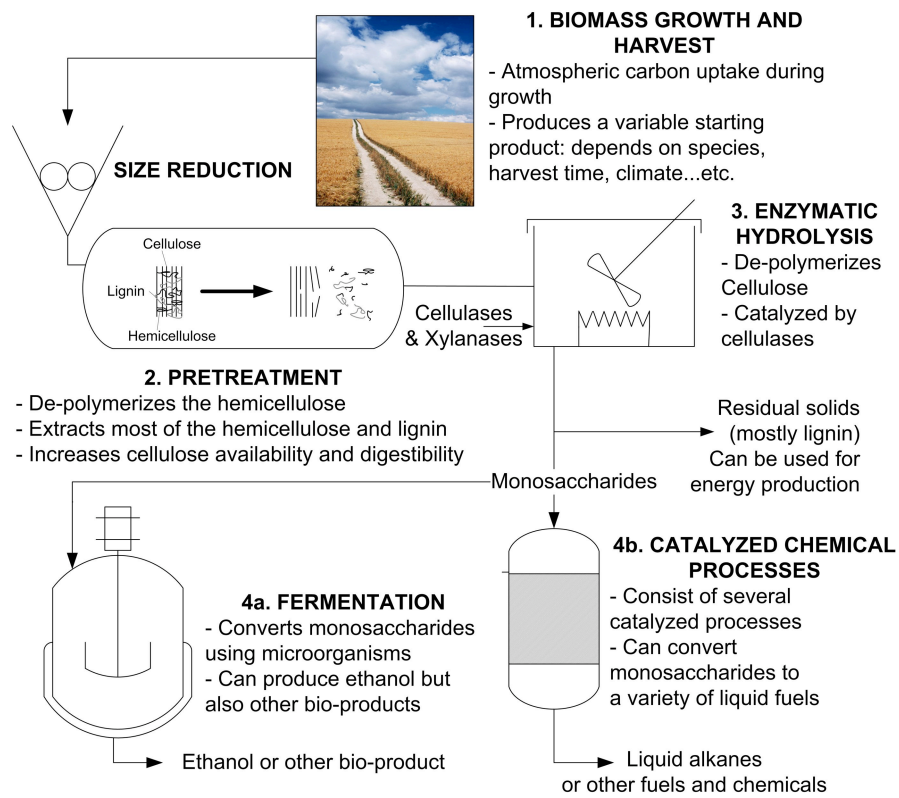


Fig. 1.2: Biomass conversion using sugar as an intermediate.

CHAPTER 2

BIOMASS DEPOLYMERIZATION

Lignocellulosic biomass is a mixture of different molecules such as sugars, proteins, lipids and organic acids, minerals. However, sugars generally constitute between 60 and 80 wt% of dry biomass [31]. These sugars are either in the form of cellulose (35-50 wt% of dry biomass), a polymer of glucose, or hemicellulose (15-35 wt% of dry biomass). Hemicellulose is a heteropolymer containing mostly xylose and some arabinose, which are 5-carbon sugars, and some 6-carbon sugars such as mannose and galactose [31]. Lignin is the third major component of biomass (between 10 and 30 wt% of dry biomass). It is also a heteropolymer, but its repeating unit is far more complex than a construction of simple sugars.

In summary, these three polymers constitute 95 wt% or more of dry biomass and are highly interlinked within the plant cell wall. Therefore, each major constituent's degradation is dependent on the degradation of the other two major constituents. For this reason, the state of knowledge regarding deconstruction of each of these three polymers is reviewed and discussed in the following three sections. The fourth section presents an overview of biomass pretreatment and enzymatic saccharification; a two-stage process which is the primary and most researched method used for biomass depolymerization. In this discussion, depolymerization is always referred to in tandem with monosaccharide degradation to unwanted byproducts. Indeed, biomass depolymerization strategies are often limited by the ability of the process in question to deconstruct biomass without destroying the product.

2.1 Cellulose depolymerization

Cellulose is a polysaccharide of glucose molecules which are connected through β -(1 \rightarrow 4)-glycosidic bonds (see Figure 2.1 A). The repeating cellobiose unit is given in its polymer form in Figure 2.1 A. This particular type of linkage in the glucose molecule allows for intra- and inter-molecular hydrogen bonds. This makes cellulose a crystalline polymer and recalcitrant to degradation. Cellulose is formed through the condensation of glucose molecules through the elimination of water. Conversely, cellulose can be depolymerized by the hydrolysis reaction shown below:



The hydrolysis reaction is made possible through the ionic stabilization of its intermediary which can take the form of either a cation or anion depending on whether a hydroxyl anion or a proton is used as a catalyst. Both mechanisms are shown in Figure 2.2. Therefore, acid or basic solutions can serve as catalysts to disrupt the β -(1 \rightarrow 4)-linkage [31]. Enzymatic reactions follow similar mechanisms. Indeed, in cellulase enzymes, carboxyl groups serve as proton donors [32]. Therefore, part of the enzyme acts as an acid catalyst while the rest of its structure further stabilizes the intermediate.

Cellulose hydrolysis can also occur in pure water. In fact, Bobleter reports that hydrolysis rates of these bonds appear to be insensitive to pH change in a pH range of 3 to 7 [31]. A mechanism that does not involve a charged intermediate is proposed, though Bobleter admits it to being controversial. Indeed, this suggestion goes against common tenets of organic chemistry, and, it is more likely that at low ion concentrations, the reaction becomes limited by other mechanistic features independent of ion concentration. In addition, at

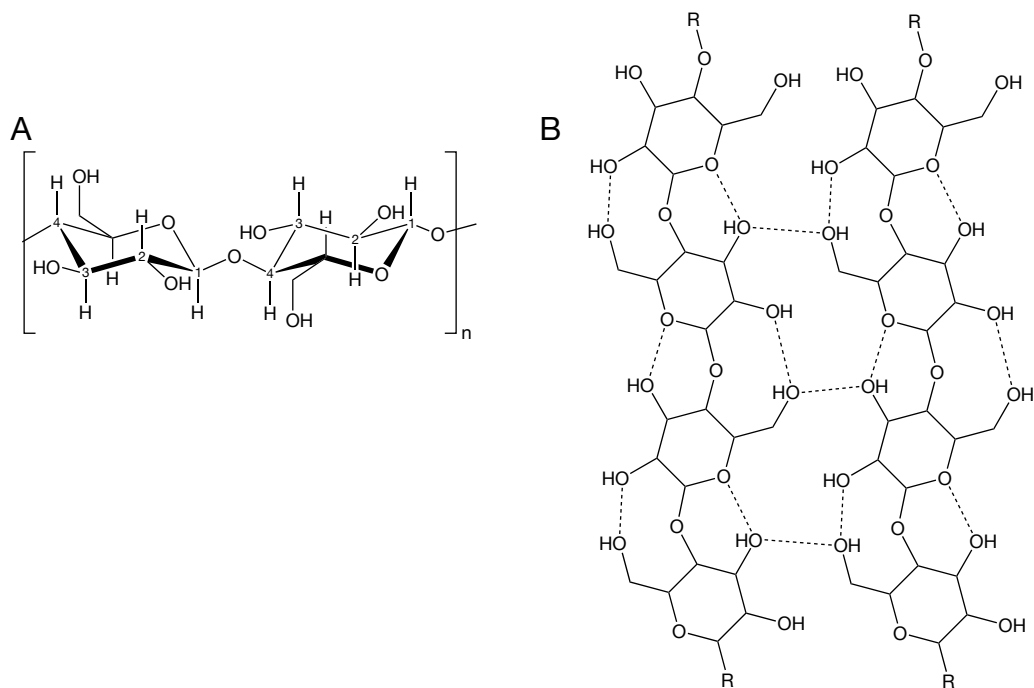


Fig. 2.1: Cellulose composition and structure. Part A shows cellobiose, the repeating unit of the cellulose polymer. Part B shows the crystalline structure of two cellulose chains with the inter- and intra-molecular hydrogen bonds depicted as dashed lines.

temperatures above 180°C, when cellobiose begins to hydrolyze in pure water [33, 34], the concentrations of acidic and basic forms of water increase significantly. Indeed the ion product of water, K_w , defined as the product of the concentrations of water's acidic and basic forms, $K_w = [H_3O^+][OH^-]$, goes from 10^{-14} M at room temperature to 10^{-11} M at around 250°C [35]. In other words, the concentration of protons and hydroxyl anions increases by a factor of 30. This allows for significant acid and base chemistry at these conditions.

The depolymerization of cellulose in liquid water (hydrothermal conditions), acid, basic and enzymatic solutions will be reviewed in the four sections that follow.

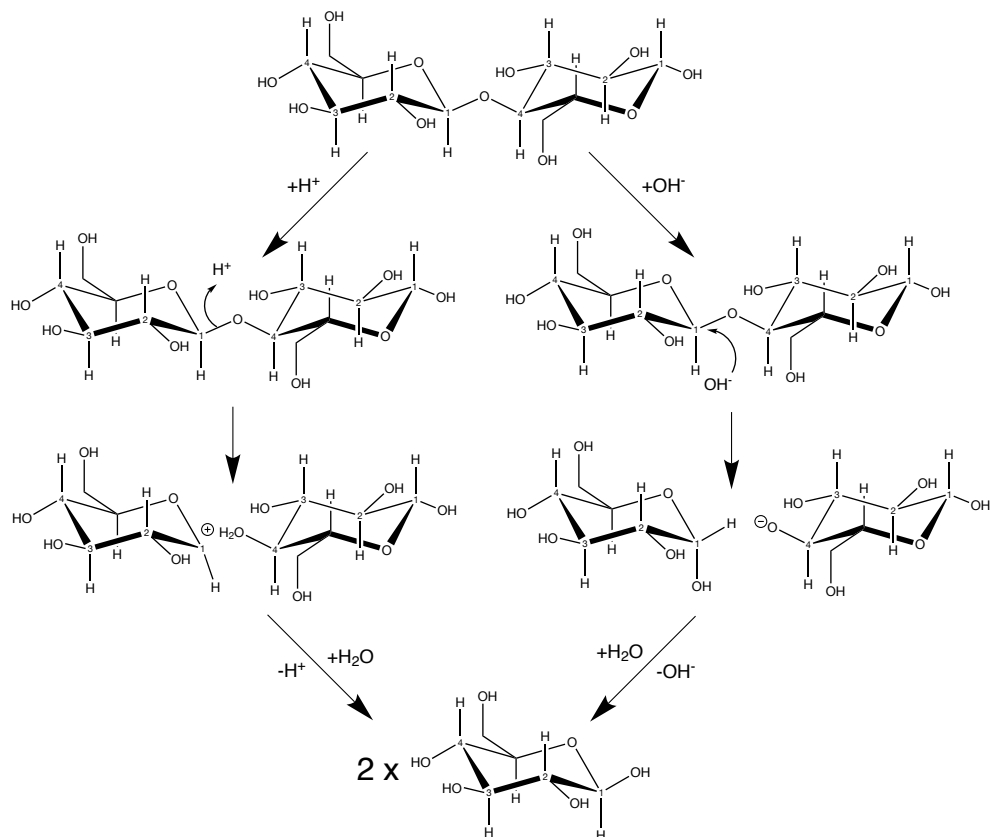


Fig. 2.2: Acid and base catalyzed mechanism of cellobiose hydrolysis

2.1.1 Cellulose depolymerization in pure water

Liquid water at temperatures above 180°C can depolymerize cellobiose, while cellulose decomposition becomes noticeable above 210°C [36, 37]. Bobleter et al. performed hydrothermal flow-through experiments to obtain elution curves for Aspen wood [33]. After removing all hemicellulose using water at 180°C, all the cellulose fraction is removed using water at 265°C in about 20 min.

Hydrolysis of cellulose leads to glucose oligomers which themselves depolymerize to glucose. However, glucose production is limited by its further degradation to other smaller molecules. Peterson et al. reported 25 identifiable degradation products from fructose or glucose in hydrothermal conditions

and slightly acidic. Of those products, only 8 are reported in 4 or more studies and are therefore considered the most important glucose degradation products. They are given in table 2.1. In addition, all of these 8 products appear below 300°C. The only product found in every study is 5-hydroxymethylfurfural (5-HMF). This confirms the common observation that, when treating lignocellulosic biomass in a hydrothermal (or acidic) environment at temperatures between 180 and 240°C, 5-HMF is the most prevalent glucose degradation product [38, 39].

Table 2.1: Glucose degradation products in hydrothermal media

Degradation product	Source
Acetic acid	[40, 41, 42, 43, 44]
Dihydroacetone	[37, 40, 41, 44]
Formic acid	[40, 41, 42, 43, 44]
Fructose	[37, 40, 41, 42]
Furfural (2-furaldehyde)	[37, 40, 43, 44]
Glyceraldehyde	[37, 40, 41, 44]
Glycoaldehyde	[37, 40, 41, 44]
5-Hydroxymethylfurfural (5-HMF)	[37, 40, 41, 42, 43, 44]
Pyruvaldehyde	[37, 40, 41, 44]

The competition between cellulose depolymerization and glucose degradation is illustrated by the variation of their first order rate constant with temperature shown in Figure 2.3. At temperatures between 250 and 350°C, glucose degradation outpaces cellulose depolymerization. However, this changes at 350°C due to cellulose’s higher activation energy. In addition to the acceleration of cellulose degradation above 320°C, the disappearance of crystallinity could have an important effect. Deguchi et al. used polarized light microscopy

to monitor birefringence loss in cellulose fibers, which corresponds to a loss of crystallinity during hydrothermal treatment [45]. By using temperature scanning experiments with water at 250 bar and heating rates between 11 and 14 K/min, they observed a drop in birefringence around 320°C. Complete breakup of the cellulose fibers followed shortly after, indicating a possible acceleration of cellulose deconstruction due to its melting.

In summary, opportunities seem to exist for effective biomass depolymerization at high temperatures and short residence times (400°C or above and reaction times of 10 to 500 milliseconds). Indeed, Sasaki et al. report a yield of 67% cellulose conversion to soluble oligo- and mono-saccharides when treating cellulose at 400°C for 50 milliseconds. They also postulated that there was a strong acceleration of the reaction kinetics when the critical point of water (374°C and 220 bar) was passed. However, when viewed with data from other groups (see Figure 2.3) this increase appears to be less dramatic. Zhao et al. obtained a yield of 54% cellulose conversion to soluble oligo- and mono-saccharides when treating cellulose at 380°C for 15 sec. Another interesting avenue of research is the use of CO₂-water mixtures. Above temperatures and pressures of 350°C and about 320 bar CO₂ and water become completely miscible [46]. This lowers the critical point of the mixture and thereby increases mass transfer. In subcritical conditions, the addition of carbon dioxide has proven to be a useful acid catalyst (through the production of carbonic acid) as demonstrated on starch and hemicellulose [47, 48]. In conclusion, opportunities for cellulose depolymerization in hot water systems exist, but much more research is needed to characterize this parameter space and to develop technologies capable of effectively reaching interesting reaction conditions.

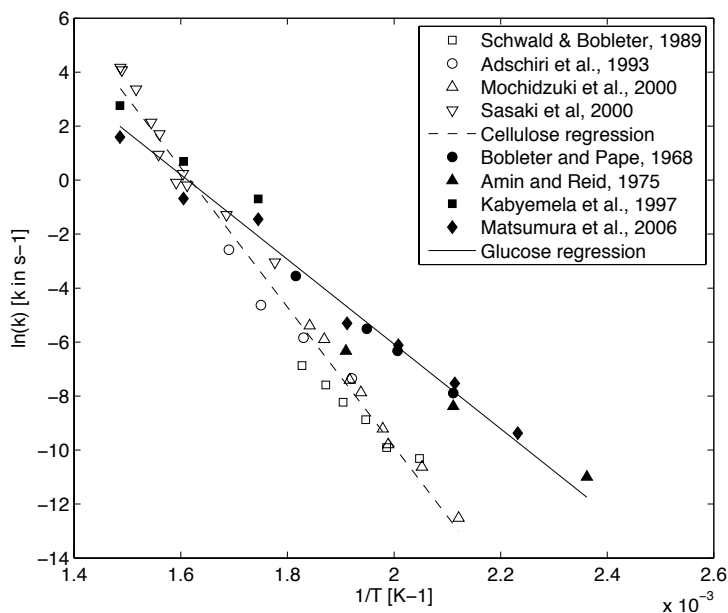


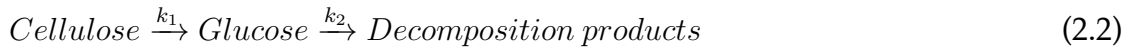
Fig. 2.3: Overlay of the Arrhenius plots of cellulose depolymerization (full symbols and line) and glucose degradation (hollow symbols and dashed line) (recreated from the figure given by Peterson et al. [13]). Data was taken from Schwald and Bobleter [36], Adschiri et al. [49], Mochidzuki et al. [50], Sasaki et al. [51], Bobleter and Pape [52], Amin and Reid [53], Kabyemela et al. [41] and Matsumura et al. [54].

2.1.2 Acid catalyzed cellulose depolymerization

The high concentration of protons present in acidic solutions are able to catalyze the cleavage of the β -(1 \rightarrow 4)-glycosidic bonds. This is demonstrated by the degradation of cellobiose in sulfuric, hydrochloric or phosphoric acid [31]. Acids are also capable of disrupting hydrogen bonding, which is why they are successful in depolymerizing cellulose. Indeed, for over 50 years, concentrated acids at room temperatures have been used to extract cellulose from biomass and completely solubilize it, which lead to the development of commercial processes [55, 56]. This technology was abandoned mainly due to the economic and environmental concerns of acids and neutralization chemicals, but the Chinese government has recently showed renewed interest in this technology by

funding a pilot-scale demonstration facility [57]. Concentrated acid treatment provides mostly oligomers that do not react further once in solution. Similarly, concentrated sulfuric acid is used to extract cellulose in the form of oligomers as an assay to measure structural carbohydrates in biomass [58]. More recently solubilizing biomass with concentrated phosphoric acid has been proposed as a possible pretreatment technology [59, 60].

Dilute acid mixtures at high temperatures (such as 2% sulfuric acid above 170°C) can completely depolymerize cellulose to glucose [61, 62]. At lower temperatures (around 120 °C), similar acid concentrations can hydrolyze soluble oligomers and are used to do so in the assay for measuring biomass structural carbohydrates [58]. However, producing glucose monomers from this principle suffers the same drawbacks as those discussed for hydrothermal depolymerization. Indeed, glucose easily degrades in acidic media through similar mechanisms, leading to similar decomposition products to those in a pure water environment [42]. Both Saeman and Fagan et al. successfully modeled cellulose depolymerization and further degradation of glucose as a pseudo-first-order sequential set of reactions [61, 62]:



where these reactions can be modeled as:

$$\frac{d[Cellulose]}{dt} = -k_1[Cellulose] \quad (2.3)$$

$$\frac{d[Glucose]}{dt} = k_1[Cellulose] - k_2[Glucose] \quad (2.4)$$

and where:

$$k_i = k_{o,i}[Acid]^{n_i} \exp\left(\frac{Ea_i}{RT}\right) \quad (2.5)$$

In the equations above, brackets denote concentrations [mol/cm³], cellulose concentration is given in moles of potential glucose per liters of reaction, acid concentration is given in wt% of sulfuric acid, k_i [hr⁻¹] is the i^{th} reaction constant, $k_{o,i}$ [hr⁻¹ wt% Acid⁻ⁿ] is the i^{th} pre-exponential factor, n_i [-] is the exponential factor for the i^{th} reaction, and E_{a_i} [kJ/mol] is the i^{th} activation energy. All variables and there descriptions are given in Table 2.2. Saeman's results were obtained for wood while Fagan's results were obtained for paper [61, 62]. Other groups have used this approach for Solka-Flok (purified cellulose) with two rate constants for accessible cellulose vs. crystalline, unaccessible, cellulose [63], or lignocellulosic biomass [64]. Glucose yields as a function of time are plotted for different temperatures and acid concentrations as in Figure 2.4 according to the model proposed by Fagan et al. [61]. This figure shows the limitations of glucose production from cellulose and, similar to cellulose depolymerization in pure water, high temperatures and short times must be achieved to obtain high yields.

It is important to note that this approach supposes that oligomer depolymerization to glucose happens extremely fast compared to cellulose depolymerization and glucose degradation, and can therefore be neglected. Nevertheless, Abatzoglou et al. detected significant amounts of oligomers in solution at short residence times (30-90 sec) and acid concentrations of 1 wt% or less [65]. Mok et al. report that for low concentrations of acid (0.05 wt% or less) and reaction times of up to an hour, oligomer production influences reaction kinetics [39]. Therefore, it appears that at lower concentrations of acid and shorter residence

Table 2.2: List of symbols and their associated description.

Parameter	Description	Units
A	Area of the wood chips	[cm ³ /L]
$[Component]$	Concentration of the <i>component</i> in question	[mol/cm ³]
$[Component]_0$	Initial concentration of the <i>component</i> in question	[mol/cm ³]
E_{a_i}	Activation energy of reaction i	[kJ/mol]
k_i	First order rate constant for reaction i	[hr ⁻¹]
$k_{o,i}$	Pre-exponential factor for the reaction i	[hr ⁻¹ wt% Acid ⁻ⁿ]
$k_{tr,j}$	Mass transfer coefficient for compound j	[cm/hr]
n_i	Acid exponential factor for reaction i	[-]
R	Ideal gas constant	[kJ/(mol K)]
T	Temperature	[K]
t	Time	[hr]
V_B	Bulk volume i	[cm ³]
V_p	Pore volume i	[cm ³]
Greek symbols		
α	Un-hydrolyzable xylan fraction	[-]
ϵ	Porosity	[-]
Subscripts		
B	Bulk	[-]
F	Fast reaction	[-]
f	Furfural	[-]
i	Component i	[-]
j	Reaction j	[-]
P	Pore	[-]
ol	Xylo-oligomer	[-]
S	Slow reaction	[-]
x	xylose	[-]

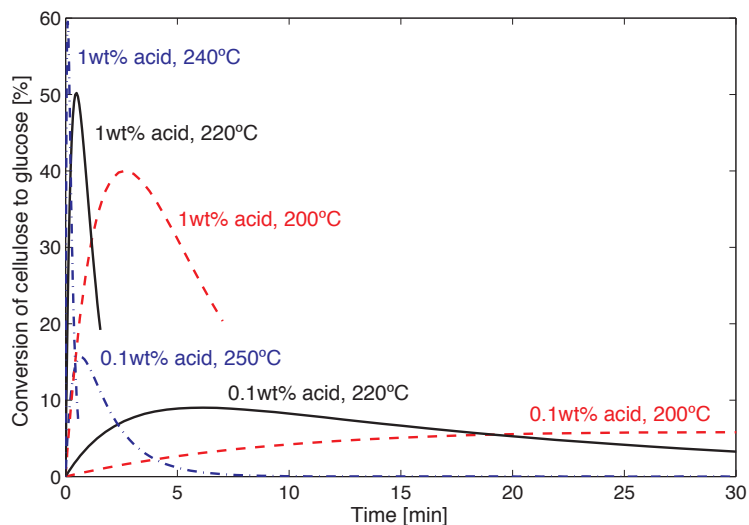


Fig. 2.4: Predicted glucose yield from cellulose as a function of time for different temperatures and sulfuric acid concentrations (based on a model proposed by Fagan et al. [61]).

times, this kinetic approximation is not valid. For pure water systems, high concentrations of oligomers are obtained as glucose degradation occurs making this approximation invalid [51, 66]. In fact, if one applies this same approximation using kinetic data obtained from cellulose depolymerization and glucose degradation data (see Figure 2.3), glucose production and degradation is overestimated. Indeed, soluble oligomers must further hydrolyze to produce glucose, which decreases glucose yields. In turn, decreased glucose concentrations lead to decreased yields of glucose degradation products.

Regardless of these considerations, Figure 2.4 accurately illustrates the trade-offs of using acid hydrolysis for glucose production from cellulose. These results suggest more experiments should be run at short times and high temperatures (perhaps closer to or above 300°C). So far, no experiments at such temperatures and in the presence of strong acids have been reported.

2.1.3 Base catalyzed cellulose depolymerization

As discussed earlier, the β -(1 \rightarrow 4)-linkage is catalyzed by hydroxyl anions. Because of this phenomenon, cellobiose depolymerizes quickly in basic solutions (0.1 M NaOH) even below 100°C [67]. However, glucose is also severely attacked by alkali even at these low temperatures and a number of degradation products are produced directly from cellobiose, from glucose and through a fructose intermediate [67].

In contrast, cellulose is quite stable even at higher temperatures and, surprisingly, sees its crystallinity index increase when it is treated with around 20 wt% sodium hydroxide at room temperature or at 100°C [68, 69]. This process, known as mercerization, is commonly used industrially to apply a glazed finish to cellulose. Therefore, basic solutions are effective at degrading glucose but are ineffective at depolymerizing it, making them very poor catalysts for monosaccharide production from cellulose. However, as will be discussed in Section 2.1.4, they can be an interesting option to increase cellulose degradability towards enzymes.

2.1.4 Enzyme catalyzed cellulose depolymerization

Given that cellulose is the most important form of carbohydrate on the surface of the earth, it is not surprising that different types of organisms have developed strategies to deconstruct and metabolize it. All of these organisms use cellulase enzymes which depolymerize cellulose through a protonated intermediate as discussed on page 11. Microorganisms such as bacteria and fungi are the most

important cellulose consumers [70]. However, insects and mollusks have been known to produce their own cellulases [71, 72]. Other cellulose utilizing species have developed symbiotic relationships with cellulolytic bacteria, such as ruminants [73] or with bacteria and/or fungi, such as termites [71, 72, 74, 75, 76].

Most cellulolytic bacteria and fungi secrete their cellulases outside their cell walls because insoluble cellulose cannot be transported through them. Therefore, the enzymes depolymerize cellulose and produce monosaccharides, which can be transported into the cell to be metabolized. This allows for easy production and harvesting of the organism's cellulase mixture or "crude" which can be used depolymerize cellulose. In a subsequent step, these monosaccharides can then be fermented or catalytically converted. Alternatively, cellulose can be converted into the desired product in a single step, either by mixing the crude with fermentative organisms, or by using anaerobic bacteria that can both, hydrolyze plant cell walls, and ferment monosaccharides to the desired product. This strategy is referred to as consolidated bioprocessing [77].

Most anaerobic bacteria and fungi do not produce free cellulases and grow very slowly. Rather, they produce multi-enzyme complexes called cellulosomes [78]. This complex is usually bound to the outer surface of the organism [79]. The enzymes present on this complex often cannot bind to cellulose on their own. However, the scaffolding protein linking them together contains a cellulose binding module allowing the unit to bind to cellulose. Efforts are currently underway to design cellulosomes with increased activity [80, 81, 82, 83]. The ability of cellulosome producing organisms to degrade cellulose as effectively as free enzyme solutions is not fully understood. Indeed, cellulosomes have much more limited access to the cellulose surface, especially the surface present

in pores, compared to free cellulases [70]. Despite these interesting questions, the narrow applications of anaerobic bacteria and their more inefficient carbon metabolism has lead most current commercial development to focus on free enzyme systems [84]. In addition, the catalytic sites present in free enzyme systems are often analogous to mechanisms found in enzymes docked to the cellulosome, which makes the study of free enzyme systems very relevant to biomass depolymerization [70].

Industrial enzyme cocktails are almost exclusively produced in aerobic fungi *Trichoderma reesei* or *Humicola insolens*, with the majority produced in *Trichoderma reesei*. Engineered strains of these organisms can produce over 100 g/L of crude cellulase protein [84]. The U.S. Department of Energy (USDOE) has been supporting the development of cellulases for the production of ethanol from lignocellulosic biomass. This has lead several companies to develop commonly used, high-activity, cellulase crudes such as Spezyme CP© or Accelerase© developed by Genencor Inc., and Celluclast© developed by Novozyme Inc. In addition, a number of bacterial and fungal systems are used to produce non-industrial cellulases mainly for research purposes.

Free cellulase types and classification

Free cellulase systems are always a mixture of a number of different proteins that have different roles and that work synergistically to depolymerize their substrate (see section 2.1.4). Cellulases are designated by a prefix *Cel* followed by their family number, followed by a letter designating the order in which they were discovered (for example: *Cel9A*). According to the CAZy website (<http://www.cazy.org>), there exists 118 families (numbered 1 through 118) of

glycoside enzymes that can be subdivided into 14 related families or “clans”. Nevertheless, cellulases can be classified into three different categories based on their catalytic action, all of which are depicted with a schematic representation of their action on cellulose on Figure 2.5:

Exocellulases. These enzymes are also known as cellobiohydrolases. They attack at chain ends of cellulose polymer chains. Depending on the enzyme, the attack will take place at a reducing or non-reducing cellulose chain end. The reducing end of cellulose designates the direction that will end in a ketone group if the open-chain form of the end sugar monomer is accessed. Exocellulases function in a processive manner, sequentially liberating cellobiose units as they travel along a cellulose chain [70, 77]. All their catalytic sites, for which the structure has been determined, are shaped like a tunnel, through which the cellulose chain threads [85, 86]. The catalytic domain (CD) containing the catalytic site is linked to a carbohydrate binding module (CBM) by a flexible linker peptide.

It has been speculated that the CBM has an important role in disrupting cellulose’s structure in addition to fixing the enzyme to the surface [87, 88, 89, 90]. In contrast, some studies have observed little disruption due to the CBM [91, 92]. However, these two studies were performed using avicel cellulose, which is a dilute acid processed form of cellulose, while all the other studies were performed on cotton fibers. It could be that in Avicel, the cellulose structure is already somewhat disrupted and is not further disrupted by the CBM. Nevertheless, the exact way that the CBMs influence cellulose hydrolysis is still not well understood.

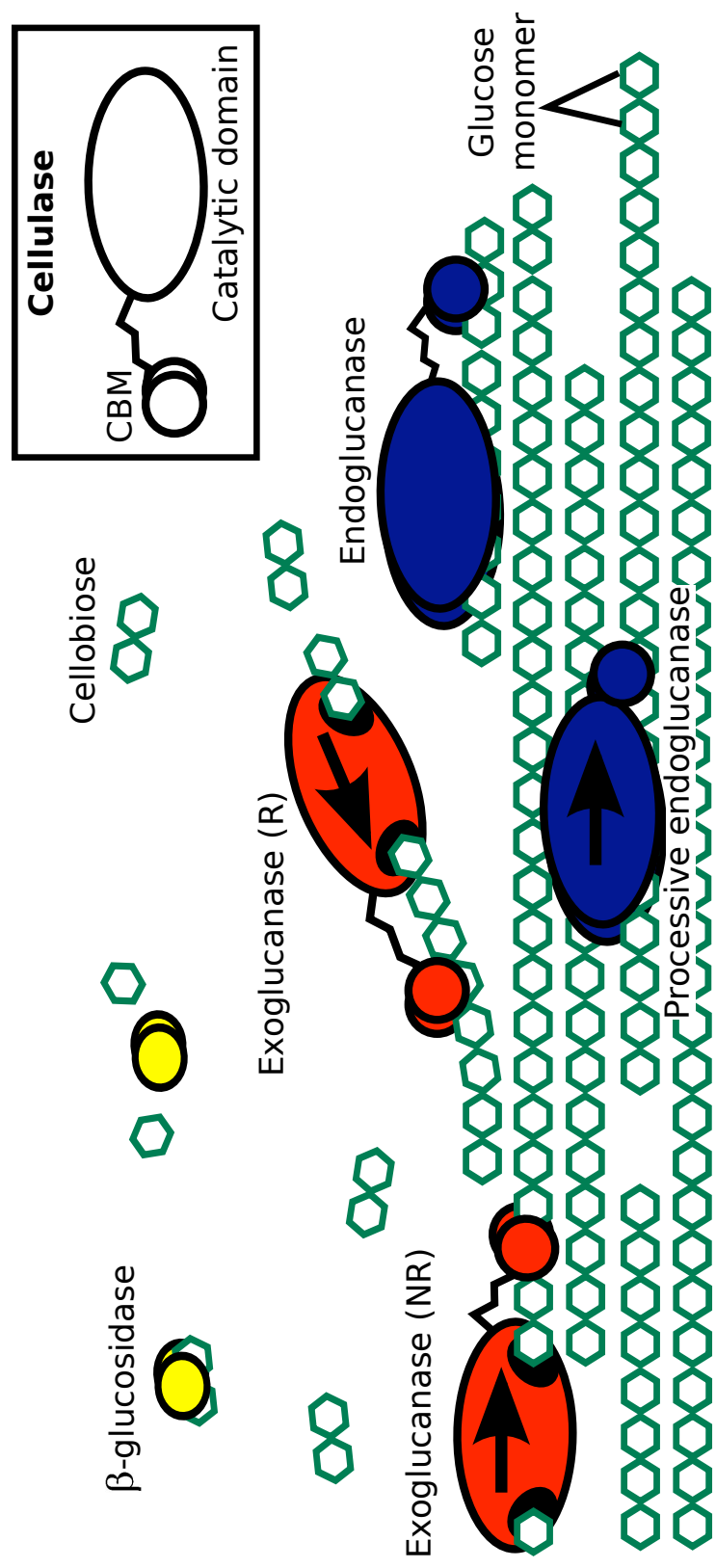


Fig. 2.5: Depiction of cellulose depolymerization by cellulase mixtures

Endocellulases. The endoglucanase catalytic domain structures that have been determined have an open “cleft-like” structure [93, 94]. This open structure allows the cellulase molecules to attack in the middle of cellulose chains, liberate oligosaccharides and expose individual cellulose chains. Endocellulases are thus usually identified by their ability to rapidly reduce the viscosity of carboxymethyl cellulose (CMC) by reducing cellulose chain length. Traditionally, endocellulase attack sites have been described as amorphous [77]. However, more recently, birefringence has been measured in these areas by Thygesen et al., indicating a certain degree of crystallinity [95]. However, Thygesen et al. still observe a discontinuity between these areas and the rest of the cellulose structure and, through the use of fluorescently labeled endocellulases, demonstrate that this is their preferential attack site.

Endocellulases contain a CBM that has been proven to be important for activity [96, 97]. Many of the considerations discussed for exocellulase CBMs apply to endocellulase CBMs. A notable exception occurs with processive endocellulases. Processive endocellulases exhibit both endo- and exocellulase qualities [96, 97]. They can attack in the middle of a cellulose chain and rapidly reduce the viscosity of CMC but produce mostly soluble oligosaccharides from insoluble cellulose [96]. The CBM differs from that of exocellulase in that it is rigidly linked to the catalytic domain and binds only weakly to cellulose [97, 98]. However, these CBMs have still been shown to be essential to the enzyme activity [97].

β -glucosidases. Cellobiose and some larger soluble oligosaccharides are hydrolyzed by enzymes known as β -glucosidases [77]. These enzymes not only help produce glucose that can be more easily metabolized, but also help avoid

the inhibition of other enzymes by cellobiose, a strong inhibitor [99, 100]. Many aerobic fungal organisms produce their own β -glucosidases. *Trichoderma reesei* produces β -glucosidases, but a large portion of these enzymes remain bound to the cell wall [101]. This leads commercial preparations that are constituted by *Trichoderma reesei* crude cellulases to be supplemented with a β -glucosidase crude from the *Aspergillus* species when biomass depolymerization experiments are conducted [102].

Synergism in cellulase systems

Shortly after the discovery of *Trichoderma reesei* cellulases, a synergistic effect was observed between its enzymes [103]. This effect is said to occur when the activity of a mixture of enzymes is greater than the summed activities of the individual enzyme. The ratio between the mixture's activity and the sum of individual activities is known as the degree of synergism [104]. A mixture of 3 enzymes has been known to have a degree of synergism of up to 8 [96]. Interestingly, anti-synergistic effects can be observed at low temperatures, when activity is low but binding still occurs, which indicates that cellulases may be competing for binding sites.

A mechanism for the synergism of endocellulases and exocellulases has been accepted for over 30 years: endocellulases, by disrupting the middle of cellulose chains create new attack sites for exocellulases to begin processive depolymerization [105, 77]. This mechanism is illustrated in Figure 2.5. For this reason, all active endocellulases show synergism with any exocellulase but usually not with each other [96, 70]. There is no evidence that this synergism is due to interactions between the enzymes, since synergism is similar between enzymes

whether or not they are produced by the same organism [70].

In subsequent enzymatic treatment experiments, it has been shown that endocellulase-treated filter paper is more readily hydrolyzed by exocellulases, but the reverse is not true [106]. Interestingly, in synergistic mixtures, endocellulase activity and exocellulase activity increase equally [96]. Wilson explains that this phenomenon could be due to a temporary and reversible disruption of the cellulose structure by the binding of exocellulases that favors hydrolysis by endocellulase [70]. Subsequent and simultaneous enzymatic studies with different exocellulases have shown synergistic effects but only if the exocellulases attacked different ends of the cellulose chains [106, 96].

Finally, there are several non-cellulase proteins that appear to enhance enzymatic hydrolysis of cellulose by cellulases. Such proteins include a class of plant proteins called expansins [107, 108] and a closely related fungal protein called swollenin [109]. Indeed, an expansin like protein produced by the bacteria *Bacillus subtilis* has been proven to stimulate the hydrolysis of corn stover by the Celluclast® cellulase crude [108]. Some organisms secrete proteins that only contain a CBM and have been shown to stimulate the activity of low-concentration cellulase mixtures. Furthermore, recent work by Novozyme Inc. found that a family 61 protein from a thermophilic fungus could increase the activity of the *Trichoderma reesei* crude severalfold even though it did not contain any cellulose binding sites [110, 111].

Accessibility to cellulose

The specific activities of cellulases on heterogeneous cellulose substrates are slow compared to those of other enzymes acting in solution and do not follow Michaelis-Menten kinetics [70, 112]. However, on soluble oligosaccharides, activities are significantly higher and Michaelis-Menten kinetics can be applied [113, 114]. This difference indicates that access of cellulases to the substrate surface is the key determining factor in cellulose depolymerization kinetics by cellulases, which has been verified by specific studies [115, 112]. Recent studies using microscopy and fluorescently labeled cellulases have shown that cellulases rapidly bind to easily accessible sites and then, in a process limited by diffusion, bind to sites located within the particle [116, 117].

As it will be further discussed in Section 2.4, to increase enzymatic hydrolysis rates and obtain near complete cellulose depolymerization by cellulases, a thermochemical pretreatment step must be applied to lignocellulosic biomass. It has been demonstrated that the main reason such a step is beneficial is due to its effect of increasing biomass accessibility to cellulases (see Section 2.4.1 and Grethlein's work [118]).

In conclusion, enzymes can completely and effectively depolymerize cellulose. In addition, because of their specificity and low temperatures (usually around 50°C for fungal systems), no degradation products are formed. However, because of the substrate heterogeneity and accessibility limitations, enzymatic cellulose depolymerization is fairly slow and maximal glucose yields are often only obtained after 1 to 7 days (see Section 2.4 for more details). This contrasts with the hydrothermal depolymerization systems that produce high yields in seconds (or less) but produces higher amounts of byproducts.

Modeling of enzymatic hydrolysis

A number of recent approaches have been used to model enzymatic hydrolysis reactions. These approaches have been recently reviewed by Bansal et al. [119] and fit into four broad categories:

Empirical correlations. Empirical models generally attempt to correlate variables with hydrolysis rates or cellulose conversion extents. These variables include substrate properties such as accessible surface area to cellulases [118, 120], lignin content [120, 121], crystallinity [120, 121] or acetyl bonds in pretreated biomass [121]. DRIFT (i.e. Diffusive Reflectance FT-IR) spectroscopic data have also been used as an input for such empirical models along with lignin content and crystallinity [122]. Stochastic models have recently been used to optimize the composition of cellulase mixtures by correlating cocktail compositions with cellulose conversion yields [123, 124].

Michaelis-Menten kinetics. As said above, cellulose-cellulase hydrolysis systems do not follow Michaelis-Menten kinetics due to substrate heterogeneity. However, a number of studies have shown that data can be fitted quite well to models based on Michaelis-Menten kinetics. Bansal et al.'s review lists 11 studies that base their modeling approach entirely on Michaelis-Menten approach [119]. However, since such an approach does not account for the heterogeneity effects that are known to occur, it can be considered a semi-empirical approach.

Models with an adsorption step. The review by Bansal et al. lists a total of 29 studies that include an adsorption step in their modeling approach. Us-

ing the Langmuir isotherm is the most common approach for binding and has been used many times to model the adsorption of cellulases on cellulose [125, 126, 119, 127]. In some models, an additional kinetic step is added after enzyme binding to account for the binding of the cellulase's catalytic domain (assuming that initially enzymes are only bound through their carbohydrate binding module) [128, 129, 130]. Most of these models implicitly assume that equilibrium is instantaneous with respect to degradation. However, Steiner suggests that this assumption may be incorrect [131].

Models with non-equilibrium adsorption. A number of models take into account an adsorption step but do not assume that an adsorption equilibrium controls the fraction of bound enzyme. Levine et al. have proposed a model that includes an adsorption step, an equilibrium complexation step (i.e. binding of the catalytic domain) and account for changes in substrate surface area [132, 133]. Gan et al. attempted to incorporate both heterogeneity factors, mass transfer and kinetics (preventing a true equilibrium), but they did not model spatial variations of concentration within a biomass particle and thus did not truly account for diffusion [134].

In summary, though many models have been proposed, there is no approach that successfully combines the multiple steps that are thought to occur during enzymatic hydrolysis: (1) diffusion through the porous substrate, (2) binding of the carbohydrate binding module to the cellulose surface, (3) binding of the catalytic domain, (4) reaction of the enzyme (if a processive action of the cellulase occurs, multiple reactions could occur) and (5) desorption of the substrate. Step 5 could be followed by a repetition starting at steps 2 or 3 depending on whether full desorption has occurred or if only the catalytic domain has disengaged.

2.2 Hemicellulose

Hemicellulose is a heteropolymer of mostly 5-carbon sugars, or pentoses (mostly xylose and some arabinose), and some 6-carbon sugars, or hexoses (glucose, mannose and galactose). It usually also contains some organic acids. Figure 2.6 shows the structure of the hemicellulose repeating unit of Vetiver grass leaves proposed by Chaikumpollert et al. [135]. As illustrated by this structure, the heterogeneity of hemicellulose composition leads to a highly branched polymer. These branches prevent the formation of hydrogen bonds and thus prevent hemicellulose from having a highly crystalline structure like cellulose. This leads hemicellulose to be much less resistant to hydrolysis than cellulose.

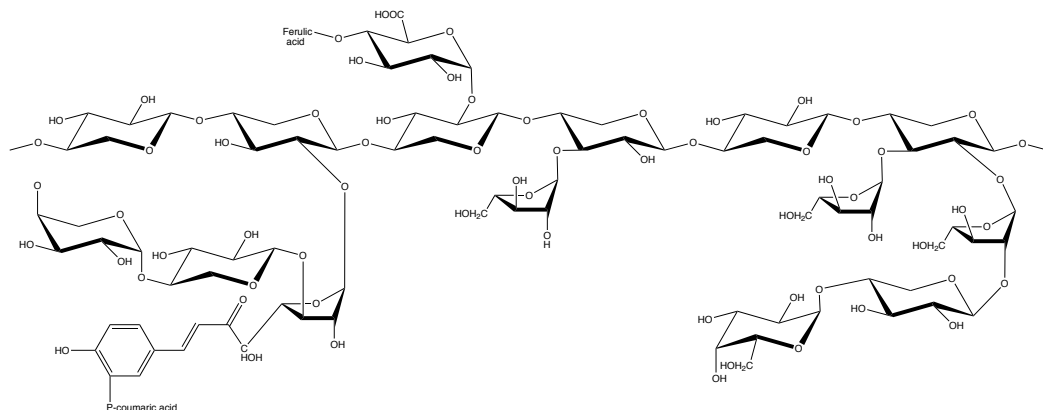


Fig. 2.6: Structure of the repeating unit of Vetiver grass leaf hemicellulose (proposed by Chaikumpollert et al. [135])

Most lignocellulosic listed on the United States Department of Energy biomass program feedstock database (http://www1.eere.energy.gov/biomass/feedstock_databases.html) have hemicellulose that are constituted of 80% or more xylan (xylose polymers). Softwoods are a notable exception because they contain important quantities of mannan (polymer of mannose) [31]. Because of the prevalence of xylose in hemicellulose, most studies have focused on xylose chemistry. Most bonds in xylose polymer and other hemicellulose

oligosaccharides are linked with the same β -(1 \rightarrow 4)-glycosidic bond that is present in cellulose. They logically follow similar depolymerization mechanisms as those presented in Figure 2.2 for cellulose. However the bonds that occur in branched oligosaccharides are generally α -(1 \rightarrow 2) or α -(1 \rightarrow 3)-glycosidic bonds [31].

Hemicellulose is highly interlinked with lignin and cellulose in the plant cell wall [30]. Therefore, isolation of pure hemicellulose is difficult and its isolation will often fundamentally alter its behavior [136]. In addition, as will be discussed, its behavior is heavily dependent on its structure and the structure of other lignocellulosic components. This makes the study of native hemicellulose much more meaningful than the study of model compounds. Furthermore, as discussed in the following paragraphs, because of its linkages with lignin, hemicellulose and lignin degradation can often be hard to differentiate.

2.2.1 Hemicellulose depolymerization in pure water

Hemicellulose depolymerization in pure water begins around 180°C. Bobleter was able to extract most of the hemicellulose fraction of Aspen wood with water at 180°C[31]. Wyman and Liu were able to extract 90% of the xylan content of corn stover, after 16 min at 180°C, by flowing water through a packed bed of biomass [137]. This removed xylan increased to 97% for the same conditions with a temperature of 220°C. In the absence of flow-through, the removed xylan dropped to 5% and 91% for 180 and 220°C, respectively. This indicates that xylan hydrolysis is limited by mass transfer. In the absence of flow-through,

yields of soluble xylose and xylo-oligomers dropped from 50 to 15% at 180°C and from 95 to 5% at 220°C. In addition to mass transfer limitations, this result indicates that xylose degrades fairly readily at these temperatures.

Xylose degradation in neutral or slightly acidic media produces mostly furfural as a degradation product, especially at temperatures close to or below 200°C [138, 139, 31]. Even at 250°C in acidic conditions, Antal et al. have shown that a furfural yield of close to 60% is obtainable. However, a number of other degradation products exist and they are listed in Table 2.3. Resin in particular is an interesting degradation product given that recently, it has been suggested that xylose degradation products could form solid residues on pretreated biomass and be mistaken for lignin [140].

Table 2.3: Xylose degradation products in hydrothermal media

Degradation product	Source
Furfural	[139, 141, 138]
2,3-Dihydroxy-2-cyclopenten-1-one	[142]
Lyxose	[139]
Acetol	[139]
Formaldehyde	[143, 144]
Glyceraldehyde	[139, 139]
Glycoaldehyde	[139, 139]
Pyruvaldehyde	[139]
Acetaldehyvde	[143, 144]
Crotonaldehyde	[143, 144]
Lactic acid	[139]
Formic acid	[138, 139]
Dihydroxyacetone	[139]
Resin	[138]

Modeling xylan depolymerization in pure water has consisted of a number of different approaches. Garrote et al. used sequential pseudo-first order reactions kinetics (xylan→high-molecular weight xylo-oligomers→low-molecular weight xylo-oligomers→xylose→furfural) [145, 146]. Garrote et al. proposed another model, in a subsequent study, where two types of xylan (fast and slow reacting) decomposed to the previously described high molecular weight xylo-oligomers [147]. Jacobsen and Wyman used a similar sequential model with two types of xylan (fast and slow reacting) that form xylo-oligomers, which then degrade to xylose, and subsequently furfural [148]. Mittal et al. proposed a similar kinetic model for wood meal and then incorporated mass transfer limitations in a model for sugar-maple xylan [149, 150]. The structure of this model is depicted in Figure 2.7. The advantage of this approach is that it incorporates mass transfer limitations that occur in xylan depolymerization and have previously been discussed in this review.

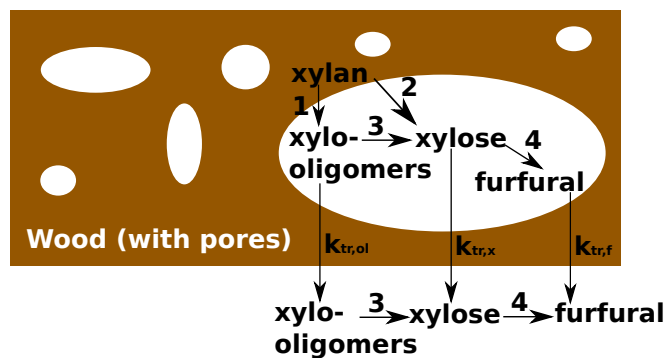


Fig. 2.7: Xylan depolymerization model (as proposed by Mittal et al. [150]). Rate constant for the i^{th} reaction is denoted by k_i while the mass transfer coefficient for compound j is denoted by $k_{tr,j}$. The subscripts ol , x and f designate xilo-oligomers, xylose and furfural, respectively.

According to Mittal et al. xylan can depolymerize from its solid form to xylose or xylo-oligomers:

$$\frac{d[Xylan]}{dt} = -(k_1 + k_2)([Xylan] - \alpha[Xylan]_0) \quad (2.6)$$

The concentration of xylo-oligomers in the pores is given by the following differential equation:

$$\begin{aligned} \frac{d[Oligomer]_P V_p}{dt} &= V_p k_1 [Xylan] ([Xylan] - \alpha[Xylan]_0) - V_p k_3 [Oligomer]_P \\ &\quad - k_{tr,ol} \frac{1+\epsilon}{2} A ([Oligomer]_P - [Oligomer]_B) \end{aligned} \quad (2.7)$$

while the concentration of xylo-oligomers in the bulk is given by:

$$\begin{aligned} \frac{d[Oligomer]_B}{dt} &= k_{tr,ol} \frac{1+\epsilon}{2V_B} A ([Oligomer]_P - [Oligomer]_B) \\ &\quad - k_3 [Oligomer]_B \end{aligned} \quad (2.8)$$

Following similar reasoning, the differential equations describing the concentrations of xylose and furfural in the bulk are given by:

$$\begin{aligned} \frac{d[Xylose]_B}{dt} &= k_{tr,x} \frac{1+\epsilon}{2V_B} A ([Xylose]_P - [Xylose]_B) \\ &\quad + k_3 [Oligomer]_B - k_4 [Xylose]_B \end{aligned} \quad (2.9)$$

and

$$\begin{aligned} \frac{d[Furfural]_B}{dt} &= k_{tr,f} \frac{1+\epsilon}{2V_B} A ([Furfural]_P - [Furfural]_B) \\ &\quad + k_4 [Xylose]_B \end{aligned} \quad (2.10)$$

In the equations above, brackets denote concentrations [mol/cm³]. The rate constant for the i^{th} reaction is denoted by k_i [hr⁻¹]. The mass transfer coefficient for compound j is denoted by $k_{tr,j}$ [cm/hr]. The subscripts ol , x and

f designate xilo-oligomers, xylose and furfural respectively. The subscripts P and B designate compounds in the pores or in the bulk, respectively. An unhydrolyzable xylan fraction is designated by α [-]. The porosity fraction and area (cm^3/gr) of the wood chips are designated by ϵ [-] and A [-], respectively. All variables and there descriptions are given in Table 2.2. The bulk volume is designated by V_B [cm^3]. The pore volume (V_p [cm^3]) is calculated through a correlation with mass loss, which is itself modeled used pseudo-first order kinetics. This approach adds two temperature dependent parameters for the correlation and rate constants (for which Arrhenius parameters have not been calculated. In addition, all mass transfer coefficients are temperature dependent and fitted for each temperature. Therefore, this approach requires many parameters to function and should be refined. However, it represents a good effort to take into account mass transfer limitations in biomass depolymerization. The xylan, xylo-oligomer, xylose and furfural yields are given as a function of time in Figure 2.8. They demonstrate that significant xylose removal is difficult without producing some furfural.

2.2.2 Acid catalyzed hemicellulose depolymerization

At room temperature, just like for cellulose, concentrated acid can be used to extract most of the hemicellulose fraction from biomass in the form of oligomers, [58]. In dilute acid, hemicellulose depolymerization is approximately 60 to 80 times faster than cellulose depolymerization under the same conditions [31]. Hydrolysis of soluble hemicellulose derived oligomers can even begin below $100^\circ C$ in dilute acid media [136]. However, presumably due to the structural

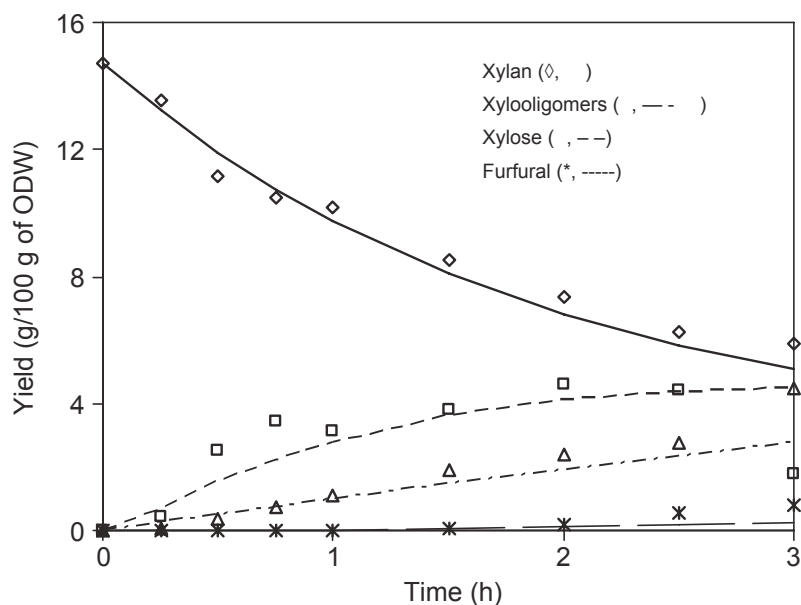


Fig. 2.8: Xylose, xylo-oligomers, xylose and furfural concentration as a function of time in hydrothermally (175°C) pretreated sugar maple wood chips (as reported and modeled by Mittal et al. [150]).

features of lignocellulosic biomass, native hemicellulose depolymerization only becomes significant above 100°C. Very similarly to the experiments that were described for pure water, Wyman et al. showed that by flowing a 0.05 wt% sulfuric acid solution through a packed bed of corn stover, they could remove over 90% of the xylan in 16 minutes [151]. Without any flow-through, only about 50% was removed. This demonstrates that mass transfer effect exist in dilute acid hemicellulose. With 0.05 wt% acid solution soluble xilan derivatives are almost exclusively xilo-oligomers, even in the absence of flow-through. However, with an 0.1 wt% acid solution about 40% of the products that are recovered are xylose, even in the presence of flow-through. Therefore, as acid concentrations rise, xylo-oligomers are increasingly rare in solution because they rapidly depolymerize to xylose.

In most cases, approaches for modeling xylan depolymerization in acidic

media have assumed that the xylo-oligomers are short lived. These studies generally use acid solutions Thus, they assume first order reactions that directly convert xylan to xylose and, subsequently, a first order reaction that converts xylose to degradation products:

$$\frac{d[Xylan]}{dt} = -k_1[Xylan] \quad (2.11)$$

$$\frac{d[Xylose]}{dt} = k_1[Xylan] - k_2[Xylose] \quad (2.12)$$

where:

$$k_i = k_{o,i}[Acid]^{n_i} \exp\left(\frac{Ea_i}{RT}\right) \quad (2.13)$$

In the equations above, brackets denote concentrations [mol/cm³], xylan concentration is given in moles of potential xylose per liters of reaction, acid concentration is given in wt% of sulfuric acid, k_i [hr⁻¹] is the i^{th} reaction constant, $k_{o,i}$ [hr⁻¹] is the i^{th} pre-exponential factor, n_i [-] is the exponential factor for the i^{th} reaction, and Ea_i [kJ/mol] is the i^{th} activation energy. All variables and there descriptions are given in Table 2.2. A second approach taken for modeling xylan depolymerization is to assume that there are two types of xylan fractions in biomass. The first is a fast-depolymerizing fraction and the second is a slow depolymerizaing fraction. Both fractions have their own kinetic parameters:

$$\frac{d[Xylan]}{dt} = \frac{d[Xylan]_F}{dt} + \frac{d[Xylan]_S}{dt} = -k_{F,1}[Xylan]_F - k_{S,1}[Xylan]_S \quad (2.14)$$

$$\frac{d[Xylose]}{dt} = k_{F,1}[Xylan]_F + k_{S,1}[Xylan]_S - k_2[Xylose] \quad (2.15)$$

where:

$$k_{j,i} = k_{j,o,i}[Acid]^{n_{j,i}} \exp\left(\frac{Ea_{j,i}}{RT}\right) \quad (2.16)$$

In the equations above, the subscripts F and S designate the fast and slow reacting xylan fractions, respectively. Reaction parameters determined for a number

of different biomass species, using both approaches described above, are given in Table 2.4. These parameters generally differ within a fairly wide range. A study by Yat et al. presents parameters that vary with particle size, biomass species and even temperature [152]. This indicates that factors that have not been accounted for undoubtedly play an important role. Structural features of biomass undoubtedly play a role. Mass transfer limitations were shown to be present by Liu and Wyman [151] and could explain variations between the kinetic parameters of particles of different sizes [152]. Another source of variations could be the inconsistent effect of the substrates deconstruction on the pH of the solution, as it has been postulated for similar cellulose depolymerization kinetics [153]. Nevertheless, it is useful to use kinetic predictions to visualize variations of xylose yields as a function of time, temperature and acid concentration. Such predictions are given in Figure 2.9 using kinetic parameters presented by Esteghlalian et al. [154]. This data seems to indicate that short reaction times at high temperatures (close to 200°C) and high acid concentrations (above 1 wt%) show the most promise for maximizing hemicellulose yields.

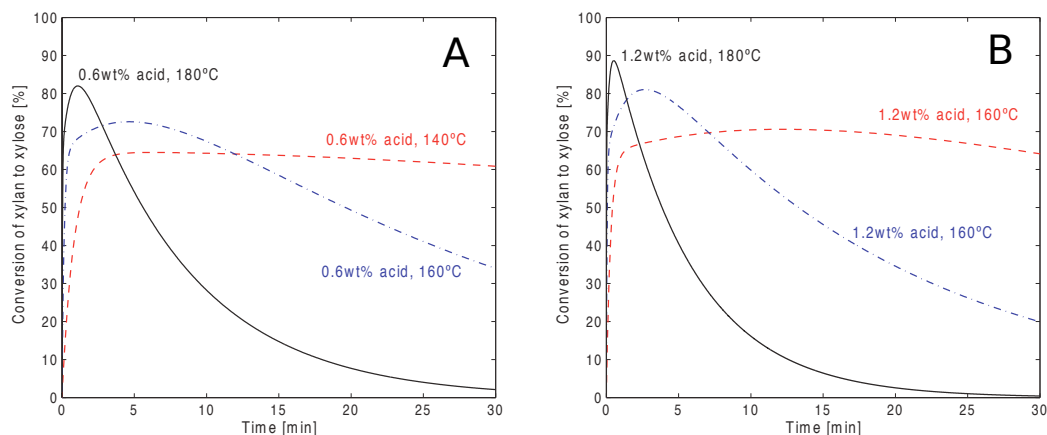
2.2.3 Base catalyzed hemicellulose depolymerization

In dilute sodium hydroxide solutions, hemicellulose can be extracted at room temperatures [160, 161]. Sills and Gossett, when pretreating switchgrass and mixed prairie biomass at room temperature with sodium hydroxide solutions, observed that though the xylan fraction in biomass decreased, the klason lignin fraction systematically decreased more [160]. By treating coastal bermuda grass at 121°C for residence times between 15 and 90 min with NaOH concentrations

Table 2.4: Kinetic parameters obtained in various studies for xylan depolymerization in acidic conditions. The top of the table lists parameters obtained by assuming a single depolymerizing xylan fraction. The lower part of the table lists parameters obtained by assuming a fast and a slow depolymerizing xylan fraction.

Biomass species	$k_{0,1}$ [min^{-1}]	n_1 [-]	E_{a1} [kJ/mol]	$k_{0,2}$ [min^{-1}]	n_2 [-]	E_{a2} [kJ/mol]	Source			
Wheat Straw	$2.25 \cdot 10^{20}$	1.55	167	$1.52 \cdot 10^{15}$	2	141	[155]			
Aspen	$1.53 \cdot 10^{11}$ - $2.65 \cdot 10^{17}$	1.75	97.18-151.85	$6.51 \cdot 10^{16}$	1	155.36	[156, 152]			
Balsam	$7.53 \cdot 10^4$ - $2.78 \cdot 10^{17}$	1.75	48.72-151.52	$7.59 \cdot 10^{15}$	0.9	147.56	[156, 152]			
Basswood	$4.46 \cdot 10^{11}$ - $2.63 \cdot 10^{20}$	1.75	102.67-179.13	$2.52 \cdot 10^{13}$	1.2	126.89	[156, 152]			
RedMaple	$5.77 \cdot 10^9$ - $1.40 \cdot 10^{17}$	1.75	88.65-149.45	$6.83 \cdot 10^{13}$	1	129.64	[156, 152]			
Switchgrass	$1.89 \cdot 10^7$ - $1.03 \cdot 10^{19}$	1.75	65.94-167.48	$3.73 \cdot 10^{17}$	1.4	165.59	[156, 152]			
Biomass species	$k_{f,0,1}$ [min^{-1}]	$n_{f,1}$ [-]	$E_{af,1}$ [kJ/mol]	$k_{s,0,1}$ [min^{-1}]	$n_{s,1}$ [-]	$E_{as,1}$ [kJ/mol]	$k_{0,2}$ [min^{-1}]	n_2 [-]	E_{a2} [kJ/mol]	Source
Beachwood pentosan	$2.56 \cdot 10^{15}$	1.15	129.2	$5.57 \cdot 10^{14}$	1.15	129.2	-	-	-	[157]
Switchgrass	$1.9 \cdot 10^{21}$	0.4	169	$4.2 \cdot 10^{23}$	2	210.7	$3.8 \cdot 10^{10}$	1.45	99.5	[154]
Poplar	$3.3 \cdot 10^{21}$	0.4	176.7	$3.3 \cdot 10^{22}$	1.5	192	$8.5 \cdot 10^{10}$	0.55	102	[154]
Corn Stover	$6.7 \cdot 10^{16}$	1.5	129.8	$6.9 \cdot 10^{19}$	1.6	167.6	$3.7 \cdot 10^{10}$	0.5	98.4	[154]
Paper Birch	$2.67 \cdot 10^{16}$	1	126.6	$1.6 \cdot 10^{19}$	1	156.5	-	-	-	[158]
Southern Red Oak	$1.04 \cdot 10^{14}$	1.54	120.1	$6 \cdot 10^{12}$	1.19	118	-	-	-	[159]

Corn stover



Poplar

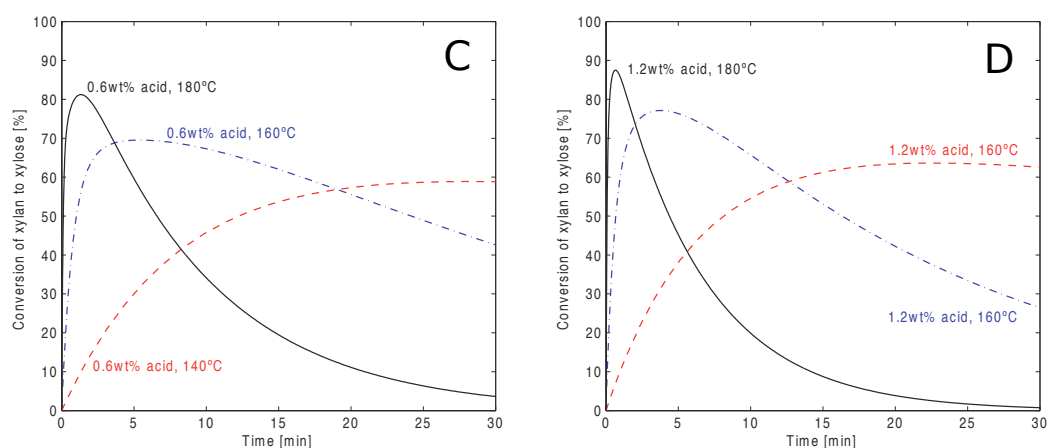


Fig. 2.9: Predicted xylose yield from xylan as a function of time for different temperatures and sulfuric acid concentrations (based on a model proposed by Esteghlalian et al. [154]). Figures A and B show results for corn stover in 0.6 and 1.2 wt% sulfuric acid solutions, respectively. Figures C and D show results for poplar in 0.6 and 1.2 wt% sulfuric acid solutions, respectively.

of 0.5 to 3 wt%, Wang et al. saw reduction in insoluble xylan contents of between 14 and 60% and klason lignin reductions between 12 and 86% [162]. Only one set of conditions led to a more important loss of xylan than klason lignin and these conditions corresponded to the least important losses for both fractions. Therefore, though it is likely that some hemicellulose depolymerization occurs, especially above 100°C, it seems that disrupting of lignin bonds is responsible

for at least some fraction of hemicellulose extraction.

2.2.4 Enzyme catalyzed hemicellulose depolymerization

When referring to enzymes that catalyze hemicellulose depolymerization, people often focus on xylanases, because xylan is usually hemicellulose's most prominent oligosaccharride. Xylanases represent the second largest group of glycoside hydrolases after cellulases, just as xylan is the second most prominent oligo-saccharride in nature after cellulose [70].

Given the similarities in substrates, xylanase and cellulases have many traits in common. They both are predominantly produced in bacteria and fungi, and can be excreted outside the cell-wall or be attached to the cell on a xylanosome (the xylanase equivalent of the cellulosome) [163]. Xylanolytic enzymes can be categorized as xylanase that break β -(1 \rightarrow 4)-linkages between xylose monomers, β -xylosidase which break xylobiose and other soluble xylo-oligomers [164]. Hemicellulose side chains are attacked by, among others, α -l-arabinofuranosidases, α -d-glucuronidases, acetyl xylan esterases, ferulic acid esterases and p-coumaric acid esterases [164]. These enzymes and the type of bond they attack are shown on Figure 2.10. Among xlanases, most are endoxy-lanases, meaning that they occur within a xylan chain. However, the discovery of a xylanase enzyme that only produced xylo-tetraose seemed to indicate an Exo-type mechanism similar to that of exocellulases [165]. However, the need for a complete absence of side-chains for such a mechanism to occur, suggests an alternate mechanism [164].

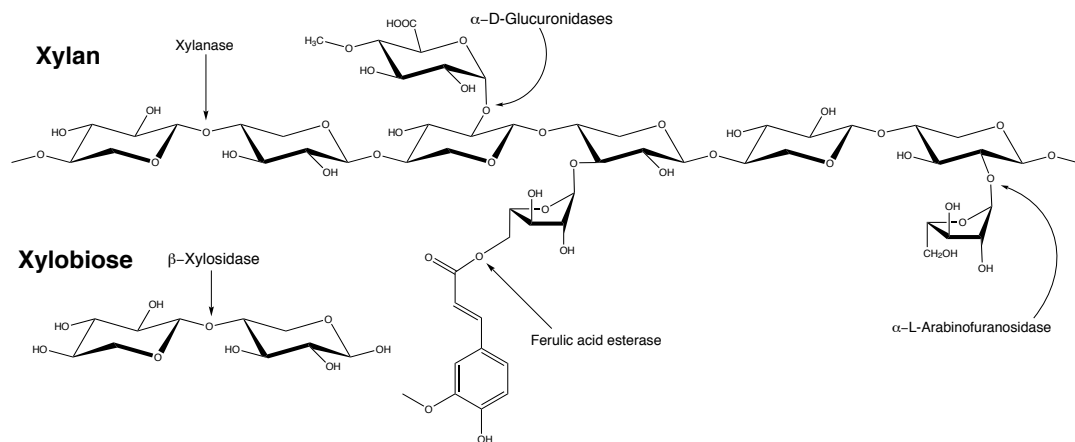


Fig. 2.10: Cellulolytic and hemicellulose side-chain attacking enzymes and their points of attack on hemicellulose (based on a representation proposed by [164]).

Similarly to cellulases, synergism seems to occur among hemicellulose cleaving enzymes. Mainly, side chain attacking enzymes improve the activity of xylanases and vice-versa [163, 164, 166, 167]. Notably, synergy between endo-xylanase and α -d-glucuronidase, between endoxylanase and arabinoxylan arabino-furanohydrolase and between endoxylanase and feruloyl esterase [167]. Furthermore, β -xylosidase enzymes show synergism with endoxylanases, similar to the synergistic behavior of β -glucosidase and cellulases [168].

Because of their ability to degrade hemicellulose, these enzymes have been applied in the pulp and paper and food industries [163, 164]. Due to the growing interest in biofuels, applications in biomass depolymerization processes may be foreseeable. Some have demonstrated that these enzymes can supplement other enzyme mixtures in order to increase xylose and other hemicellulose sugar recovery and, simultaneously, facilitate the access to cellulose by cellulases [169, 170, 171, 172, 173, 174, 175]. Indeed, xylanase supplementation has improved both glucose and xylose recovery. The most commonly used en-

zyme mixture is Genencor Inc.'s Multifect®xylanase. The timescale of xylan and other hemicellulose sugars hydrolysis by enzymes remains on the order of hours to days (similar to cellulose depolymerization by enzymes) and therefore, remains much slower than thermochemical depolymerization.

2.3 Lignin

Lignin is a complex heteropolymer that is much more complex than hemicellulose. Three phenolic subunits are the structural building blocks of all lignins: coumaryl alcohol, coniferyl alcohol and sinapyl alcohol (all three are shown in Figure 2.11). However, its repeating monomer is much more complex. A famous example is given by Nimz when he proposed a structure for beech lignin [176].

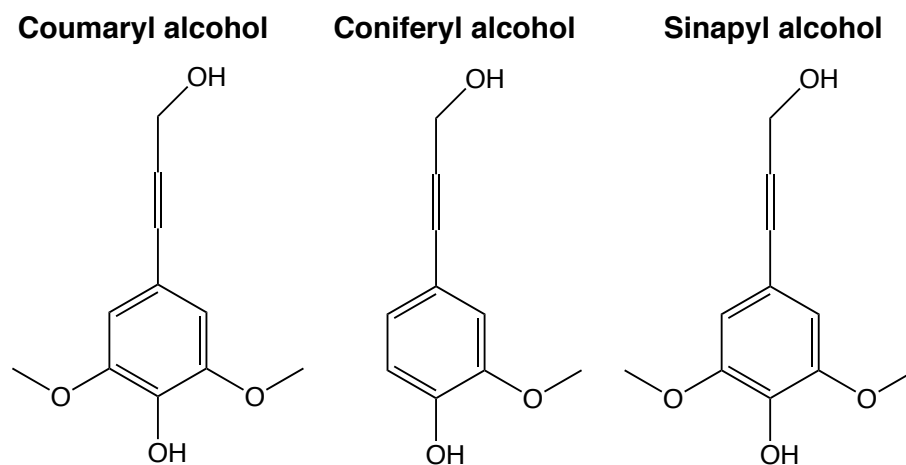


Fig. 2.11: The three basic molecular subunits of lignin.

Referring to the complex array of molecules that form lignin as a single entity can suggest that the chemical behavior of this polymer is somewhat uniform. However, this is not the case. Different chemical bonds will behave differently

in different environments, which complicates lignin characterization and understanding. The isolation of lignin, similarly to the isolation of hemicellulose, can never be achieved without altering its structure. Many studies have suggested that, once solubilized through chemical treatment, lignin rapidly re-condenses [177, 178, 31]. Bobleter and Sannigrahi et al. even found an increase in cross-linking during this re-condensation process [177, 31]. Furthermore, differentiating hemicellulose and lignin can often be complicated. Indeed, they are often extracted simultaneously in acidic and hydrothermal processes [151, 179]. In addition, hemicellulose degradation products have been known to form insoluble condensation products that are often mistaken for lignin during the Klason lignin analysis¹ [140].

Since lignin is not a polysaccharide polymer, the recovery of its constitutive molecules for use as starting products for other processes is not addressed here. Nevertheless, a number of researchers have suggested possible processes to extract valuable chemicals from lignin [180, 181, 182, 183, 184, 185]. However, since it is structurally intertwined with cellulose and hemicellulose in lignocellulosic biomass, its deconstruction can heavily affect the depolymerization of its neighboring polysaccharides. Therefore, it is worth understanding lignin's fate in environments used to depolymerize cellulose and hemicellulose.

¹A description of the Klason lignin analysis can be found in the analytical procedure by Sluiter et al. [58].

2.3.1 Lignin deconstruction in pure water

The lignin fraction of lignocellulosic biomass can be partially extracted with hot water, even at temperatures below 200°C. By flowing water through corn stover, Liu and Wyman were able to remove 30% of Klason lignin at 180°C, 65% at 200°C and 75% at 220°C. In the absence of flow-through, lignin removal was reduced to 30% or less in all cases, suggesting possible lignin re-condensation. In the high-flow-through experiments, there is an excellent correlation between xylan and Klason lignin removal. Therefore, it is unclear whether lignin bonds are actually being broken or if lignin removal is just occurring due to it being cross-linked with xylan, which is known to depolymerize at these conditions. Masselter et al. did a similar flow-through experiment with water at 200°C and detected a number of lignin degradation compounds [186], which indicates that limited lignin degradation does indeed occur at those temperatures. These compounds, along with those identified after water or steam pretreatment by two other studies are listed in Table 2.5. They are almost all phenolic derivatives.

Lignin's reactivity at higher temperatures has been explored mainly in the interest of biomass gasification [189, 190]. Waldner and Vogel proposed a simplified reaction network for lignin and its interaction with other degrading lignocellulosic molecules in water close to its critical point (300-400°C), which is given in Figure 2.12 [190]. They also observed that the addition of a Raney-Nickel catalyst heavily favored the production of small organic molecules and, eventually, gases, avoiding tar and coke formation.

Experiments with lignin isolated using concentrated acid (or Willstätter lignin) demonstrated that extracted lignin was much more stable than native lignin [31]. Indeed, no more than 70% of lignin can be extracted below 270°C.

Table 2.5: Lignin degradation products in hydrothermal media

Degradation product	Source
1-(4-hydroxyphenyl)propan-1-one	[186]
Syringaldehyde	[186, 187, 188]
Vanillin	[186, 188]
Ferulic acid	[186]
Syringic acid	[186, 187, 188]
Vanillic acid	[186, 187, 188]
Vanillyl alcohol	[188]
4-hydroxybenzoic acid	[186, 187, 188]
3-hydroxybenzoic acid	[187]
Furan-2-carboxylic acid	[186]
Coniferylalcohol	[187]
3,5-Dimethoxy-4-hydroxycinnamyl alcohol	[187]
4-hydroxybenzaldehyde	[187, 188]
Cinnamic acid	[187]
Cinnamaldehyde	[187]
1,2-Dimethoxybenzene	[188]

Furthermore, Bobleter observed that after the initial degradation, the amount of soluble lignin products would drop from as high as 90% to 60-70%, presumably due to re-condensation [31].

2.3.2 Acid catalyzed lignin deconstruction

According to the Klason lignin analysis, treating wood with a strong concentrated acid (such as H₂SO₄) removes all carbohydrates, leaving lignin and ash

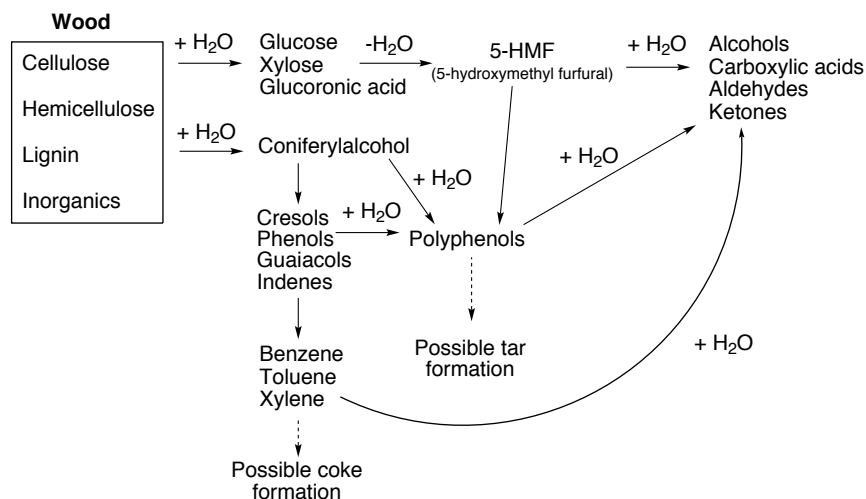


Fig. 2.12: A simplified reaction network for lignin in water close to the critical point [190].

[58]. However, at higher temperatures, lignin can be completely solubilized in a refluxing 10:1 mixture of dioxane-water containing 0.2 M HCl in a process known as “acidolysis” [191]. The products are an oily substance and high molecular weight compounds soluble in the ether solution. Presumably, solubilization in the ether avoids re-condensation of the lignin on the biomass. It was found that this treatment cleaved mostly β -ether linkages [191]. Vazquez et al. found that they could delignify pine wood using refluxing concentrated acetic acid and some hydrochloric acid [192]. However, they observed rapid re-condensation of lignin on the biomass surface.

At temperatures between 160 and 220°C, Yang and Wyman showed that with 0.1 wt% sulfuric acid solutions they could remove almost 90% of the lignin from corn stover in a flow-through system. In the absence of flow-through (i.e. batch experiments), at the same conditions, lignin removal was limited to 30 %. Once again, this phenomenon is thought to occur because of lignin re-condensation. Lignin forms insoluble products that can precipitate on the biomass when left in the reactor. This phenomenon was further documented by

Selig et al. who observed the formation of lignin droplets on the surface of pre-treated biomass and filter paper in the presence of dissolved lignin above 130 °C [178]. These results were obtained both in neutral and acidic conditions.

2.3.3 Base catalyzed lignin deconstruction

Alkali compounds prove to be excellent catalysts for lignin degradation. Both α -ether and β -ether bonds are readily cleaved in strongly basic environments [191]. For this reason the SODA and Kraft delignification processes are widely used in the paper industries to produce a lignin free pulp. Both processes use sodium hydroxide as a catalyst for lignin removal [193, 194, 195]. In addition, the Kraft pulping uses sulfates that readily bind to lignin fragments and, thus, further favor delignification [193].

In the context of lignocellulosic biomass depolymerization for sugar production, delignification reactions have proven to be successful in increasing cellulose and hemicellulose depolymerization by enzymes and microorganisms. Therefore, lignin depolymerization must contribute to increasing the available surface area to depolymerizing enzymes (see Section 2.4.1). Pavlostathis and Gossett showed that biodegradability of wheat straw could be greatly enhanced with room temperature treatment with a solution of up to 50 gr/L of NaOH Sodium hydroxide pretreatment and enzymatic hydrolysis of coastal [196, 197]. They observed that biomass “consumed” some of the sodium hydroxide. This was probably due to the liberation of organic acids by biomass, leading to a partial neutralization of sodium hydroxide. In addition, they observed that the ma-

jority of the dissolved organic carbon was in the form of aromatic compounds, which were undoubtedly by-products of lignin degradation [196].

Several studies have successfully used sodium hydroxide solutions from room temperature up to 121°C to enhance cellulose and hemicellulose depolymerization by enzymes [160, 162, 161]. With a 2% NaOH solution Xu et al. observed a Klason lignin reduction in Switchgrass of about 60 to 80% for temperatures of 20 and 121°C, respectively [161]. Wang et al. pretreated coastal bermuda grass at 121°C with varying concentrations of NaOH [162]. They observed that up to 85% of Klason lignin could be removed from the solid residue. This result was accompanied by the most important reduction in xylan content (about 61%) of all their experiments. Kim and Holzapple used lime at room temperature or slightly above (55°C) to enhance the enzymatic digestion of corn stover [198, 199, 200]. Up to 75% of the lignin was removed at 55°C [200]. Dale's research group from Michigan State University has done multiple studies on using ammonia and water mixtures to enhance digestibility of various lignocellulosic feedstocks [201, 202, 203, 204]. They attribute the increases in digestibility to a decrease in cellulose crystallinity, and breakage of the ester linkages between lignin and hemicellulose [202].

2.3.4 Biological lignin deconstruction

In nature, some organisms such as bacteria and fungi are able to degrade lignin [205, 206]. These enzymes allow the organism to gain access to cellulose or hemicellulose but also to metabolize lignin. However, no organism has been

shown to grow with lignin as its sole carbon/energy source [206]. Lignin degrading enzymes are an array of oxidoreductase enzymes that include:laccases, oxidases and peroxidases facilitated by organic acid and hydrogen peroxide producing catalases [207, 205]. The most successful lignin degrading organisms are fungi known as white rot fungi. It produces three well characterized groups of iso-enzymes: lignin peroxidase, manganese peroxidase and laccases [205]. The two former enzymes use hydrogen peroxide as an oxidant while the later uses molecular oxygen as the oxidant. All of these enzymes catalyze a free radical mediated oxidation of lignin bonds. Most enzymes are excreted but some enzymes have been shown to be cell bound [206].

Lee et al. showed that by pretreating Japanese red pine with different white rot fungi they could remove 14.5% of the lignin but also 7.8% of the holocellulose (cellulose and hemicellulose) fraction [208]. This lead to increased digestibilities by commercial cellulase mixtures. However, these increased digestibilities (from 14% to a maximum of 20%) were very small compared to the increase in digestibilities that occur with thermo-chemical pretreatment (see Section 2.4). Ray et al. exposed pine sapwood to white rot fungus *Coniophora puteana* for 20 days and saw glucose yields of around 70%. Another possibility that has yet to be explored is the supplementation of commercial enzyme mixtures with lignin degrading enzymes.

2.4 Pretreatment and Enzymatic Saccharrification

Lignocellulosic depolymerization in various environments using different catalysts provides multiple avenues for monosaccharide production. However, some technologies are closer to their desired industrial application. Dilute and concentrated acid technologies have been implemented at industrial or pilot-plant scales at various periods [31, 57]. However, important by-product formation and the important environmental and economic burden of the required acidifying and neutralizing agents have led most to turn away from such processes. Both pure water and acidic systems seem to offer interesting opportunities where high cellulose to glucose yields can be reached at high temperatures and short residence times. However, the absence of reliable technologies or even experimental setups to successfully reach such conditions makes this process far from commercial development. This has led to pretreatment and enzymatic hydrolysis as being the main focus of research of monosaccharide production from plants [30].

The use of enzymes mixtures can successfully produce quasi-complete cellulose and hemicellulose conversion to monosaccharides, but only under the right conditions. Indeed, as discussed for cellulases, the issue of accessibility is critical. The available surface area to the enzymes, which increases tremendously with an initial thermochemical (or “pretreatment”) step, has been shown to dictate the initial rate of hydrolysis[118].

2.4.1 Biomass pretreatment provides accessibility for cellulases

Heterogeneous catalysis research has shown that, in the case of a reactant diffusing to a heterogeneous catalyst's surface, the pore size distribution was a key factor in mass transfer limited systems [209]. Indeed, surface area is a key factor in designing a catalyst and is heavily influenced by the pore size distribution. In addition, diffusion of a particle into a pore is influenced by the pore size even if this pore is considerably larger than the particle. This leads heterogeneous catalysts to be frequently designed with a bimodal pore distribution comprising very small and very large pores, favoring both surface area and diffusion [209]. Enzymatic hydrolysis of cellulose is essentially a reverse heterogeneous catalysis system, where the enzyme (catalyst) has to diffuse to the surface of the heterogeneous cellulose (substrate) and, therefore, the same considerations apply.

To obtain near complete cellulose depolymerization by cellulases, a thermochemical pretreatment step must be applied to lignocellulosic biomass. In fact, the effect of available surface area on enzymatic hydrolysis of cellulose has been well documented, while the effect of the pore size distribution on diffusion remains to be explored. Indeed, Grethlein demonstrated that the key feature of the pretreatment step's effect on enzymatic hydrolysis was the increase of the available surface area to the enzymes [118]. Grethlein measured the pore size distribution of biomass using solute exclusion chromatography, which allows the samples to remain in water during the analysis and hence avoid pore collapse [118, 210]. He then showed that the surface area available to cellulases correlated perfectly with the initial rate of hydrolysis (his results are shown in Figure 2.13).

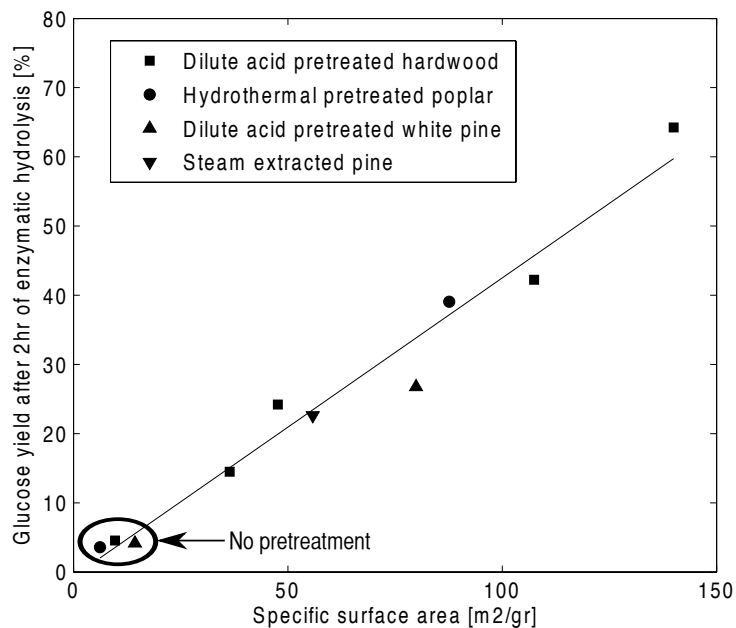


Fig. 2.13: Relationship between initial rates of cellulose hydrolysis and available surface area to cellulases (particles with a size of 510 nm) on pretreated and non-pretreated lignocellulosic biomass (based on results obtained by Grethlein [118]).

In addition, the final conversion of structural carbohydrate to monomers also increases tremendously with pretreatment, making this step unavoidable in enzymatic depolymerization processes [211, 212]. This dependence on pretreatment is probably also due to accessibility. Unconvertible structural carbohydrate are probably completely inaccessible to enzymes even during and after hydrolysis due to other plant constituents recalcitrant to deconstruction (lignin etc.). Therefore, this fraction of inaccessible polysaccharides seems to be heavily dependent on the quality of pretreatment step. The effect of the pretreatment step is illustrated schematically in Figure 2.14. This figure illustrates pretreatment's effect on lignin and hemicellulose fragments that are intertwined with crystalline cellulose fibers. The rupture of these fragments by a pretreatment step opens up the plant constituents' structure, increasing the internal surface area.

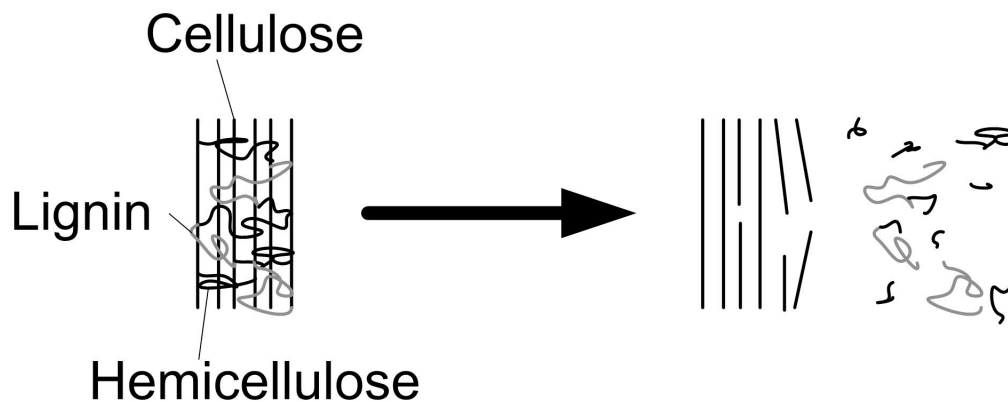


Fig. 2.14: Diagram of pretreatment's effect on biomass (based on a diagram created by [213]).

As discussed above, accessibility has been demonstrated to be a key factor controlling biomass depolymerization. This has been demonstrated by Grethlein and confirmed more recently by Jeoh et al. and Rollin et al. [214, 115, 118]. Grethlein and others have used accessibility in empirical correlations used for predicting rates and extent of cellulose conversion [118, 120]. Levine et al. have attempted to capture changes in reactive surface area during enzymatic hydrolysis through changes in particle morphology [132, 133]. However, despite the proven importance of accessibility and the many efforts to model enzymatic hydrolysis (see Section 2.1.4), the effect of pore size distribution on initial hydrolysis rates observed by Grethlein (see Figure 2.13) has not been successfully explained through a theoretical approach.

2.4.2 Challenges facing current pretreatment technologies

Despite its advantages, the pretreatment and enzymatic hydrolysis process has several limitations that researchers are still trying to address. These issues can be regrouped into the following four categories:

Yield. Biomass structural carbohydrates must be nearly completely converted to monosacharrides in order to minimize process and starting material costs. Indeed, a low yield will require that important amounts of materials are processed to obtain a certain amount of product. This leads to increased equipment sizes and inputs of biomass feedstock, which negatively affect process costs and life cycle environmental performance [215, 216].

Pretreatment byproducts. As was discussed earlier, the high temperatures and acid or alkaline environments associated with a thermochemical step can lead to a byproduct formation. It is straightforward to see that these by-products, if produced from monosaccharrides, limit the obtainable yield. In addition, they can also be detrimental to the rest of the process and hinder enzymatic hydrolysis, poison a catalyst and inhibit fermentation. Furfural, 5-HMF, acetic acid, formic acid, and levulinic acid, in particular, are well documented fermentation inhibitors [217, 218, 219].

Fuel/energy and catalyst usage. The thermochemical pretreatment step uses a chemical catalyst and, generally, fairly extreme temperatures (and sometimes pressures), which require some sort of fuel or electrical input. Chemical inputs can have important embedded life cycle environmental burdens and associated costs. In addition, these chemicals typically lead to a removal, neutralization and/or detoxification step downstream of pretreatment. In summary, chemical catalysts could prove to be a key factor in the overall environmental performance of the process life cycle [216]. Enzyme requirements during the hydrolysis step also have non-negligible effects on the overall environmental performance of the process [220]. Furthermore, enzymes were systematically a key economic concern for ligno-

cellulosic ethanol production. In fact, the US Department of Energy has financed several import enzyme cost-cutting programs to improve biofuel technology prospects [84]. The fuel needed to meet process energy requirements can often be produced from the unconverted biomass or by burning part of the fuel that was produced (lowering the final product yield) [221, 222]. However, another option is to convert the unconverted biomass to electricity or gaseous fuels and generate co-products [57]. In this case, lowering process energy requirements can improve co-product production.

Solid content. Recent process design and life cycle assessment studies in our group have shown that solid content is a key design parameter in the biomass to ethanol conversion process [216]. A similar correlation between solid content and process economics has been shown by Wingren et al. [223]. Indeed, solid content will determine total reacting volume and final product concentration and hence capital, operating and energetic costs. Most importantly, since ethanol must be separated from water for use as a fuel (typically through distillation) separation costs increase exponentially with decreasing final ethanol concentrations, which depend on solid content [224]. Commercial starch-based ethanol conversion processes are commonly run with solid contents close to 30 wt% where final ethanol contents of 16-17 v/v % are reached [225]. If similar yields are expected for lignocellulosic biomass technologies, solid contents around 40 wt% will have to be used throughout the process. Indeed, using a typical lignocellulosic feedstock, and assuming that roughly 90% of all structural carbohydrates can be converted to monomers, about 60 gr of sugars can be extracted from 100 gr of biomass. Assuming a yield of 0.5 wt/wt of

ethanol from these sugars, a 15 wt% ethanol (19 v/v%) solution would require an initial biomass mixture of 44 wt% solids. Similarly, a 30 wt% starting solution would lead to an 8 wt% ethanol solution (10 v/v %) and a 20 wt% solution would lead to a 4.6 wt% ethanol solution (5.8 v/v %).

2.4.3 Leading pretreatment technologies

As it will be discussed, depending on pretreatment and hydrolysis conditions, many different yields can be achieved and different amounts of byproducts are produced. This often leads to trade-offs amongst different processes. Different pretreatment technologies use more or less chemical catalyst. The trade-off between pretreatment usage and enzyme loading has not been studied in a systematic way. However, most pretreatment are run with a given activity of enzyme, which, with variations in enzyme mixtures, can be achieved independently of a certain amount of protein [226, 212]. Solid contents (i.e. for the biomass water mixture) up to 62.5% can be used in pretreatment [204]. However, most enzymatic hydrolysis experiments were performed with washed solids and a solid content below 5 wt% [226, 212]. This is an effective way of determining pretreatment efficacy, but it overlooks a number of issues that influence enzymatic hydrolysis of an unwashed high solids mixture. Above 15 wt% solids the initial viscosity of the solution is extremely high and, starting at 20 wt% solids, no free water is observed. This leads to mixing and mass transfer limitations. In addition, enzymatic activity is progressively dampened by product inhibition [227] and other inhibitors such as lignin [228] or pretreatment degradation products [229].

In summary, many different approaches exist. Thanks to a consortium of researchers (Consortium for Applied Fundamentals and Innovation: CAFI), experiments with various pretreatment technologies have been performed with the same biomass feedstock, systematic enzyme loadings and hydrolysis conditions [213, 211, 102, 230, 231, 212]. Though experiments were performed in a systematic way, analyses of environmental and economic trade-offs have not been systematically explored between these technologies. In fact, of the four issue categories listed above, only the effect of these technologies on yield was thoroughly explored. Nevertheless, the technologies that they have explored are often presented as the leading pretreatment technologies. Therefore, they are presented and discussed below. So far the results for two biomass species, corn stover and poplar, have been published. As the results will show, these two feedstocks represent two extremes of ease of depolymerization. Indeed, corn stover has proven to be fairly easy to depolymerize and usually requires milder pretreatment conditions, while poplar is just the opposite. The glucose and xylose yields are presented with pretreatment process conditions for each relevant technology in Tables 2.6 (corn stover) and 2.7 (poplar).

Hot water pretreatment

Pure water as been known to offer an interesting medium for pretreatment. It's main advantage is that it does not require any chemicals to run and very few, if any, for neutralization and buffering of the enzymatic reaction. However, even when using pure water, the reaction mixture does not remain neutral. Pretreated biomass releases organic acids, which usually lowers the pH to the point where some refer to this process as auto-hydrolysis (where biomass

itself provides its hydrolysis catalysts) [147, 145, 146, 237, 149, 238, 239]. These acids are liberated in steam and liquid hot water pretreatments and so they fall in the same category. Liquid hot water pretreatment was notably used to pretreat poplar, corn stover and dry distillers grain as part of the CAFE studies [234, 240, 241, 242, 232]. Impressive glucose and xylose yields of 89 and 82% were obtained for corn stover, respectively, but these yields were lower for poplar (50 and 67%) [234, 232]. In both cases solid loadings of 15 and 16% were used. Liu and Wyman used a water flow-through system to pretreat corn stover [137, 243]. The rapid removal of soluble oligosaccharides in this system led to virtually no degradation and, thus, impressive yields of 90% for glucose and 98% for xylose. However, this system requires high flow rates and therefore dilute hemicellulose and cellulose fractions. No study was performed for poplar.

Another process involving pure water as a pretreatment medium is steam explosion. This process involves using steam close to the condensation pressure at similar temperature to those used in liquid water pretreatment. The reaction is rapidly heated and pressurized by injecting steam in the reactor and explosively depressurized at the end of the process. CAFE researchers have used steam explosion to pretreat corn stover and obtained impressive yields of 98% for xylose and 100% for glucose [174]. However, a personal communication with Bura revealed that the solid content was only between 3 and 15 wt%. It could be that rapid pressurization and depressurization enhances enzymatic hydrolysis rates and extent because of mechanical disruptions caused to the substrate. Nevertheless, Bura communicated that this same technology did not work well with poplar and that SO₂ addition was required to obtain high yields (see dilute acid section). Interestingly, steam exploded wheat straw at higher

solid contents (195°C, 6 min, 23-28 wt% solids) gave slightly lower, but similar yields (90% glucose yield) [244].

Dilute acid pretreatment

CAFI researchers have used dilute sulfuric acid to pretreat corn stover and poplar [226, 212]. Lloyd and Wyman [226] obtained glucose and xylose yields of 92 and 94%, respectively. A pilot scale reactor led to glucose and xylose yields close to 70% using a solid content 20 wt% [245]. However, as it is often the case with dilute acid technologies, important amounts of degradation products are produced. Up to 30% furfural yields were obtained during their runs and only one run led to yields below 10%. Dilute acid pretreatment of poplar (2 wt% H₂O₄, 190°C for 1.1 min) led to glucose and xylose yields of 85 and 65%, respectively [212]. A study reporting similar yield in the same pilot reactor used a solid content of 15 wt% [246]. Liu and Wyman used a dilute acid flow-through system to treat corn stover [151]. Once again, the rapid removal of soluble oligosaccharides in this system led to little degradation and close to 100% of xylose/xylo-oligomer recovery. However, this system requires high flow rates and therefore dilute hemicellulose and cellulose fractions. No study was performed for poplar.

Sulfur dioxide catalyzed steam explosion was also explored by CAFI researchers [174, 175]. Poplar pretreated with catalyzed steam explosion (3 wt% SO₂, 200°C, 5 min, from a personal communication with Bura: 8-15% solid content), can reach glucose yields of 93% and xylose yields of 97% [174]. Given these high yields important amounts of degradation products are unlikely to have been produced. However, SO₂ catalyzed steam explosion retains the other

disadvantages of dilute acid pretreatments such as the important amount of required chemical catalyst and a required neutralization/detoxification step.

Ammonia catalyzed pretreatment

The most well known of ammonia catalyzed pretreatments is known as ammonia fiber explosion (AFEX). This process involves treating biomass with a mixture of water and a very important fraction of ammonia (often an equal amount of biomass and ammonia) at high temperatures (90-180 °C) and important pressures (700 psi) [201, 202, 247, 203, 173, 204, 169]. AFEX pretreatment gave glucose yields of and 82% for corn stover (90°C, 5 min, 62.5% solids) [204]. Ammonia fiber explosion's main advantages are its high-solid content (30 to 62.5 wt% depending on the feedstock) and, for processes run close to 100°C, its low amount of produced byproducts. However, the amount of ammonia required is an important drawback. Even in the case where 99% of ammonia is recycled, 1 kg of ammonia must be added for every 100 kg of biomass. Glucose and xylose yields of 93% and 76% were obtained for switchgrass (with a temperature of 120°C, a 5 min residence time and a 20 wt% solid content), demonstrating AFEX's ability to successfully pretreat herbaceous crops, albeit at slightly higher temperatures and lower solid contents [201]. However, woody biomass, such as poplar, has proven harder to degrade than the aforementioned species. Using standard enzyme loadings, 48% glucose yields and only 27% xylose yields are obtainable, despite pretreatment temperatures of 180°C (5 min residence time and a 30 wt% solids loading) [202].

A system where high-temperature (170-185°C) ammonia-water mixtures (15-20 wt% ammonia solutions) are flowed through a packed bed of biomass has

also been explored [235, 233]. Glucose yields of 90 and 73% and xylose yields of 78 and 70% can be reached for corn stover and poplar, respectively. However, like all flow-through processes, ammonia recycle percolation will undoubtedly suffer from dilution issues if adapted to industrial scales.

Lime catalyzed pretreatment

High-solid lime (calcium hydroxide, 8gr solids added per 100 gr biomass) and water mixtures have been used to pretreat corn stover at low temperatures (55 °C) [248, 198, 200]. However, this pretreatment was extremely slow and a residence time of 4 weeks was used to obtain glucose yields of 90% and xylose yields of 98%. The mild temperatures and atmospheric temperatures make this long residence within reason for practical purposes. However, as with all chemically catalyzed processes, lime pretreatment requires important chemical inputs and a neutralization step prior to enzymatic hydrolysis. Interestingly, much more extreme conditions (160°C, 2hr residence time and 40 gr of calcium hydroxide per 100 gr biomass) were used for poplar pretreatment to obtain glucose and xylose yields of 92 and 66%. This illustrates a common issue with alkaline pretreatments. Indeed, they often have problems successfully pretreating woody feedstocks.

Other pretreatment technologies

Other technologies besides those presented by the CAFI consortium are also promising. Sodium hydroxide pretreatment at room temperatures can lead to glucose and xylose yields above 70-90% for herbaceous crops, while producing

virtually no degradation products [160, 162]. Of course, the issue of catalyst inputs and chemical neutralization may hinder this process's development. However, the absence of any degradation means that solid washing followed by pretreatment medium recycling can be used to alleviate these problems [196, 197].

Kim and Hong used pure CO₂ and CO₂-H₂O mixtures to pretreat lignocellulosic biomass and obtained yields close to 80% for aspen wood with solid contents around 40wt% [249]. In addition, several studies [250, 48] used a water-rich liquid phase, containing dissolved CO₂, to pretreat corn stover and aspen wood between 180 and 220°C. They suggest that this environment may be more advantageous than pure water for pretreatment especially with respect to the production of furfural. These different results suggest that CO₂-H₂O mixtures may be interesting media for pretreatment and that more research is needed on this subject.

Zhang et al. used concentrated phosphoric acid at low temperatures (about 50 °C) to pretreat biomass with 97% glucose yields obtained for corn stover, switchgrass and poplar [59]. The drawback of such a process is of course the important costs and/or the recovery of the chemical catalysts. More recently, ionic liquids have been used to very effectively pretreat lignocellulosic biomass [251, 252, 253, 254]. Ionic liquid's main issue is the important cost associated with its production. However, these technologies are still in the early phases of development and more research is needed. Mainly for this reason, the ionic liquid environment and its effect on biomass was not discussed in this review.

2.4.4 Conclusions

Biomass pretreatment followed by enzymatic hydrolysis can effectively and, in some cases, almost completely convert biomass to monosaccharides. However, this is often done at the cost of high chemical or enzymatic catalyst usage, low solid content or long residence times (especially compared to direct thermochemical conversion). Issues that must be improved in concert for a technology to become profitable and sustainable, are yield, by-product formation, energy/fuel and chemical usage and solid content. So far, leading technologies have often addressed one or more of these issues but not all of them.

Table 2.6: Parameters and monosaccharide yields for leading **Corn stover** pretreatment technologies

Pretreatment method	Chemical addition (wt ratio to dry biomass) [%]	Temperature [°C]	Nominal pretreatment time [min]	Pressure [bar]	Solids loading [wt% of total mixture]	Cellulose loading [FPU/gr cellulose]	Xylanase loading [mg protein/gr cellulose]	Maximum xylose yield [%]	Maximum glucose yield [%]	Source
Dilute acid	1.96% H ₂ SO ₄	160	20	7 ^a	25	15	0	94	92	[226]
Steam explosion	–	190	5	12.6	8–15 ^b	10	6	98	100	[174]
Catalyzed steam explosion	3% SO ₂	190	5	12.6	8–15 ^b	10	6	64	100	[174]
Hot water	–	190	15	>13 ^a	16	15	0	82	89	[232]
AFEX	100 % NH ₃ (99% rec.)	90	5	15	62.5 ^c	15/60	0	55/69	81/90	[204]
Ammonia flow-through	20% NH ₃	170	10	25	<10 ^d	15	0	78	90	[233]
Lime	8% CaO	55	4 weeks	atm	5-20	15	0	76	93	[200, 102]
Flow-through hot water	–	200	24	>16 ^a	<10 ^d	15	0	98	90	[211]

^aEstimated from boiling pressure

^bSource: personal communication with Bura

^cDoes not include ammonia

^dAssumed to be low due to flow-through

Table 2.7: Parameters and monosaccharide yields for leading Poplar (hardwood) pretreatment technologies

Pretreatment method	Chemical addition (wt ratio to dry biomass) [%]	Temperature [°C]	Nominal pretreatment time [min]	Pressure [bar]	Solids loading [wt% of total mixture]	Cellulase loading [FPU/gr cellulose]	Xylanase loading [mg protein/gr cellulose]	Maximum xylose yield [%]	Maximum glucose yield [%]	Source
Dilute acid	2% H ₂ SO ₄	190	1.1	>13 ^a	N/A	15	0	65	85	[212]
Catalyzed steam explosion	3% SO ₂	190	5	12.6	8-15 ^b	10	6	97	93	[174]
Hot water	–	200	10	>16 ^a	15	15	0	67	50	[234]
AFEX	100% NH ₃ (99% rec.)	180	5	47	30 ^c	15	0	27 ^e	48 ^e	[202]
Ammonia flow-through	15% NH ₃	185	27.5	20-28	<10 ^d	15	31.5	70	73	[235]
Lime	40% CaO	160	120	15	6	15	0	66	92	[236]

^aEstimated from boiling pressure

^bSource: personal communication with Bura

^cDoes not include ammonia

^dAssumed to be low due to flow-through

^e168 hr of hydrolysis instead of 72 hr

CHAPTER 3

OBJECTIVES

As discussed in the two previous chapters, the focus of the work presented in this thesis is to develop new strategies for improving biomass depolymerization. An overview of the current state of biomass depolymerization research in Chapter 2 demonstrated that two important challenges for this area are: (1) improving the sustainability and economic feasibility of biomass pretreatment and enzymatic hydrolysis and (2) helping guide these improvements by using a theoretical framework rather than random optimization. These two important challenges form the basis for the two overarching objectives of the work presented in this thesis, which are presented below.

3.1 Objective 1: Sustainably and economically producing concentrated solutions of monosaccharides from biomass

In Chapter 2, four major hurdles for pretreatment development were identified and discussed: (1) eliminating or reducing chemical usage, (2) increasing solid content throughout the process, (3) successfully treating different species of biomass and their mixtures and (4) maximizing monosaccharide yield while limiting byproduct formation. Biphasic CO₂-H₂O mixtures at high pressures used as pretreatment media can help overcome some of these hurdles with CO₂ acting as an easily separable green co-solvent and weak acid catalyst. If CO₂ acts as a weak acid catalyst, it could be an interesting substitute for acids that are used in a number of pretreatment processes. Using CO₂ as an easily separable co-solvent could help reduce water usage (i.e. increase solid content).

In combination with the use of biphasic CO₂-H₂O mixtures, exploring various pretreatment temperatures and residence times could help design a process that can successfully pretreat multiple biomass species and their mixtures while maximizing sugar yields and minimizing the formation of unwanted byproducts.

In **Chapter 4**, a study is described that used a 25 ml unstirred reactor for rapidly testing multiple biphasic CO₂-H₂O pretreatment temperatures and residence times on multiple biomass species. Switchgrass, corn stover, big bluestem and mixed perennial grasses (a co-culture of big bluestem and switchgrass) were pretreated at 40 wt% solids. Operating temperatures ranged from 150°C to 250°C, and residence times from 20 s to 60 min. However, these experiments were run with small biomass particles (< 1 mm, too small to be industrially relevant) and without any mixing (which could lead to temperature gradients. Therefore, in **Chapter 5** a 1 L stirred reactor is used to test the effect of using larger (< 0.95 cm) particles and the effect of mixing.

In the same chapter, results from testing two-temperature stage pretreatment are presented. This study attempts to increase glucose and hemicellulose sugar yields while maintaining or lowering byproduct formation. Indeed, given the typical reaction chemistry of biomass in acidic or neutral media, it may be advantageous to use a range of pretreatment temperatures. As was shown in Chapter 2, short high-temperature stages might be advantageous for depolymerizing cellulose and hemicellulose without producing excessive amounts of byproducts. Hemicellulose depolymerization produces oligomers that depolymerize to monomers that can degrade to unwanted byproducts such as furfural. The sequential nature of this reaction network entails that furfural production lags behind that of oligo- and monosaccharides. Thus, it may be advantageous

to use a high pretreatment temperature for a short period during this initial lag in degradation product formation, and then pursue pretreatment for a longer time at lower temperatures, at which monomer degradation is less pronounced.

The conversion yields presented in Chapters 4 and 5 were obtained after dilute enzymatic hydrolysis of the washed solids. Though this is an effective way of characterizing biomass digestibility, it effectively negates any effect of using a high-solids pretreatment process. In **Chapter 6**, biomass pretreated at the optimal conditions determined in Chapter 5 were used for high-solids enzymatic hydrolysis of unwashed solids. The objective of the work presented in Chapter 6 is to determine the effectiveness of using biphasic CO₂-H₂O mixtures during pretreatment and produce concentrated monosaccharide solutions after high solids enzymatic hydrolysis.

3.2 Objective 2: Developing a modeling framework for understanding the relationship between pretreatment and enzymatic hydrolysis and forming a basis for the rational design of these conversion processes

As demonstrated in Chapter 2, until now, most efforts to improve carbohydrate production from biomass through pretreatment and enzymatic hydrolysis have used random optimization and/or educated guessing. In fact, the approach that was used to optimize pretreatment parameters and that is presented in Chapters 4, 5 and 6 could be described as educated guessing. Such efforts could employ a rational design process if they were guided by a modeling framework that

captured the key mechanisms governing the relationship between pretreatment and enzymatic hydrolysis. In **Chapter 7**, a fluorescence confocal microscopy method was developed for observing and measuring the binding and reaction of cellulase cocktails and their substrates *in situ*. The Spezyme CP cellulase cocktail was supplemented with a small fraction of fluorescently labeled *T. Reesii* Cel7A, which served as a reporter to track cellulase binding onto the physical structure of bacterial microcrystalline cellulose (BMCC). Kinetic models were fitted to fluorescence intensity data and were compared to bulk cellulose conversion experiments. The goal was to demonstrate that fluorescence experiments could be relevant and provide useful insights into cellulose hydrolysis by commercial cellulase cocktails.

To accurately model enzymatic hydrolysis of real biomass, a reaction and diffusion model was developed and is presented in **Chapter 8**. The goal of the proposed reaction and diffusion model was to attempt to predict the well-known relationship between accessible surface area and initial enzymatic hydrolysis rates. Therefore, this model's predictions are compared to the previously discussed data published by Grethlein (see Chapter 2 and work by Grethlein [118]). In addition, this model was used to determine at which conditions and to which degree mass transfer limits enzymatic hydrolysis and could form the basis for the rational design of biomass depolymerization processes.

CHAPTER 4

HIGH-SOLIDS BIPHASIC CO₂-H₂O BIOMASS PRETREATMENT

Large portions of this Chapter have appeared as a published manuscript in the Journal *Biotechnology & Bioengineering* [38].

4.1 Introduction

As discussed in Chapter 2, one of the most specific and versatile routes to produce fuels or other bio-products is to obtain monosaccharides from biomass. Selectively producing sugars from lignocellulosic biomass is challenging and typically involves several stages. The initial or pretreatment stage consists of, depending on the process, partially extracting the cellulose, hemicellulose and/or lignin fraction of biomass while avoiding the production of unwanted degradation products. Pretreatment increases accessibility of cellulase and xylanase enzymes to their substrate when they are added, during the next stage, to depolymerize cellulose and remaining hemicellulose.

Some of the pretreatment approaches reviewed in Chapter 2 have included using acid or base solutions or simply pure water (often at higher temperatures) to deconstruct hemicellulose and lignin [213, 211, 212, 102]. Some of these technologies involve either flowing the reacting media through the biomass [151, 235] or an explosive decompression of the total mixture in the case of steam explosion [174] or ammonia fiber explosion (AFEX) [202, 204]. However, as mentioned earlier major remaining hurdles for pretreatment development include: (1) eliminating or reducing chemical usage, (2) increasing solid content throughout the process, (3) successfully treating different species of biomass

and their mixtures and (4) maximizing monosaccharide yield while limiting byproduct formation. Chemical usage has economic and environmental costs and necessitates either a neutralization or separation step to detoxify the pretreatment liquor. Increasing solid content dramatically decreases water usage, reducing equipment size, energy and separation costs [223]. Finally, using mixtures of different species and/or biomass grown in mixed culture will maximize year-round inputs and make production more sustainable [255]. Hence, advances in such areas will improve life cycle sustainability, which is essential to the biomass conversion process [256, 222, 257].

To address these issues, CO₂-H₂O mixtures could be used as a pretreatment medium. At high pressures (200 bar or above) and between 160 and 250°C, a supercritical CO₂ phase, with densities similar to that of a liquid, contains up to 30 mol% water while a liquid water phase contains up to 2 mol% CO₂. According to an approach proposed by Duan and Sun [258], a specific interaction model was used to estimate liquid phase behavior and an equation of state to estimate gas phase behavior. Duan and Sun report predictions within 7% of experimental values for this method. Polysaccharides already react in hot liquid water and the addition of CO₂ acts as an acid catalyst [13], while the supercritical CO₂ phase offers high diffusivities and was proven to have a swelling effect on plant material [259]. At atmospheric conditions, CO₂ is immiscible in water allowing it to be easily separated and recycled.

Kim and Hong [249] used pure CO₂ and CO₂-H₂O mixtures to pretreat lignocellulosic biomass. However, they do not refer to any specific phases that may be present. In addition, they do not explore temperatures above 165°C or residence times other than 1 hr and only study wood. Several studies [250, 48]

used a water-rich liquid phase, containing dissolved CO₂, to pretreat corn stover and aspen wood between 180 and 220°C. However, the biomass was not in direct contact with a supercritical CO₂ phase. In this study, a biphasic mixture of supercritical CO₂ saturated with water and of liquid water saturated with CO₂ was used to pretreat biomass. An initial attempt was made to use a single water saturated supercritical CO₂ phase, but this proved ineffective. Phase calculations and the details regarding the single-phase experiments are given in Appendix A.

4.2 Materials and methods

4.2.1 Biomass: species and analysis

Five different species of biomass were used: mixed hardwood (obtained from MESA® inc., Auburn, NY, harvested in NY, 2007), switchgrass, mixed perennial grasses (a co-culture of switchgrass and big blue stem), big bluestem grass (all were harvested near Ithaca, NY in fall 2009) and corn stover (obtained from the National Renewable Laboratory or NREL, Golden, CO, in 2009). All species of biomass were dried (moisture contents of 7 to 12 wt%). The biomass was size reduced using a cutting mill (IKA® Wilmington, NC) with a 1mm screen. The particles were sieved using a 38µm mesh screen to eliminate small particles that would be lost during filtering (U.S. Standard 400 sieve, E. H Sargent and Co., Chicago, IL). The moisture content of the biomass, before and after pretreatment, was determined by weighing it prior to and following its placement in an oven at 105°C for 12 hr and in a desiccator for 5 hr.

Biomass feedstocks were analyzed for neutral detergent fibers (NDF), acid detergent fibers (ADF) and acid detergent lignin (Lignin). All these analyses were performed by Dairy One® (Ithaca, NY) using methods described by Van Soest et al. [260]. NDF content is determined by measuring the leftover organic matter after an extraction with neutral detergent solution, -amylase and sodium sulfite at 70°C. ADF content is determined by measuring the leftover organic matter after an extraction with acid detergent solution at 70°C. Lignin content is determined by measuring the leftover organic matter after a 3 hr, 72 wt% sulfuric acid extraction. Biomass feedstocks were further analyzed for glucan, xylan arabinan and mannan using the protocol developed Sluiter et al. [58]. The amount of galactan liberated during this assay was so small (below 0.5 wt% in most cases and below 1% for corn stover) that it was neglected. Results for all species used in this study are given in Table 4.1.

4.2.2 Pretreatment

Biomass particles were mixed with deionized water to obtain the desired moisture content (80 or 60 wt% moisture in this study). The resulting slurry (2 g of dry matter and 3 or 8 g of H₂O) was loaded into a stainless steel reactor (see Figure 4.1 and caption for description). Once closed, the reactor was purged by pressurizing and venting it 5 times with 30 to 35 bar of CO₂. Liquid CO₂ is loaded from a siphon tank into the reactor resulting in a pressure of 60 bar. A fluidized sand bath (Techne® Burlington, NJ) was preheated to a temperature of about 50 to 20°C above the target reaction temperature. The reactor was then dropped into the sand bath and the bath temperature was set 10 to 20°C above the target reactor temperature. At that point, the pressure raised and reached

Table 4.1: Results of biomass analyses. NDF stands for neutral detergent fiber and ADF stands for acid detergent fiber. Acid detergent fiber corresponds to the addition of the lignin and cellulose fractions of biomass. Neutral detergent fiber corresponds to the addition of the lignin, cellulose and hemicellulose fractions of biomass. Glucan, xylan, mannan and arabinan measurements are provided with a range representing their 90% confidence interval.

	Cellulose = ADF – Lignin [wt%]	Glucan [wt%]	Hemicellulose = NDF – ADF [wt%]	Xylan [wt%]	Mannan [wt%]	Arabinan [wt%]	Lignin [wt%]
Mixed Hard-wood	55.8	42.8 ±0.5	22	13.4 ±0.1	1.8 ±0.01	0.6 ±0.01	16.1
Switchgrass	45.6	30.0 ±3.6	27.3	18.4 ±2.1	0.3 ±0.09	2.0 ±0.3	8.6
Big bluestem	44.4	37.6 ±0.1	28.6	19.9 ±0.1	0.4 ±0.01	2.4 ±0.02	6.9
Corn stover	40.6	38.5 ±0.1	33.6	21.6 ±0.2	0.5 ±0.02	2.6 ±0.03	4.2
Mixed perennial grasses	41.6	36.0 ±0.3	27	21.5 ±0.1	0.5 ±0.04	2.5 ±0.03	7

200 bar in 20 to 30 sec. The reactor was, from then on, progressively vented to maintain the reactor at 200 ± 10 bar. Water losses were considered minimal because the exiting gas was at room temperature (see Figure 4.1) and water saturation concentrations in CO_2 are small under those conditions (see Appendix, A). The internal reactor temperature reached the target temperature ($\pm 5^\circ\text{C}$) within 10 ± 1 min (typical reactor temperature profiles are given in Appendix A). The initial sand bath temperature was chosen to satisfy this condition. Internal reactor temperature was maintained within 5°C of the target temperature over the course of the residence time. Hence, all residence times reported in this study correspond to the time between the end of the heating period and the transfer of the reactor to an ice bath. Submerging the reactor in the ice bath caused the reactor temperature to drop below 100°C in about 20 sec reducing reaction rates to negligible values [31, 249, 149]. The resulting slurry was filtered using Miracloth® filtering cloth (Merck® Darmstadt, Germany, $38\mu\text{m}$ openings) and washed with 1 L of deionized water.

4.2.3 Enzymatic hydrolysis

The washed solids were hydrolyzed in a 1 wt% cellulose solution of 0.05 M sodium citrate buffer (pH 4.8) with 15 FPU/(g cellulose) of spezyme CP® cellulases, 30 (mg protein)/(g cellulose) of Multifect® xylanase (both from Genecor, Copenhagen, DK) and 30 CBU/(g cellulose) of Novo188® -glucosidase (Novozyme, Davis, Ca) at 50°C . Cyclohexamide (30 mg/L) and Tetracycline (40 mg/L) were added to prevent growth. A mass balance was carried out to determine cellulose content (assuming no cellulose loss during pretreatment). Samples of 150 *mul* were taken at 4, 24, 72 and 144 hr. Hydroly-

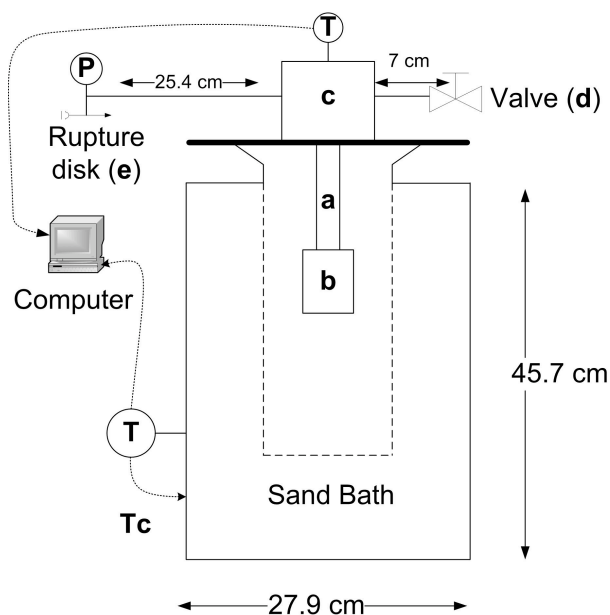


Fig. 4.1: Diagram of the batch pretreatment apparatus. The stainless steel pretreatment reactor was made with 20.3 cm (8) of 2.54 cm (1) O.D. (outer diameter) medium pressure tubing (**a**) and the corresponding end fitting (**b**) (Autoclave Engineers®, Erie, Pa). A thermocouple (**T**) was fed into the top of the reactor and placed 2 cm from the bottom of the reactor in the center of the packed bed of biomass. The top of the reactor was connected to a steel insulation plate and to a 4-way medium pressure fitting (**c**) that connected to a needle valve (**d**) (Autoclave Engineers®, Erie, Pa), a pressure gauge (**P**) and a rupture disk (**e**) (ETS, Erie, Pa, pressure rating: 282 bar) using 0.635 cm (1/4) O.D. medium pressure tubing (Autoclave Engineers®, Erie, Pa). This resulted in a nominal reactor volume of 25ml. The sand bath heaters were controlled by a temperature feedback loop (**Tc**).

sis was ended by heating the samples at 95°C for 5 min in a microplate heating block.

To determine the amount of oligomers in the pretreatment liquids, 10 ml of 0.05 M sodium citrate buffer (pH 4.8) with 2 ml of pretreatment liquid, 0.01 FPU/ml of spezyme CP, 0.02 CBU/ml of Novo188 -glucosidase and 0.03 mg/ml of Multifect® xylanase protein were incubated at 50°C for 72 hr. All enzymatic hydrolysis experiments were carried out in triplicates in order to calculate a 90%

confidence interval for our results.

4.2.4 Liquid analysis

Pretreatment liquids, enzymatic hydrolysis samples and the samples resulting from the oligomer assay were analyzed for glucose, xylose, mannose, arabinose, furfural and 5-hydroxymethylfurfural (5-HMF) using a Shimadzu liquid chromatography system (Shimadzu, Kyoto, Japan) with an Aminex P-Column (Biorad, Hercules, CA). Standards for the analysis were purchased from Sigma-Aldrich (St. Louis, MO).

4.3 Results

4.3.1 Yield

Concentrations of glucose, xylose, mannose, arabinose, 5-HMF and furfural measured during pretreatment and enzymatic hydrolysis were used to calculate yield. Yield coefficients, Y_i , are reported as the molar percentage of the maximal possible output of this compound during pretreatment and after 72 hr of enzymatic hydrolysis:

$$Y_g = \frac{Mo_{g,Pr} + Mo_{g,E} + Mo_{g,Ol}}{P_g} \times 100 \quad (4.1)$$

$$Y_h = \frac{Mo_{x,Pr} + Mo_{x,E} + Mo_{x,Ol} + Mo_{m,Pr} + Mo_{m,E} + Mo_{m,Ol} + Mo_{a,Pr} + Mo_{a,E} + Mo_{a,Ol}}{P_x + P_m + P_a} \times 100 \quad (4.2)$$

$$Y_f = \frac{M_{O_f,Pr}}{P_x + P_a} \times 100 \quad (4.3)$$

$$Y_5 = \frac{M_{O_5,Pr}}{P_g + P_m} \times 100 \quad (4.4)$$

The variables $M_{O_{i,j}}$ and P_i designate moles of monomers or polymers of compound i obtained during process j . The subscripts $g, h, x, m, a, 5$ and f designate glucose, hemicellulose sugars (i.e. xylose, mannose and arabinose), xylose, mannose, arabinose, 5-HMF or furfural, respectively. The subscripts Pr, E and Ol designate compounds obtained during pretreatment (Pr), 72 hr of enzymatic hydrolysis (E) or the oligomer assay (Ol), respectively. Glucose and, to a far lesser extent, xylose, can produce degradation products besides 5-HMF and furfural, and all degradation products can further degrade, especially at temperatures close to 240°C [37, 138]. However, these products are still a good indicator of sugar degradation during pretreatment. Organic acids are often released as well and tend to lower the pH of the pretreatment liquor. However, they are not quantified in this study.

4.3.2 Hardwood pretreatment

20 wt% pretreatment and saccharification

The 20 wt% solids slurry of hardwood was pretreated at temperatures between 150 and 200°C and residence times between 20 seconds and 60 min. The highest measured Y_g obtained after enzymatic hydrolysis of pretreated hardwood were between 75 and 77% (see Figure 4.2A). All three Y_g measurements in this range were statistically equivalent with values differing by 2 to 3.6 percentage points. The highest yields were obtained in a temperature range of 170 to 180 °C

with residence times of 20 to 60 min. After 4 hr of enzymatic hydrolysis, yields reached 53 to 68% of their 72 hr yield (Y_g) for pretreatment temperatures above 170°C. For 170°C and below, yields reached between 39 and 47% of their 72 hr value after 4 hr. At pretreatment temperatures below 200 °C , between 90 to 95% of the glucose monomers measured and used to calculate Y_g was produced during enzymatic hydrolysis. For temperatures of 225 to 230 °C and for 250 °C, enzymatic hydrolysis was responsible for 83 to 88% and 56 to 75% of the total glucose produced, respectively. These results are corroborated by the increased mass loss with increasing temperature that occurred during pretreatment (from 6% at 150°C and 1 hr residence time to almost 80% at 250°C and 1 min residence time). This is consistent with the important glucan depolymerization reported by Bobleter for temperatures above 220°C[31].

As shown on Figure 4.2B, Y_h values increased almost linearly with decreasing temperature up to a value of $28 \pm 1\%$ for 160°C and 60 min before dropping down at 150°C . However, the Y_h of $31 \pm 5\%$ was obtained at 200°C and a residence time of 20 min. Between 60 and 90% of the hemicellulose sugar yield was due to sugars released during enzymatic hydrolysis. This range narrowed between 63 to 68% for pretreatment temperatures below 200°C demonstrating that, at higher temperatures, a large fraction of hemicellulose sugars released during pretreatment had degraded.

Figure 4.2C shows that a small amount of 5-HMF is produced in all experiments, with 4-5% being produced for pretreatment temperature of 215 to 230°C. This was due to much higher xylose than glucose production during pretreatment. Furfural yields up to 23% were observed for pretreatment temperatures of 200°C and 230°C with residence times of 20 and 2 min, respectively. Consis-

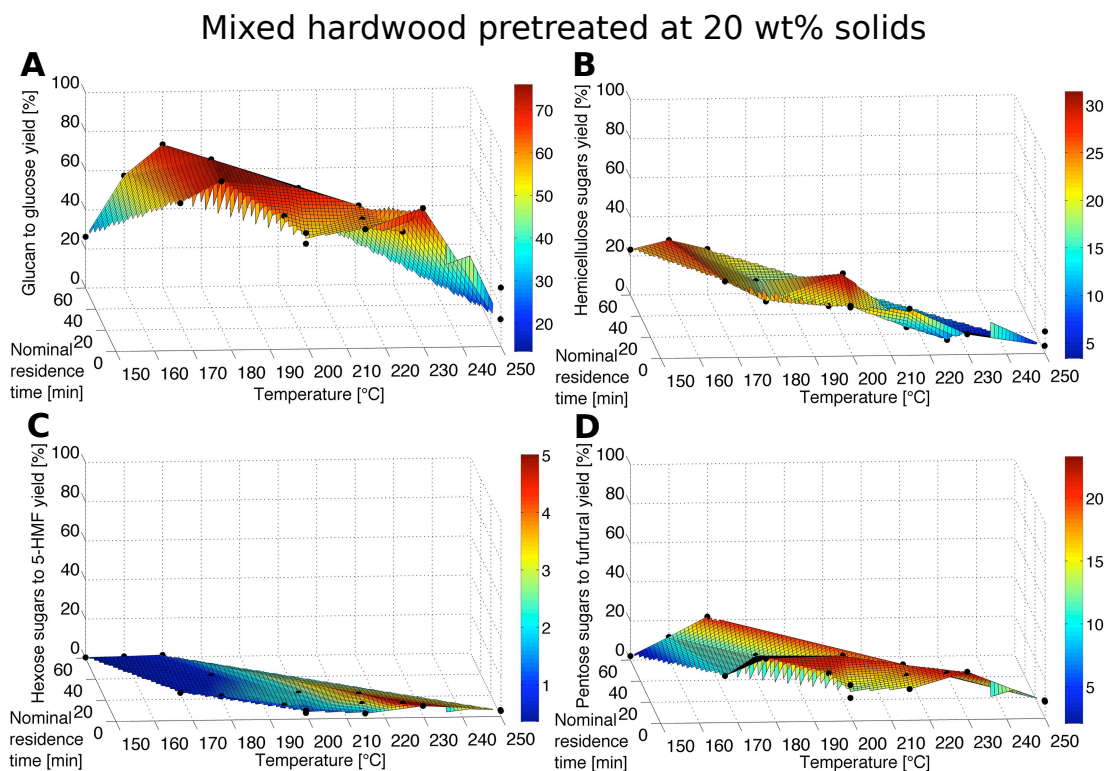


Fig. 4.2: Combined yields from pretreatment of a 20 wt% solids (biomass water mixture) slurry of mixed hardwood as a function of pretreatment time and temperature at 200 bar. Yields are obtained after 72 hr of enzymatic hydrolysis (15 FPU/g cellulose or 19.6 FPU/g glucan). (A) Glucan to glucose yields. (B) xylan, arabinan and mannan (hemicellulose sugars) to xylose, arabinose and mannose yields. (C) Glucan and mannan (hexose sugars) to 5-HMF yields. (D) Xylan and arabinan (pentose sugars) to furfural yields.

tent with the release during pretreatment of pentose sugars, furfural yields tend to decrease with decreasing temperature and residence times but increase from 250 to 230°C, which could be due to decomposition of the furfural at temperatures closer to 250°C [37, 13].

40 wt% pretreatment and saccharification

Given the lower yields and higher byproduct formation observed for pretreatment of 20 wt% solids mixtures at temperatures above 200°C, the experimental range was restricted to temperatures between 150 and 200°C for 40 wt% solids mixtures.

As shown in Figure 4.3A, the highest Y_g was $73 \pm 5\%$ for a pretreatment temperature of 170°C and a nominal residence time of 60 min. The three Y_g values reported in the range of 67 to 69% are statistically equivalent suggesting limited sensitivity in the temperature range of 160 to 180 °C and retention times of 30 to 60 min. Thus, once again, maximal Y_g are observed at low temperatures and long residence times or higher temperatures with shorter residence times. Between 87 and 95% of Y_g was obtained as monomers during enzymatic hydrolysis, confirming that very little glucan was depolymerized at temperatures below 200°C. After 4 hr of enzymatic hydrolysis, yields reached between 78 to 89% of their 72 hr value (Y_g) for pretreatment temperatures above 160°C. Below that temperature, yields reached between 53 and 64% of their 72 hr value after 4 hr.

Hemicellulose sugar yields (Figure 4.3B) of 18 and 19% were observed for temperatures of 150 to 160°C with residence times of 60 min, and a maximum Y_h of $24 \pm 5\%$ at 190°C with a 15 min residence time. This maximum Y_h coincided with the lowest fraction of sugars released during enzymatic hydrolysis (53%). For other pretreatment conditions, 62 to 85% of the Y_h value was produced during enzymatic hydrolysis. Figure 4.3C shows, once again, low Y_s values indicating limited hexose degradation. Furfural yields, shown in Figure 4.3D, increased with temperature and residence time up to values of 15 to 19%.

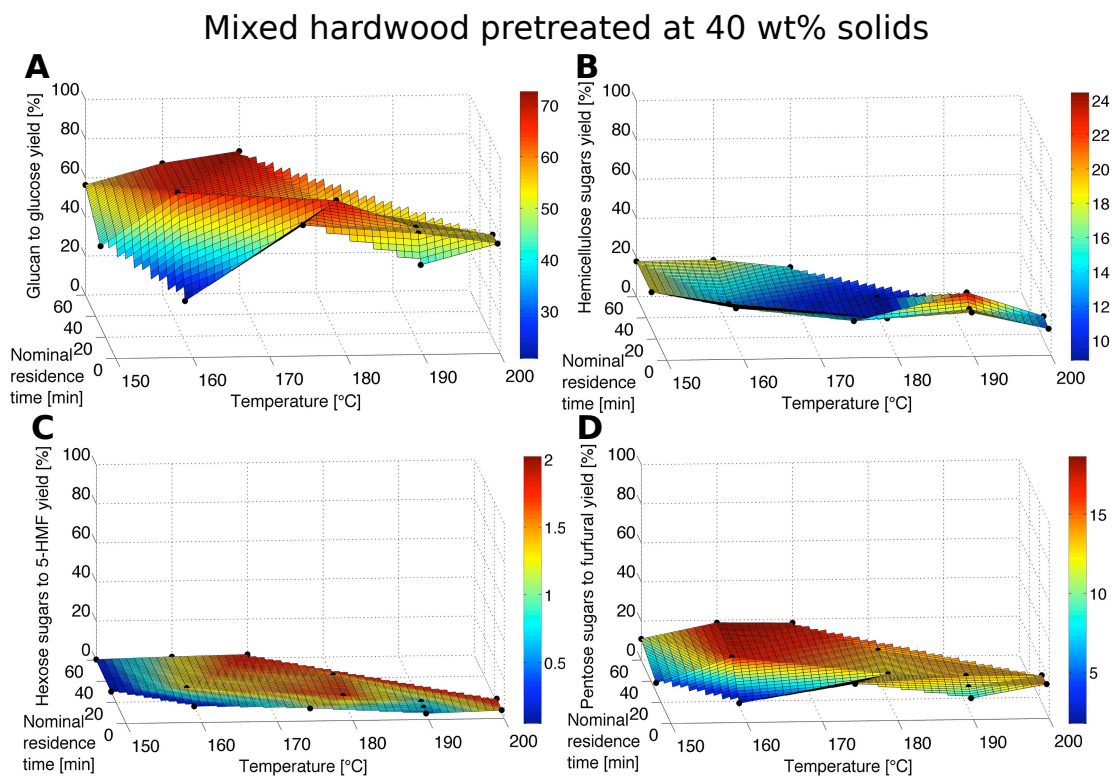


Fig. 4.3: Combined yields from pretreatment of a 40 wt% solids (biomass water mixture) slurry of mixed hardwood as a function of pretreatment time and temperature at 200 bar. Yields are obtained after 72 hr of enzymatic hydrolysis (15 FPU/g cellulose or 19.6 FPU/g glucan). (A) Glucan to glucose yields. (B) xylan, arabinan and mannan (hemicellulose sugars) to xylose, arabinose and mannose yields. (C) Glucan and mannan (hexose sugars) to 5-HMF yields. (D) Xylan and arabinan (pentose sugars) to furfural yields.

4.3.3 Switchgrass pretreatment and saccharification

Pretreatment of 20 and 40 wt% solids slurries of mixed hardwood led to similar yields. Considering the process advantages linked with higher solid content, the pretreatment runs that followed were only performed with slurries containing 40 wt% dry solids at temperatures between 150 and 200°C with nominal residence times of 5 to 60 min.

Glucose yields (Figure 4.4A) were the highest for temperatures of 160 and

170°C and a residence time of 60 min, with yields of 79 and 81%. As shown in Table 4.2, pretreated switchgrass had Y_g values that were 8 times larger than the value obtained for un-treated biomass. A Y_g of 72% was reached with a pretreatment temperature of 180°C and a 15 min residence time. All other yields ranged from 50 to 70%. After 4 hr of enzymatic hydrolysis, yields had reached between 80 to 92% of their 72 hr value. For pretreatment temperatures below 200 °C, between 92 and 95% of glucose yields were due to glucose monomers released during enzymatic hydrolysis. For a pretreatment temperature of 200°C, the fraction of Y_g due to enzymatic hydrolysis was between 83 and 87%.

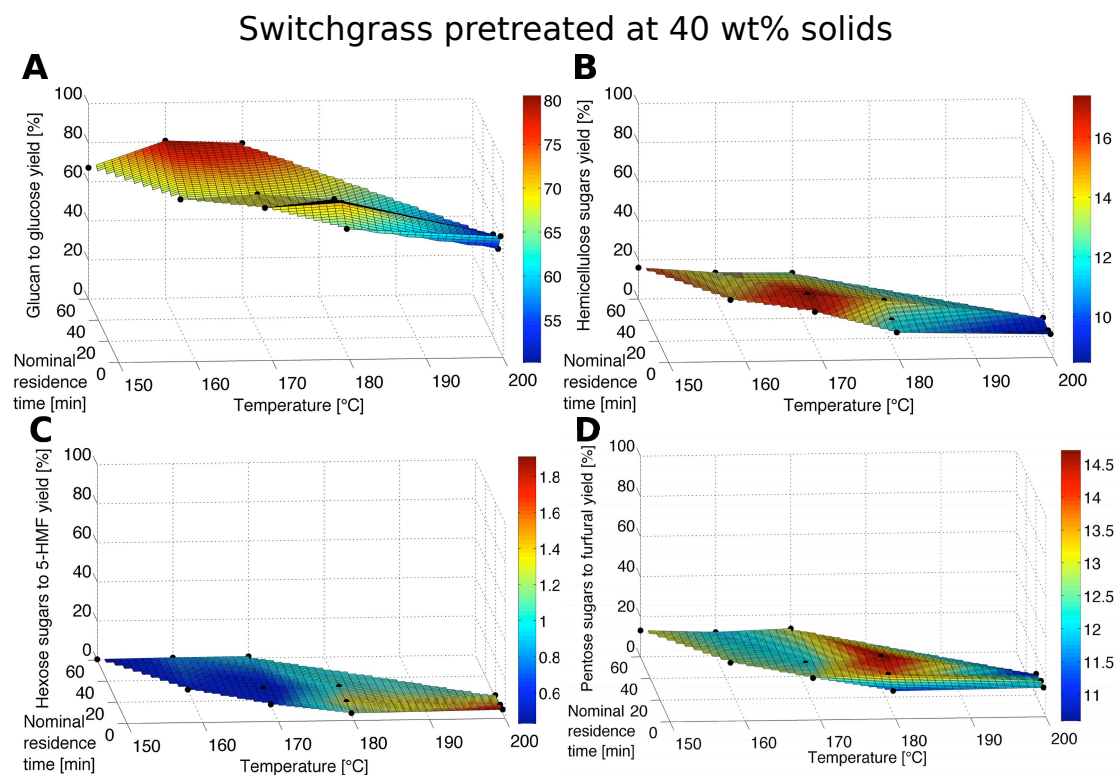


Fig. 4.4: Combined yields from pretreatment of a 40 wt% solids (biomass water mixture) slurry of switchgrass as a function of pretreatment time and temperature at 200 bar. Yields are obtained after 72 hr of enzymatic hydrolysis (15 FPU/g cellulose or 22.8 FPU/g glucan). (A) Glucan to glucose yields. (B) xylan, arabinan and mannan (hemicellulose sugars) to xylose, arabinose and mannose yields. (C) Glucan and mannan (hexose sugars) to 5-HMF yields. (D) Xylan and arabinan (pentose sugars) to furfural yields.

Hemicellulose sugar yields (Figure 4.4B) were as high as 16 to 17% for pretreatments at 170°C with 15 and 30 min residence times and 150°C with a residence time of 60 min. Other combination of temperature and residence time led to yields between 9 and 15%. Contribution of sugars released during enzymatic hydrolysis for these combined yields ranged from 62 to 73%. Conversion of pentoses to furfural (Figure 4.4D) varied little with temperature and residence time, staying confined to a yield range of 10 to 15%.

4.3.4 Mixed perennial grasses pretreatment and saccharification

Mixed perennial grasses were pretreated using slurries containing 40 wt% dry solids at temperatures between 150 and 200°C with nominal residence times between 5 and 60 min. Experiments were limited to 40 wt% solids for the same reasons given previously.

As shown on Figure 4.5A, the highest Y_g values, $68 \pm 1\%$, was observed for pretreatment temperatures of 170°C with nominal residence times of 15 and 60 min. This corresponded to a Y_g value 5 times greater than the value for untreated biomass (see Table 4.2). After 4 hr of enzymatic hydrolysis, yields had reached between 79 to 86% of their 72 hr yield (Y_g). Between 87 and 94% of the glucose reported was released during enzymatic hydrolysis. The highest Y_h value (Figure 4.5B) was of 9% for a pretreatment temperature of 160°C and a residence time of 60 min. All other yields ranged from 5 to 8%. Furfural yields produced from pentose degradation, shown in Figure 4.5D, ranged from 14% for 180°C and 15 min of pretreatment to 4% for 150°C and 60 min of pretreat-

Table 4.2: Combined sugar and degradation product yields given for various pretreatment conditions and biomass species. All yields are provided with a range representing their 90% confidence interval.

	No pretreatment		Pretreatment at 160° C for 1hr				Pretreatment at 170° C for 1hr			
	Glucan yield [%]	Hemicellulose sugars yield [%]	Glucan yield [%]	Hemicellulose sugars yield [%]	5-HMF yield [%]	Furfural yield [%]	Glucan yield [%]	Hemicellulose sugars yield [%]	5-HMF yield [%]	Furfural yield [%]
Mixed Hard-wood (20 wt%)	5.1 ±0.3	3.9 ±0.8	57 ±2	28 ±1	0.6 ±0.1	11.6 ±0.2	77 ±4	27 ±3	1.1 ±0.1	21.7 ±0.3
Mixed Hard-wood (40 wt%)			67 ±2	18 ±3	1.3 ±0.1	16.6 ±0.3	73 ±5	14 ±2	1.9 ±0.3	16 ±1
Switchgrass	10.4 ±0.4	6.6 ±0.4	81 ±1	13 ±1	0.8 ±0.2	11.8 ±0.5	79 ±1	12 ±1	0.9 ±0.1	13.1 ±0.6
Big bluestem	17 ±1	5.0 ±0.4	56 ±2	9.9 ±0.3	0.9 ±0.3	14 ±1	66 ±2	13 ±1	1.0 ±0.2	15 ±1
Corn stover	36 ±1	17 ±1	85 ±2	10 ±1	1.3 ±0.1	11.2 ±0.5	67 ±2	10 ±2	1.2 ±0.1	9.1 ±0.2
Mixed perennial grasses	12.2 0.4	3.5 ±0.3	65 ±2	8.7 ±0.4	0.6 ±0.1	5.5 ±0.2	68 ±1	6.2 ±0.3	1 ±0.1	12 ±0.1

ment.

Mixed perennial grasses pretreated at 40 wt% solids

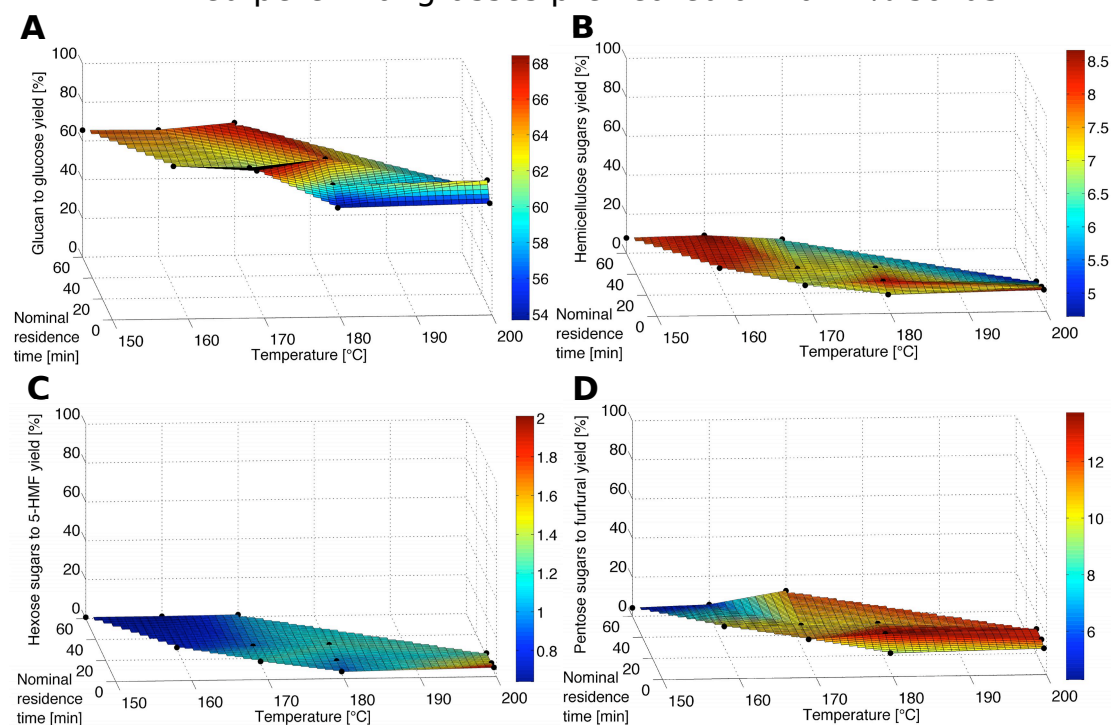


Fig. 4.5: Combined yields from pretreatment of a 40 wt% solids (biomass water mixture) slurry of mixed perennial grasses as a function of pretreatment time and temperature at 200 bar. Yields are obtained after 72 hr of enzymatic hydrolysis (15 FPU/g cellulose or 17.3 FPU/g glucan). (A) Glucan to glucose yields. (B) xylan, arabinan and mannan (hemicellulose sugars) to xylose, arabinose and mannose yields. (C) Glucan and mannan (hexose sugars) to 5-HMF yields. (D) Xylan and arabinan (pentose sugars) to furfural yields.

4.4 Discussion

4.4.1 Effect of solids content

As shown by comparing Figure 4.2A and 4.3A, changes in biomass solids content seem to have a limited affect on final glucose yields. The variation in Y_g

between solids loading of 40 wt% and 20 wt% was always under 10 percentage points. Furthermore, the final 72 hr yield was reached earlier with solid loadings of 40 wt%. No significant change in yield ever occurred after 72 hr of enzymatic hydrolysis. The surfaces depicted in Figures 4.2A and 4.3A are similar with maximal yields achieved under similar temperature and retention time. However, at the higher solids content Y_g is less sensitive to temperature. The change in Y_g with temperature for the 20 wt% (Figure 4.2A) is more dramatic between 170 and 150°C than it is for the 40 wt% (Figure 4.3A). Heat transfer could be an important cause of this difference. Indeed, a slurry with a higher solid content seemed to lower heat-transfer rates. Thus, it required an initial sand bath temperature that was about 20°C higher than for the experiments with 20 wt% solids slurries to achieve the same heat-up time. This increased sandbath temperature could lead to a greater temperature gradient within the reactor, which would, have increased the yields for pretreatment experiments at lower temperatures by subjecting part of their mixture to higher temperatures.

Hemicellulose sugar yields, obtained with 40 wt% slurries, are about half those obtained for pretreatment with 20 wt%. However, the response surfaces shown in Figures 4.2B and 4.3B exhibit similar trends to glucose yields (see Figure 4.2A and 4.3A). Once again, yields are less sensitive to temperature changes for the higher solids content experiments. Lower Y_h values could be due to increased pentose sugar degradation or decreased hemicellulose depolymerization during pretreatment. However, neither furfural nor 5-HMF yields significantly increased with solids content. Water limitations and hot spots in the reactor could have led to locally accelerated pyrolysis of hemicellulose. This explanation is consistent with observations of Serapiglia et al., who reported biomass degradation between 175-220°C for 2 min of continuous heating [261].

4.4.2 Effect of biomass species

The biomass species appeared to shift yield numbers (see Figures 4.3, 4.4 and 4.5) by a more-or-less constant value. Indeed, yield variations stay essentially the same with different conditions. For example, Y_g values for switchgrass are always greater than those of other species by about 10 percentage points regardless of conditions. Yield maxima always occur at pretreatment temperatures between 160 and 170°C with a 1 hr residence time. Hemicellulose sugars yield was the highest for wood, slightly less for switchgrass and lower for mixed perennial grasses. Furfural yields logically show similar variations.

4.4.3 Comparison with leading pretreatment technologies

For 40 wt% mixed hardwood slurries, a Y_g of $73 \pm 5\%$ was obtained with a pretreatment temperature of 170°C and a residence time of 60 min. Kim and Hong (2001) obtained a similar result using aspen wood (165°C, 1 hr), indicating that the phase behavior is probably analogous. Poplar pretreated with catalyzed steam explosion (3 wt% SO_2 , 200°C, 5 min, from a personal communication with Bura: 8-15% solid content), can reach glucose yields of 100% [174]. Dilute acid pretreatment of poplar (2 wt% H_2O_4 , 190°C for 1.1 min) led to glucose yields of 83% [212]. A study reporting similar yield in the same pilot reactor used a solid content of 15 wt% [246]. Our pretreatment of 40 wt% solids slurries led to Y_g values of $81 \pm 1\%$ for switchgrass and $85 \pm 2\%$ for corn stover (see Table 4.2). In comparison, dilute acid pretreatment gave yields of 91% for switchgrass and 92% for corn stover (switchgrass: 180°C, 0.5 min, 1.2% H_2O_4 , solids content not given and corn stover: 160°C, 20 min, 0.49% H_2O_4 , 25 wt% solids) [262, 211].

AFEX pretreatment gave glucose yields of 93% for switchgrass and 82% for corn stover (switchgrass: 100°C, 5 min, 20 wt% solids and corn stover: 90°C, 5 min, 62.5% solids) [201, 204]. Corn stover pretreated with hot water (190°C, 15 min, 16 wt% solids) and steam explosion (190°C, 5 min, 8-15 wt% solids) gave yields of 89 and 100%, respectively. Finally, steam exploded wheat straw (195°C, 6 min, 23-28 wt% solids) gave a 90% glucose yield [244].

Glucose yields reported here are often less than 10 percentage points below those obtained with leading pretreatment technologies despite the absence of additional chemicals and a higher solid content. Furthermore, yields for leading technologies are often obtained in larger and, sometimes, mixed reactors. Thus, introducing mixing could improve our process by increasing temperature homogeneity and mass transfer rates. This could increase hemicellulose sugar yields, which are much lower than those of leading technologies and decrease furfural yields, which are comparable to values reported for dilute acid pretreatment [245]. Furthermore, contrary to most leading technologies, our optimal pretreatment conditions are nearly identical for different biomass species, which could allow processing their mixtures in the same reactor. Nevertheless, increased capital costs can be incurred due to high-pressure equipment and must be outweighed by the benefits if this process is to be commercialized.

4.5 Conclusions

Biphasic CO₂-H₂O pretreatment can produce glucose yields of 73% for wood, 81% for switchgrass and 85% for corn stover using very similar experimental conditions (160-170°C and a 60 min residence time), high solid contents

(40 wt%) and no additional chemicals. However, further improvements are needed to increase hemicellulose sugars yields and reduce furfural formation. To address this, efforts were focused on designing a mechanically agitated high-pressure reactor to increase temperature homogeneity and mass transfer rates. These efforts are described in Chapter 5

CHAPTER 5

TWO-TEMPERATURE STAGE BIPHASIC CO₂-H₂O PRETREATMENT OF LIGNOCELLULOSIC BIOMASS AT HIGH SOLID LOADINGS

Large portions of this Chapter have appeared as a published manuscript in the Journal *Biotechnology & Bioengineering* [263].

5.1 Introduction

In Chapter 4, it was demonstrated that pretreatment using biphasic CO₂-H₂O mixtures at high pressures could help overcome some the remaining hurdles that biomass conversion processes face on the road to commercialization. These hurdles include (1) eliminating or reducing the use of chemical catalysts, (2) reducing the amount of water carried through the process, (3) successfully pretreating different types of biomass and their mixtures and (4) obtaining high monosaccharide yields and limiting byproduct formation. Carbon dioxide can act as an easily separable green co-solvent and weak acid catalyst when mixed with water and, thus, help address some of these issues. In Chapter 4, temperatures between 150 and 250°C were explored at 200 bar to pretreat mixed hardwood, switchgrass, mixed perennial grasses, big bluestem and corn stover at 40 wt% (or weight percent) solids loadings (water-biomass mixture). Glucan to glucose yields of 73% for wood, 81% for switchgrass and 85% for corn stover were obtained under very similar experimental conditions (160-170°C and a 60 min residence time) and no additional chemicals. Water and CO₂ mixtures have also been used to pretreat aspen wood, guayule bagasse and wheat straw [264, 249, 265]. However, all these studies were performed in externally heated reactors without any agitated mixing. In addition, the biomass used in

all of these experiments were ground to a size ranging between 0.5 to 2 mm; this is probably unrealistically small for use in a biorefinery. In this work, the results for biphasic CO₂-H₂O pretreatment of mixed hardwood and switchgrass in a larger (1 L) stirred reactor at both the original (<1 mm) and a larger (<0.95 cm) particle size are compared to the results of the previous work presented in Chapter 4 (obtained in a small, 25 ml unstirred reactor) to assess the effect of particle size and mixing on pretreatment performance.

The vast majority of pretreatment studies published in the literature are conducted using a single temperature stage (i.e. one temperature for a given residence time). However, given the typical reaction chemistry of biomass in acidic or neutral media, it may be advantageous to use a range of pretreatment temperatures, which may help alleviate the production of unwanted byproducts. Indeed, hemicellulose depolymerization produces oligomers that depolymerize to monomers that can degrade to unwanted byproducts such as furfural [154, 149, 150]. The sequential nature of this reaction network entails that furfural production lags behind that of oligo- and monosaccharides. Indeed, when maple and aspen wood are treated with water at 175°C xylose and xylo-oligomer concentrations have to increase significantly before furfural starts to appear [150]. Thus, it may be advantageous to use a high pretreatment temperature for a short period during this initial lag in degradation product formation, and then pursue pretreatment for a longer time at lower temperatures, at which monomer degradation is less pronounced. According to a recent literature search, this particular staged pretreatment scheme has not been presented before. However, a number of approaches have used a low temperature stage to depolymerize hemicellulose while avoiding degradation, followed by a high temperature stage to successfully pretreat the remaining cellulose

[266, 267, 268]. This approach is often successful in increasing yields and reducing by-product formation. However, separating the solubilized hemicellulose sugars with a filtering and washing step is required to avoid their degradation during the second high-temperature stage. Such a separation step is present in all of the studies mentioned above. Biomass washing adds significant amounts of water to the process and filtering can significantly add to economic and energetic costs.

The objective of the work presented in this Chapter was to assess the effect of mixing, particle size and the benefit of using two temperature stages for mixed hardwood and switchgrass by subjecting them to a short (0-24 min) stage at 200-210°C followed by a longer (30-60 min) pretreatment stage at 150-190°C.

5.2 Materials and Methods

5.2.1 Biomass: species and analysis

Field dried (moisture content: 9-12 wt%) mixed hardwood (obtained from MESA® inc., Auburn, NY, harvested in NY, 2007) and sunburst switchgrass (harvested near Ithaca, NY in fall 2009) were used in this work. Biomass was size reduced in a hammermill (Schutte Buffalo LLC, Buffalo, NY) with a 3/8" (0.95 cm) screen to produce large particles (most of which are between 0.5 and 1 cm in length and about 0.2-0.4 cm wide). These particles were further size reduced in a cutting mill (IKA®, Wilmington, NC) with a 1 mm screen to produce particles smaller than 1 mm. Biomass was then sieved with a 38 μ m mesh screen to remove dust-like particles that would be lost during filtering (U.S. Standard

400 sieve, E. H. Sargent and Co., Chicago, IL). Biomass moisture content was determined by weighing it before and after its drying in an oven at 105°C for 12 hr and in a desiccator for 5 hr. Biomass was analyzed for neutral detergent fibers, acid detergent fibers, acid detergent lignin, glucan, xylan, arabinan and mannan (galactan is neglected) as described in Chapter 4 and these results are given in Table 4.1.

5.2.2 Pretreatment

Biomass particles were mixed with deionized water to obtain the desired dry solids content of 40 wt%. The resulting slurry (60 g of dry matter and 90 g of water) was loaded into a 1 L stirred reactor (see Figure 5.1). The reactor was purged of air by pressurizing it with CO₂ to a pressure of 20 bar and venting it 5 times. Liquid CO₂ was then loaded into the reactor resulting in a pressure of about 60 bar. The reactor was then heated-up to the target temperature with an electric heating jacket. The reactor was progressively vented to maintain 200 ±10 bar using a backpressure regulator (BPR). The target temperature (±5 °C) was reached after 30 to 45 min of heating (typical reactor temperature profiles are given in Appendix B). All residence times reported in this work correspond to the time at which the reactor was within 5 °C of the target temperature. The reaction was stopped by flowing water through a cooling coil within the reactor, which reduced the reactor temperature to below 100°C in about 1 min.

When a second stage of pretreatment was performed, additional CO₂ was loaded into the reactor to compensate for CO₂ vented during the first stage. Heating, temperature control, pressure control and cooling were performed

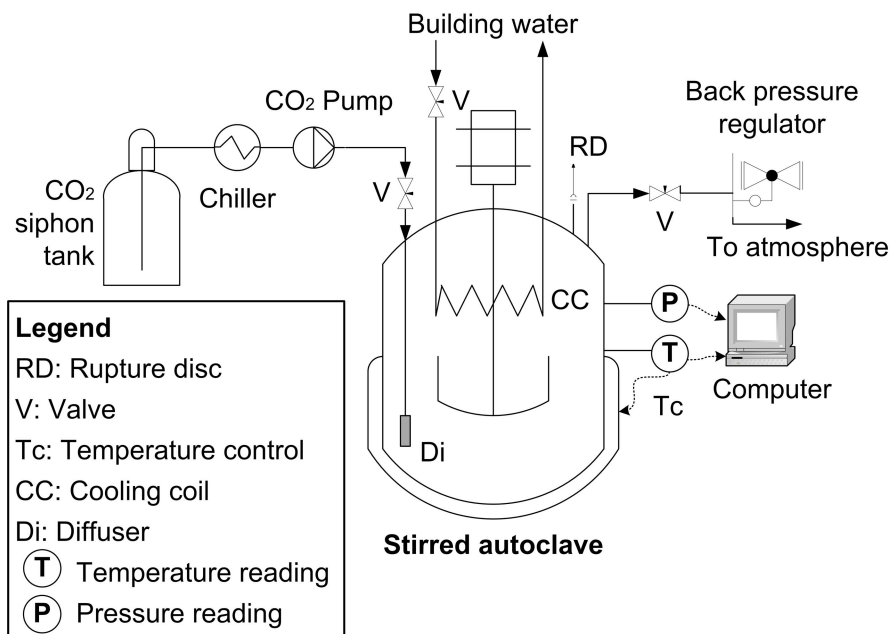


Fig. 5.1: Stirred pretreatment reactor schematic. A high-pressure stainless-steel vessel was stirred with a magnetically controlled shaft and impeller (system obtained from Autoclave Engineers®, Erie, Pa). A custom impeller was machined to optimize biomass mixing throughout the process (a description and pictures are available in Appendix B). Liquid CO₂ was delivered from a CO₂ siphon tank through a CO₂ pump (Thar® Process, Pittsburg, Pa) hooked up to a chiller (Thermo-Fisher® Scientific, Waltham, Ma) to avoid CO₂ phase change during compression. To maximize CO₂ distribution upon entry, it was delivered through a porous metal diffuser that was supplied with the reaction system. A colloidal cooling coil (supplied with the reaction system) was hooked up to the building water through a valve to enable rapid cooling of the reactor. An electrical heating jacket was used for temperature control. Pressure was maintained at the target pressure with a backpressure regulator (BPR, Tescom®, Elk River, Mn). Heating tape (Omega Engineering®, Stamford, Co) was used to prevent excessive cooling of the BPR during CO₂ decompression.

in the same way as during the initial stage. The resulting biomass was then washed and filtered using Miracloth® filters (Merck®, Darmstadt, Germany, 38µm openings) and 1 L of deionized water. To determine the quantity of oligomers present in the washwater, acid hydrolysis was performed in a 4 wt% sulfuric acid solution according to the NREL procedure [269].

5.2.3 Enzymatic hydrolysis

Washed solids were hydrolyzed in a 1 wt% solution of original glucan (i.e. all glucan was assumed to be conserved) at 50°C according to NREL methods for assessing biomass digestibility [270]. A 0.05 M sodium citrate buffer (pH 4.8) was used with 15 FPU/(g cellulose) (FPU, filter paper units) of spezyme CP® cellulases, 30 (mg protein)/(g glucan) of Multifect® xylanase (Genencor, Copenhagen, DK) and 30 CBU/(g glucan) (CBU, cellobiase unit) of Novo188® β-glucosidase (Novozyme, Davis, Ca). To prevent growth, 30 mg/L Cyclohexamide and 40 mg/L Tetracycline were added. Samples were taken at 4, 24 and 72 hr. Reactions were quenched by heating the samples at 95°C for 5 min in a microplate heating block.

5.2.4 Yield calculations

Pretreatment, enzymatic hydrolysis and oligomer assay liquids were analyzed for glucose, xylose, mannose, arabinose, furfural and 5-hydroxymethylfurfural (5-HMF) using liquid chromatography as described in Chapter 4 . Various yields, $Y_{i,r}$, are calculated based on those concentrations. They represent the

molar percentage of the maximal possible output of the product of interest, expressed as:

$$Y_g = \frac{M_{Og,Pr} + M_{Og,E} + M_{Og,Ol}}{P_g} \times 100 \quad (5.1)$$

$$Y_h = \frac{M_{Ox,Pr} + M_{Ox,E} + M_{Ox,Ol} + M_{Om,Pr} + M_{Om,E} + M_{Om,Ol} + M_{Oa,Pr} + M_{Oa,E} + M_{Oa,Ol}}{P_x + P_m + P_a} \times 100 \quad (5.2)$$

$$Y_f = \frac{M_{Of,Pr}}{P_x + P_a} \times 100 \quad (5.3)$$

$$Y_5 = \frac{M_{O5,Pr}}{P_g + P_m} \times 100 \quad (5.4)$$

$$Y_T = \frac{Y_g \times (P_g) + Y_h \times (P_x + P_m + P_a)}{P_g + P_x + P_m + P_a} \times 100 \quad (5.5)$$

The variable $M_{O_{i,j}}$ designate moles of monomers of compound i obtained during process j . The variable and P_i designates the structural polymer of compound i (see Table 4.1). The subscripts $g, h, x, m, a, 5$ and f designate glucose, hemicellulose sugars (i.e. xylose, mannose and arabinose), xylose, mannose, arabinose, 5-HMF or furfural, respectively. The subscripts Pr, E and Ol designate compounds obtained after pretreatment (Pr), after 72 hrs of enzymatic hydrolysis (E) or after the oligomer assay (Ol), respectively. Though furfural and 5-HMF are not the sole degradation products of xylose and glucose, they are the main products at temperatures below 220-240°C (especially furfural in the case of xylose) and thus, are a good indicator of degradation in the range explored here [37, 138]. A total sugar yield (Y_T), which combines, on a molar basis, the glucan to glucose and hemicellulose sugar yields was also determined.

Losses of reactant mass (water and biomass) after pretreatment, typically between 4 and 9% , are omitted for the purpose of yield calculations. Indeed, these losses do not correlate with temperature and extent of pretreatment and are thus assumed to be due to losses during material transfer and biomass sticking to the reactor walls. In some cases, specifically when switchgrass was pretreated at a high temperature (210°C) for long times (6 min or more), mass losses exceeded 10 wt% (up to 17%). In such cases, any mass loss beyond 10 wt% is accounted as non-glucan biomass lost during pretreatment, which is included into yield calculations by assuming that this lost mass increases the glucan proportion in the pretreated biomass.

5.3 Results and Discussion

5.3.1 Single temperature stage results: effect of mixing and particle size

Mixed hardwood pretreatment

When 40 wt% solids mixed hardwood was pretreated in the 25 ml unstirred reactor at 160°C and 170°C for 60 min, glucan to glucose yields (Y_g) of 67 and 73% and hemicellulose sugar yields (Y_h) of 18 and 14% were obtained (see Chapter 4). As shown in Figure 5.2, when the same small particles (<1mm) were pretreated in the 1 L stirred reactor at 160°C and 170°C for 60 min, Y_g decreased from 67 to 22% and from 73 to 57%, while Y_h increased from below 20% to 39 and 42%, respectively. However, with temperatures of 180 or 190°C for 60 min,

a Y_g of 69% was obtained.

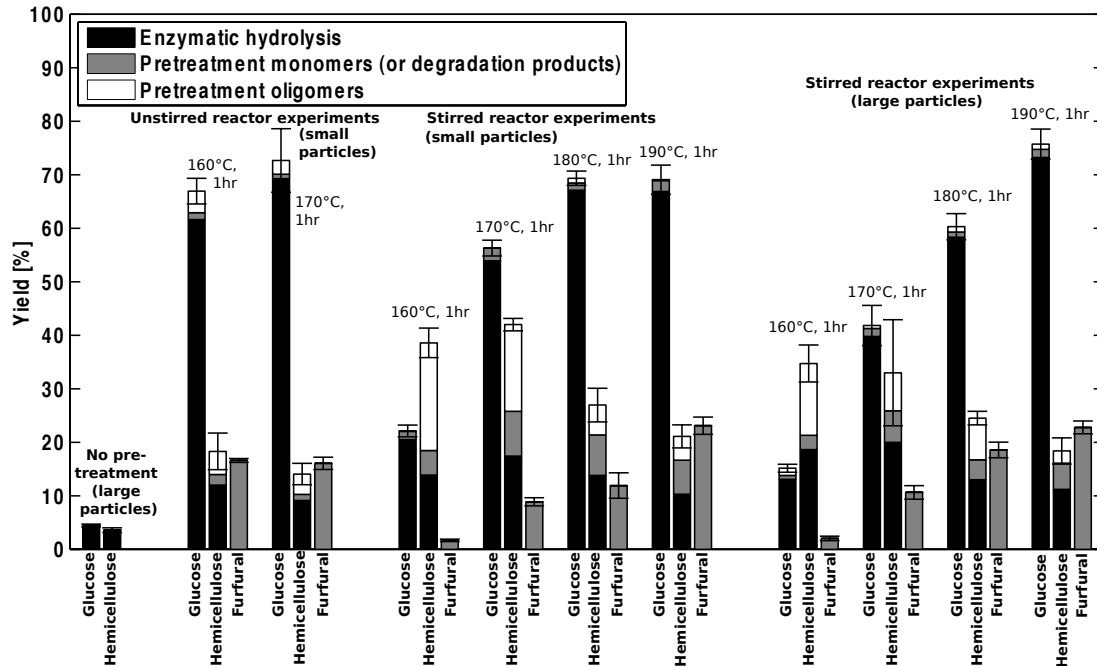


Fig. 5.2: Yields for single-temperature stage pretreatment of 40 wt% solids (water biomass mixture) mixed hardwood. All yields were obtained after pretreatment (unless no pretreatment is indicated) and 72 hr of enzymatic hydrolysis (15 FPU/gr glucan). Pretreatment was performed at 200 bar, while temperature and residence time are indicated above each set of yields. Bars represent glucan to glucose yields (indicated by *glucose*), xylan, arabinan and mannan to xylose, arabinose and mannose yields (indicated by *hemicellulose*) and xylan and arabinan to furfural yields (indicated by *furfural*). Error bars represent the results 95% confidence interval based on triplicate sampling. *Unstirred reactor experiments* designates results obtained in the small unstirred reactor and previously discussed in Chapter 4. *Stirred reactor experiments* designates results obtained in the 1 L stirred reactor. *Large particles* designates results obtained with large particles (<0.95 cm) *small particles* designates results obtained with small particles (<1 mm).

As discussed in Chapter 4, this difference in yields indicates the presence of temperature gradients in the unstirred system. These gradients lead to higher temperatures in certain areas of the reactor (which increases Y_g compared to the mixed system which has a more uniform temperature), but they also degrade hemicellulose sugars by creating hot spots within the reactor (which decreases

Y_h and increases Y_f compared to the mixed system). In addition, as shown in Chapter 4, a higher moisture content of 80 wt% (vs. 60 wt% here) led to a quicker drop in Y_g with pretreatment temperature. It was suggested that a drier substrate seemed to increase heat gradients and to “flatten” yield variations with temperature. An analogous phenomenon seems to be occurring here, except that gradients are reduced through mixing instead of by increased conductivity of the mixture. To obtain yields similar to those from unstirred reactor while using the 1 L stirred reactor, a temperature of 180°C or more had to be applied for 60 min, which may indicate that this is in fact the average temperature in the unstirred reactor. However, when comparing results from various pretreatment runs, it should be noted that throughout this work the estimated uncertainty (represented in Figure 5.2 by error bars equal to 95% confidence intervals) was estimated based on the variability obtained during enzymatic hydrolysis runs rather than through separate pretreatment runs. When experiments were repeated, pretreatment variability did not exceed that of enzymatic hydrolysis; however, error may be slightly underestimated for certain runs.

When larger particles (<0.95 cm) were pretreated in the stirred reactor, glucose yields were generally about 10 percentage points lower than those obtained for small particles (<1 mm) pretreated at identical conditions (see Figure 5.2). The only exception was for pretreatment at 190 for an hour, which yielded a Y_g of 76%. All hemicellulose sugar yields (Y_h) were lower for larger particles while furfural yields (Y_f) were roughly equivalent. Therefore, mass transfer limitations due to increased particle size seem to hinder yields, and higher temperatures are required to obtain yields similar to those obtained with smaller particles. Finally, it should be noted that pretreated hardwood can achieve dramatically superior glucan and hemicellulose conversion yields to that of untreated

hardwood (Y_g is 15 times and Y_h is 8-10 times superior).

Switchgrass pretreatment

The yields obtained in both the unstirred and stirred reactors with small or large switchgrass particles are presented in Figure 5.3. The use of the stirred reactor consistently led to lower Y_g values (by 10-15 percentage points) than for the unstirred reactor. However, Y_h values were generally higher except at 190°C. Again, this is attributed to the more uniform temperatures in the stirred system.

The Y_g values obtained with smaller particles pretreated in the stirred reactor increased quickly but quickly leveled off around 60%. However, with larger particles, Y_g values continually increased with temperature coming within 10 percentage points of those obtained with the unstirred reactor. Hemicellulose sugar yields (Y_h) initially increased with temperature until 170°C, after which they dramatically decreased with increasing temperature. An important increase in Y_h observed with the stirred compared to the unstirred reactor with a pretreatment of 170°C for 60 min (to 48% from 13%) further indicates the presence of temperature gradients. Furfural yields (Y_f) however, were either larger or identical to the unstirred reactor when the stirred reactor was used. Therefore, it seems that the absence of temperature gradients may have decreased the degradation of furfural itself or reduced other forms of hemicellulose degradation such as pyrolysis.

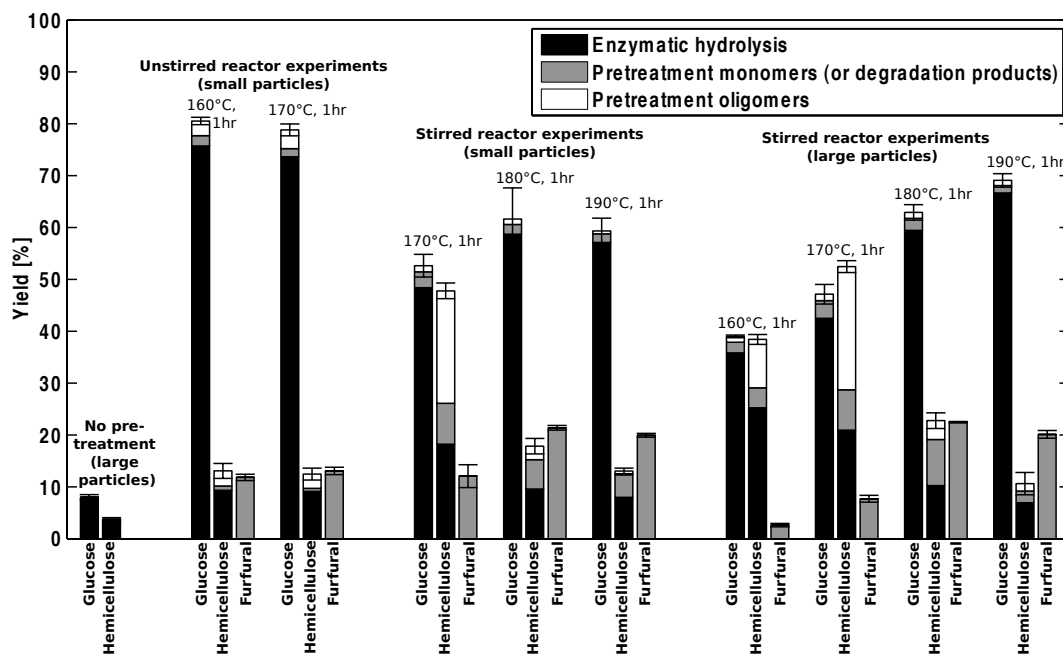


Fig. 5.3: Yields for single-temperature stage pretreatment of 40 wt% solids (water biomass mixture) switchgrass. All yields were obtained after pretreatment (unless no pretreatment is indicated) and 72 hr of enzymatic hydrolysis (15 FPU/g glucan). Pretreatment was performed at 200 bar, while temperature and residence time are indicated above each set of yields. Bars represent glucan to glucose yields (indicated by *glucose*), xylan, arabinan and mannan to xylose, arabinose and mannose yields (indicated by *hemicellulose*) and xylan and arabinan to furfural yields (indicated by *furfural*). Error bars represent the results 95% confidence interval based on triplicate sampling. *Unstirred reactor experiments* designates results obtained in the small unstirred reactor and previously discussed in Chapter 4. *Stirred reactor experiments* designates results obtained in the 1 L stirred reactor. *Large particles* designates results obtained with large particles (<0.95 cm) *small particles* designates results obtained with small particles (<1 mm).

5.3.2 Two-temperature stage results

Mixed hardwood pretreatment

Following the reasoning discussed in Section 5.1, two temperature stages were used in an attempt to increase Y_g and Y_h values. A short high-temperature stage was applied (200°C-210°C for 0-24 min, with 0 min representing just the heating phase) followed by a longer low-temperature stage (160-170°C for 60 min) to pretreat the large (<0.95 cm) hardwood particles. The results are shown in Figure 5.4.

Glucan to glucose yields consistently increased and plateaued once they reached a residence time of about 16 min (see Figure 5.4, A1, B1 and C1). The highest Y_g (83%) was obtained at 210°C for 16 min followed by 160°C for 60 min. Hemicellulose sugar yields (Y_h) varied more with retention time with a general trend showing a decrease in yield with increasing 1st stage residence time (see Figure 5.4, A2, B2 and C2). Higher Y_h values were obtained after 4 min at 200°C, 1 min at 200°C and 8 min at 210°C as shown in Figure 5.4, A2, B2 and C2, respectively, with the highest Y_h obtained at 200°C for 4 min and 160°C for 60 min. Thus, a lower 2nd stage temperature of 160°C yielded the highest Y_g and Y_h values. In contrast, Y_f values increased and then plateaued at 20% around 8 min of high-temperature pretreatment regardless of other parameters. Importantly, 5-HMF yields (Y_5) were insignificant for all runs, suggesting that very little hexose degradation occurred with staged heating.

Heating the mixture to 200°C did not have a measurable effect given that the yields for 200°C for 0 min and 160 or 170°C for 60 min were statistically identical (the two yields were well within their confidence intervals) to those obtained at

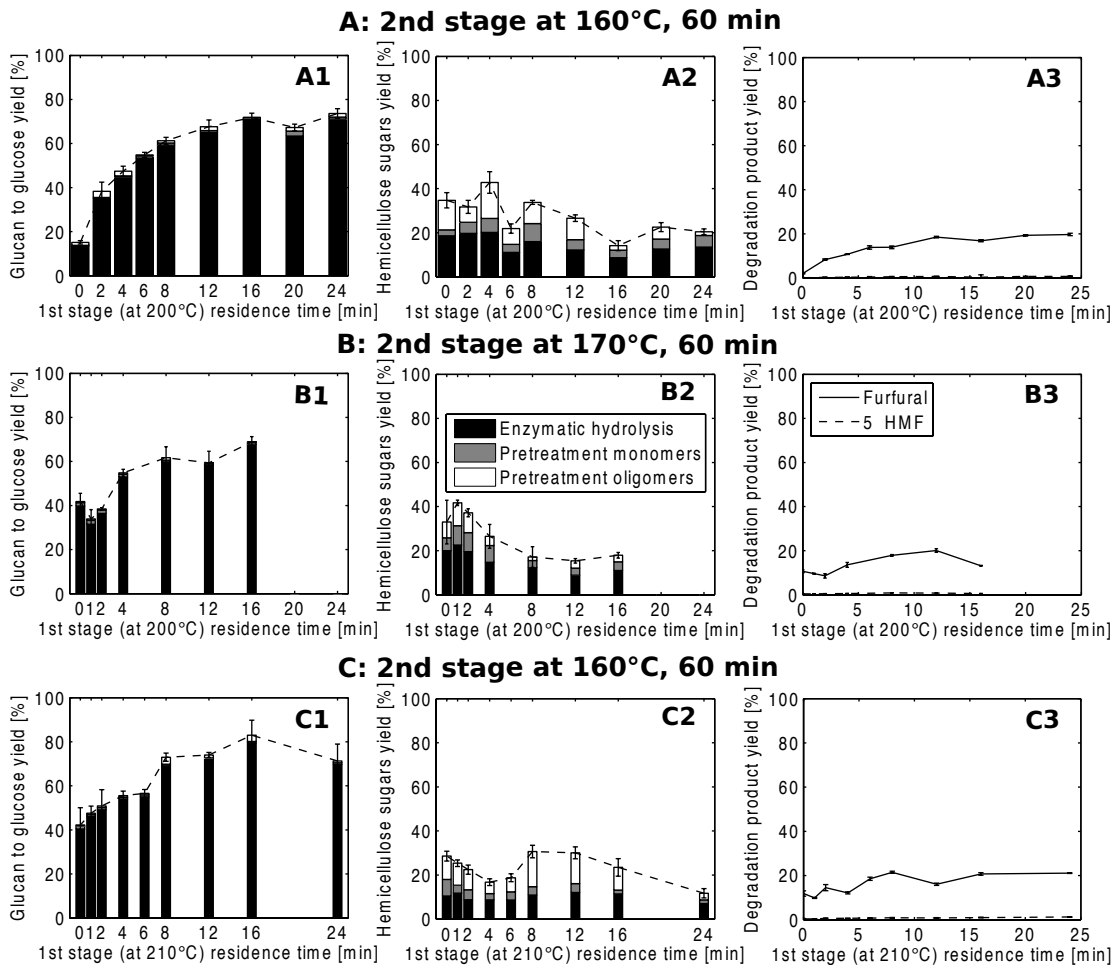


Fig. 5.4: Yields for two-temperature stage pretreatment of 40 wt% solids (water biomass mixture) large particle mixed hardwood. All yields were obtained after pretreatment and 72 hr of enzymatic hydrolysis (15 FPU/g glucan). Pretreatment was performed at 200 bar. Lines A and B present results obtained for pretreatments at 200°C for varying residence times with a 2nd stage at 160°C and 170°C for an hour, respectively. Line C presents results obtained for pretreatments at 210°C for varying residence times with a 2nd stage at 160°C for an hour. Column 1 shows glucan to glucose yields. Column 2 shows xylan, arabinan and mannan to xylose, arabinose and mannose yields. Column 3 shows degradation product yields (xylan and arabinan to furfural and glucan and mannan to 5-HMF). Error bars represent the results 95% confidence interval based on triplicate sampling.

160 and 170°C for 60 min (see Figure 5.4). Heating to 210°C had a much more significant effect (more than doubling Y_g and Y_f and significantly increasing Y_h). Yields obtained for 210°C, 0 min were more or less equivalent to yields for 200°C, 2-4 min (followed by 160°C for 60 min in both cases) which corresponds to the time spent at $200\pm 5^\circ\text{C}$ during the heating phase. Therefore, a couple of minutes spent above 195°C seems to have a much more significant effect than the 5-10 min spent between 150°C and 195°C (see heating curves in Appendix B). Following this initial optimization, further tests were done to determine the effects of modifying the temperature and residence time of the 2nd stage, but this failed to improve yields (see results in Appendix B).

Switchgrass pretreatment

Given the results for wood, the range of pretreatment conditions explored for switchgrass was reduced to a first stage at 210°C and a second stage at 160°C for 60 min. Results are given in Figure 5.5. Contrary to wood, the glucose yields for switchgrass were the highest at short residence times and rapidly decreased as pretreatment time was extended beyond 6 min (see Figure 5.5, 1). The maximum observed Y_g was 80% at 210°C for 1 min and 160°C for 60 min (statistically equivalent to the Y_g of 77% obtained at 210°C for 6 min). The heating stage to 210°C had a much more significant effect for switchgrass than it did for wood, given that a 50% increase of Y_g was observed when comparing results for 210°C, 0 min and 160°C for 60 min with 160°C for 60 min (see Figure 5.3).

Similar to the results obtained for hardwood, hemicellulose sugar yields (Y_h) had a varied response with changing high-temperature stage residence times (see Figure 5.5, 2). Yields of 42 and 27% were obtained after 0 and 4 min at

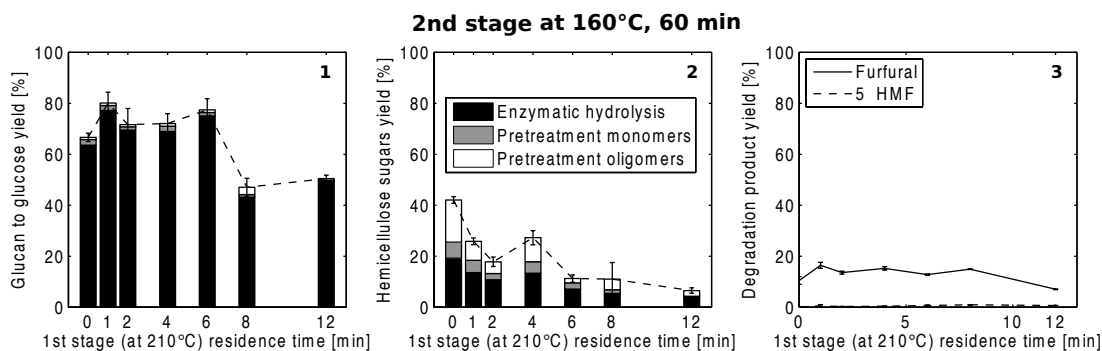


Fig. 5.5: Yields for two-temperature stage pretreatment of 40 wt% solids (water biomass mixture) large particle switchgrass. All yields were obtained after pretreatment and 72 hr of enzymatic hydrolysis (15 FPU/g glucan). Pretreatment was performed at 200 bar with a first stage at 210°C for varying residence times and a 2nd stage at 160°C for an hour. Column 1 shows glucan to glucose yields. Column 2 shows xylan, arabinan and mannan to xylose, arabinose and mannose yields. Column 3 shows degradation product yields (xylan and arabinan to furfural and glucan and mannan to 5-HMF). Error bars represent the results 95% confidence interval based on triplicate sampling.

210°C and 160°C for 60 min, respectively. Furfural yields rapidly increased to about 15% after 1 min at 210°C and remained stable until 12 min, after which they decreased (indicating possible furfural degradation). As with hardwood, further tests were done to determine the effects of modifying the temperature and residence time of the 2nd stage. Once again, these changes did not further improve yields as reported in Appendix B.

5.3.3 Tradeoff between Glucose and Hemicellulose sugar yields

Total molar sugar yields (Y_T) are given in Figure 5.6 for high-yield experiments using both single or dual temperature stages and for both mixed hardwood or

switchgrass. However, treating hemicellulose sugars and glucose equivalently (on a molar basis), though theoretically straightforward, does not necessarily reflect their true relative value. Indeed, microorganisms tend to favor glucose over hemicellulose sugar consumption and thus fermentation of the latter sugars is usually less productive [271].

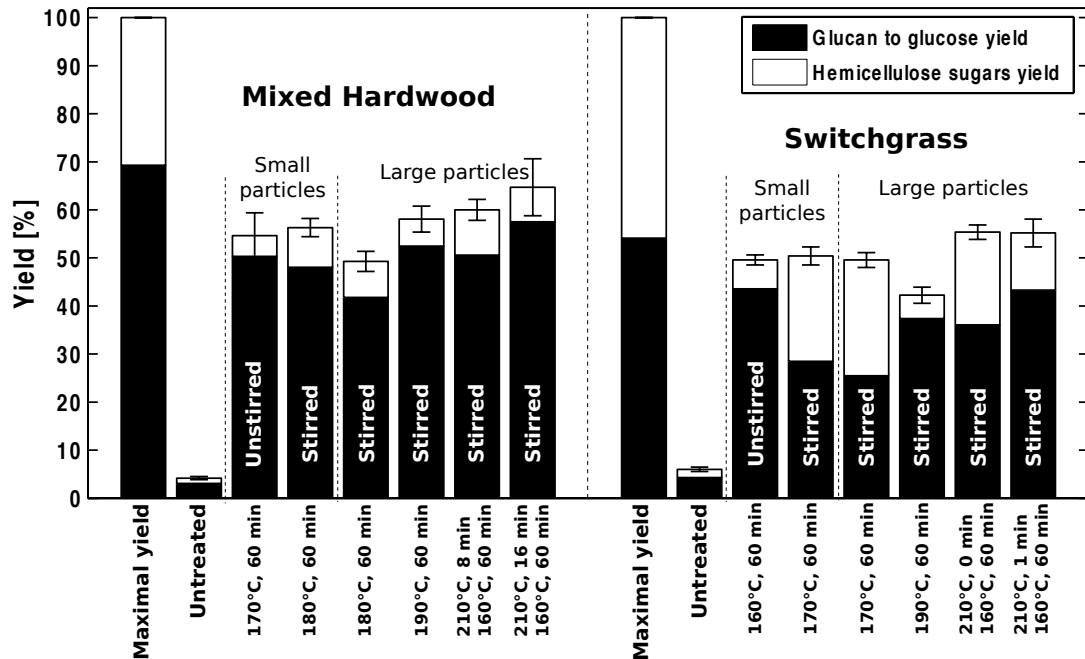


Fig. 5.6: Total molar sugar yields (Y_T) for two-temperature stage pretreatment of 40 wt% solids (water biomass mixture) mixed hardwood (left section) and switchgrass (right section). Error bars represent the results 95% confidence interval based on triplicate sampling. All yields were obtained after pretreatment at 200 bar (unless labeled as *untreated*, in which case no pretreatment was performed) and 72 hr of enzymatic hydrolysis (15 FPU/g glucan). Maximal yield shows the breakdown of the total yield if both glucan to glucose (Y_g) and hemicellulose sugars yield (Y_h) is equal to 100%.

The highest overall sugar yield was 65% for wood (at 210°C 16 min and 160°C, 60 min) and 55% for switchgrass (at 210°C, both 0 and 1 min and 160°C, 60 min). All single temperature stage yields presented in Figure 5.6 illustrate the difficulty of simultaneously obtaining high glucan and high hemicellulose sug-

ars yield. For wood, Y_h decreases from 180°C to 190°C while Y_g increases; and for switchgrass, Y_h drastically decreases from 170°C to 190°C while Y_g drastically increases a trend that persisted but became less pronounced when using a two-temperature stage process. Indeed, the fact that the two-temperature yields presented in Figure 5.5 are systematically lower than their single-stage counterparts is largely due to the fact that for equivalent or higher Y_g values they can achieve higher Y_h values. This confirms the hypothesized benefits of two-stage processing on hemicellulose degradation described in the Introduction.

5.3.4 Comparison to other pretreatment processes

For a 40 wt% solids mixture of large particles (<0.95 cm) of mixed hardwood, a Y_g of $83 \pm 3\%$ was obtained with a pretreatment temperature of 210°C for 16 min and 160°C for 60 min. These were 10% higher than those obtained by Kim and Hong with Aspen wood using water and CO₂-water mixtures at 165°C for 60 min [249]. Most other technologies reporting similar yields use chemical catalysts. Poplar pretreated with catalyzed steam explosion (3 wt% SO₂, 200°C, 5 min, from a personal communication with Bura: 8-15% solid content), could reach glucose yields around 100% [174]. Dilute acid pretreatment of poplar (2 wt% H₂SO₄, 190°C, 1.1 min) led to a glucose yield of 83% [212]. McMillan et al. reported a similar yield for poplar in the same pilot reactor with a solid content of 15 wt% [246]. Those pretreated poplar particles went through a 1/4 in screen (0.64 cm) and were thus slightly smaller than those used in this work. Lime pretreatment (140-160°C, 120 min) reached glucose yields close to 100% despite a 40 wt% solids loading but necessitated the use of 20 wt% lime [212]. Therefore, in other technologies, successful pretreatment of hardwood is systematically

carried out at fairly low solids and/or with high chemical catalyst loadings.

For 40 wt% solids switchgrass, Y_g values of $80 \pm 1\%$ were obtained with a pretreatment at 210°C, 1 min and 160°C, 60 min. Similar yields were obtained when Guayule bagasse was pretreated in water-CO₂ mixture (40 wt% solids as well and a particle size <2 mm) at 200°C for 20 min to obtain glucose yields of 77% [265]. In comparison, yields of 91% were obtained for switchgrass pretreated with dilute sulfuric acid (180°C, 0.5 min, 1.2% H₂SO₄, solids content and particle size not reported) [262]. Ammonia fiber explosion pretreatment gave glucose yields of 93% for switchgrass (100°C, 5 min, 20 wt% solids, particle size not reported) [201]. Finally, steam exploded wheat straw (195°C, 6 min, 23-28 wt% solids, 6-10 cm long) gave a 90% glucose yield [244]. Therefore, interesting yields can be obtained for grasses with and without chemical catalyst addition. However, so far successful pretreatment above 30 wt% solids has not been presented elsewhere.

5.4 Conclusions and outlook

Using a stirred reactor to study CO₂-H₂O pretreatment of lignocellulosic biomass allowed exploring the effect of using larger particles and the effect of mixing, which had not been done for similar systems. Using two temperature stages, the hypothesized benefits of using a range of temperatures during pretreatment was confirmed. Two-temperature stage pretreatment was introduced to obtain glucan to glucose conversion yields of 83% for mixed hardwood and 80% for switchgrass. These yields were similar to those obtained with dilute acid pretreatment for wood (a major technology for wood conversion) and

within 10% of major technologies for switchgrass despite the absence of chemical catalysts, the use of larger particles and the significantly higher solid content (40 wt%). This high solids processing along with the shorter residence times at higher temperatures used in the staged approach could reduce equipment capital costs by allowing smaller reactor volumes to be used. However, for this technology to be attractive, all these benefits must outweigh the issue of lower xylose recovery and higher equipment capital costs linked with high-pressure processing.

CHAPTER 6

**PRODUCING CONCENTRATED SOLUTIONS OF MONOSACCHARIDES
USING BIPHASIC CO₂-H₂O MIXTURES**

Large portions of this Chapter have appeared as a published manuscript in the Journal *Energy & Environmental Science* [272].

6.1 Introduction

The successful implementation of a number of biomass to biofuels or biomaterials conversion processes hinges on the development of a robust biomass saccharification platform that can yield low-cost sugars. In particular, as discussed in previous chapters, sustainably and economically producing concentrated solutions of monosaccharides remains a key hurdle for such processes (i.e. obtaining sugars without overwhelming energetic, chemical and/or monetary inputs). In yeast fermentation, which is used in various biofuel production processes and notably in bioethanol production, it is often desirable to have high sugar concentrations to drive high rates and extents of product formation, increase volumetric productivity and lower subsequent product separation costs [225, 273, 274]. Indeed, typical starch or sugar concentrations used in the bio-ethanol industry range from 20 to 30 wt% , which allows the production of ethanol solutions of 10 to 17 % v/v [225, 273], without which the additional cost of distillation and larger equipment size would be prohibitive. In addition, thermal conversion efficiency and overall process sustainability of similar biomass to fuel conversion technologies have been shown to be highly influenced by initial solid contents [222]. Similarly, the conversion of sugars to dimethyl-furan, a proposed biofuel, begins with the dehydration of 30 wt% solutions of fructose and lower feed

concentration would inevitably lead to lower energetic efficiency and higher processing costs [28].

As discussed in previous chapters, different media used in biomass pretreatment for monosaccharide production have included acid or base solutions, pure water at high-temperatures or mixtures of various solvents such as ammonia, carbon dioxide and/or ionic liquids [201, 202, 173, 251, 232, 160, 275, 211, 212, 102, 249]. However, most of these studies employ a dilute pretreatment stage (<20 wt%) followed by the enzymatic hydrolysis of the washed solids at 1-3 wt% solids.

Kristensen et al. reviewed a number of high-solids enzymatic hydrolysis studies performed with air-dried pretreated biomass [227]. Their review reported that observed glucose yields were below 50% for high solids enzymatic hydrolysis carried out at or above 30 wt% solids. One of the reviewed studies, by Jorgensen et al., used a drum with a rotating shaft and paddles to hydrolyze air dried pretreated biomass at solid contents up to 40 wt% [244]. They observed decreasing glucose yields from 90 to 40% as saccharification's initial solids content was increased from 2 to 40 wt% . The factors leading to these lower yields at high solid contents were identified as increased mass transfer limitations due to the increase in viscosity of the mixture and enzyme inhibition. This inhibition was attributed to lignin [228], lignin derivatives (notably tannic acid) [276], oligo- and monosaccharide products [277] and pretreatment degradation products [229]. Substrate washing can help overcome some of these issues by removing solubilized lignin derivatives and pretreatment by-products; but such a step would add significant amounts of water to the process reducing any advantage gained from high-solids processing.

Only a single study involving dilute acid pretreated corn stover was able to successfully carry out enzymatic hydrolysis with solid loadings up to 30 wt% without drying the pretreated substrate [278]. This led to glucose yields of 40 to 60% after 48 hr and 60 to 90% after 168 hr of hydrolysis depending on the enzyme loading. However, such pretreatment experiments typically require the use of 2-3 kg of sulfuric acid (assuming a 1-2 wt% acid solution) and roughly equivalent molar amounts of sodium hydroxide (for neutralization) for every 100 kg of biomass [278, 245].

In Chapter 4, it was demonstrated that CO₂-H₂O mixtures at high pressures (100-200 bar) are an interesting alternative to dilute acid solutions and other biomass pretreatment media, especially for high-solids pretreatment. Using a small (25 ml) unstirred reactor, temperatures between 150 and 250°C were explored with a single pretreatment stage at 40 wt% solids. Glucan to glucose yields of 73% for wood, 81% for switchgrass and 85% for corn stover were obtained under very similar experimental conditions (160 or 170°C and a 60 min residence time) and with no additional chemicals.

In this work, a two-temperature stage approach was used to take advantage of biomass's presumed temperature dependent depolymerization reaction sequence. Hemicellulose depolymerization occurs rapidly during pretreatment to produce oligomers. These oligomers further depolymerize to monomers that can degrade to unwanted byproducts such as furfural [154, 149, 150]. Because these reactions occur in sequence, furfural production lags behind that of oligo- and monosaccharides. This has been documented in the modeling and experimental results obtained by Mittal et al. for maple and Aspen wood pretreated in water at 175°C [150]. Because of this sequence, a short high-temperature pre-

treatment stage (i.e. minutes at 200-210°C) could take advantage of this lag, while a subsequent longer low-temperature pretreatment (i.e. 0.5-1 hour at 160-180°C) stage could pursue pretreatment at a temperature at which monomer degradation is less pronounced. According to a recent review of the literature search, this 2-stage pretreatment system has not yet been attempted. However, several studies have used a reversed approach: a low temperature pretreatment step is used to extract the hemicellulose fraction that is then separated by washing [266, 267, 268, 279]. The leftover solids are then subjected to a high temperature pretreatment step to increase cellulose digestibility. This alternative approach is successful at increasing hemicellulose yields and decreasing the formation of unwanted by-products while maintaining high glucose yields. However, a separation and washing step is necessary and is present in all of the aforementioned studies. Separation and dewatering through a filter press is difficult beyond 20 wt% solids and can collapse biomass pores, which decreases enzymatic hydrolysis yields [266, 280]. Furthermore, this washing step would add significantly to the amount of water carried through the process resulting in an overall low-solids approach.

In Chapter 5, it was demonstrated that, contrary to results obtained using a single temperature stage, using two temperature stages simultaneously increased cellulose and hemicellulose conversion yields without increasing furfural production. In addition, the optimal pretreatment conditions for the proposed two-temperature stage approach was determined. The resulting yields at these optimal pretreatment conditions are presented in Table 6.1 and discussed in Section 6.3.1. During the optimization, a standardized, high-throughput dilute enzymatic hydrolysis assay of the washed pretreatment solids was used (1 wt% glucan, 1-2 wt% solids, following a methodology proposed by the Na-

tional Renewable Energy Laboratory [270]) to assess the potential monosaccharide yield of the resulting biomass. In this work, unwashed pretreatment solids were used to study high solids enzymatic hydrolysis. As demonstrated by the results presented here, dilute washed hydrolysis yields correlated well with yields from unwashed biomass, making the optimization relevant to this work.

Therefore, the effect of using unwashed pretreatment solids and of varying the enzymatic hydrolysis solid content on the temporal extent of hydrolysis was explored. Optimally pretreated mixed hardwood and switchgrass were used in this work. A custom-built “rotating drum high-solids enzymatic hydrolysis system was used for the saccharification of these pretreatment solids, which could accommodate up to twelve separate rotating drum reactors.

6.2 Material and Methods

6.2.1 Biomass: species and analysis

Field dried (moisture content: 9-12 wt%) mixed hardwood (obtained from MESA® inc., Auburn, NY, harvested in NY, 2007) and sunburst switchgrass (harvested near Ithaca, NY in fall 2009). The biomass was size reduced in a hammermill (Schutte Buffalo LLC, Buffalo, NY) with a 3/8” (0.95 cm) screen. The resulting particles were used in all experiments. Biomass was analyzed for neutral detergent fibers (NDF), acid detergent fibers (ADF), acid detergent lignin (Lignin), glucan, xylan, arabinan and mannan (galactan is neglected) and results are given in Table 4.1. Biomass moisture and dry matter content was de-

terminated by weighing it before and after its drying in an oven at 105°C for 12 hr and in a desiccator for 5 hr.

6.2.2 Two-temperature stage biphasic CO₂-H₂O pretreatment

Deionized water was mixed with biomass particles to obtain a 40 wt% solids mixture. Following this, 150 g of the resulting slurry (60 g of dry matter and 90 g of water) was loaded into a 1 L stirred reactor (see Figure 6.1, Part A). Air was purged from the reactor by pressurizing and venting it 5 times with 20 bar of CO₂. The reactor was then filled with liquid CO₂ resulting in a pressure of about 60 bar. The reactor was heated with an electric heating jacket resulting in a rapid increase in pressure. The reactor pressure was maintained at 200 ±10 bar with a backpressure regulator (BPR). Reported residence times refer to the time at which the reactor was within 5°C of the target temperature. The first pretreatment stage was ended by flowing water through a cooling coil located within the reactor, bringing the reactor to room temperature. Additional liquid CO₂ was then pumped into the reactor up to 60 bar to compensate for CO₂ vented during the first stage. The reactor was then heated to the 2nd stage's target temperature and stopped as it was for the first stage. Optimal pretreatment conditions were used (see Table 6.1): mixed hardwood was pretreated at 210°C for 16 min followed by 160°C for 60 min and switchgrass was pretreated at 210°C for 1 min followed by 160°C for 60 min.

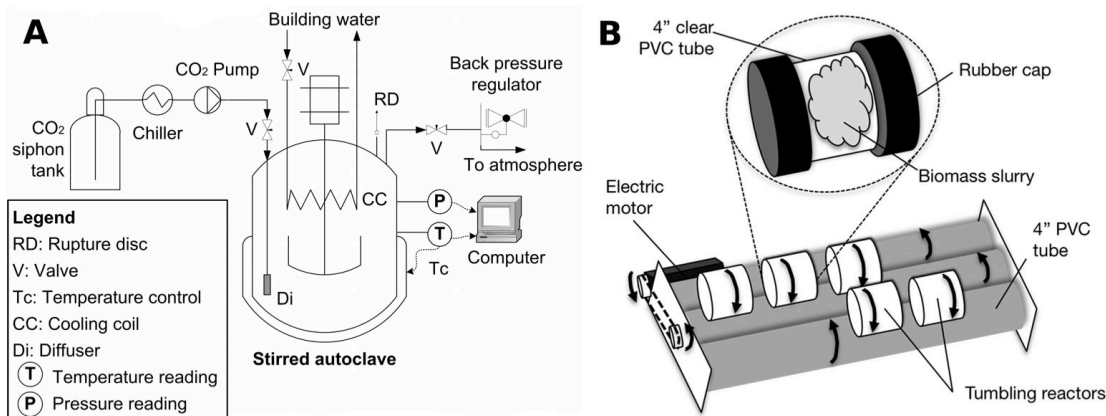


Fig. 6.1: High-solids biomass conversion setup. Part A shows the pretreatment reactor which is described in detail in Chapter 5. A stirred high-pressure stainless-steel vessel (system obtained from Autoclave Engineers®, Erie, Pa) was hooked up to a CO₂ injection system consisting of a siphon tank and a CO₂ pump (Thar® Process, Pittsburg, Pa) hooked up to a chiller (Thermo-Fisher® Scientific, Waltham, Ma) to avoid CO₂ phase change during compression. Pressure was controlled with a backpressure regulator (BPR, Tescom®, Elk River, Mn). Part B shows the high-solids enzymatic hydrolysis reaction system. The “rotating drum” reactors were custom built using 4” segments of 4” schedule 40 clear PVC pipe and rubber caps (Fernco, Davison, MI). For each reactor, one cap was glued using silicon sealant and the other was left unattached to allow access to the reactor. During an experiment, vacuum grease was applied inside the movable rubber caps to improve the seal while the reactors were maintained shut with rubber bands. The roller setup consisted of three 30” segments of 4” schedule 40 opaque PVC pipe mounted to a custom-built stainless steel frame using ball bearings. The central roller was rotated at 30 rpm by a fixed speed electric motor (Bodine, Chicago, IL) using a chain and gear setup, while the other two rolled freely.

6.2.3 High-solids enzymatic hydrolysis

Unmodified pretreatment mixtures obtained after pretreatment were used in all experiments. Unless otherwise specified, solid content refers to the original solids content prior to pretreatment. For 5 and 10 wt% solids experiments, 20 g of total solution was hydrolyzed in agitated 50 ml tubes with 0.5 M sodium

citrate buffer (pH 4.8), 30 mg/L of Cyclohexamide and 40 mg/L of Tetracycline to prevent growth and sugar consumption. The samples were centrifuged and the supernatant was sampled after 4, 24, 48 and 72 hr of hydrolysis. Each experiment was run in triplicate.

For experiments of 15 wt% solids or more, 112.5 g of wet pretreated material (45 g of original dry solids prior to pretreatment) were loaded into a 0.77 L rotating drum reactor. This setup required significantly less pretreated biomass per reactor than the setup proposed by Jorgensen et al. (45 g vs. 3 kg or more) and can accommodate more simultaneous reactions (12 vs. 5 reactors) while still achieving thorough mixing using the rotating drum configuration [244]. A schematic and general description of the reaction system is given in Figure 6.1, part B. Up to twelve rotating drum reactors fit on this system at the same time. It is a simple, low cost system made with inexpensive piping material and a motor. A picture of the entire setup along with a couple of reactors is available in Appendix C.

To prevent growth and consumption of sugars, 1 mg/(g of initial dry solids) of Cyclohexamide and Tetracycline were added to the mixture. Sodium carbonate (Na_2CO_3) was added until the pH of the slurry was approximately 4.8. The exact amount was determined by titrating a 10 wt% solids aqueous solution of pretreated biomass with Na_2CO_3 until the appropriate pH was reached (this amount ranged from 30 to 40 mg/g initial dry biomass). The pH remained relatively constant and within optimal values for cellulase activity during the course of the experiment (between 4.6 and 4.9). Approximately 1 g of the reaction slurry was sampled in triplicate at 4, 24, 48 and 72 hr (the error estimated from sampling a single reactor three times was statistically equivalent to sam-

pling three different reactors once, see Section C.2 in Appendix C). These samples were diluted by the addition of 10 ml of water and the resulting liquid was sampled for hydrolysate analysis (see below). Any reactions occurring in this diluted solution were quenched by heating the samples at 95°C for 5 min in a micro-plate heating block to denature the enzymes.

Unless otherwise specified, all reactions were run at 50°C with 7.5 FPU/(g initial solids) of spezyme CP® cellulases, 15 (mg protein)/ (g initial solids) of Multifect® xylanase (Genecor, Copenhagen, DK) and 15 CBU/(g initial solids) of Novo188® β -glucosidase (Novozyme, Davis, Ca). Cellulase loadings were set with respect to total solids to be consistent with most high-solids enzymatic hydrolysis studies [244, 227, 281]. However, they can easily be translated into loadings based on initial glucan content (17.5 FPU/(g glucan) for wood and 25 FPU/(g glucan) for switchgrass). Studies have shown that xylanase supplementation can moderately improve hemicellulose sugar and glucose yields for acidic and pure water pretreatment and can greatly improve these yields for alkaline pretreatments [160, 172, 282]. To take advantage of the moderate increase in overall monosaccharide yields, xylanase is added to the reaction solution (by analogy with work by Wyman et al., a comparable protein mass of xylanase to cellulase protein mass was added [212]). Temperature was controlled by placing the shaking flacon tubes or the “rotating drum reactor in an Innova® incubator (New Brunswick Scientific, Edison, NJ) as illustrated in Figure C.1 of the Appendix C.

6.2.4 Liquid analysis and yield calculations

Hydrolysate samples were analyzed for glucose, xylose, mannose, arabinose, furfural and 5-hydroxymethylfurfural (5-HMF) using liquid chromatography as described in Chapter 4. Yields were calculated based on concentrations of glucose, xylose, mannose, arabinose, 5-HMF and furfural measured after enzymatic hydrolysis. They represent the molar percentage of the maximal possible output of the product of interest. The details of the yield calculations have been reported in Chapter 5.

6.3 Results and Discussion

6.3.1 Optimal pretreatment results

The optimal pretreatment conditions and their associated yields are given in Table 6.1. Glucan to glucose conversion yields of 83% for mixed hardwood and 80% for switchgrass were obtained after treatment at 210°C for 16 min and 1 min, respectively, followed in both cases by a stage at 160°C for 60 min. The longer residence time required for wood compared to switchgrass during the initial stage reflects the increased pretreatment intensity that is often required for hardwood. Bura et al. were only able to obtain yields above 90% for wood using steam explosion at 200°C for 5 min after impregnation with 3% SO₂, while similar yields were obtained for corn stover after treatment using only pure steam at 190°C for 5 min [174]. Ammonia fiber explosion (AFEX) pretreatment of switchgrass gave glucose yields of 93% after treatment at 100°C for 5 min but

a treatment at 180°C for 30 min was required to reach glucose yields of 73% for poplar at similar enzyme loadings [201, 202].

The total molar sugar yields, corresponding to the molar addition of glucose and hemicellulose sugar yields, were about 10 percentage points above those obtained with a single temperature stage (see Chapter 4 and 5), despite a 10-fold increase in particle size (0.95 cm vs. 1 mm). This demonstrated the advantage of the two-temperature stage approach. The hardwood yields obtained here compare favorably to the 6 technologies used to pretreat and convert poplar (using identical cellulase loadings to ours) recently reviewed by the Consortium for Applied Fundamentals and Innovation (CAFI) [212]. The glucose yield obtained after dilute acid treatment is around 80% which is equivalent to ours and is higher than the yields obtained for AFEX, ammonia recycle percolation (ARP) and controlled pH (i.e. hot water) pretreatment. Both steam explosion with SO₂ impregnation and high temperature lime pretreatment obtain glucose yields close to 100%. For switchgrass, glucose yields of 93% and 91% are obtained with AFEX and dilute acid pretreatment, respectively [201, 262]. The hemicellulose sugar recovery presented here is generally lower than that of most aforementioned pretreatment studies. This difference in yield cannot be explained by degradation product formation alone, which only accounts for 20% of hemicellulose sugars. In Chapter 4, it was hypothesized that hemicellulose could undergo pyrolysis in low moisture environments potentially lowering yields. Therefore, two-stage biphasic CO₂-H₂O pretreatment can obtain yields within about 10% of major pretreatment technologies, despite the use of high solid loading (40 wt%) and the absence of additional chemical catalysts.

Table 6.1: Optimal pretreatment conditions and their associated yields. Yields were obtained after pretreatment and enzymatic hydrolysis of the washed solids (at 1 wt% glucan or 2 wt% solids) according to the NREL methods described by Selig et al. [270]. An NREL assay was used to determine oligomers [269]. Yield measurements are provided with a range representing their 95% confidence interval. These yields were the optimal results obtained in Chapter 5.

	Optimal pretreatment conditions	Hemicellulose sugar yield [%]			Furfural yield [%]	Glucan to glucose yield [%]				
	1 st stage	2 nd stage	Oligomers from pre-treatment	Monosaccharides from pre-treatment	Monosaccharides from enzymatic hydrolysis	Total	Oligomers from pre-treatment	Monosaccharides from enzymatic hydrolysis	Total	
Mixed Hard-wood	210°C 16 min	160°C 60 min	10±1	2±0.3	11±0.7	23±2	2.9±0.3	0.6±0.1	79±6	83±7
Switch-grass	210°C 1 min	160°C 60 min	8±0.6	5±0.5	13±1	26±2	1±0.1	2±0.2	77±4	80±4

6.3.2 High-solids enzymatic hydrolysis

Mixed hardwood

Temporal glucan to glucose and hemicellulose sugar yields are shown for different mixed hardwood initial solids contents in Figure 6.2. For comparison purposes, the hydrolysis results as a function of time for washed solids (1 wt% glucan) reported in Table 6.1 are shown as well. In the case of glucan to glucose yields (Figure 6.2, part A), a maximum yield of about 80% was rapidly reached with washed solids while the yields obtained with unwashed solids and higher solid content increased more slowly. This could indicate enzyme inhibition by the pretreatment byproducts or increased mass transfer limitations as has been suggested in the literature [227, 276]. The 10 and 20 wt% experiments showed a statistically equivalent (the two average measurements were within each others confidence intervals) progression of yield with time; however, yields for 30 wt% solids were not only lower, but also showed a more linear and less logarithmic temporal response. This could be due to increased mass transfer limitation, as increasing solids content creates more viscous solutions and decreases the amount of free liquid that is present. Additionally, the concentrations of lignin derivatives, pretreatment byproducts and of monosaccharides produced by enzymatic hydrolysis increase significantly with solids content, all of which have been suggested as possible inhibitors of enzymatic activity [227, 229, 277, 276, 283]. Furthermore, the final yields for unwashed solids were always lower than those for washed solids, further indicating possible enzyme inhibition or mass-transfer limitations. Indeed, the absence of pretreatment byproducts and the lower solid content could lead to less enzyme inhibition over time for washed solids. Simultaneously, increased mass transfer limitations in

the high-solids system could have slowed down enzymatic hydrolysis reducing the amount of sugars liberated before product inhibition became significant.

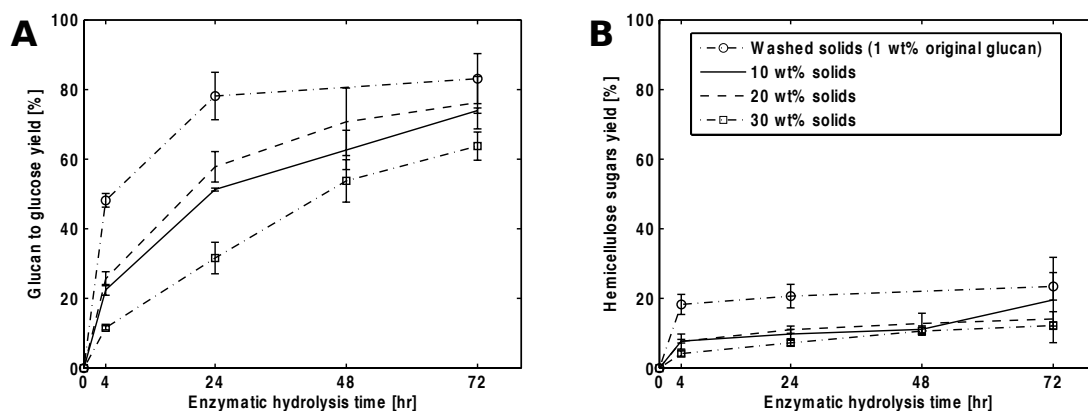


Fig. 6.2: Temporal glucan to glucose (part A) and hemicellulose sugar (xylan, arabinan and mannan to xylose, arabinose and mannose) (part B) yields for optimally two-temperature stage $\text{CO}_2\text{-H}_2\text{O}$ pretreated mixed hardwood (210°C , 16 min and 160°C , 60 min) for different initial solids contents (before pretreatment). Washed solids results correspond to the yields obtained from the enzymatic hydrolysis of the washed solids (see Table 6.1). All other results (10, 20 and 30 wt% solids) were obtained using unmodified pretreatment mixtures for enzymatic hydrolysis. Error bars represent the results 95% confidence interval based on triplicate sampling.

Hemicellulose sugar yields always reached a large fraction of their maximum yield after 4 hr, primarily because about half of the maximum potential hemicellulose sugar yield was generated during pretreatment (see Table 6.1). Yields of all unwashed experiments were lower than that obtained for washed solids, indicating possible xylanase inhibition by pretreatment by-products.

The effects of pH control (addition or absence of sodium carbonate) and of doubling the amount of loaded cellulase activity (from 7.5 FPU/(g solids) to 15 FPU/(g solids), with β -glucosidase and xylanase activity kept constant) were explored for enzymatic hydrolysis at 30 wt% solids. Temporal glucan to glucose and hemicellulose sugar yields are shown in Figure 6.3. In the absence

of sodium carbonate, the pH remains below 4 (typically 3.3-3.8 depending on the pretreatment run and based on measurements with a 10% solids mixture). This lower pH seems to completely inactivate enzymatic activity since the glucan to glucose and hemicellulose sugar yield correspond to the yields of soluble carbohydrate obtained after pretreatment (see Table 6.1). In contrast, doubling the cellulase activity increases the rate and extent of hydrolysis for both sugar yields. The maximal glucose yield is reached after 48 hr (as opposed to 72 hr for the lower cellulase activity). Furthermore, with an increased cellulase content, the initial hydrolysis rate was much faster, with the curve shape more logarithmic than linear as opposed to the 7.5 FPU/(g solids) experiments. The evolution of hemicellulose yields with time shows a similar pattern despite the fact that the xylanase content was constant throughout these two experiments. This trend indicates that an increase in glucan hydrolysis by cellulases may increase accessibility to hemicellulose, increasing its extent of hydrolysis.

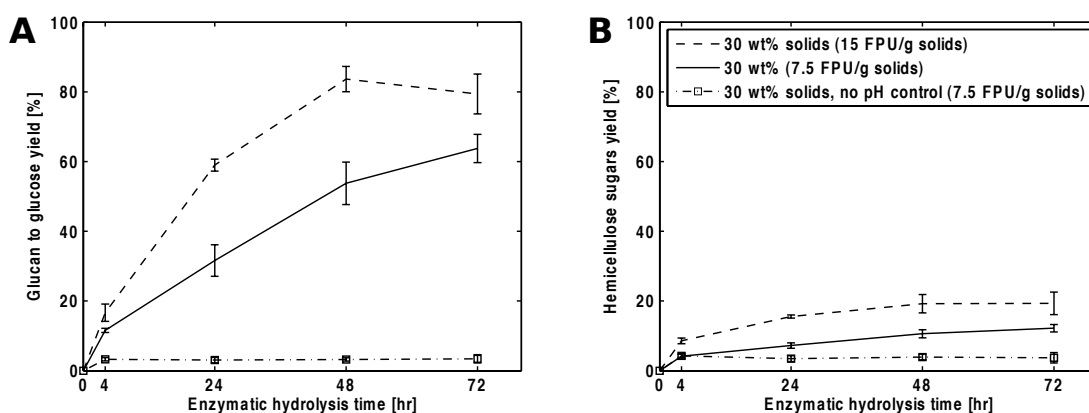


Fig. 6.3: Temporal glucan to glucose (part A) and hemicellulose sugar (xylan, arabinan and mannan to xylose, arabinose and mannose) (part B) yields for optimally two-temperature stage CO₂-H₂O pretreated mixed hardwood (210°C, 16 min and 160°C, 60 min) for 30 wt% of initial solids content (before pretreatment) and varying enzyme and sodium carbonate loadings. Experiments for which no sodium carbonate was added are indicated by *no pH control*. Error bars represent the results 95% confidence interval based on triplicate sampling.

Switchgrass

Glucan to glucose and hemicellulose sugar yields are shown for different switchgrass initial solid contents in Figure 6.4. Once again, glucan to glucose yields were higher for washed solids than for unwashed solids at higher solids contents. However, most yields are within their respective 95% confidence intervals. This could have been due to higher pretreatment byproducts concentrations, higher sugar concentrations and high solid contents (see Figure 6.4, part A). Similar to the results obtained with hardwood, most of the hemicellulose sugar yield was obtained after 4 hr of hydrolysis (see Figure 6.4, part B). Unwashed experiments systematically showed a slightly higher hemicellulose sugar yield than the washed solids experiment due to more sugars being released during enzymatic hydrolysis (though this difference was often within the yields' confidence interval). This could be due to xylanase inhibition, which has been shown to occur in similar ways to cellulase inhibition in the presence of lignin [283]. Just as xylanase can increase cellulose conversion, cellulases increase xylan conversion. Thus, the aforementioned cellulase inhibition could also negatively effect hemicellulose conversion. The absence of a decrease in yield with increasing solids concentration could be due to the increase in xylanase concentration that accompanies the increase in solids content (due to the constant enzyme to solids content ratio). The fact that the highest hemicellulose sugar yield is obtained for 30 wt% solids strengthens this hypothesis.

As shown on Figure 6.5, unlike the results observed with hardwood, some enzymatic activity was maintained in the absence of pH control, with the yields exceeding those attributable to the soluble oligosaccharides produced during pretreatment (see Table 6.1). Doubling the cellulase activity increased the rate

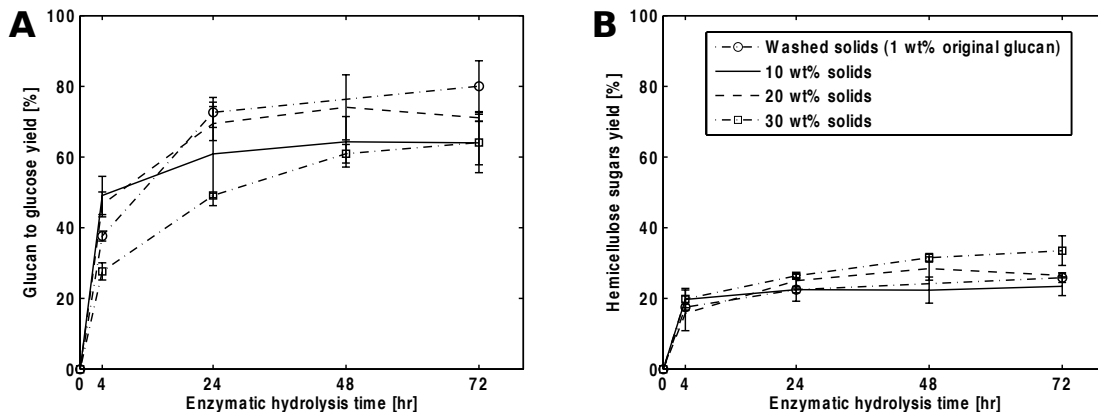


Fig. 6.4: Temporal glucan to glucose (part A) and hemicellulose sugar (xylan, arabinan and mannan to xylose, arabinose and mannose) (part B) yields for optimally two-temperature stage $\text{CO}_2\text{-H}_2\text{O}$ pretreated switchgrass (210°C , 1 min and 160°C , 60 min) for different initial solids contents (before pretreatment). Washed solids results correspond to the yields obtained from the enzymatic hydrolysis of the washed solids (see Table 6.1). All other results (10, 20 and 30 wt% solids) were obtained using unmodified pretreatment mixtures for enzymatic hydrolysis. Error bars represent the results 95% confidence interval based on triplicate sampling.

and extent of hydrolysis for glucan to glucose yields, but did not affect hemicellulose sugar yields. Thus, these hemicellulose yields appear to be less sensitive to changes in cellulase concentrations and glucan hydrolysis than the yields obtained with wood.

6.3.3 Solid content effect

Mixed hardwood

Glucan to glucose yields and hemicellulose sugar yields are shown as a function of initial solids content, for different hydrolysis times (4, 24 and 48 hr) in Figure 6.6, part A and part B, respectively. At 4 hr of hydrolysis, yield initially

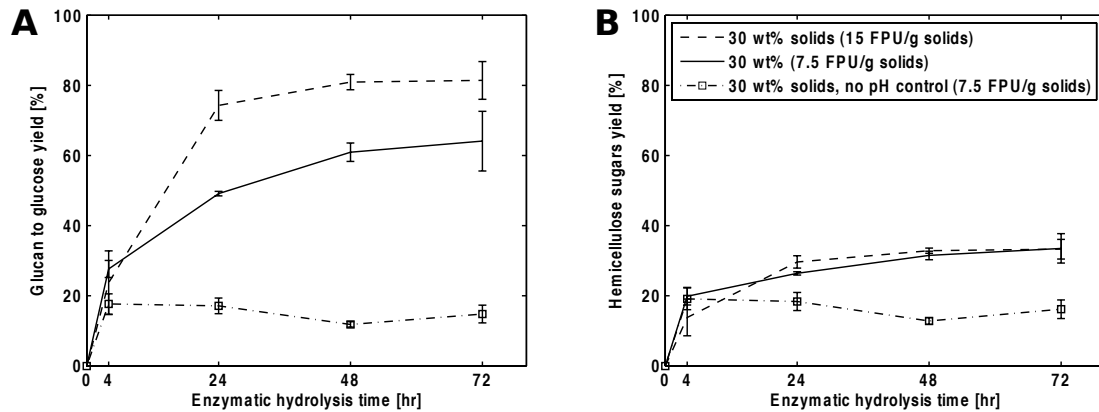


Fig. 6.5: Temporal glucan to glucose (part A) and hemicellulose sugar (xylan, arabinan and mannan to xylose, arabinose and mannose) (part B) yields for optimally two-temperature stage $\text{CO}_2\text{-H}_2\text{O}$ pretreated switchgrass (210°C , 1 min and 160°C , 60 min) for 30 wt% of initial solids content (before pretreatment) and varying enzyme and sodium carbonate loadings. Experiments for which no sodium carbonate was added are indicated by *no pH control*. Error bars represent the results 95% confidence interval based on triplicate sampling.

decreased sharply between 5 and 10 wt%, then remained more or less constant and dropped at 30 wt% solids (see Figure 6.6, part A). After 24 hr of hydrolysis, a similar drop in yield occurred between 5 and 15 wt% of initial solid content. Yield then rose between 15 and 25 wt% solids content before, once again, dropping at 30 wt% solids. Very similar trends occur after 48 hr of hydrolysis but are slightly dampened. Except for the measurement at 10 % solids, hydrolysis yields at 72 hr were always statistically equivalent to yields at 48 hr.

The increase and decrease pattern could be due to two competing effects. On the one hand viscosity, which increases mass transfer limitations, and inhibitor concentrations increase with solid content. These effects could be decreasing yields initially and take over after 30 wt% solids. On the other hand, enzyme concentrations increase with solid content (the ratio of initial solid content to cellulase is constant), which could explain the increasing yields between 10-15

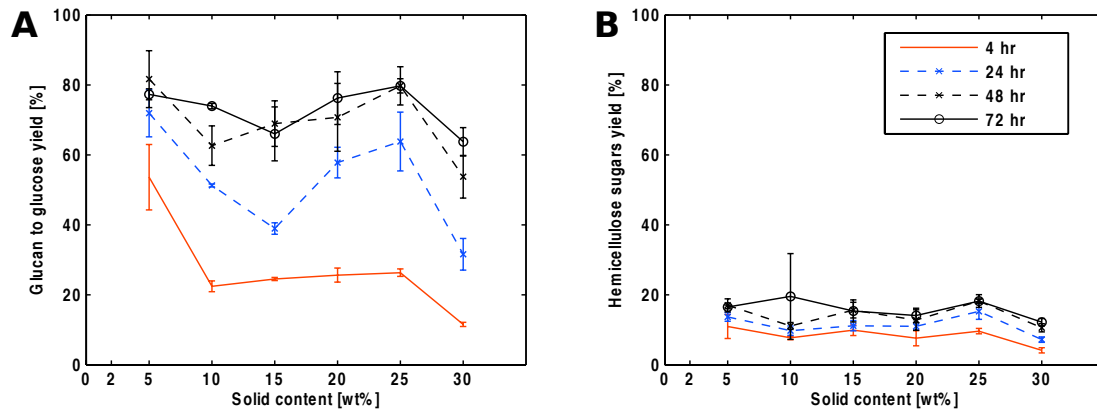


Fig. 6.6: Glucan to glucose (part A) and hemicellulose sugar (xylan, arabinan and mannan to xylose, arabinose and mannose) (part B) yields for optimally two-temperature stage CO₂-H₂O pretreated mixed hardwood (210°C, 16 min and 160°C, 60 min) as a function of solid content for different enzymatic hydrolysis residence times. Error bars represent the results 95% confidence interval based on triplicate sampling.

and 25 wt% solids.

The 48 and 72 hr glucan to glucose yields obtained at 5 wt% solids were close to 80% and were thus comparable to the yields obtained for washed solids at 1 wt% glucan (about 1.5-2% solids). In addition, when doubling the cellulase content to 15 FPU/(g solids) at 30 wt% solids, a glucan to glucose yield close to 80% (see Figure 6.3, part A) was once again achieved. Therefore, this doubling seems to reverse the sharp drop in yield that occurs between 25 and 30 wt% solids (see Figure 6.6, part A). Interestingly, this effect is not observed after 4 hrs of hydrolysis, where doubling the cellulase content led to a glucan to glucose yield of about 20% which was slightly below the yield obtained with half the cellulase content. This could indicate that increasing the enzyme content helps slow inhibition by the produced sugars or the liberated lignin, which are gradually released throughout enzymatic hydrolysis.

Hemicellulose sugar yields are shown in Figure 6.6, part B, for different hy-

drolsis times. As observed previously, there is little difference in yields for different hydrolysis times due to the amount of soluble oligosaccharides liberated during pretreatment contributing to the yield. Solid content does not seem to have a significant effect before 30 wt%, at which point (similar to glucan to glucose yield) a drop in yield occurs. Interestingly, this drop was eliminated when the cellulase content was doubled, which led to a yield of about 20% (see Figure 6.3, part B) as opposed to 10% (while the xylanase content remained unchanged). Thus, a limiting factor in hemicellulose hydrolysis could be the restriction of its access by cellulose. However, all hemicellulose yields remain below those obtained with washed solids, suggesting that hemicellulases could be inhibited by pretreatment byproducts.

Switchgrass

For glucan to glucose yields, all three hydrolysis times show almost identical yield patterns as a function of solids content (see Figure 6.7, part A). Yields progressively increase between 5 and 20 or 25 wt% of initial solids and then sharply decrease between 25 and 30 wt%. Once again, this could be indicative of competing effects between increasing enzyme concentration and increasing mass transfer limitations and inhibitor concentrations. However, pretreatment inhibitors seem to somewhat affect yields at low solid because the 72 hr yield for washed solids (about 80%, see Table 6.1) was significantly higher than the maximal yield for 5 wt% solids. Like hardwood, doubling the cellulase content increased the yield to around 80% (see Figure 6.5, part A), reversing the decrease occurring between 25 and 30 wt%. Hemicellulose sugar yields (see Figure 6.7, part B) increased with solid content for 24, 48 and 72 hr of hydrolysis

even though these yields were initially lower than the maximum yield obtained with washed solids, which was close to 30% (see Table 6.1). This increase in yield was probably due to the increasing enzyme concentrations that accompany the increasing solids content. Unlike with wood, doubling the cellulase content did not influence hemicellulose sugar yields (both hemicellulose sugar yields were around 30% for a 30 wt% solids content, see Figure 6.5, part B). This may indicate that, for switchgrass, hemicellulose hydrolysis was not limited by cellulose restricting its accessibility.

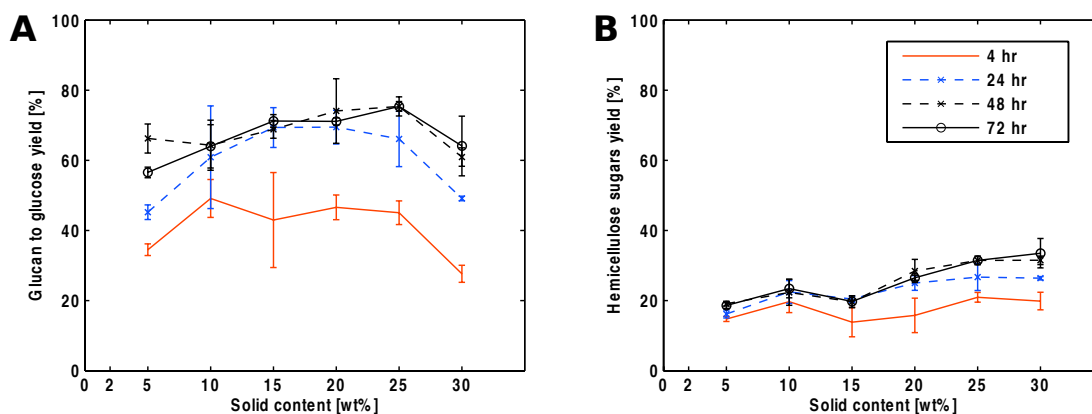


Fig. 6.7: Glucan to glucose (part A) and hemicellulose sugar (xylan, arabinan and mannan to xylose, arabinose and mannose) (part B) yields for optimally two-temperature stage CO₂-H₂O pretreated switchgrass (210°C, 1 min and 160°C, 60 min) as a function of solid content for different enzymatic hydrolysis residence times. Error bars represent the results 95% confidence interval based on triplicate sampling.

6.3.4 Comparison to other pretreatment and high-solids enzymatic hydrolysis processes

Several other studies have explored the effect of increasing the solids content on sugar yields for high-solids enzymatic hydrolysis of different lignocellulosic materials obtained from different pretreatment processes, including: corn stover

from dilute acid pretreatment [278], wheat straw from steam explosion [244] and olive wood from liquid hot water pretreatment or steam explosion (sometimes followed by an alkali delignification process) [281]. For comparison, the maximum glucan to glucose yields obtained from those studies are plotted in Figure 6.8 for varying initial dry matter content (in this case, initial refers to the beginning of enzymatic hydrolysis). Dry matter was used instead of the initial solids content prior to pretreatment for consistency with the aforementioned studies. Thus, the highest initial solids content used in this work was 30 wt%, but the highest initial dry matter used in enzymatic hydrolysis was around 25 wt%, due to part of the biomass being converted to volatile compounds during pretreatment. Jorgensen et al. used 7 FPU/(g initial dry matter), Cara et al. used 15 FPU/(g initial dry matter) and Hodge et al. used 40 (mg protein)/(g initial dry matter), while in this work about 9 FPU/(g initial dry matter) or about 18 (mg protein)/(g initial dry matter) was used.

Figure 6.8 shows that glucan to glucose yields behave differently as a function of initial dry matter for acid-catalyzed and non-acid-catalyzed processes. Dilute acid pretreated corn stover shows a fairly constant yield as a function of dry matter and suddenly drops above 30 wt% dry matter. Other technologies (all of them partially uncatalyzed) show a more or less linear decrease in yield as a function of increasing dry matter. This alternate pattern could be indicative of a fundamental difference in the internal structure, viscosity (which could affect mass transfer limitations) and/or chemistry of their pretreated biomass mixtures. In contrast, CO₂-H₂O pretreated hardwood or switchgrass showed an increase in yield with dry matter until 25 wt% and then a sudden drop thereafter. This behavior is generally consistent to what is observed for dilute acid pretreatment and contrasts with the other technologies, indicating that CO₂-H₂O

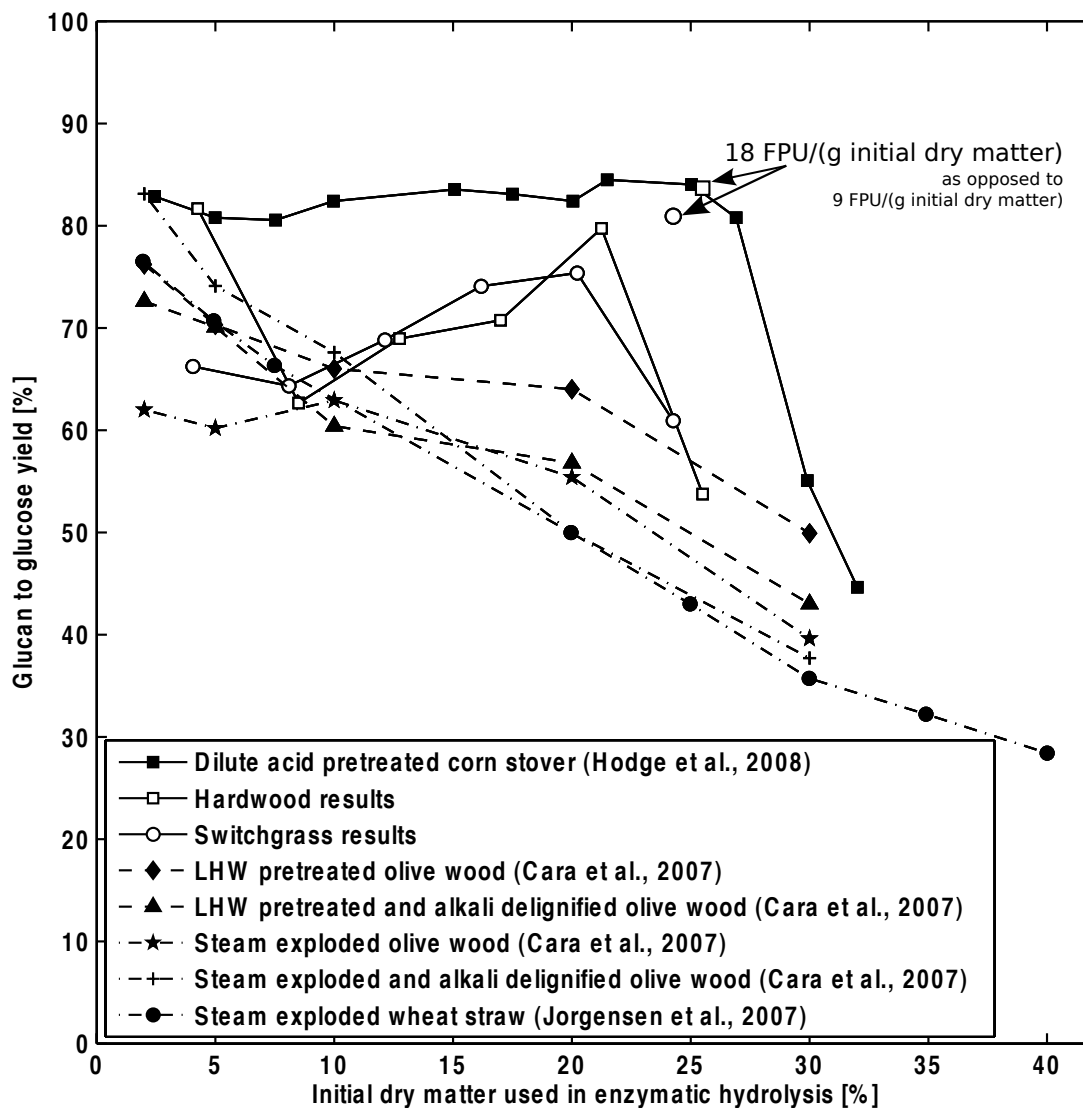


Fig. 6.8: Comparison of glucan to glucose yields obtained with different pretreatment technologies in different studies as a function of the initial dry matter used in enzymatic hydrolysis. Dry matter is defined differently than the previously used “initial solids content”, and refers to the dry matter (as determined by a drying assay, see Section 6.2.1) at the start of enzymatic hydrolysis. This alternate metric is used to more accurately compare different technologies. Hardwood and switchgrass results refer to the yields obtained in this work after 48 hrs of enzymatic hydrolysis (after which, they were almost always at their maximum level), at 9 FPU/(g initial dry matter) (i.e. previously described as 7.5 FPU/(g solids)). For comparison, several yields obtained with an enzyme loading of 18 FPU/(g initial dry matter) (i.e. previously described as 15 FPU/(g solids)) are also shown.

pretreatment acts more like an acid catalyzed than an uncatalyzed or alkali-catalyzed pretreatment process. The initial increase in yield observed in this work, which is absent for the dilute acid results, could be due to the lower enzyme content used here (about half as much protein was used in this work). Indeed, a higher enzyme loading could decrease the system's sensitivity to increasing dry matter. It also seems to postpone the sudden drop in yield. As shown in Figure 6.8, when the amount of cellulase was doubled for a dry matter content of about 25 wt%, a yield greater than at 20 wt% dry matter was obtained. Incidentally, this resulted in similar yields to those obtained for dilute acid pretreated corn stover, which was hydrolyzed at similar cellulase loadings [278].

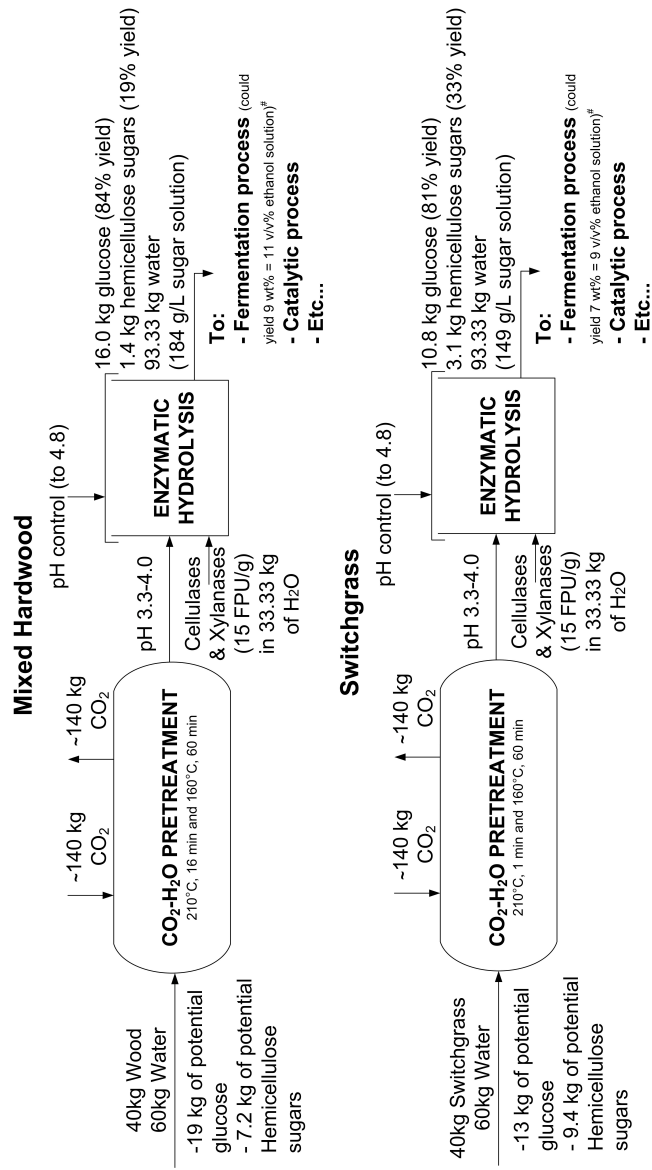
Therefore, doubling the cellulase loading compensated for the reduction in glucose yield brought on by the increasing solid between 20 and 25 wt% dry matter. This is consistent with findings by Sills and Gossett [160]. They showed that, in the presence of cellulase, β -glucosidase and xylanase, enzymatic hydrolysis yields were quite sensitive to increasing enzyme loadings up to about 40-50 (mg protein)/(g initial solids), after which yields remained more or less constant. In this work, doubling the cellulase content led to an increase in total enzyme loading (including, cellulase, xylanase and β -glucosidase) of 33 to 48 (mg protein)/(g initial solids), which is within this range in which yields are quite sensitive to enzyme loadings. However, as demonstrated by the varying effects of increasing enzyme loadings for poplar pretreated with different technologies, the effect of increasing the cellulase content varies with the pretreatment technology [282]. This is demonstrated in Figure 6.7; Cara et al. obtained significantly lower yields in the hydrolysis of olive wood with 15 FPU/(g initial dry matter) than was obtained here with 9 FPU/(g initial dry matter). There-

fore, the ability of increased enzyme loadings to significantly increase yields of CO₂-H₂O pretreated biomass is a collateral benefit of this pretreatment technology.

6.3.5 Process overview

Figure 9 summarizes the overall process mass balance for both mixed hardwood and switchgrass for a 100 kg mixture of starting material (60 kg water, 40 kg biomass). The amount of CO₂ to be added was calculated by estimating the amount of free volume present in the stirred pretreatment reactor and by using the density of pure CO₂ calculated at the relevant pressures and temperatures [284]. However, the process is likely to require far less CO₂ because the estimated amount far exceeds the necessary quantity needed to saturate water and form a ternary phase of equal volume to the water that is present. For a 100 kg mixture of starting material, assuming that the densities of water and CO₂ are equal to their pure values, this would correspond to less than 4 kg of CO₂ to saturate the water and less than 18 kg of CO₂ to produce a supercritical phase equal in volume to the water-rich phase [284, 258].

As shown in Figure 9, using 40 wt% CO₂-H₂O pretreatment with two temperature stages (210°C, 16 min and 160°C, 60 min for mixed hardwood or 210°C, 1 min and 160°C, 60 min for switchgrass) followed by high-solids enzymatic hydrolysis at 30 wt% (initial solids content) with 15 FPU/(g initial solids content) of cellulases and 15 mg/(g initial solids content) of xylanase, glucan to glucose yields above 80% can be obtained for switchgrass and mixed hardwood. Therefore, sugar solutions of 185 g/L (170 g/L of glucose and cellobiose 15 g/L of



[#]Assuming a conversion of monosaccharides to ethanol of 0.5 wt/wt

Fig. 6.9: Overall biomass pretreatment and saccharification mass balance for 100 kg of a 40 wt% solids biomass-water mixture (40 kg biomass, 60 kg water). The amount of added CO₂ added was based on the approximate amount present in the stirred pretreatment reactor based on the density of pure CO₂ calculated at the relevant pressures and temperatures [284]. To calculate a potential ethanol solution concentration after fermentation an optimistic conversion factor of monosaccharides to ethanol of 0.5 wt/wt was used (based on a theoretical yield of 0.511 wt/wt for both glucose and xylose fermentation where 1 mole of glucose yields 2 of ethanol and 2 of CO₂ and where 3 moles of xylose yield 5 of ethanol and 5 of CO₂).

hemicellulose sugars) and 149 g/L (115 g/L of glucose and cellobiose 34 g/L of hemicellulose sugars) were obtained for mixed hardwood and switchgrass, respectively, without any drying, separation or additional chemical catalysts.

In comparison, other uncatalyzed processes such as steam explosion or liquid hot water demonstrate glucan to glucose yield in the neighborhood of 80% with low-solids enzymatic hydrolysis (2-5 wt%), but they often see this yield drop by almost half for higher solids contents [244, 281]. In addition, biomass with a lower solids content was systematically used during pretreatment (20-28 wt% for wheat straw and 17 wt% for olive wood) and required subsequent drying. In contrast, dilute acid pretreatment was able to maintain glucan to glucose yields above 80% at high solids contents (35 wt% and 30 wt% for pretreatment and enzymatic hydrolysis respectively) without any drying [278]. A 202 g/L sugar solution was produced (which exceeds the results presented here due to a high hemicellulose sugar yield of 74%). However, such pretreatment processes typically require the use of 2 to 3 kg of sulfuric acid (assuming a 1 to 2 wt% acid solution) and roughly equivalent molar amounts of sodium hydroxide (for neutralization) for every 100 kg of biomass [245, 278]. In addition, to achieve these yields required 168 hr of enzymatic hydrolysis while only 48 hr were required using the approach presented here. Finally, dilute acid results were obtained with corn stover, which can often produce higher yields than other substrates for similar pretreatment conditions as demonstrated by the fairly high yield obtained with untreated substrates (20-30% vs. 3-5% for hardwood) [212, 285].

6.4 Conclusions

When performing high solids enzymatic hydrolysis on biphasic CO₂-H₂O pretreated biomass, the competing effects of increasing solid content, enzyme concentration and inhibitor concentration on monosaccharide yields were observed. Mass transfer limitations due to increased viscosity and increased inhibitor concentrations contributed to sharply decreasing yields between 25 and 30 wt% solids. This sudden drop in yield as solid content increased above 25-30% was also observed for results obtained with dilute acid pretreatment. However, these sharply declining yields are markedly different than those observed with uncatalyzed and alkali catalyzed pretreatment technologies, which showed a gradual and continuous decrease in glucose yields with increasing solid content. The continuous decline in yields appears to be more detrimental to commercial processing because it would prevent obtaining high yields at high-solids contents.

Therefore, it seems that CO₂ acts as an easily recyclable acid catalyst and co-solvent, and that two-temperature stage biphasic CO₂-H₂O pretreatment could be a viable alternative to catalyzed pretreatment processes such as those requiring acids. In addition to offering similar glucan to glucose yields, the resulting CO₂-H₂O pretreated biomass has a similar behavior during high-solids enzymatic hydrolysis. Furthermore, unlike dilute acid pretreatment, CO₂-H₂O pretreatment combined with high-solids enzymatic processing (up to 30 wt%) has been tested for multiple substrates (mixed hardwood and switchgrass). Glucan to glucose yields above 80% and sugar concentrations of 185 and 149g/L were obtained for mixed hardwood and switchgrass, respectively, without any drying, separation or additional chemical catalysts. Apart from results obtained

with dilute acid pretreated corn stover, these are the highest concentration values reported without any substrate drying.

CHAPTER 7

**OBSERVING AND MODELING BMCC DEGRADATION BY
COMMERCIAL CELLULASE COCKTAILS WITH FLUORESCENTLY
LABELED *TRICHODERMA RESEII* CEL7A THROUGH CONFOCAL
MICROSCOPY**

Large portions of this Chapter will appear as a published manuscript in the *Journal Biotechnology & Bioengineering* [286].

7.1 Introduction

As was shown in Chapters 4, 5 and 6, the structural polysaccharides present in biomass can be depolymerized into fermentable sugars that could be converted to fuels and/or chemicals. However, producing carbohydrates from biomass economically and sustainably remains a key bottleneck to successfully commercializing this process [29]. A specific challenge has been to improve the efficacy and lower the cost of cellulase cocktails used to depolymerize biomass's cellulose fraction [30].

In Chapters 4, 5 and 6, pretreatment and enzymatic hydrolysis yields were increased by modifying pretreatment parameters. Though careful consideration was used to choose the different parameters that were varied and how they were varied, this procedure was not guided by a theoretical framework that would describe important structural changes occurring during pretreatment. Indeed, a modeling approach could be used as a tool for the rational design of pretreatment processes.

A number of recent studies have focused on improving cellulase cocktails

and have suffered from the same type of limitations. Banerjee et al. have used large data sets to create stochastic models to optimize these mixtures [123, 124]. Though effective, this approach provides limited insight into mechanisms of cellulose hydrolysis by cellulases and can only be used to find optimal enzyme mixtures within the explored range of parameters. Alternative approaches have included using (1) empirical models, (2) Michaelis-Menten kinetics and (3) models that include an adsorption step, often modeled by a Langmuir isotherm [119], and more recently (4) with non-equilibrium Langmuir kinetics [132, 133]. The latter approach couples enzyme binding with hydrolysis by including an adsorption step, an equilibrium complexation step and a final catalysis step, while accounting for changes in exposed surface area [132, 133].

All of these studies use the final sugar concentrations or the solubilized fraction of cellulose to validate and/or fit their models. By focusing on final sugar yield, they ignore both cellulase binding and changes in cellulose structure when comparing models to experimental results, even though these are important phenomena that influence depolymerization rates and final yields [115, 118]. Therefore, several researchers have used fluorescence confocal microscopy [287] or scanning electron microscopy (SEM) [178, 288] to image cellulosic substrates at various stages after pretreatment and/or enzymatic hydrolysis. The drawback of these studies is that they observe the reacting mixture once the reaction is no longer in progress. In contrast, some researchers have been able to observe enzyme-cellulose interaction *in situ* using fluorescence microscopy [117, 116] or atomic force microscopy [289, 290]. While these microscopy studies have been used to observe enzymes at dilute concentrations, they have not been used for concentrated cellulase mixtures at 50°C (the optimal temperature for most cellulase cocktails), which are necessary conditions

for effective biomass depolymerization [291, 285]. In fact, no *in situ* study has been done at 50°C or in the presence of a mixture of more than two cellulase species.

The goal of this study was to visualize the process of cellulose depolymerization by a commercial cellulase cocktail, in real time and at reactive temperatures, by simultaneously imaging BMCC and bound cellulases through confocal fluorescence microscopy. The data were fitted to kinetic models, which were validated using independent measurements of carbohydrates released in bulk experiments.

7.2 Materials and Methods

7.2.1 Cellulase preparation

T. reesei Cel7A was purified from the *T. reesei* culture broth as described by Bothwell et al. [126]. The enzyme was labeled with the Alexa Fluor 647 dye (AF647, Invitrogen, Carlsbad, CA) using a solid-phase labeling protocol and purified by anionic exchange fast protein liquid chromatography [292]. All Cel7A enzymes used in this study had a degree of labeling of three and exhibited hydrolytic activity on BMCC within 15% of that of the unlabeled enzyme (see Appendix D).

7.2.2 Microscopy sample preparation

A suspension of BMCC (Monsanto Cellulon, San Diego, CA) was labeled with the fluorescent dye 5-(4,6-dichlorotriazinyl)-aminofluorescein (DTAF) and sonicated to obtain a uniform suspension using previously described protocols [116, 293]. A glass coverslip (40 mm, BiopTechs, Butler, PA) was rendered hydrophilic by treatment in an oxygen plasma cleaner (Harrick, Ithaca, NY) for 2 min. It was then placed on a hotplate set at 70°C where 100 ml of a 1 g/L solution of DTAF-BMCC was spread on the coverslip. The solution was left to dry for 20 min. The glass slide was then placed in a heated micro-fluidic chamber (see Figure 7.1, FCS2 chamber assembly, BiopTechs, Butler, PA) and 15 ml of Milli-Q water was flushed through the chamber to wash the BMCC. Following this, 5 ml of 10% bovine serum albumin (BSA) solution was added and left to incubate overnight to block any non-specific binding. The effects of DTAF labeling, substrate drying and BSA used during sample preparation on enzymatic hydrolysis are discussed in Appendix D. Prior to imaging, the blocking buffer was washed away by flushing 30 ml of Milli-Q water through the chamber followed by 30 ml of 0.05 M sodium citrate buffer (pH 4.8) containing 30 mg/L Cyclohexamide and 40 mg/L Tetracycline to prevent microbial contamination. The experiment was started when 4.75 ml of sodium citrate buffer containing 5nM of AF647-Cel7A, 0.003 FPU/ml of Spezyme CP (Genencor, Copenhagen, Denmark) and 0.006 CBU/ml of Novo 188 β -glucosidase (Novozyme, Davis, Ca) was added. The *T. reesei* cellulase Cel7A is the often the most prevalent and most active component of the *T. reesei* crude which is the source of the spezyme CP cellulase cocktail [96]. Therefore, it is assumed here that a small fraction of AF647-Cel7A acts as an accurate reporter for the cellulase mixture.

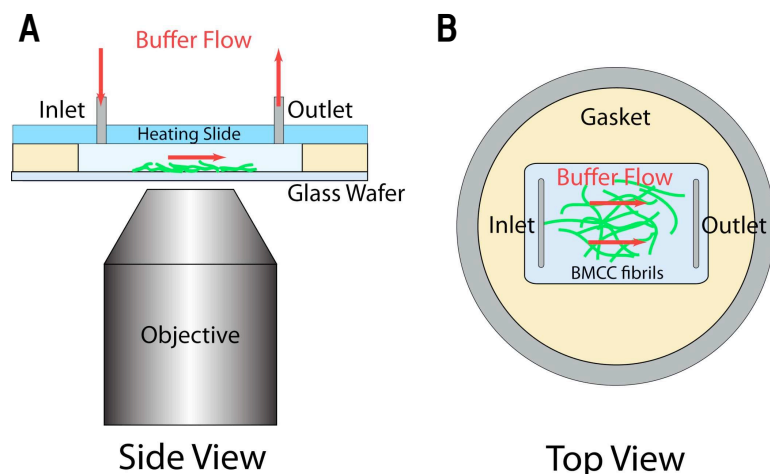


Fig. 7.1: Imaging chamber setup. Part A shows the side view with the confocal microscope objective and Part B shows the top view facing the surface on which the sample is deposited.

7.2.3 Confocal microscopy imaging

DTAF-BMCC and bound AF647-Cel7A were imaged using an Olympus IX81-FV1000 confocal microscope equipped with a UPLFLN 60x/NA 0.9 objective (Olympus, Center Valley, PA). Lasers at 488 and 635 nm were used to excite the DTAF and AF647 dyes, respectively (both at 2% laser power, gain=1, photomultiplier voltage 550 V, 20 msec/pixel dwell time and a 100 mm confocal aperture). Signals from each dye were collected in separate channels with bandpass filters at 555/100 nm (DTAF) and 705/100 nm (AF647). The Olympus Fluoview Software (v2.1c) was used for automated acquisition of z-stack images (covering the thickness of the sample) at regular time intervals on up to four predefined areas. Photobleaching of the dyes was corrected for as described in Appendix D.

7.2.4 Image processing

For each collection channel and each area being imaged at a given time, a z-stack of images was processed in order to obtain a mean fluorescence intensity signal (see Figure 7.2). The intensity for each pixel within the z-stack of images was integrated along the z-axis using Image J (NIH, Bethesda, Maryland) to create a two-dimensional sum projection of the area of interest. To identify those pixels where the intensity was saturated, a two-dimensional maximum intensity projection image was also created for each z-stack. The time-series of sum projection and maximum projection images for every area were then aligned using the Stackreg plugin for Image J to correct for stage drift [294]. Following this, a custom Matlab routine (Mathworks, Natick, Ma) was used to create a mask in order to eliminate certain areas from further analysis. For a given area, this mask was created from a time-averaged image of all the sum projections. A threshold was applied based on the mean intensity of a user-selected background area to separate the pixels that were considered “signal” from those that were considered “background”. Small holes in the signal mask created by the threshold were filled, so that the mask represented a continuous region. Finally, areas containing saturated pixels (identified from maximum projections) and small isolated areas (speckle noise outside the cellulose) were removed from the signal mask so as not to be further analyzed. Once this mask was obtained, it was applied to the time series sum projections and the mean intensity and standard deviation were calculated for each time point.

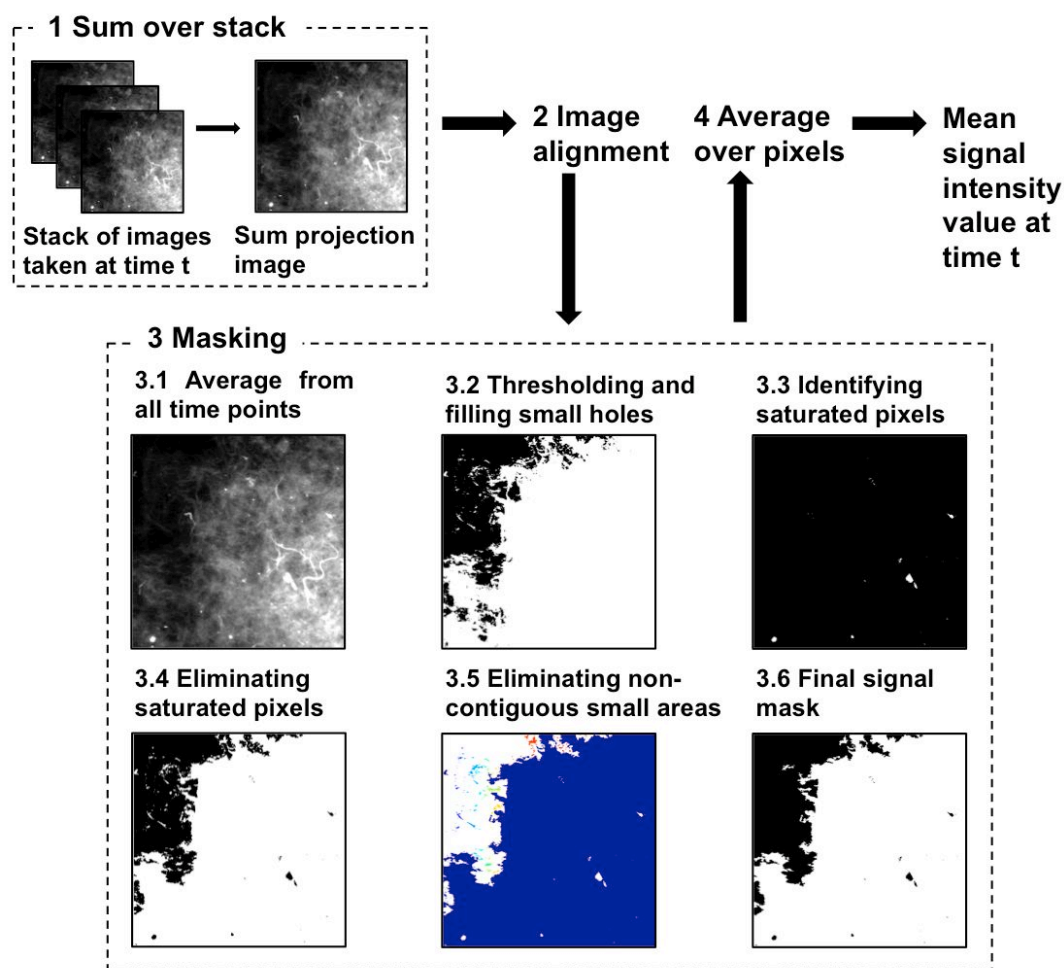


Fig. 7.2: Illustration of the image processing method. The method converts a vertical stack of images for a given fluorescence collection channel to a fluorescence intensity value using these four illustrated operations.

7.2.5 Bulk experiments

For each time-point, triplicate reactions were prepared by drying 100 ml of the 1 g/L labeled BMCC solution a glass surface of a 50 mm MatTek glass bottom dish as described above (MatTek Corp., Ashland, MA). The dish containing the BMCC was then incubated overnight in a fridge while immersed in 2 ml of 10% BSA blocking buffer. The buffer was removed with a pipette and the substrate was washed with 1.5 ml of 0.05 M Sodium Citrate buffer containing the growth

inhibitors tetracycline and cyclohexamide and was placed in an incubator set at 50°C. The reaction was started by adding 1.5 ml 0.05 M sodium citrate buffer heated to 50°C containing 0.003 FPU/ml (or 0.006 mg/ml of protein measured using the Bradford assay [295]) of Spezyme CP and 0.006 CBU/ml of Novo 188 b-glucosidase. Released sugars were sampled by removing all the liquid in the dish and heating it to 95°C for 5 min to inactivate the enzymes. Samples were analyzed for glucose and cellobiose by liquid chromatography using previously described methods described in Chapter 4.

7.2.6 Model development

Fluorescence signal characterization

As it has been previously shown, DTAF tagged BMCC can be used to track cellulose throughout degradation, demonstrating that the dye uniformly tags BMCC [293]. Therefore, the fluorescence signal emitted by this dye (I_S) was assumed to be proportional to the total amount of BMCC present and thus to the total number of cellulase binding sites contained within BMCC (S_{tot}). A description of all the symbols and their units is given in Table 7.1.

$$I_S = \alpha [S_{tot}] \quad (7.1)$$

Normalizing by the DTAF-BMCC signal ($I_{S,0}$) measured at $t = 0$:

$$\frac{I_S}{I_{S,0}} = \frac{[S_{tot}]}{[S_{tot}]_0} \quad (7.2)$$

As discussed in the Material and Methods, the fluorescence signal emitted by AF647-Cel7A is assumed to be proportional to the total amount of bound en-

Table 7.1: List of symbols and their associated description.

Parameter	Description	Units
$[E]$	Bulk cellulase concentration	$[\text{mol}/\text{g}_{BMCC}]$
$[ES]$	Surface concentration of bound cellulase	$[\text{mol}/\text{g}_{BMCC}]$
I_S	Total measured DTAF-BMCC fluorescence intensity	[-]
I_{ES}	Total measured AF647-Cel7A fluorescence intensity	[-]
k_1	Cellulase irreversible binding rate constant	$[\text{FPU}/(\text{ml min})]$
$k_{r,1}$	Cellulase reversible binding rate constant	$[\text{FPU}/(\text{ml min})]$
$k_{r,-1}$	Cellulase reversible unbinding rate constant	$[\text{min}^{-1}]$
k_i	Cellulose binding site exposure rate constant	$[\text{FPU}/(\text{ml min})]$
k_2	Cellulose degradation rate constant (irreversible model)	$[\text{min}^{-1}]$
$k_{r,2}$	Cellulose degradation rate constant (reversible model)	$[\text{min}^{-1}]$
$k_{i,2}$	Cellulose degradation rate constant (instantaneous model)	$[\text{min}^{-1}]$
$[P]$	Hydrolysis product concentration	$[\text{mol}/\text{g}_{BMCC}]$
$[S]$	Surface concentration of free (exposed) binding sites	$[\text{mol}/\text{g}_{BMCC}]$
$[S_i]$	Concentration of inner (unexposed) binding sites	$[\text{mol}/\text{g}_{BMCC}]$
$[S]_0$	Initial surface concentration of free (exposed) binding sites	$[\text{mol}/\text{g}_{BMCC}]$
$[S_{tot}]$	Concentration of total binding sites in cellulose	$[\text{mol}/\text{g}_{BMCC}]$
t	Time	$[\text{min}]$
$[X]_{t=0}$	Initial (surface, if applicable) concentration of X (at $t=0$)	[-]
α	DTAF-BMCC-fluorescence proportionality constant	$[(\text{mol}/\text{g}_{BMCC})^{-1}]$
β	Enzyme-fluorescence proportionality constant	$[(\text{mol}/\text{g}_{BMCC})^{-1}]$
λ_i	i th eigenvalue	[-]
ψ	Initial fraction of available sites (exposed over total sites)	[-]

zyme:

$$I_{ES} = \beta [ES] \quad (7.3)$$

The AF647-Cel7A signal can also be normalized by $I_{S,0}$:

$$\frac{I_{ES}}{I_{S,0}} = \frac{\beta [ES]}{\alpha [S_{tot}]_0} \quad (7.4)$$

Irreversible and reversible binding models

Given that BMCC is an easily accessible substrate [126], as a first approximation, it could be assumed that all the binding sites ($[S_{tot}]$) are exposed and available for binding during the reaction. Therefore, at any given time, the total number of exposed free sites ($[S]$) added to the total number of bound sites ($[ES]$) equals the total number of binding sites ($[S_{tot}]$):

$$[S_{tot}] = [S] + [ES] \quad (7.5)$$

In what will be referred to as the irreversible binding model, cellulases are assumed to bind to unoccupied cellulose binding sites (S) through an irreversible reaction (k_1). In a subsequent reaction (k_2), the bound enzyme (ES) can react to form a soluble oligosaccharide product (P):



These reactions can be described by the following three differential equations:

$$\frac{d[S]}{dt} = -k_1 [S] [E] \quad (7.7)$$

$$\frac{d[ES]}{dt} = k_1 [S] [E] - k_2 [ES] \quad (7.8)$$

$$\frac{d[P]}{dt} = k_2 [ES] \quad (7.9)$$

with initial conditions defined as:

$$[S]_{t=0} = [S]_0 = [S_{tot}]_0 \quad (7.10)$$

$$[ES]_{t=0} = 0 \quad (7.11)$$

$$[P]_{t=0} = 0 \quad (7.12)$$

where $[S]_0$ is defined as a non-zero initial surface concentration of cellulose binding sites which, since all sites are exposed and unbound at $t = 0$, is equal to

the initial total number of sites in BMCC ($[S_{tot}]_0$). The bulk enzyme concentration $[E]$ is assumed to stay constant throughout the experiment. This assumption was verified experimentally (see Section in D.7 Appendix D). Therefore, the system of Equations 7-12 can be solved (see details in Appendix D) and rearranged using Equations 2, 4 and 5 to produce the following results:

$$\frac{I_S}{I_{S,0}} = \frac{[S]}{[S_{tot}]_0} + \frac{[ES]}{[S_{tot}]_0} = \exp(-k_1 [E] t) + \frac{k_1 [E]}{k_2 - k_1 [E]} (\exp(-k_1 [E] t) - \exp(-k_2 t)) \quad (7.13)$$

$$\frac{I_{ES}}{I_{S,0}} = \frac{\beta [ES]}{\alpha [S_{tot}]_0} = \frac{\beta k_1 [E]}{\alpha k_2 - k_1 [E]} (\exp(-k_1 [E] t) - \exp(-k_2 t)) \quad (7.14)$$

$$\frac{[P]}{[S_{tot}]_0} = \frac{k_2}{k_2 - k_1 [E]} (1 - \exp(-k_1 [E] t)) - \frac{k_1 [E]}{k_2 - k_1 [E]} (1 - \exp(-k_2 t)) \quad (7.15)$$

This model can be slightly modified to produce what will be referred to as the reversible model by assuming that cellulases bind to unoccupied cellulose binding sites (S) through a first reaction ($k_{r,1}$) and unbind through a second reaction ($k_{r,-1}$). As was the case for the irreversible model, in a third reaction ($k_{r,2}$), the bound cellulose-enzyme complex (ES) can react to form a soluble oligosaccharide product (P):



These reactions can be modeled and expressed in a similar procedure to that applied for the irreversible binding model to obtain (see details in Appendix

D):

$$\frac{I_S}{[S_{tot}]_0} = \frac{[S]}{[S_{tot}]_0} + \frac{[ES]}{[S_{tot}]_0} = \frac{1}{\sqrt{\frac{k_{r,1}^2 [E]^2 + k_{r,-1}^2 + k_{r,2}^2 + 2k_{r,1} [E] k_{r,-1}}{-2k_{r,1} [E] k_{r,2} + 2k_{r,-1} k_{r,2}}}} \times \left[\exp(\lambda_1 t) \left(k_{r,-1} + k_{r,2} + \sqrt{\frac{k_{r,1}^2 [E]^2 + k_{r,-1}^2 + k_{r,2}^2 + 2k_{r,1} [E] k_{r,-1}}{-2k_{r,1} [E] k_{r,2} + 2k_{r,-1} k_{r,2}}} \right) - \left(k_{r,-1} + k_{r,2} - \sqrt{\frac{k_{r,1}^2 [E]^2 + k_{r,-1}^2 + k_{r,2}^2 + 2k_{r,1} [E] k_{r,-1}}{-2k_{r,1} [E] k_{r,2} + 2k_{r,-1} k_{r,2}}} \right) \exp(\lambda_2 t) \right] \quad (7.17)$$

$$\frac{I_{ES}}{I_{S,0}} = \frac{\beta [ES]}{\alpha [S_{tot}]_0} = \frac{\beta}{\alpha} \frac{k_{r,1} [E]}{\sqrt{\frac{k_{r,1}^2 [E]^2 + k_{r,-1}^2 + k_{r,2}^2 + 2k_{r,1} [E] k_{r,-1}}{-2k_{r,1} [E] k_{r,2} + 2k_{r,-1} k_{r,2}}}} \times [\exp(\lambda_1 t) - \exp(\lambda_2 t)] \quad (7.18)$$

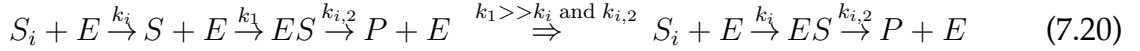
$$\frac{[P]}{[S_{tot}]_0} = \frac{k_{r,1} [E]}{\sqrt{\frac{k_{r,1}^2 [E]^2 + k_{r,-1}^2 + k_{r,2}^2 + 2k_{r,1} [E] k_{r,-1} - 2k_{r,1} [E] k_{r,2} + 2k_{r,-1} k_{r,2}}{\lambda_1} - \frac{(1 - \exp(\lambda_2 t))}{\lambda_2}}} \quad (7.19)$$

Where λ_1 and λ_2 are the eigenvalues (see definition in Appendix D).

7.2.7 Instantaneous binding model

Rather than assuming that all the sites are exposed and available for binding at the start of the reaction, one can assume that only a fraction (ψ) of the total

binding sites are exposed at the start of the reaction. A simplified reaction (k_i) catalyzed by enzymes (E) is assumed to create newly exposed free sites (S) from inner unexposed sites (k_i). In addition, for reasons that will be discussed in the Results and Discussion section, if the binding reaction (k'_1) is assumed to be much faster than the reaction exposing inner sites (k_i) or the reaction creating product ($k_{i,2}$), it can be omitted from the reaction sequence:



Henceforth, this model is referred to as the instantaneous binding model. These assumptions lead to the exact same problem definition as that of the reversible binding model except that the initial conditions for unexposed binding sites ($[S_i]$) and bound enzyme ($[ES]$) depend on the fraction of initially exposed binding sites (ψ):

$$[S_i]_0 = [S_{tot}]_0 (1 - \psi) \quad (7.21)$$

$$[ES]_0 = [S_{tot}]_0 \psi \quad (7.22)$$

Otherwise the two problems are identical leading to the following solutions (see details in Appendix D):

$$\frac{I_S}{I_{S,0}} = \frac{[S_i]}{[S_{tot}]_0} + \frac{[ES]}{[S_{tot}]_0} = (1 - \psi) \exp(-k_b [E] t) + \psi \exp(-k_{i,2} t) + \frac{(1 - \psi) k_i [E]}{k_{i,2} - k_i [E]} (\exp(-k_i [E] t) - \exp(-k_{i,2} t)) \quad (7.23)$$

$$\frac{I_{ES}}{I_{S,0}} = \frac{\beta [ES]}{\alpha [S_{tot}]_0} = \frac{\beta}{\alpha} \left(\psi \exp(-k_{i,2} t) + \frac{(1 - \psi) k_i [E]}{k_{i,2} - k_i [E]} (\exp(-k_i [E] t) - \exp(-k_{i,2} t)) \right) \quad (7.24)$$

$$\begin{aligned}
[P] = [S_{tot}]_0 & \left(\psi - (1 - \psi) \frac{k_i [E]}{k_{i,2} - k_i [E]} \right) (1 - \exp(-k_{i,2} t)) + \\
& (1 - \psi) \frac{k_{i,2} [S_{tot}]}{k_{i,2} - k_i [E]} (1 - \exp(-k_i [E] t))
\end{aligned} \tag{7.25}$$

Normalized fluorescence intensity data were fitted to the three models as defined by equations 13 and 14 (irreversible model), 17 and 18 (reversible model) and 23 and 24 (instantaneous binding model). Details are given in the Supplementary Information.

7.3 Results and discussion

7.3.1 Cellulose and cellulase imaging

Independent acquisition of fluorescence images of DTAF-BMCC and AF647-Cel7A allowed us to track the evolution of cellulose as it is degraded, and the binding of cellulase cocktails onto this substrate by imaging a fraction of one of their main components (Cel7A). The results are illustrated by the images shown in Figure 7.3. As expected, at time zero the cellulose can be observed (1st row) without any enzyme present (2nd row). But after 13 min plenty bound enzyme has appeared. After that, both the cellulose and enzyme signals start to fade as the cellulose is degraded and enzymes have less and less substrate to bind to, and completely disappears after 6 hr. This timeframe is comparable to that over which pretreated biomass hydrolyzes in industrial scenarios (i.e. about 24-48 hrs as discussed in Chapter 6). Since the total volume of the microfluidic chamber is 1.5 ml, the total enzyme loading used here is of about 45 FPU/g

cellulose, which is comparable to loadings used for pretreated biomass (15-60 FPU/g see [291]). Interestingly, when enzyme concentrations of 0.15 FPU/ml (which are standard for degrading pretreated biomass [270]) were employed, complete degradation occurred in minutes (see Appendix D). Therefore, both enzyme concentration and loading seem to affect cellulose degradation.

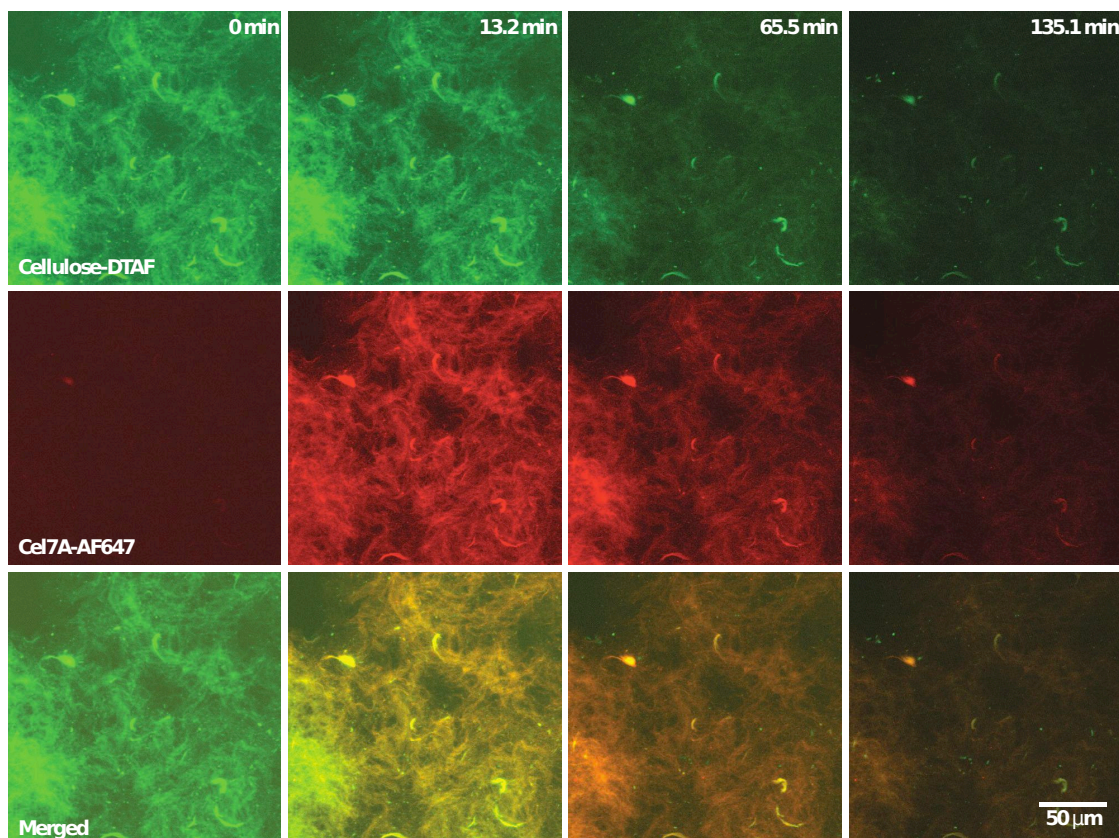


Fig. 7.3: Confocal fluorescence imaging of DTAFT-labeled BMCC and AF647-labeled Cel7A acting as a reporter for the Spezyme CP cellulase cocktail (Genencor, Copenhagen, Denmark). The green channel (row 1) represents the DTAF labeled BMCC. The red channel (row 2) represents the Spezyme CP cocktail as represented by the AF647-labeled Cel7A fraction. The bottom row shows the overlay of both images.

Quantitative intensity data extracted from such images confirmed the observations discussed above (see Figure 7.4, Parts A, B and C). The DTAF signal rapidly dropped as BMCC degradation began. Simultaneously, the bound cellulase (or AF647) signal increased before it eventually started decreasing as there

Table 7.2: Average fitting results and their standard deviation (obtained from 10 fits) for the reversible and irreversible models.

Irreversible binding model		Reversible binding model			
$k_1[E]$ [min^{-1}]	k_2 [min^{-1}]	$k_{r,1}[E]$ [min^{-1}]	$k_{r,-1}$ [min^{-1}]	$k_{r,2}$ [min^{-1}]	β/α [-]
0.019 ± 0.001	0.068 ± 0.019	0.021 ± 0.021	$3 \cdot 10^{-4} \pm 2 \cdot 10^{-3}$	0.068 ± 0.017	5.8 ± 3.5

was less and less cellulose available for binding. As will be further discussed, this increase in intensity could be due to cellulase binding to existing or newly exposed binding sites.

7.3.2 Irreversible and reversible binding models

Parts A, B and C of Figure 7.4 show three examples of data fitting to the reversible and irreversible binding models. The reversible model (dashed lines) can be difficult to distinguish because its predictions are nearly identical to those of the irreversible model. This is due to the fitting algorithm estimating the average value of the unbinding rate constant to values about 100 times smaller than those of the other rate constants (see Table 7.2). Mathematically, if the unbinding rate is significantly smaller than the binding rate it can be neglected, and the irreversible and reversible models become near identical. Because of its low value, the standard deviation on $k_{r,-1}$ is quite large but even its standard deviation remains over an order of magnitude smaller than all other rate constants. In some cases, the standard deviations for the parameters are close to the fitted values. However, this does not call into question the order of magnitude of the estimated values.

Since a mixture of cellulase was used, and since the exact composition of Spezyme CP is proprietary, the exact molar concentration of cellulases is un-

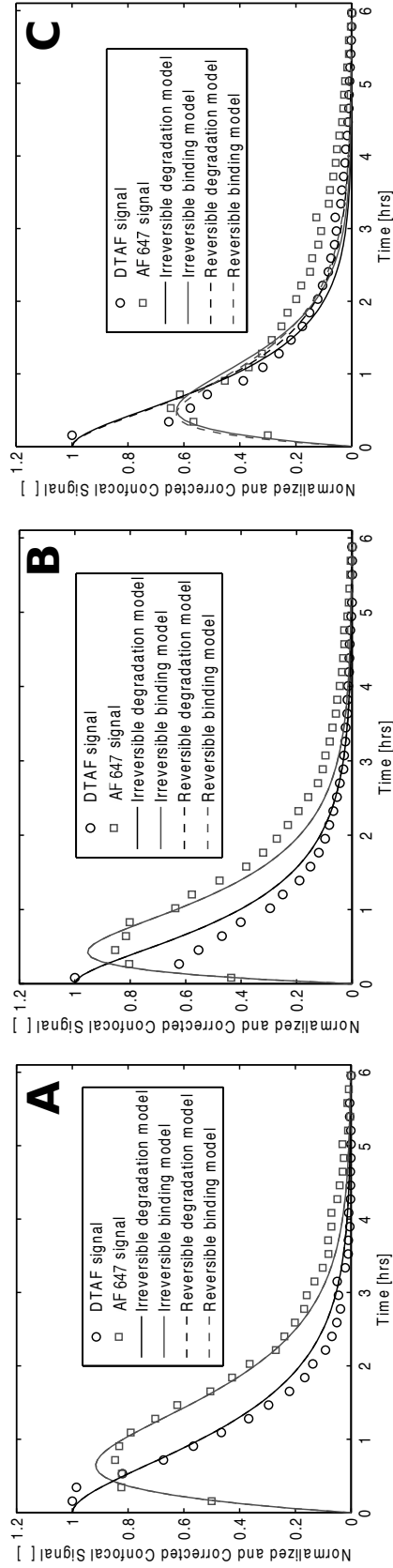


Fig. 7.4: Three examples of data fitting to the reversible and irreversible binding model. Parts A, B and C show the data and the fitted model for separate areas and separate experiments. *Irreversible* or *Reversible degradation model* refers to the predicted evolution of the normalized DTAF-labeled BMCC signal predicted by irreversible and irreversible binding models, respectively.

known. However, it is assumed that a molar mass of 60 kDa, which is a good approximation for cellulase molar mass [126], can be used to calculate an approximate binding rate constant (k_1) from the fitting result ($k_1[E]$). This results in a k_1 value of about $0.2 \text{ min}^{-1}\text{mM}^{-1}$. This binding rate constant is about 100-200 times smaller than binding rate values obtained in previous studies done at 20°C a temperature at which a smaller binding rate would have been expected [116]. Furthermore, though the results of Moran-Mirabal et al. were obtained with *Thermobifida fusca* enzymes, they were in agreement with previously reported half saturation times on cellulose obtained for *T. reesei* crude extracts [296]. Under the conditions used here, a binding rate of $30 \text{ min}^{-1}\text{mM}^{-1}$ would lead to a characteristic binding time ($1/(k_1[E])$) of 20 sec rather than the characteristic binding time of 50 min as predicted from the fitted value (see Table 7.2).

A possible explanation for this discrepancy is that binding is instantaneous with respect to the measurement capabilities used here. Given that the measure of AF647 fluorescence reflects changes in enzyme surface concentration that are mostly due to binding of the cellulase's binding module, this does contradict recent reports that a limiting factor could be the binding of a cellulose chain to the enzyme's catalytic domain [128]. In the case of instantaneous binding, the increase in the signal of bound cellulase would be due to an increase in the number of binding sites. Furthermore, during imaging moving fibers were observed as tension was released during degradation. This could have led to new sites being created between fibers that may have been inaccessible due to the dense packing of the cellulose chains within BMCC microfibrils. The hypotheses of instantaneous binding and new site creation are used as a basis for the instantaneous binding model, the results of which are discussed in section 3.3.

7.3.3 Instantaneous binding models

Parts A, B and C of Figure 7.5 detail three separate examples of data fitting to the instantaneous binding model. The two fitted rate constants (k_i and $k_{i,2}$) have very similar values to those of the irreversible binding model (see Table 7.3) because the predicted initial fraction of exposed sites (ψ) is only 2% (as ψ approaches 0 these two models become mathematically identical). However, these two models have very different implications. For the instantaneous binding model, only 2% of the available sites are predicted as exposed at the start of the reaction vs. 100% in the case of the irreversible binding model. This accounts for an important part of the spread between the estimated ranges of the ratio of fluorescence proportionality constants (a/b) observed between the two models (see Table 7.2 and II). When only 2% of the sites are accessible, b multiplies a concentration of bound sites approximately 50 times smaller (see Equation 3) and thus, should be at least 50 times larger (while a remains approximately the same for both models). If an equilibrium process is in fact taking place rather than just irreversible binding, the predicted fraction ψ could be interpreted as the fraction of occupied sites (regardless of whether they are exposed or unexposed). The increase in accessible binding sites would still be responsible for the increase in bound cellulase through a modification of the equilibrium conditions. An equilibrium process could help explain why the degradation occurs in minutes when the enzyme concentration is 50 times higher (see Appendix D). Therefore, exposing binding sites appears to be an important rate-limiting process in cellulose degradation.

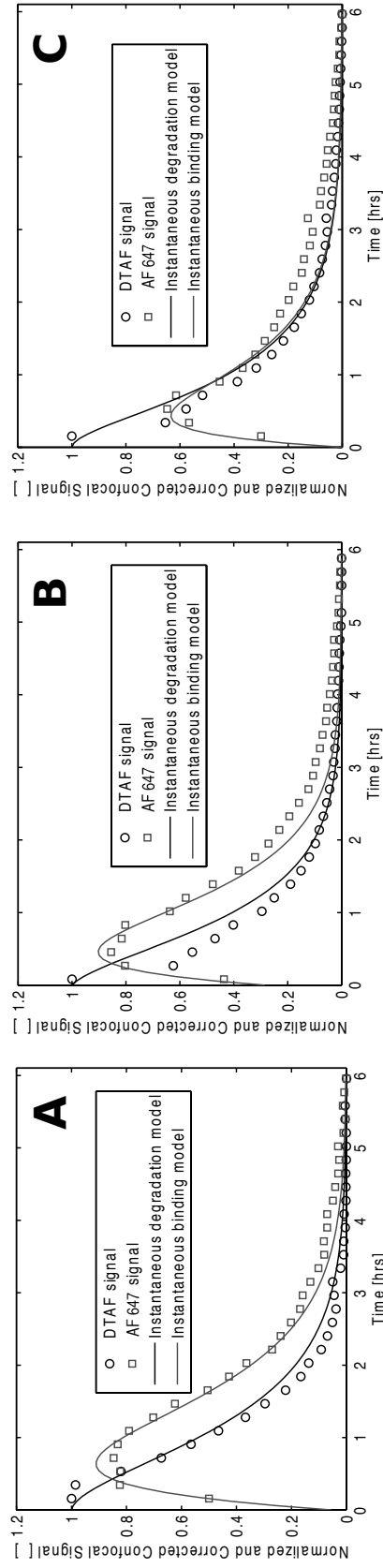


Fig. 7.5: Three examples of data fitting to the instantaneous binding model. Parts A, B and C show the data and the fitted model for separate areas and separate experiments. Instantaneous degradation model refers to the predicted evolution of the normalized DTAF-labeled BMCC signal predicted by instantaneous binding model.

Table 7.3: Average fitting results and their standard deviation (obtained from 10 fits) for the instantaneous binding model.

$k_{i,1}[E]$ [min^{-1}]	$k_{i,2}$ [min^{-1}]	ψ [-]	β/α [-]
0.019 ± 0.002	0.064 ± 0.018	0.022 ± 0.002	0.003 ± 0.005

7.3.4 Model validation

The soluble product yield predicted by the irreversible and reversible binding model is compared to soluble product measurements from independent experiments (see Figure 7.6). Carbohydrate oligomers larger than cellobiose were not detected. The comparison shows that all experimental measurements fall within the model's standard deviation. Given the mathematical similarity of the irreversible binding model to the two other models, its soluble product predictions are just as accurate even though it seems to more accurately reflect cellulase-binding kinetics (see Figure 7.7). This demonstrates that kinetic models constructed on the basis of the optical measurements can accurately predict degradation, as measured by soluble product formation.

7.4 Conclusions

In this study, a way of observing cellulose degradation by a commercial cellulase cocktail *in situ* at temperatures relevant for catalysis (i.e. 50°C) was presented. It allows tracking both the degrading cellulose and the bound enzyme. These images were used to generate quantitative information that was fitted to three kinetic models. Comparing the modeling results to those obtained in the literature allowed us to reach conclusions regarding rate-limiting processes in BMCC degradation: specifically, that exposing new binding sites is an impor-

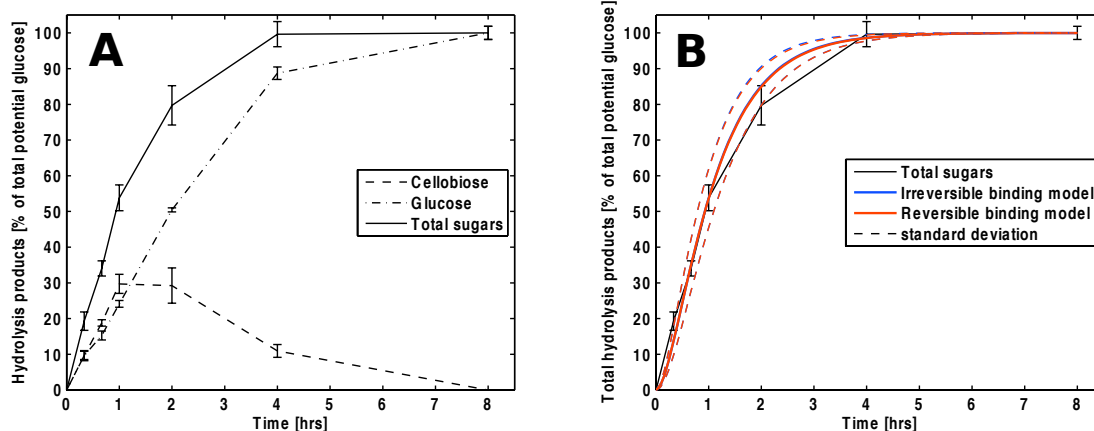


Fig. 7.6: Comparison of bulk sugar concentrations measured during the enzymatic hydrolysis of BMCC with the predictions obtained from the irreversible and reversible binding model (the irreversible binding model is barely noticeable because both models fall on top of each other). Part A shows the amount of glucose and cellobiose measured in solution with their sum as the molar percentage of the total potential glucose. Part B shows the amount of potential glucose liberated predicted by the irreversible and reversible binding models and the sum of glucose and cellobiose measured in solution. Error bars represent the standard deviation of the sugar measurements and dashed lines represent that of the models.

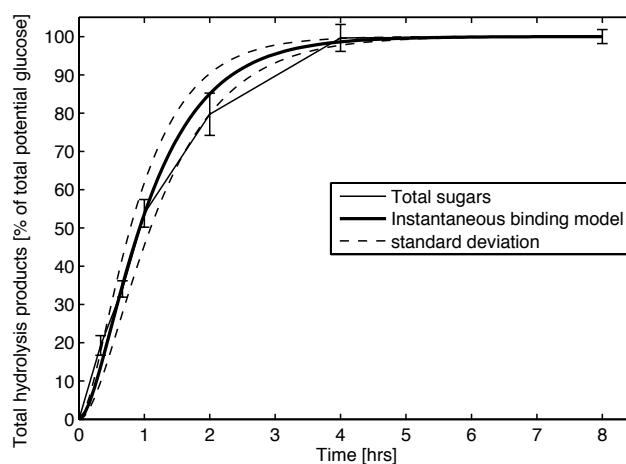


Fig. 7.7: Comparison of total bulk sugar concentrations measured during the enzymatic hydrolysis of BMCC with the predictions obtained from the instantaneous model. Error bars represent the standard deviation of the sugar measurements and dashed lines represent that of the instantaneous binding model.

tant rate-limiting step. This study also demonstrates that models constructed from optical measurements can form the basis for predictions of cellulose conversion to soluble products. In summary, the confocal microscopy methods together with the development of kinetic models could be useful in guiding the development of cellulase cocktails by improving the understanding of the key mechanisms and rate-limiting steps that occur during cellulose degradation.

CHAPTER 8

A PORE-HINDERED DIFFUSION AND REACTION MODEL CAN HELP EXPLAIN THE IMPORTANCE OF PORE SIZE DISTRIBUTION IN ENZYMATIC HYDROLYSIS OF BIOMASS

Large portions of this Chapter appear in a manuscript that was submitted to the Journal *Biotechnology & Bioengineering* [297].

8.1 Introduction

Producing carbohydrates is a key bottleneck in the biomass conversion [29]. Improving conversion yields, lowering enzyme costs and increasing product concentration are major challenges to successful carbohydrate production from biomass (see Chapters 4, 5 and 6 and Lynd et al. [29]). In Chapter 3, a methodology enabling the *in situ* imaging of enzymatic hydrolysis and a model was introduced to better understand enzymatic hydrolysis of BMCC. A better understanding of enzymatic hydrolysis could help guide a rational design process for improving cellulolytic enzyme cocktails.

Indeed, so far, most advances in enzymatic hydrolysis, but also biomass pretreatment, have been made through random optimization. This is illustrated somewhat by the work presented in Chapters 4, 5 and 6 but especially by the recent interest in high-throughput pretreatment methods that allow for rapid screening of a wide array of pretreatment parameters [298, 299, 300, 301]. Similarly, high throughput activity assays have been developed to assess the rate and extent of biomass enzymatic hydrolysis [300, 302, 303]. Moreover, some researchers have used large data sets to create empirical statistical models to

further optimize enzyme mixtures [123, 124].

Though all of these methods are effective, none are based on comprehensive theoretical modeling. The complexity of lignocellulosic substrates is partially to blame, because it makes understanding and modeling pretreatment, enzymatic hydrolysis and their relationship very difficult. However, important results obtained by Grethlein showed that initial enzymatic hydrolysis rates are strongly correlated with the reactive surface area available to enzymes, which greatly increases during pretreatment [118]. The significance of reactive surface area compared to other parameters such as lignin removal was recently confirmed by Rollin et al. [214]. However, to our knowledge, no study has provided a model to successfully explain this correlation.

The importance of reactive surface area indicates that accessibility of the substrate to the enzymes is a key factor controlling hydrolysis. Enzymatic hydrolysis should be modeled as an inherently heterogeneous catalysis process where enzyme diffusion and surface reactions occur. Such an approach differs from models using bulk concentrations such as Michaelis-Menten kinetics or only surface reactions such as Langmuir binding without accounting for diffusion. These modeling efforts were recently reviewed by Bansal et al. [119]. In Chapter 7, BMCC degradation by a commercial cellulase cocktail was modeled using Langmuir binding kinetics. Heterogeneity was accounted for by assuming that only a fraction of the substrate was at the surface at the start of the reaction. Similarly, Gan et al. attempted to incorporate both heterogeneity factors and kinetics, but they did not model spatial variations of concentration within a biomass particle and thus did not truly account for diffusion [134]. Instead, they account for the heterogeneity of the particle through an accessibility factor. In contrast,

the objective of this Chapter is to introduce a model of enzymatic hydrolysis of biomass as a diffusion and surface reaction process in a porous substrate. This approach is then used to model and explain the dependence of initial rates of enzymatic hydrolysis of biomass on accessible surface area as reported in the literature [118].

8.2 Methods

8.2.1 Model

Biomass particles were modeled as porous cylinders of infinite length containing a fraction of their total mass (x_A) that is accessible to degrading cellulases (see Figure 8.1, Parts A and B). As shown in images taken with a confocal microscopy system, a non-shrinking cylindrical geometry with a decreasing density is a reasonable geometry for hydrolyzing biomass (see supplemental information). The accessible biomass mass fraction (x_A) reacts while the inaccessible fraction ($1 - x_A$) is unaffected by enzymes. Assuming cellulose is evenly distributed within the particles, the accessible mass fraction (x_A) can be estimated from the final yield of cellulose conversion to glucose (Y_C).

$$x_A = Y_C \tag{8.1}$$

Part B of Figure 8.1 illustrates our definition of accessible and inaccessible biomass fractions. Table 7.1 contains a list and description of all the symbols used below. To integrate over evolving densities, accessible mass fractions must be translated into accessible volume. If a uniform and unchanging biomass density (ρ_B , not including void volume) is assumed, then the accessible mass frac-

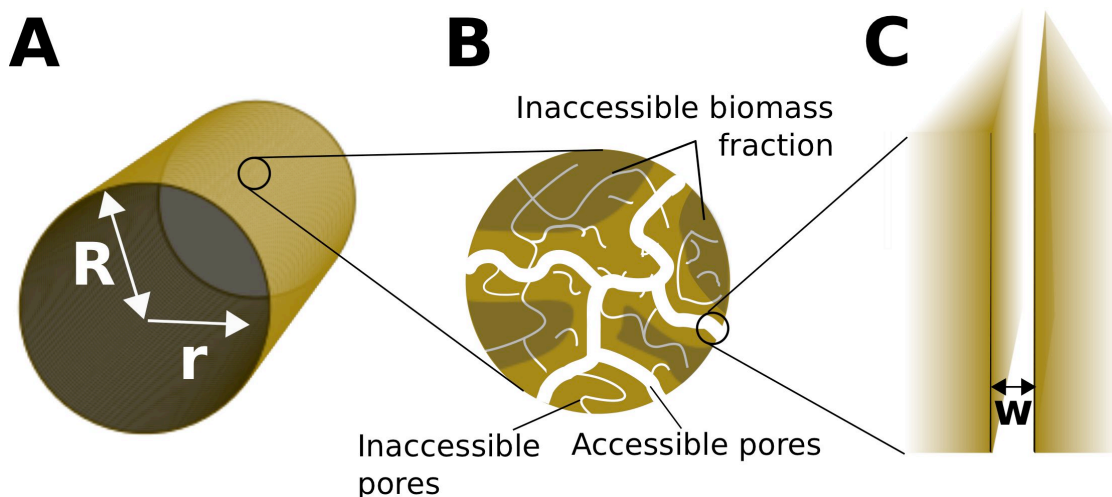


Fig. 8.1: Assumed biomass geometry. Part A shows the entire biomass particle modeled as a cylinder of radius R . Part B shows a close-up of the pore geometry with large accessible pores (i.e. wider than 51 \AA) and small inaccessible pores. An assumed inaccessible fraction of biomass is shown with darker shading. Part C shows the assumed pore geometry as an infinite slit.

tion (x_A) will be equal to the accessible biomass volume fraction ($x_{A,v}$), which is the fraction of biomass volume occupied by accessible biomass, not including void volume:

$$x_{A,v} = \frac{\rho_B}{\rho_B} x_A = x_A \quad (8.2)$$

If one assumes that the inaccessible void volume (i.e. pores smaller than 51 \AA , the approximate size of a cellulase (Grethlein, 1985)) is equally distributed within the accessible and inaccessible biomass, as shown in Part B of Figure 8.1, then the fraction of inaccessible pores located within the accessible fraction of biomass can be assumed to be equal to the fraction of accessible biomass volume. Therefore, the specific volumes (including void volume) occupied by the accessible (V_A) and inaccessible (V_I) fraction per mass of biomass, which do

Table 8.1: List of symbols and their associated source. Dependent variables listed as *Dep. var.* and can be calculated from one of the equations while independent variables are listed as *Indep. var.*

Parameters	Description	Units	Value	Source
D_{bulk}	Cellulase diffusivity in the bulk solution	[cm ² /min]	$7.35 \cdot 10^{-5}$	Estimated from Young et al. [304]
D_E	Cellulase effective diffusivity in the pores	[cm ² /min]	Dep. var.	-
\bar{D}_p	Average cellulase diffusivity in the pores	[cm ² /min]	Dep. var.	-
$D_{p,j}$	Cellulase diffusivity in pore j	[cm ² /min]	Dep. var.	-
d_c	Molecular diameter of a cellulase	[Å]	51	[118]
W_j	Diameter of pore j	[Å]	Indep. var.	From pore size distributions data [118]
$E(\tau,t)$	Enzyme concentration in a pore	[mol/cm ³]	Dep. var.	-
$[E]_{bulk}$	Bulk enzyme concentration	[mol/cm ³]	Dep. var.	From the enzyme concentration (0.93 mg/ml) with an estimated molar mass of 60 kDa [118, 126].
h	Length of finite difference radial section	[cm]	R/n	-
k_1	Cellulase binding rate constant	[cm ³ /(mol min)]	$3 \cdot 10^4$	[116]
k_2	Cellulase surface reaction rate	[min ⁻¹]	0.068	Chapter 7
M_{AorI}	Mass of the accessible (A) or inaccessible (I) fraction of a biomass particle	[g]	Dep. var.	-
M_p	Average mass of cellulose liberated per mole of cellulase during one binding-reaction cycle	[g/mol]	58'000	Estimated value corresponds to 360 glucan monomers.
$M_{tot,HorL}$	Mass of the particle's total, hemicellulose or lignin fractions	[g]	Indep. var.	[118]
n	Number of radial sections used to solve the problem numerically.	[-]	50	-
r	Radial distance	[cm]	Indep. var.	-
R	Particle radius	[cm]	$2.5 \cdot 10^{-3}$	The particle radius was assumed to be 10% of the screen size opening (0.25 mm) [118].
S	Surface area per pore volume	[cm ² /cm ³]	Dep. var.	-
t	Time	[min]	Indep. var.	-
V_{AorI}	Accessible (A) or inaccessible (I) specific volume (i.e. per initial particle mass $M_{tot,0}$) of the particle	[cm ³ /g]	Dep. var.	-
$V_{p,j}$	Specific volume (i.e. volume per initial particle mass $M_{tot,0}$) of pore j	[cm ³ /g]	Indep. var.	Based on data from pore size distributions [118].
x_A or $x_{A,v}$	Mass or volume fraction of accessible biomass	[-]	Dep. var.	-
X_0	Variable X at time 0	[-]	-	-
Y_C	Final cellulose conversion yield	[-]	Indep. var.	Taken as the 24-hr yield reported by Grethlein [118].
ϵ	Porosity	[cm ³ /cm ³]	Dep. var.	-
η	Fraction of pore surface that is not cellulose (i.e. that cannot bind cellulases)	[-]	Dep. var.	-
$\vartheta(\tau,t)$	Fraction of occupied binding sites	[-]	Indep. var.	-
$\rho_A(\tau,t)$	Density of accessible fraction (with void)	[g/cm ³]	Dep. var.	-
ρ_B	Density of biomass (excluding void)	[g/cm ³]	1.49	Calculated from the proportion of cellulose, hemicellulose and lignin [118] with density values for each fraction Ehrnrooth [305].
σ	Maximum cellulase surface concentration on cellulose	[mol/cm ²]	$2.1 \cdot 10^{-12}$	Based on the estimated projection of a cellulase [125].
ρ_I	Density of the inaccessible fraction (including void)	[g/cm ³]	Dep. var.	-
τ	Tortuosity	[-]	2	Estimated parameter (constrained between 1 and 3)

not change with the reaction, can be defined as:

$$V_A = \left(\frac{1}{\rho_B} + \sum_{i=0}^{51\text{\AA}} V_{p,i} \right) x_{A,v} + \sum_{i=51\text{\AA}}^{\infty} V_{p,i} = \frac{x_{A,v}}{\rho_{A,0}} \quad (8.3)$$

$$V_I = \left(\frac{1}{\rho_B} + \sum_{i=0}^{51\text{\AA}} V_{p,i} \right) (1 - x_{A,v}) = \frac{(1 - x_{A,v})}{\rho_{I,0}} \quad (8.4)$$

As shown in Equation 8.1, the accessible specific volume V_A contains a fraction of the inaccessible pores but also the entirety of the accessible pores. By definition, the accessible pores can only be found within the accessible biomass fraction (see Figure 8.1, Part B). On the other hand, the inaccessible volume only contains the inaccessible volume fraction of biomass and an equal fraction of inaccessible void volume. The total mass of the particle is calculated by integrating over both specific volumes as defined in equations 3 and 4 and multiplying by the initial particle mass:

$$M_{tot} = M_A + M_I = M_{tot,0} \left(\int_{V_A} \rho_A(r, t) + \int_{V_I} \rho_I \right) = M_{tot,0} \left(\int_{\frac{x_{A,v}}{\rho_{A,0}}} \rho_A(r, t) + \int_{\frac{1-x_{A,v}}{\rho_{I,0}}} \rho_I \right) \quad (8.5)$$

The proposed mass transfer and reaction model is based on mass balance equations for enzyme in solution (Equation 8.6), surface bound enzymes (Equation 8.12) and biomass density (Equation 8.13) in the accessible fraction of the particle. For the mass balance of enzyme in solution, accumulation of enzyme is controlled by radial diffusion through the accessible porous structure, removal of enzyme through surface binding, and addition of enzyme when product formation is catalyzed and enzyme unbinds from the surface (see Figure 8.2 for an illustration of this kinetic model within a pore):

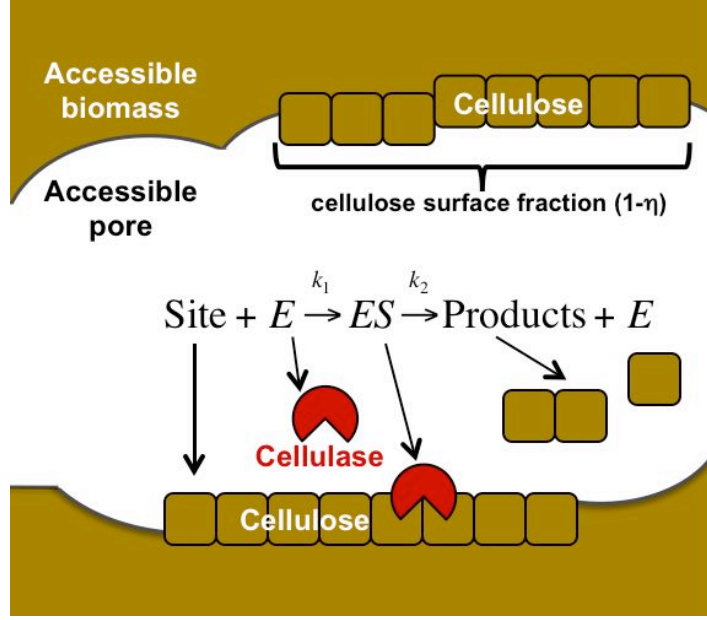


Fig. 8.2: Illustration of the proposed cellulase reaction mechanism in an accessible biomass pore. Cellulose only covers a fraction $(1 - \eta)$ of the pore surface. Cellulases (E) react with available cellulose binding sites (k_1) to form a surface-bound enzyme (ES) and a second reaction (k_2) produces soluble oligosaccharides from cellulose and liberates the enzyme.

$$\frac{\partial E(r, t)}{\partial t} = D_E \frac{1}{r} \frac{\partial}{\partial r} \left(r \frac{\partial E(r, t)}{\partial r} \right) - S(1 - \eta) \sigma (1 - \vartheta(r, t)) k_1 E(r, t) + S(1 - \eta) \sigma \vartheta(r, t) k_2 \quad (8.6)$$

Radial diffusion through pores is proportional to the effective diffusion coefficient (D_E). For liquids, this coefficient can be expressed as a function of the bulk diffusion coefficient (D_{bulk}), the tortuosity factor (τ) and the pore size distribution (adapted from Harriott to express diffusion per pore volume as opposed to total volume [209]):

$$D_E = \frac{\bar{D}_p}{\tau} = \frac{1}{\tau} \frac{\sum_{j=51\text{\AA}}^{\infty} D_{p,j} V_{p,j}}{\sum_{j=51\text{\AA}}^{\infty} V_{p,j}} = \frac{1}{\tau} \frac{D_{bulk} \sum_{j=51\text{\AA}}^{\infty} \left(1 - \frac{51\text{\AA}}{w_j}\right)^4 V_{p,j}}{\sum_{j=51\text{\AA}}^{\infty} V_{p,j}} \quad (8.7)$$

The width of pore j (w_j) is calculated from the pore size distribution. If a set of pores is accessible to a molecule of 51 Å but not 90 Å, the average pore diameter

is assumed to be mid-way between those two molecular diameters (70.5 Å). For consistency with Grethlein, pores are assumed to be infinite slits, which are only characterized by their width (see Figure 8.1, Part C) [118]. Though it is assumed that pores widen during hydrolysis as a result of degradation, as a first approximation, it was assumed that effective diffusivity does not change during hydrolysis. The validity of this assumption is discussed further in the results and discussion section.

In Equation 8.6, removal of enzyme through surface binding is defined as the product of the number of binding sites on the surface of a pore per pore volume ($S\sigma(1-\eta)$) and the rate of change of the fraction of occupied sites ($(1-\vartheta)k_1(r,t)$). Given the assumed pore geometry (see Figure 8.1, Part B), the surface area per pore volume (S) is calculated as a volume average of the inverse of the pore diameter w :

$$S = \frac{\sum_{j=51\text{\AA}}^{\infty} V_{p,j} \frac{1}{w_j}}{\sum_{j=51\text{\AA}}^{\infty} V_{p,j}} = \frac{\sum_{j=51\text{\AA}}^{\infty} V_{p,j,0} \frac{\epsilon_A(r,t)}{\epsilon_{A,0}} \frac{1}{w_{j,0} \frac{\epsilon_A(r,t)}{\epsilon_{A,0}}}}{\sum_{j=51\text{\AA}}^{\infty} V_{p,j,0} \frac{\epsilon_A(r,t)}{\epsilon_{A,0}}} = S_0 \frac{\epsilon_{A,0}}{\epsilon_A(r,t)} \quad (8.8)$$

In the case where pores widen during degradation, pore volume and pore width evolve linearly with increasing porosity. Therefore, as shown in Equation 8.8 S can be rewritten as a function of its initial value (S_0) and the porosity of the accessible fraction (ϵ_A), which evolves as a function of density according to the following relationship:

$$\epsilon_A = 1 - (1 - \epsilon_{A,0}) \frac{\rho_A(r,t)}{\rho_{A,0}} \quad (8.9)$$

where the initial porosity of the accessible fraction can be calculated as follows:

$$\epsilon_{A,0} = \frac{\sum_{j=51\text{\AA}}^{\infty} V_{p,j}}{V_A} \quad (8.10)$$

The amount of surface area per volume (S) is multiplied by the total number of cellulases that can fit on a surface (σ), which is calculated based on the area occu-

pied by a single Cel7A cellulase [125]. A fraction (η) of the total biomass surface is assumed to have a negligible enzyme binding capacity. This non-binding surface fraction is assumed to be equal to the fraction of lignin and hemicellulose. This assumption is based on *in situ* observations of pretreated biomass during enzymatic hydrolysis using fluorescence confocal microscopy (see supplemental information), which show that after most of the cellulose has solubilized, far fewer enzymes seem to be bound to biomass. Therefore, if some non-specific binding does occur on lignin or hemicellulose, it is assumed to be negligible in hydrolysis systems such as those described here, where the total cellulase loading is much larger than the binding capacity of biomass. If one assumes that lignin and hemicellulose are little affected by cellulases, the fraction of surface that cannot bind can be described as the surface fraction occupied by hemicellulose and lignin. If the densities of all biomass components are assumed to be the same, this surface fraction can be described as a function of density (ρ_A) and the initial mass fraction of hemicellulose and lignin (η_0):

$$\eta = \frac{M_H + M_L}{M_{tot}} = \frac{M_{H,0} + M_{L,0}}{M_{tot,0}} \frac{\rho_{A,0}}{\rho_A(r, t)} = \eta_0 \frac{\rho_{A,0}}{\rho_A(r, t)} \quad (8.11)$$

Similar to enzyme removal, enzyme addition through reaction and unbinding can be described as the multiplication of the number of sites on the surface of a pore per pore volume ($S(1 - \eta)\sigma$) and the rate of change of the fraction of available sites ($\vartheta(r, t)k_2$).

The mass balance for surface-bound enzyme can be expressed as the well-known expression describing the fraction of available binding sites coverage ($\vartheta(r, t)$):

$$\frac{\partial \vartheta(r, t)}{\partial t} = (1 - \vartheta(r, t))k_1 E(r, t) - \vartheta(r, t)k_2 \quad (8.12)$$

Finally, a biomass mass balance describes the change of the accessible fraction's

density (ρ_A) as proportional to the rate of reaction and unbinding of enzymes per pore volume (as described in Equation 8.6) multiplied by the porosity of the accessible fraction (ϵ_A) and the amount of mass liberated per mole of enzyme during one binding/ reaction cycle (M_p):

$$\frac{\partial \rho_A(r, t)}{\partial t} = -\epsilon_A M_p S (1 - \eta) \sigma \vartheta(r, t) k_2 = -\epsilon_{A,0} M_p S_0 (1 - \eta) \sigma \vartheta(r, t) k_2 \quad (8.13)$$

Due to the dependence of porosity on density (see Equation 8.9), evolving density is linked to the exposure of previously unexposed cellulose as surface cellulose depolymerizes.

Equation 8.6 requires two boundary conditions: the no-flux boundary condition at the center of the particle and a fixed concentration ($[E]_{bulk}$) at the edge of the particle:

$$\left(\frac{\partial E(r, t)}{\partial r} \right)_{r=0} = 0 \quad (8.14)$$

$$E_{r=R} = [E]_{bulk} \quad (8.15)$$

Similarly, Equations 8.6, 8.12 and 8.13 all require initial conditions, which are:

$$E_{t=0} = 0 \quad (8.16)$$

$$\vartheta_{t=0} = 0 \quad (8.17)$$

$$\rho_{A,t=0} = \rho_{A,0} \quad (8.18)$$

This system of partial differential equations can be solved numerically (see Computational Methods in the Supplemental Information) and can be used to predict the effect of available surface area to a 51 Å molecule (the approximate size of a cellulase) (Grethlein, 1985). The experimental data set is given in the Supplemental Information. Most model parameters are obtained from the literature (see Table 8.1) and only two, which are difficult to obtain experimentally,

required estimation: tortuosity (τ) and the average amount of biomass liberated per binding/ reaction cycle (M_p). Tortuosity represents the average length of the tortuous path through pores relative to the straight-line distance through the particle and, thus, should reasonably be between 1 and 3[209] . Parameter estimation details are given in the Supplemental Information. These two values were therefore chosen as fitting bounds for tortuosity while M_p was allowed to vary by more than one order of magnitude (10-10'000 glucan monomers units).

8.3 Results and discussion

8.3.1 Proposed model

Parameter estimation results are given in Table 8.2. A tortuosity (τ) of 2.9 is an expected value for a random network of pores [209]. An M_p value corresponding to about 430 glucan monomers is of the same order of magnitude as a reported value for Cel7A, which was of 180 Glucan units on bacterial cellulose [306]. The higher value obtained in this work could be explained by differences between this study and theirs; notably, the use of real biomass, the higher temperature used in this work (50°C vs. room temperature) and the use of cellulase cocktails rather than pure components.

The concentration profile as a function of time and radial coordinate as predicted by Equation 8.6 using estimated parameters is given in Figure 8.3, Part A. The concentration reaches a uniform concentration, which is equal to the bulk concentration ($[E]_{bulk}$) within 30 min. In contrast, the characteristic diffusion time ($(R^2t)D_E$) for the process is about 1 min. Therefore, in the absence of

Table 8.2: Parameter estimation results. The result is given with the fit's estimate of the parameter's 95% confidence interval. The details of the parameter estimation method are given in the Supplemental Information.

Parameter	Units	Starting value	Bounds for constrained parameter estimation	Result	95% confidence interval
Mp	[glucan unit]	360	10-10000	430	242-447
τ	[-]	2	1-3	2.9	1.1-3.9

binding, a uniform concentration would be reached 30 times faster. However, instead of transporting molecules to reach a certain concentration in solution, molecules transported by diffusion fill surface binding sites. Due to specific binding, surface concentrations are much higher than concentrations in solution and the process takes more time. The effect of filling binding sites is apparent in the concentration jump that occurs once all the sites are filled (see Figure 8.3, Parts A and B).

The fact that diffusion plays no part in the kinetics of the process after 30 min validates the earlier stated assumption concerning the evolution of the pore geometry. It was assumed that the effective diffusion constant remained constant during the process. The effect of pore widening would have indeed been minimal because it would have only influenced the process during the first 15 min, and pores were unlikely to widen much during such a short timeframe. Furthermore, any widening would increase the diffusion coefficient and hence further reduce the time during which diffusion plays a role.

Figure 8.3, Part B shows the evolution of the radial fraction of available binding sites on the biomass surface. Binding clearly appears to be almost instantaneous with respect to changes in concentration and in density. As soon as the

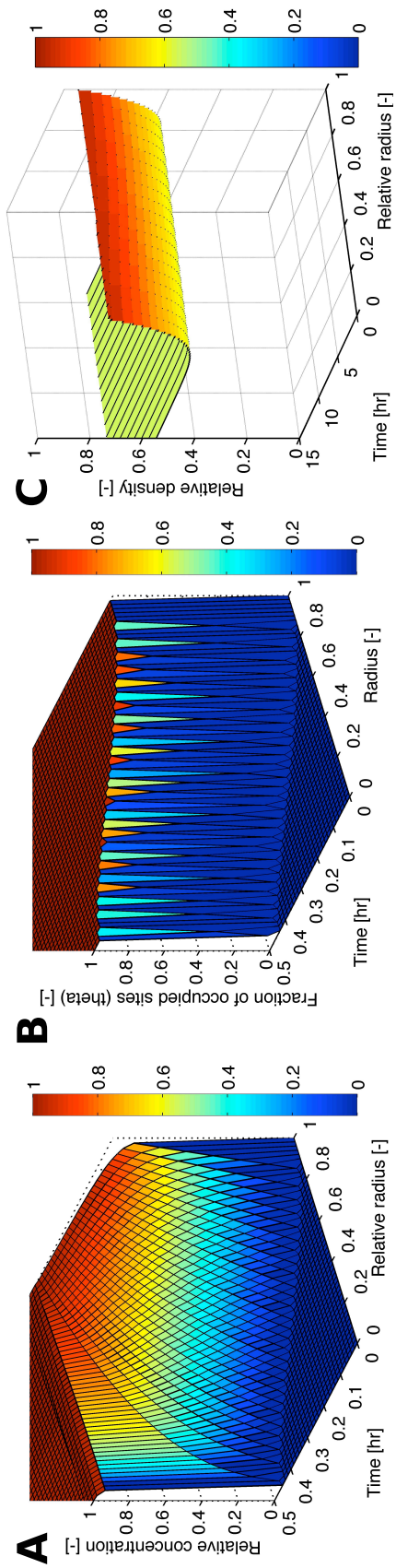


Fig. 8.3: Resulting time and radial profiles of the three mass balance equations that form the basis of the model for mixed hardwood pretreated in 1% acid for 7.8 sec at 220°C. Part A shows the results for cellulase concentration in solution (C_E). Relative radius denotes the ratio of the radial position over the particle radius (r/R) and relative concentration (C_E). Relative radius denotes the ratio of cellulase concentration within the particle over the concentration outside of the particle (CC_E/C_{Bulk}). Part C shows the results for the fraction of occupied binding sites on the surface of the biomass pores (θ).

concentration in solution was non-zero, the surface was almost instantaneously covered. A similar conclusions had been reached in Chapter 7 regarding the rapidity of binding. Furthermore, as a first approximation in this work, a binding rate constant obtained at 35°C was used [116]. Binding at 50°C is likely to lead to a higher binding constant. However, since binding is already much faster than all other processes, an increasing binding rate should not affect results. Indeed, increasing the binding rate constant 10-fold had little effect on any of the model's predictions.

Figure 8.3, Part C, shows the evolution of density with time. Contrary to concentration or surface coverage, density evolves over the course of 5-6 hr and is, by far, the slowest evolving variable. The evolution of density with time is fairly uniform throughout the particle and is only very slightly skewed by diffusion. This suggests that the rate-limiting factor in enzymatic hydrolysis is the need for material to be degraded in order to expose more material. This explains the importance of initially available surface area, which controls the rate at which new material is exposed.

The evolution of cellulose conversion yield with time is shown for three differently treated hardwood samples and compared to experimental measurements in Figure 8.4, Part A. Though the yield measurements are accurately predicted, according to the model, yields reach their maximum at a faster rate than is typical for pretreated biomass, which typically takes at least 24 hr (see Chapters 4, 5 and 6). This could be due to the very small biomass particle size (< .25mm) and severe pretreatment conditions. However, it could also be due to the fact that the model fails to take into account rate slowing factors such as product or pretreatment by-product inhibition, or differences in cellulose recal-

citranse [227]. In a future study, more data points could be obtained between 2-48 hr to better understand rates. Nevertheless, as shown in Figure 8.4, Part B, this model can accurately predict the dependence of initial rates on available surface area, which was first demonstrated by Grethlein [118]. As discussed earlier, though diffusion somewhat affects the 2-hr cellulose conversion yield, it seems to be mostly dependent on the rate at which previously unexposed cellulose is exposed after the degradation of cellulose at the surface. Therefore, increasing surface area will increase the rate at which cellulose is exposed and increase conversion rates.

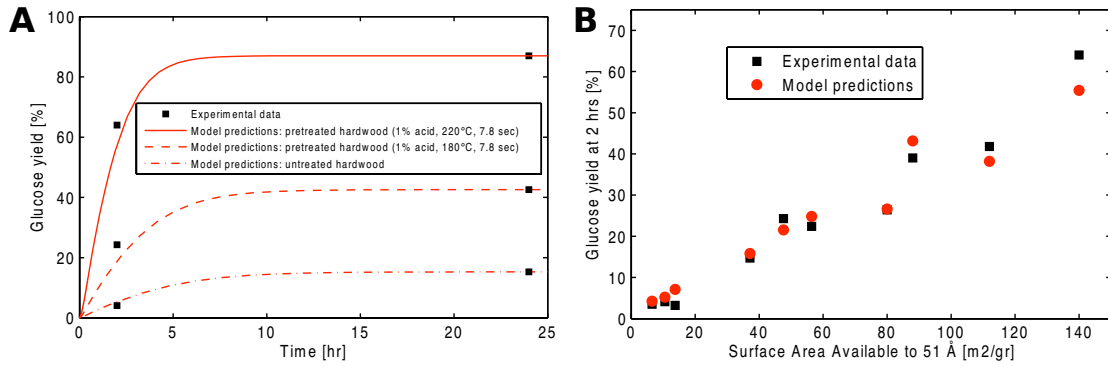


Fig. 8.4: Comparison between modeling and experimental results. Part A shows cellulose to glucose conversion yields vs. time for three types of pretreated and untreated hardwood. Part B shows the cellulose to glucose conversion yields after 2 hr of hydrolysis for all the substrates vs. the surface area available to a cellulase (or a 51 Å molecule).

8.3.2 Effect of neglecting diffusion

As discussed, diffusion seems to play a minimal role in the enzymatic hydrolysis process. If the effect of diffusion is completely neglected, Equation 8.13 can become (with $\vartheta = 1$):

$$\frac{d\rho_A(t)}{dt} = -\varepsilon_{A,0}M_pS_0(1 - \eta)\sigma k_2 = -\varepsilon_{A,0}M_pS_0 \left(1 - \eta_0 \frac{\rho_{A,0}}{\rho_A(t)}\right) \sigma k_2 \quad (8.19)$$

Using the definition of η from Equation 8.11, Equation 8.19 can be solved:

$$t = \frac{\rho_{A,0}}{\varepsilon_{A,0}M_pS_0\sigma k_2} \left[1 - \frac{\rho_A}{\rho_{A,0}} + \eta_0 \ln \left(\frac{1 - \eta_0}{\frac{\rho_A}{\rho_{A,0}} - \eta_0} \right) \right] \quad (8.20)$$

Equation 8.20 can be used to predict yields as a function of time. Further reflecting the limited effect of diffusion, the predictions made from Equation 8.20 (see Figure 3S in the Supplementary Information) deviate only very slightly from those shown in Figure 8.4.

The effect of diffusion on yield can be visualized through the effect of particle size on yield as is shown in Figure 8.5. In the case of a particle with a 2.5×10^{-3} cm radius as is used in this work, when comparing yields predicted by Equations 8.13 (full line) and 8.20 (dashed line), the effect of diffusion is barely apparent after 2 hr of hydrolysis and is completely absent after 4 and 24 hr of hydrolysis. This in part explains the simple dependence of initial yields on accessibility observed by Grethlein [118]. He conveniently used a particle size that was small enough that diffusion could be discounted. However, for larger particles the effect of diffusion becomes quite significant, reducing yields by as much as 90%. One of the benefits of our methodology is that it could guide experimental design by revealing a maximum particle radius for which the simple analytical solution given by Equation 8.20 is a good approximation for describing hydrolysis. Interestingly, in previous work, when larger pretreated hardwood particles were used (1 mm to 1 cm), we usually saw upwards of 40-50% and 80-90% of the maximal yield being reached after 4 and 24 hr, respectively contradicting what is predicted in Figure 8.5 (see Chapters 4, 5 and 6). This indicates that, beyond a certain size, biomass particles most likely contain large fissures that allow for convective transport in a mixed system. When higher solid contents are used and the mixture's viscosity significantly increases, yield after 4 and 24 hr can be reduced by as much as half (see Chapter 6). This could be due to

reduced convective transport at least in part of a particle. In summary, particles beyond a certain size should probably be modeled as multiple independent smaller particles, the size of which could change depending on the mixture's viscosity and/or solid content.

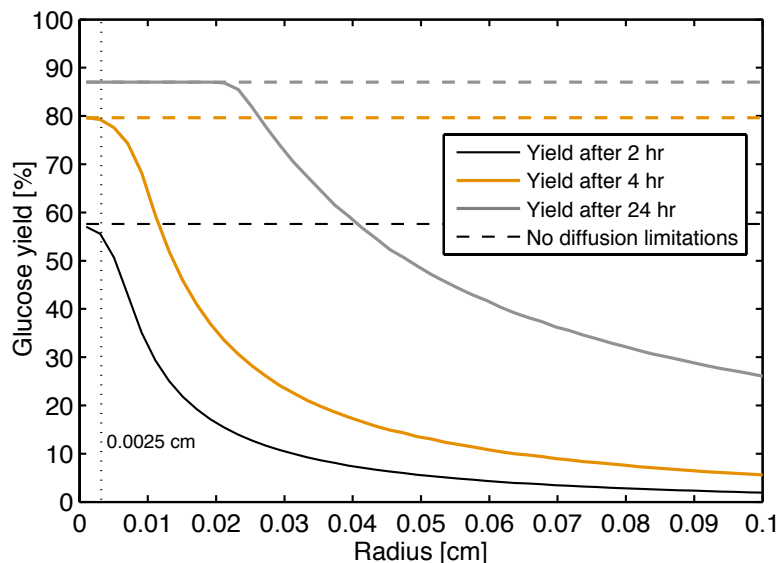


Fig. 8.5: Effect of the particle radius and diffusion on glucose yield after 2, 4 and 24 hr of enzymatic hydrolysis for pretreated hardwood (1% acid, 220°C 7.8 sec). Dashed lines show the yield predicted in the absence of diffusion limitations. The dotted line indicates the particle radius used in this study.

8.3.3 Predictive variant

A disadvantage of the model that has been discussed so far is that one of the model parameters is the measure of the final cellulose conversion yield which is used to calculate the mass fraction of inaccessible biomass (x_A) (see Equation 8.1). In order to make this model only dependent on pore size distribution data, it may be useful to find a way to predict the fraction of accessible biomass based on porosity data. One possible approximation is to assume that the fraction of

accessible biomass is equal to the ratio of accessible pores over the total pore volume (this is referred to as the equality model):

$$x_A \approx \frac{\sum_{j=51\text{\AA}}^{\infty} V_{p,j}}{\sum_{j=0}^{\infty} V_{p,j}} \quad (8.21)$$

As shown in Figure 8.6, in most cases, this model underestimates the fraction of biomass accessible for conversion. One explanation for this is that the equality model implicitly assumes that all inaccessible pores (<51 Å) are contained in the inaccessible fraction while only the accessible pores are contained in the accessible fraction. If the inaccessible pores are evenly distributed throughout the biomass particle, as illustrated in Figure 8.1, this implicit assumption leads to an underestimation of the pore volume fraction in the accessible fraction of biomass, and thus, to an underestimation of this accessible fraction. To improve the estimate, the ratio of pore volume can be recalculated based on the initial estimate of x_A , which is used to re-allocate a fraction of the inaccessible pore volume to the accessible fraction (referred to as the iterative model):

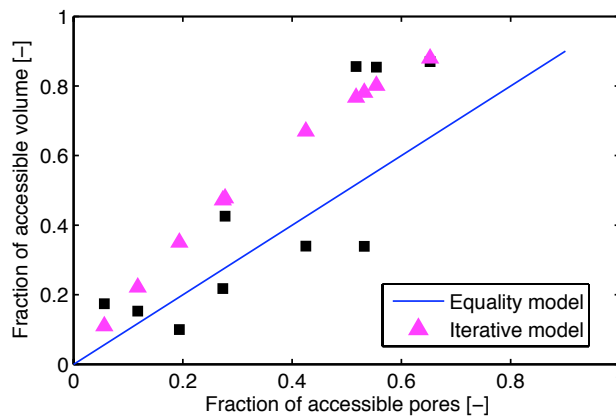


Fig. 8.6: Estimation of the fraction of accessible (or convertible) cellulose from the fraction of accessible pores. The equality model assumes that two are equal while the iterative model uses the equality model to improve the estimate of the true pore volume distribution between the accessible and inaccessible fraction.

$$x_A \approx \frac{\sum_{j=51\text{\AA}}^{\infty} V_{p,j} + x_A \sum_{j=0}^{51\text{\AA}} V_{p,j}}{\sum_{j=0}^{\infty} V_{p,j}} \quad (8.22)$$

Yield predictions based on both estimates of the accessible fraction of biomass are shown in Figure 8.7. As demonstrated by Part A of Figure 8.7, both models accurately predict 2 hr yields. The correlation between initial hydrolysis rates and available surface area depicted in Figure 8.7, Part B is successfully predicted by both models, though the iterative model shows slightly less error for high surface areas and high yields. As shown in Figure 8.7, Part A the correction introduced by the iterative model significantly reduces the final yield error for high yield substrates. Therefore, with this model, final yields can be predicted within 5-10 percentage points based only on pore size distribution data.

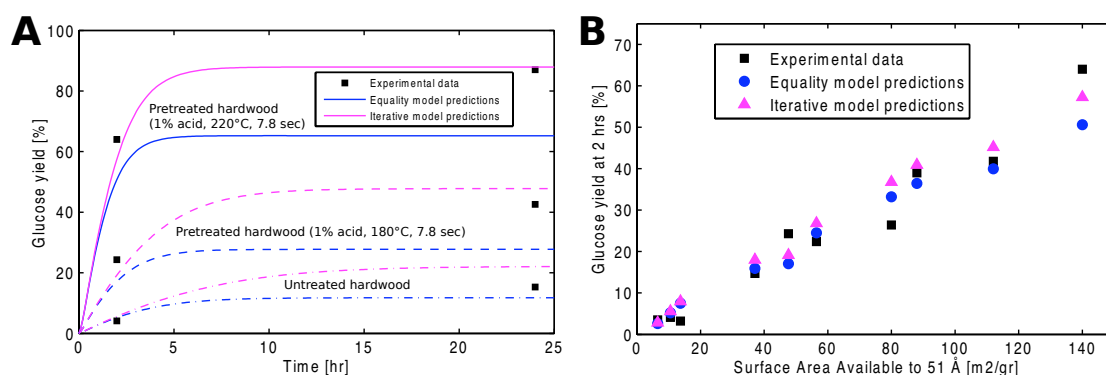


Fig. 8.7: Comparison between experimental results and two sets of modeling results. The equality model assumes that the accessible fraction of biomass is equal to the fraction of accessible pore volume while the regression assumes these two are linearly dependent. Part A shows cellulose to glucose conversion yields vs. time for three types of pretreated and untreated hardwood. Part B shows the cellulose to glucose conversion yields after 2 hr of hydrolysis for all the substrates vs. the surface area available to a cellulase (or a 51 Å molecule).

8.4 Conclusions

This Chapter presents a model that accurately predicts the dependence of initial cellulose hydrolysis rates on surface area available to a cellulase-size molecule. In addition, this model reveals that for particles smaller than 5×10^{-3} cm the key rate-limiting step is the exposure of previously unexposed cellulose after cellulose on the surface has hydrolyzed rather than enzyme binding or diffusion. In the absence of diffusion, a simple analytical solution can be used instead of the numerical one. For larger particles, diffusion may play a more significant role. Therefore, the proposed model can be used to design experiments that produce results that are either affected or unaffected by diffusion. In the model, the fraction of accessible cellulose can either be measured as the final cellulose yield or predicted from pore-size distribution data. Therefore, cellulose yields can be predicted using only the pore-size distribution and compositional data. This could form the basis for the rational design of pretreatment technologies or cellulase cocktails as opposed to using random optimization techniques.

CHAPTER 9

CONCLUSIONS

9.1 Summary of work

9.1.1 Can biphasic mixtures of CO₂ and water be used to successfully produce concentrated solutions of monosaccharides from biomass?

In Chapter 4, a 25 ml unstirred reactor was used to rapidly screen a large array of pretreatment conditions for different biomass species. It was demonstrated that biphasic CO₂-H₂O pretreatment could be used produce glucose yields of 73% for wood, 81% for switchgrass and 85% for corn stover using very similar experimental conditions (160-170°C and a 60 min residence time), high solid contents (40 wt%) and no additional chemicals. However, those results were accompanied with low hemicellulose sugars yields (below 20%) and fairly high furfural yields (around 20%). Since hemicellulose yields were higher when a higher moisture content was used which increased the biomass heat conductivity, temperature gradients within the reactor could have been partially responsible for byproduct formation and low hemicellulose recovery .

Therefore, in Chapter 5, a 1 L stirred reactor is presented and was used to increase homogeneity during CO₂-H₂O pretreatment of lignocellulosic biomass. The larger reactor also allowed for exploring the effect of using larger particles (0.95 cm vs. 1 mm). Temperature gradients were found to have significant

effects and a larger particle size was found to lower glucose yields by about 10 percentage points. Using the stirred reactor, the benefits hypothesized in Chapter 2 and 5 of using using high temperatures and short times and a range of temperatures during pretreatment were confirmed. Two-temperature stage pretreatment was introduced, with a high-temperature and short residence time stage (16 min and 1 min at 210°C for hardwood and Switchgrass, respectively) followed by a longer lower temperature stage (160 °C for 60 min). With this method, glucan to glucose conversion yields of 83% for mixed hardwood and 80% for switchgrass were obtained. These yields were similar to those obtained with dilute acid pretreatment of wood (the major technology for wood conversion) and within 10% of major technologies for switchgrass despite the absence of chemical catalysts, the use of larger particles and the significantly higher solid content (40 wt%).

The optimally pretreated biomass was used in high solids enzymatic hydrolysis experiments. The competing effects of increasing solid content and increasing enzyme concentration and increasing inhibitor concentration were observed on monosaccharide yields. Similar to results reported in the literature for dilute acid pretreated biomass, monosaccharide yields decreased sharply between 25 and 30 wt% solids. Possible causes for this phenomenon could include increased mass transfer limitations and increased inhibitor concentrations contributed. These sharply declining yields were markedly different from those observed with uncatalyzed and alkali catalyzed pretreated biomass, which showed a gradual and continuous decrease in glucose yields with increasing solid content. Such a continuous decline in yields would be more detrimental to commercial processing because it would prevent obtaining high yields at high-solids contents.

Therefore, guided by optimization results presented in Chapters 4 and 5, Chapter 6 presents experiments that used high-solids enzymatic hydrolysis to obtain glucan to glucose yields above 80% and sugar concentrations of 185 and 149g/L for mixed hardwood and switchgrass, respectively, without any drying, separation or additional chemical catalysts. Apart from results obtained with dilute acid pretreated corn stover (see Chapter 6), these are the highest concentration values reported without any substrate drying. In conclusion, high-solids biphasic CO₂-H₂O biomass pretreatment combined with high-solids enzymatic hydrolysis provides high yields, could reduce equipment capital costs by allowing smaller reactor volumes to be used and avoids the use of costly and unsustainable chemical catalysts. However, for this technology to be attractive, all these benefits must outweigh the issue of lower xylose recovery and higher equipment capital costs linked with high-pressure processing when compared to competing technologies.

9.1.2 Can modeling help better understand the relationship between biomass pretreatment and enzymatic hydrolysis and provide a basis for the rational design of biomass depolymerization processes?

As discussed in Chapter 2, most efforts to improve sugar production from biomass through pretreatment and enzymatic hydrolysis have been based on random optimization and/or educated guessing. Better understanding the depolymerization mechanisms of cellulosic substrates by cellulase cocktails and

their relationship with pretreatment could be a critical step towards rationally optimizing the production of monosaccharides from biomass. In Chapter 7, fluorescence confocal microscopy was used to observe the Spezyme CP cellulase cocktail depolymerize bacterial microcrystalline cellulose (BMCC), which was immobilized on a glass surface *in situ*. The enzyme mixture was supplemented with a small fraction of fluorescently labeled *T. reesei* Cel7A, which served as a reporter to track cellulase binding onto the physical structure of the cellulosic substrate. BMCC structure was observed throughout degradation by labeling it with a fluorescent dye. This method allowed us to measure the binding of cellulases *in situ* and follow the temporal morphological changes of cellulose during its depolymerization by a commercial cellulase mixture. Using three kinetic models that were fitted to fluorescence intensity data to predict the soluble sugar concentrations that were liberated from BMCC in bulk experiments demonstrated that fluorescence imaging experiments could successfully be used to gain insights into and successfully predict cellulose hydrolysis. Comparing binding and kinetic parameters from models with different assumptions to previously reported constants in the literature led us to conclude that exposing new binding sites is an important rate-limiting step in the hydrolysis of crystalline cellulose.

On the basis of the kinetic approach that was used in Chapter 7, a pore hindered diffusion and kinetic model was proposed for enzymatic hydrolysis of biomass (see Chapter 8). When compared to data available in the literature, this model accurately predicts the well-known dependence of initial cellulose hydrolysis rates on surface area available to a cellulase-size molecule. Modeling results suggest that, for particles smaller than 5×10^{-3} cm, a key rate-limiting step is the exposure of previously unexposed cellulose occurring after cellulose

on the surface has hydrolyzed, rather than binding or diffusion. However, for larger particles, according to the model, diffusion plays a more significant role. Therefore, the proposed model can be used to design experiments that produce results that are either affected or unaffected by diffusion. Finally, by using pore size distribution data to predict the biomass fraction that is accessible to degradation, this model can be used to predict cellulose hydrolysis with time using only pore size distribution and initial composition data.

Due to the model's ability to predict the importance of surface area available to enzymes in biomass and to predict the fraction of degradable biomass, this proposed pore hindered diffusion model could become a useful tool for the rational design of pretreated biomass and cellulolytic cocktails. It could provide the basis for an optimization based on biomass pore size distribution rather than the more opaque measure of final carbohydrate yields.

9.2 Outlook and future research

Though promising from a sustainability, energy use and economic perspective, high-solids biphasic CO₂-H₂O pretreatment is still limited in its ability to achieve high hemicellulose sugar yields and limit furfural production. Depending on society's future emphasis on process energy usage and process sustainability, these issues could become acceptable trade-offs given this pretreatment's advantages. This could become even more realistic if biphasic CO₂-H₂O pretreatment was coupled with subsequent sugar conversion systems that could tolerate and/or even successfully convert unwanted byproducts such as furfural. In a fermentation process, this could occur with furfural-tolerant and/or

metabolizing microorganisms. In a catalytic processes, this could occur in the case of a reaction system that already considers furfural as an intermediate in sugar conversion, which is already the case for carbohydrate dehydration based processes [307]. Integrating biphasic CO₂-H₂O pretreatment with a process that could successfully take advantage of unconverted hemicellulose and cellulose but also leftover lignin to produce a useful co-product. Several recent Master's thesis projects associated with the work presented here have explored *in silico* using biomass gasification to produce synthetic natural gas as a co-product [308, 216]. These two projects have demonstrated that coupling biphasic CO₂-H₂O pretreatment for ethanol production with hydrothermal gasification for synthetic natural gas production increases biomass conversion's energy efficiency and lowers it's overall environmental impact. Further exploring the integration of additional sustainable energy production processes will undoubtedly reveal similar benefits.

Suggesting that process integration can alleviate some of the drawbacks of CO₂-H₂O pretreatment is in no way indicative that those drawbacks themselves cannot be addressed or even eliminated. The addition of a short, high-temperature stage could during pretreatment increased overall carbohydrate yields without increasing byproduct formation. This confirmed trends observed in the literature and discussed in Chapter 2, that, because polysaccharide depolymerization appears to have a higher activation energy than monosaccharide degradation, high temperatures and short residence times could potentially successfully depolymerize biomass while producing limited amounts of unwanted byproducts. Higher temperatures were not explored in this work due to the limitations of the heating system in the 1 L stirred reactor presented in Chapter 5. An improved heating system enabling increased heating rates could

allow the exploration of higher temperatures and show a benefit that was even more important than the one that was presented in Chapter 5.

A major limitation of pretreatment research, including that presented in this work and discussed above, is that it is largely based on random optimization and educated guessing. In the case of the work presented here, multiple temperatures and residence times were tested out based on trends observed in the data that had already been obtained. The fastidiousness of this process encouraged the development of the model presented in Chapter 8. This model explains the link between increased available surface area to enzyme, which was known to be the main benefit provided by pretreatment, and increased biomass conversion rates and conversion extents. In the future this model could serve as a tool for rational design and optimization of biomass conversion processes. One could imagine engineering pretreatment processes that are targeted for providing improved available surface area in biomass rather than simply increased yields. This could improve the understanding of the key mechanisms that control enzymatic hydrolysis yields during pretreatment and help design more innovative pretreatment strategies. This tool could even be used at the anterior stage, and help engineer plants that are more degradable because they already have or can easily provide increased accessible surface areas for enzymes.

In conclusion, by demonstrating the usefulness of high temperatures or of a two-temperature stage pretreatment process and by explaining the link between increased available surface area and increased enzymatic hydrolysis rates and conversions, the work presented in this thesis has, at the very least, shown that there exists many more research paths to explore.

APPENDIX A
APPENDIX FOR CHAPTER 4

A.1 Thermodynamic equilibrium of the CO₂-H₂O system

According to an approach proposed by Duan and Sun [258], we used a specific interaction model to estimate liquid phase behavior and an equation of state to estimate gas phase behavior of the CO₂-H₂O system. Duan and Sun report predictions within 7% of experimental results for this method. Figure A.1 shows the calculated phase equilibrium data obtained using the Duan and Sun methodology.

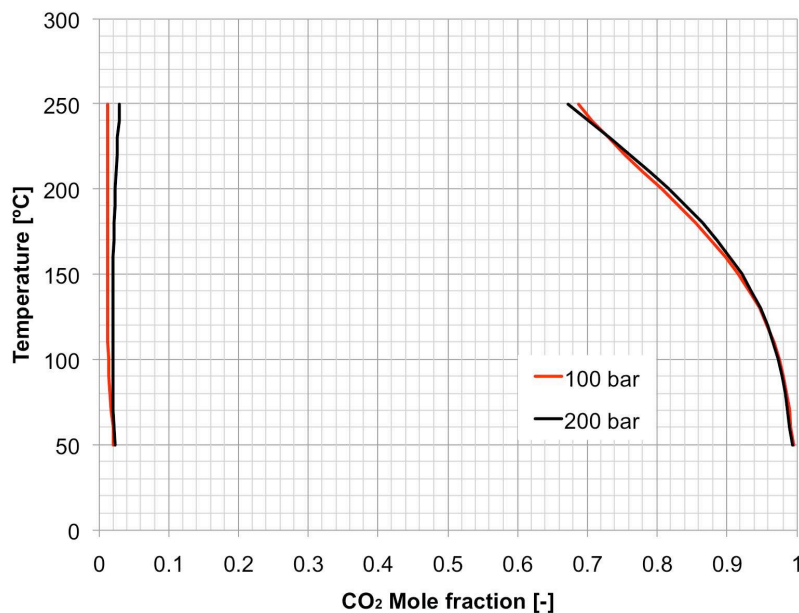


Fig. A.1: Isobaric phase equilibrium data (100 and 200 bar) for the CO₂-H₂O biphasic system.

Using this data, we estimate that, during the course of our experiments (at 200 bar), 20 wt% solids biomass will see maximum of between 1.7 (at 150°C) and 3.8 mol% (at 250°C) of its water transferred to the supercritical CO₂ phase

and that 40 wt% solids biomass will see a maximum of between 4.5 (at 150°C) and 10 mol% (at 200°C) of its water transferred to the supercritical CO₂ phase.

A.2 Heating curves

Figure A.2 shows two typical reactor temperature profiles measured during an experiment using a thermocouple imbedded in the center of the biomass slurry (see Figure 1).

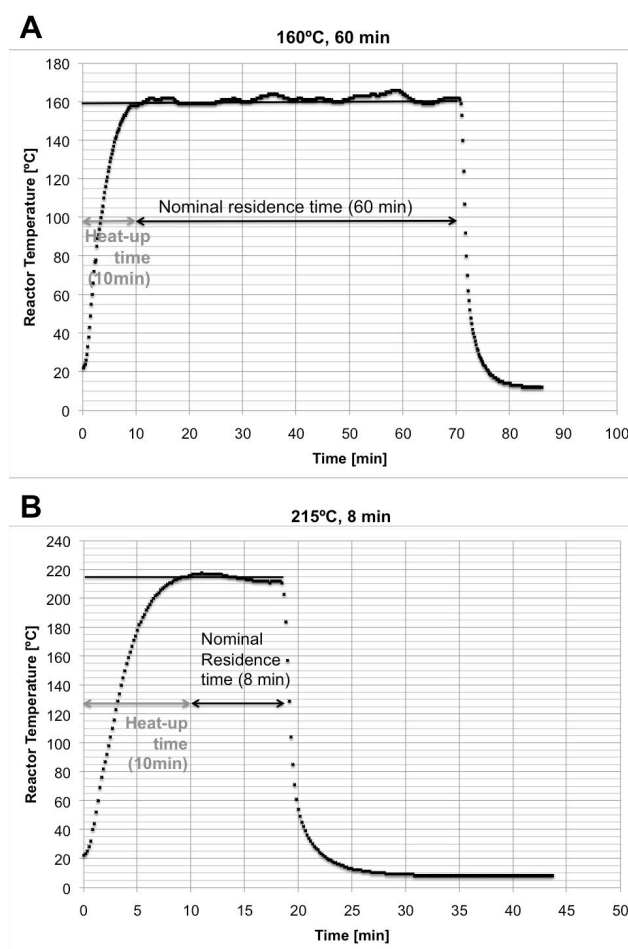


Fig. A.2: Reactor temperature profiles: (A) for a pretreatment experiment at 160°C with a 60 min nominal residence time and (B) for a pretreatment experiment at 215°C with an 8 min nominal residence time.

A.3 Water-saturated supercritical CO₂ pretreatment

Initially, it was attempted to use a unique phase of water-saturated supercritical CO₂ as a pretreatment medium. A biomass slurry was added to the reactor containing just enough water to saturate the CO₂ at the target temperature, pressure and reactor volume. This amount was calculated using a model published by Duan and Sun as described in Section A.1 [258].

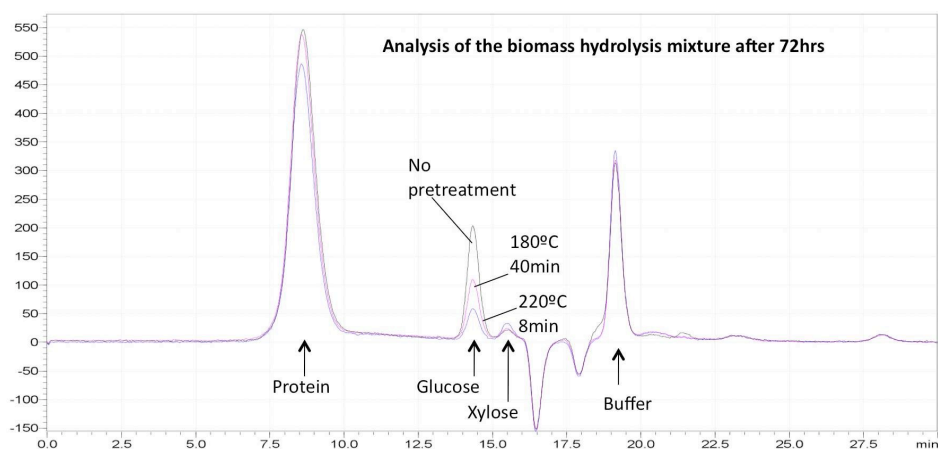


Fig. A.3: Chromatogram overlay for enzymatically hydrolyzed pretreated and non-pretreated hardwood.

Figure A.3 shows a comparison between the HPLC chromatogram of a solution of enzymatically digested non-pretreated hardwood, and those of the same biomass pretreated at various conditions and subsequently subjected to enzymes. Initial glucan loadings were identical for all samples. Contrary to all experiments presented in Chapter 3 of this study, pretreatment seems to decrease glucose and xylose yields and is, therefore, ineffective. This could be due to pyrolysis instead of hydrolysis of the hemicellulose, which could be caused by the absence of sufficient water in the supercritical phase. Indeed, blackening of the biomass was observed during the pretreatment stage.

APPENDIX B
APPENDIX FOR CHAPTER 5

B.1 Mixing impeller

A custom impeller was machined for the 1-L stirred reactor system purchased from Autoclave Engineers® (Erie, PA). Both a close-up of the impeller and a picture of the impeller attached to the shaft and placed over the reactor enclosing are shown in Figure B.1.

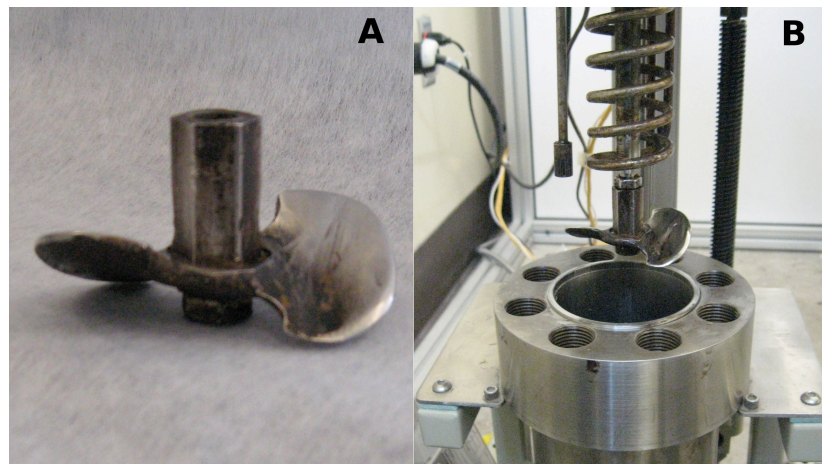


Fig. B.1: Pictures of the custom-machined biomass impeller. Part A shows a close-up of the impeller. Part B shows the impeller attached to the shaft and placed over the reactor.

B.2 Heating curves

Figure B.2 shows two typical reactor temperature and pressure profiles measured during an experiment using a thermocouple imbedded within the biomass slurry and a pressure transducer, respectively (see Figure 5.1). Total

heat-up time typically lasted about 40 min, but only about 8-13 min (depending on whether the target temperature was 200 or 210°C) were spent above 150°C (below this temperature, changes in the biomass glucan to glucose yields after such small residence times was comparable to that due the experimental variability).

B.3 Additional optimization of two-temperature stage CO₂-H₂O pretreatment

B.3.1 Mixed Hardwood pretreatment

Following an initial optimization, where the residence time of a 1st stage at 200°C or 210°C was modified with an unchanged 2nd stage at 160 or 170°C for 60 min, further tests were done to determine the effects of modifying the temperature and residence time of the 2nd stage. Therefore, two first stage conditions were chosen (210°C, 1 min and 210°C, 16 min). The longer residence time, which was the previously determined optimal time, was used to explore the effects of a less harsh or slightly modified 2nd stage. The shorter residence time was chosen to explore the effect of such a stage with a harsher 2nd stage. The results for these experiments are shown in Figure B.3, with a set of five experiments for the 16 min residence time shown on the left and a set of five experiments for the 1 min residence time shown on the right. In the case of the 16 min experiments, all three yields reported in Figure B.3 show statistically insignificant changes with the optimal conditions remaining 210°C for 16 min and 160 for 60 min. In the case of the 1 min experiments, most variations of the 2nd stage did not produce

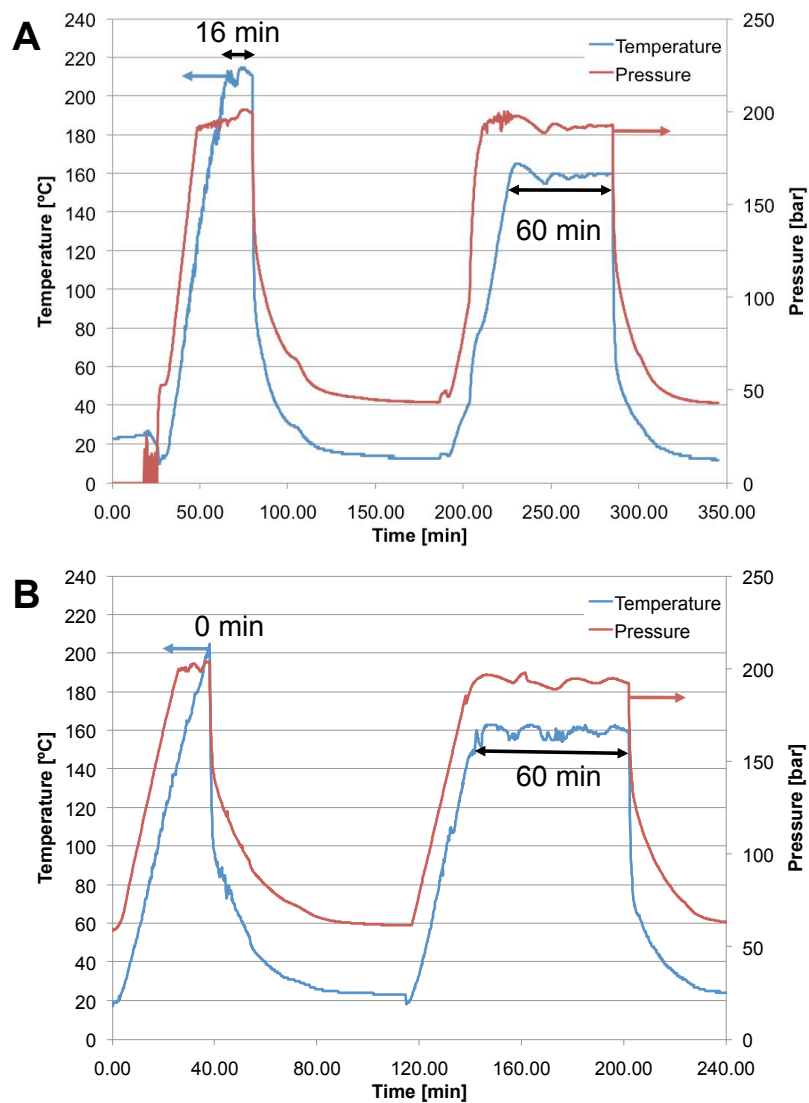


Fig. B.2: Typical temperature and pressure profiles during a two-temperature stage pretreatment experiment. Part A shows results obtained for a pretreatment at 210°C for 16 min and 160°C for 60 min. Part B shows results obtained for a pretreatment at 210°C for 0 min and 160°C for 60 min.

significant changes. The only exception was observed for a 2nd stage at 190°C and 30 min for which increases of Y_g to 67% from yields around 50% of Y_f to 20% from values around 10% were observed.

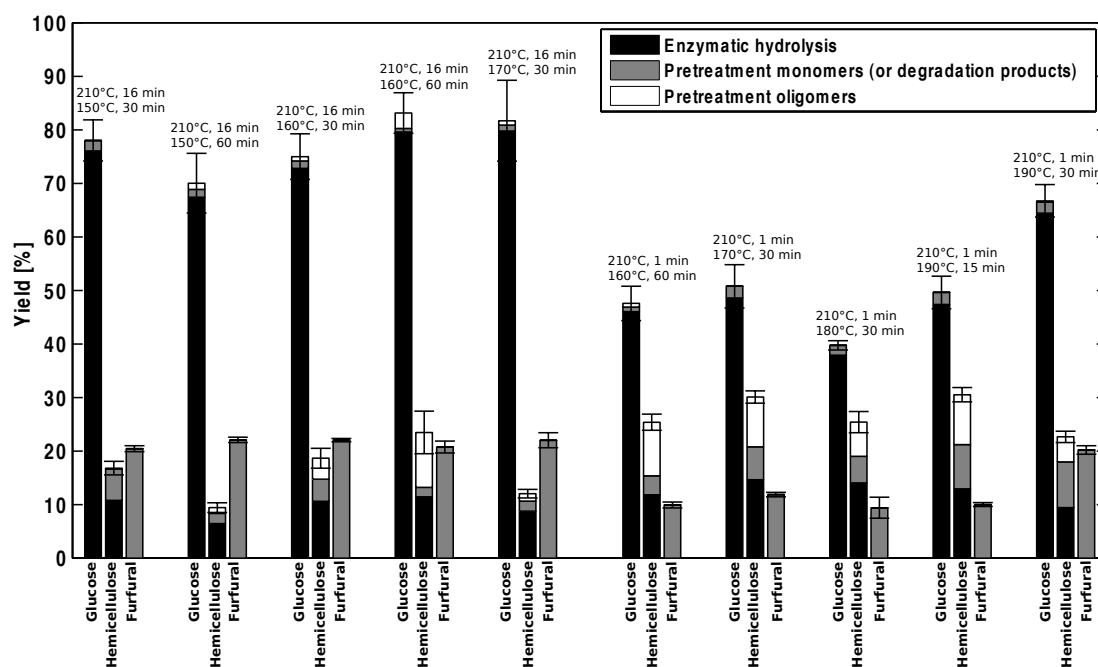


Fig. B.3: Additional yields for two-temperature stage pretreatment of 40 wt% solids (water biomass mixture) large particle mixed hardwood. All yields were obtained after pretreatment at 200 bar and 72 hr of enzymatic hydrolysis (15 FPU/g glucan). Pretreatment conditions are indicated above each set of yields. Bars represent glucan to glucose yields (indicated by *glucose*), xylan, arabinan and mannan to xylose, arabinose and mannose yields (indicated by *hemicellulose*) and xylan and arabinan to furfural yields (indicated by *furfural*). Error bars represent the results 95% confidence interval based on triplicate sampling.

B.3.2 Switchgrass pretreatment

Further tests were done to determine the effects of modifying the temperature and residence time of the 2nd stage on switchgrass pretreatment as well. Once again, two first stage conditions were chosen (210°C, 0min and 210°C, 1 min).

The results for these experiments are shown in Figure B.4, with a set of five experiments with a 1 min residence time shown on the left and a set of five experiments with a 0 min residence time shown on the right. In the case of the 1 min experiments, Y_g increased and Y_h decreased with increasing 2^{nd} stage temperature and retention time. This indicates that given the shortness of the 1^{st} stage, the conditions of the 2^{nd} stage have a bigger impact on yields. In addition, since a significant proportion of pretreatment reactions occur during the heat-up stage, this variability-prone step may introduce more variability in the final yield. Therefore, a Y_g over 80% is observed when the 2^{nd} stage is brought to 160°C for 60 min as opposed to values around 50% obtained at shorter times or lower temperatures. Similar trends are observed for furfural yields (Y_f) and inverse trends are observed for hemicellulose yields (Y_h). Less variation was observed when a residence time of 0 min at 210°C was followed by harsher 2^{nd} stage conditions. All values of Y_g were close to 65% while Y_h values reached above 40% for 2^{nd} stages at 160°C for 60 min and 180°C for 15 min while other Y_h values were around 25%.

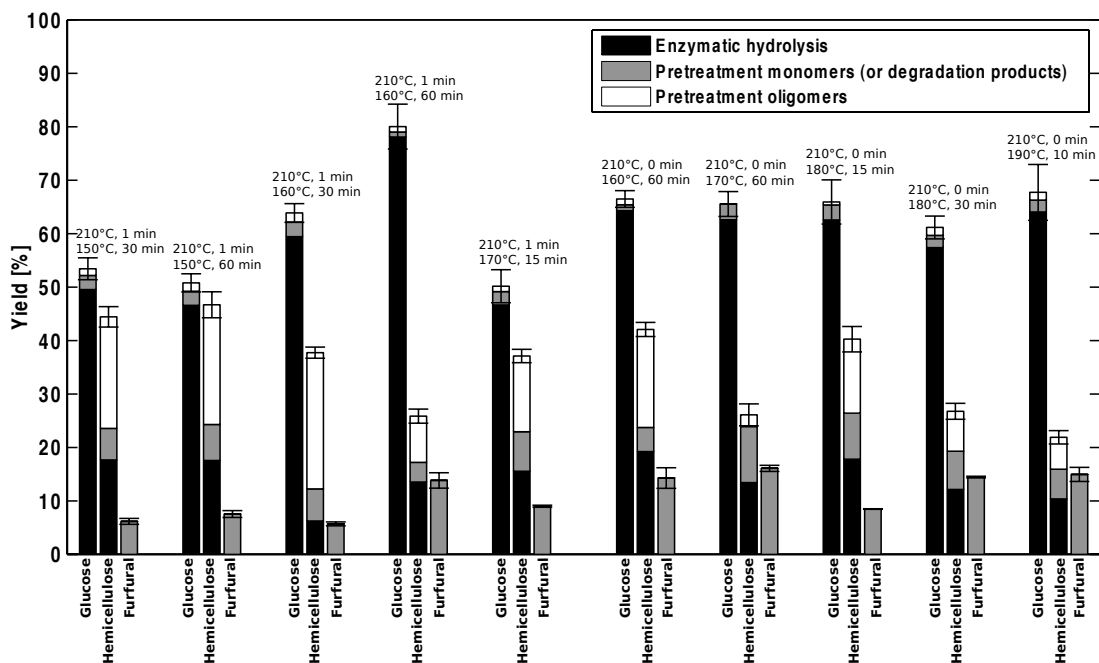


Fig. B.4: Additional yields for two-temperature stage pretreatment of 40 wt% solids (water biomass mixture) large particle switchgrass. All yields were obtained after pretreatment at 200 bar and 72 hr of enzymatic hydrolysis (15 FPU/g glucan). Pretreatment conditions are indicated above each set of yields. Bars represent glucan to glucose yields (indicated by *glucose*), xylan, arabinan and mannan to xylose, arabinose and mannose yields (indicated by *hemicellulose*) and xylan and arabinan to furfural yields (indicated by *furfural*). Error bars represent the results 95% confidence interval based on triplicate sampling.

APPENDIX C
APPENDIX FOR CHAPTER 6

C.1 High-solids enzymatic hydrolysis reaction system

A custom high-solids enzymatic hydrolysis reaction system was built for this study. This setup consists of a set of rollers that can roll up to 12 "rotating drum" reactors. A picture of this setup is available in Figure C.1.



Fig. C.1: Picture of the custom-built high-solids enzymatic hydrolysis reaction system. The set of motorized rollers is shown with 6 reactors on the back row and one on the front row. In the background, the incubator, in which the whole setup is placed for temperature control purposes, is shown.

C.2 Characterization of sampling error

Given that a single pretreatment run could only process 60 g of initial dry solids, multiple pretreatment runs are required to run multiple high-solids enzymatic hydrolysis reactions (which require 45 g of initial dry solids each). Therefore, we attempted to determine whether sampling the same reactor three times introduced more error than sampling a single reactor three times. We compared the yields and their 95% confidence intervals (based on triplicate sampling) obtained for the high-solids enzymatic hydrolysis of untreated corn stover in three separate reactors. The corn stover was obtained in 2009 from the National Renewable Energy Laboratory (NREL). Corn stover was chosen as a substrate because of it offered high yields (close to 30%) even when untreated. This allowed us to run these experiments without pretreating biomass. Corn stover composition was given in Table 4.1.

As the yields and their respective 95% confidence intervals demonstrate in Figure C.2, the error resulting from sampling a given reactor is comparable to that of the error between two separate reactors. Indeed, except for a single point (hemicellulose sugar yields, 30 wt% solids, 24 hr) all average reactor yields fall within each other's confidence intervals. In addition, for over half the data points, the error resulting from sampling exceeds the differences between the average reactor yields. The implication of these results is that sampling a given reactor three times leads to just as accurate an estimate of the uncertainty involved in high-solids enzymatic hydrolysis as sampling three separate reactors. This allowed us to use one reactor and only 45 g of initial dry solids of pretreated biomass per experiment reducing the amount of pretreatment runs necessary to complete this study.

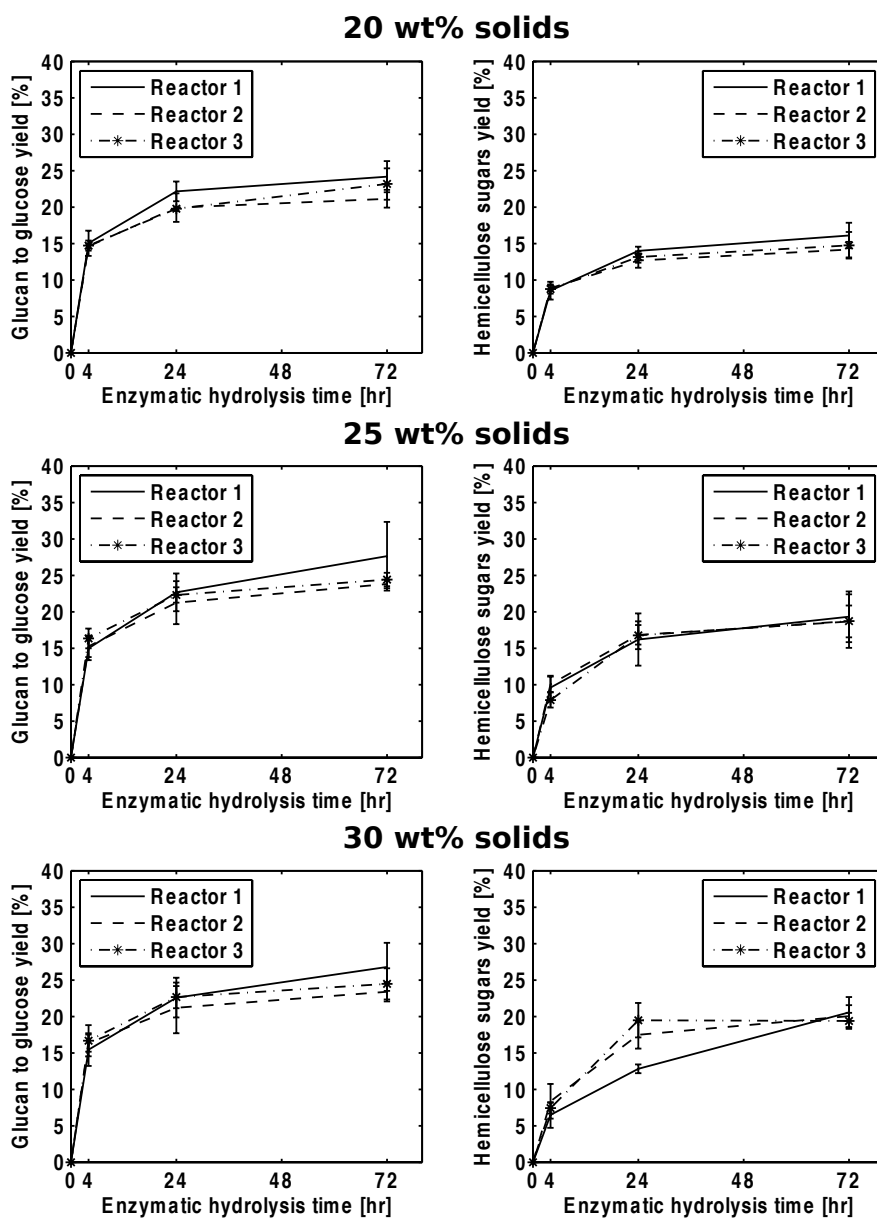


Fig. C.2: Glucan and hemicellulose sugar yields obtained as a function of enzymatic hydrolysis time for untreated corn stover at varying initial solid contents. Reactors 1, 2 and 3 refer to three separate reactors that were loaded with identical reaction mixtures and sampled at the same time. Error bars represent 95% confidence intervals.

APPENDIX D
APPENDIX FOR CHAPTER 7

D.1 Hydrolytic activity of fluorescently labeled Cel7A

The hydrolytic activity of labeled Cel7A was quantified on BMCC by measuring the total amount of oligosaccharide produced during hydrolysis and comparing this amount to that produced using the same quantity of unlabeled Cel7A. The detailed methods of this assay are given in a previous study [292]. Results are shown in Figure D.1. As shown below, the AF647-Cel7A hydrolytic activity is within 15% of the native (unlabeled) activity, while their respective standard deviat

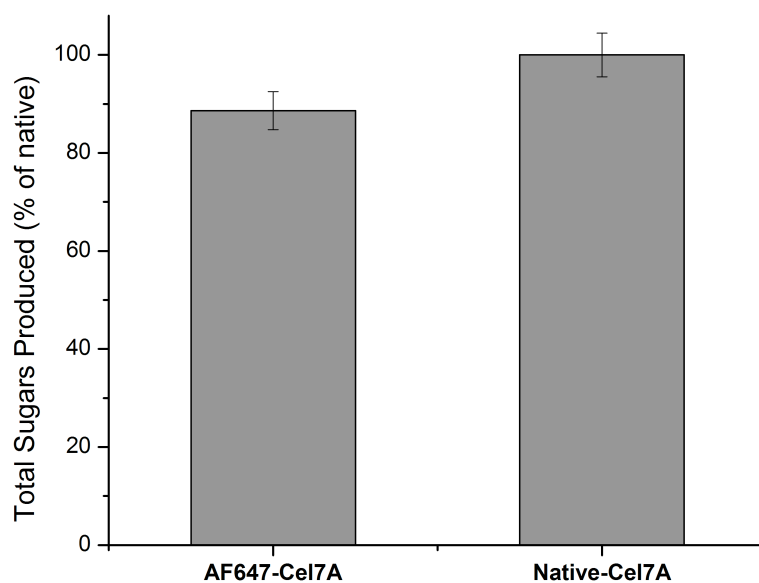


Fig. D.1: Comparison of the hydrolytic activity of labeled and unlabeled (or native) cellulase Cel7A as measured by total oligomers released from BMCC during the hydrolysis assay. Error bars represent the standard deviation calculated from triplicate measurements.

D.2 Correcting for photobleaching

To assess the effect of photobleaching several control imaging experiments were run under identical conditions (i.e. same laser intensity and microscope settings, same temperature, 50°C and same buffer) as those employed in the degradation studies. To assess the effect of photobleaching on the DTAF signal, which is used to measure the presence of BMCC, DTAF labeled BMCC was imaged in the 0.05 M sodium citrate buffer described in the Materials and Methods section but in the absence of cellulases to avoid degradation. The collected signals are shown in Figure D.2.

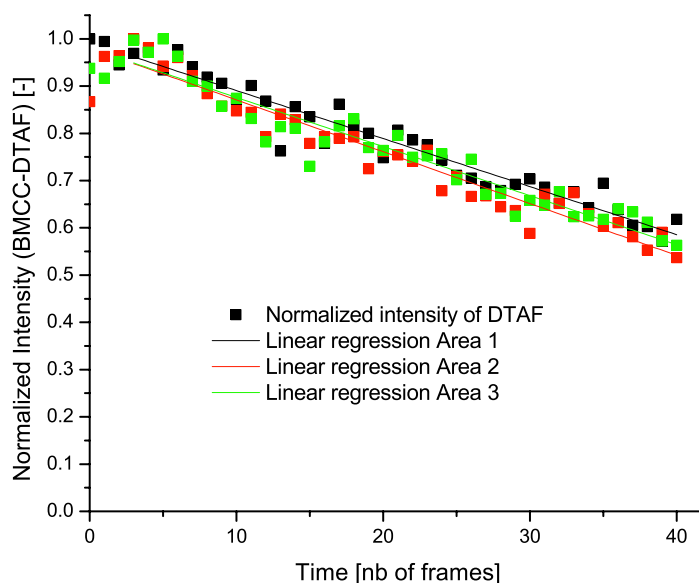


Fig. D.2: Normalized DTAF labeled BMCC fluorescence signal (normalized over the highest signal of each area) as a function of number of frames (or image stacks) that were taken. A linear regression was added to the signal of each individual area.

For each area, a linear regression was done on that set of data. The first three data points were excluded due to often-erratic behavior. The average decrease

in signal per frame was calculated as the average of that determined from each of the three linear regressions.

To assess the effect of photobleaching on the AF647 signal, which is used to measure the presence of Cel7A, DTAF labeled BMCC was imaged the presence of 5 nM of Cel7A in 0.05 M sodium citrate buffer. BMCC had been left to incubate at room temperature overnight and to equilibrate at 50°C for 1 hr. No Spezyme CP was added in order to minimize degradation. The resulting fluorescence signals are shown in Figure D.3.

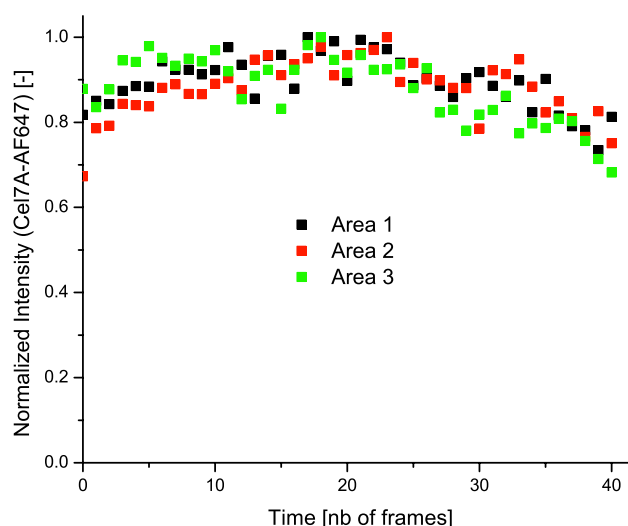


Fig. D.3: Normalized AF647 labeled Cel7A fluorescence signal (normalized over the highest signal of each area) as a function of number of frames (or image stacks) that were taken.

In contrast with the signals obtained for the DTAF control experiments, those for the AF647 control experiments did not show a marked decrease as a function of the number frames. Over the course of the experiment all signals stayed within about 30% of their maximal value. The signals seemed to increase until about the 20th frame and then decrease after that. This increase and decrease could be due to the activity exhibited by the enzyme at 50°C rather than any

photobleaching effect. Indeed, since the enzyme is active at these temperatures and even though its concentration is fairly low (5 nM), it could be that Cel7A is affecting the number of available sites creating a parabolic shape analogous to that observed in the main experiments (see Figure 7.4, in Chapter 7). In any case, this behavior seems unlikely to be due to photobleaching and thus, no correction was applied.

D.3 Model development

As discussed in Chapter 7, three models were developed for this study: the irreversible binding model, the reversible binding model and the instantaneous binding model. All symbols and their associated units are given in Table D.1 The development and solving of these models, from reaction sequence to differential equations to their solutions, are detailed below.

D.3.1 Irreversible binding model

This model takes into account an irreversible binding reaction (k_1) of cellulases (E) on unoccupied cellulose binding sites (S) and a second reaction (k_2) involved the reaction of bound cellulase and cellulose (ES) to form an oligosaccharide product (P):



Table D.1: List of symbols and their associated description.

Parameter	Description	Units
A_i	Integration constant i	[-]
$[E]$	Bulk cellulase concentration	[mol/g _{BMCC}]
$[ES]$	Surface concentration of bound cellulase	[mol/g _{BMCC}]
\mathbf{h}_i	i th eigenvector	[-]
\mathbf{I}	Identity matrix	[-]
k_1	Cellulase irreversible binding rate constant	[FPU/(ml min)]
$k_{r,1}$	Cellulase reversible binding rate constant	[FPU/(ml min)]
$k_{r,-1}$	Cellulase reversible unbinding rate constant	[min ⁻¹]
k_i	Cellulose binding site exposure rate constant	[FPU/(ml min)]
k_2	Cellulose degradation rate constant (irreversible model)	[min ⁻¹]
$k_{r,2}$	Cellulose degradation rate constant (reversible model)	[min ⁻¹]
$k_{i,2}$	Cellulose degradation rate constant (instantaneous model)	[min ⁻¹]
\mathbf{M}	Matrix M	[-]
$[P]$	Hydrolysis product concentration	[mol/g _{BMCC}]
$[S]$	Surface concentration of free (exposed) binding sites	[mol/g _{BMCC}]
$[S_i]$	Concentration of inner (unexposed) binding sites	[mol/g _{BMCC}]
$[S]_0$	Initial surface concentration of free (exposed) binding sites	[mol/g _{BMCC}]
$[S_{tot}]$	Concentration of total binding sites in cellulose	[mol/g _{BMCC}]
t	Time	[min]
$[X]_{t=0}$	Initial (surface, if applicable) concentration of X (at t=0)	[-]
\mathbf{X}	Vector X	[-]
\mathbf{X}'	Differential form of vector X	[-]
α	DTAF-BMCC-fluorescence proportionality constant	[(mol/g _{BMCC}) ⁻¹]
β	Enzyme-fluorescence proportionality constant	[(mol/g _{BMCC}) ⁻¹]
λ_i	i th eigenvalue	[-]
ψ	Initial fraction of available sites (exposed over total sites)	[-]

These two reactions along with the equation governing product concentration can be rewritten as the following differential equations:

$$\frac{d[S]}{dt} = -k_1 [S] [E] \quad (\text{D.2})$$

$$\frac{d[ES]}{dt} = k_1 [S] [E] - k_2 [ES] \quad (\text{D.3})$$

$$\frac{d[P]}{dt} = k_2 [ES] \quad (\text{D.4})$$

with initial conditions defined as:

$$[S]_{t=0} = [S]_0 \quad (\text{D.5})$$

$$[ES]_{t=0} = 0 \quad (\text{D.6})$$

$$[P]_{t=0} = 0 \quad (\text{D.7})$$

where $[S]_0$ is defined as an arbitrary non-zero initial surface concentration of cellulose binding sites. The bulk enzyme concentration $[E]$ is assumed to stay constant throughout the experiment. This assumption was verified experimentally (see Section D.7). The solution of Equation D.2 can therefore be written as:

$$[S] = A_1 \exp(-k_1 [E] t) \quad (\text{D.8})$$

where A_1 is a constant. When the initial condition defined in Equation D.5 is applied, Equation D.8 can be rewritten as:

$$[S] = [S]_0 \exp(-k_1 [E] t) \quad (\text{D.9})$$

By using equation D.9, Equation D.3 becomes:

$$\frac{d[ES]}{dt} = -k_2 [ES] + k_1 [E] [S]_0 \exp(-k_1 [E] t) \quad (\text{D.10})$$

Equation D.10 is an inhomogeneous differential equation, which is solved by combining a homogeneous and particular solution:

$$[ES] = A_2 \exp(-k_2 t) + \frac{k_1 [E] [S]_0}{k_2 - k_1 [E]} \exp(-k_1 [E] t) \quad (\text{D.11})$$

where A_2 is a constant. By applying the initial condition as defined in Equation D.6, Equation D.11 can be rewritten as:

$$[ES] = \frac{k_1 [E] [S]_0}{k_2 - k_1 [E]} (\exp(-k_1 [E] t) - \exp(-k_2 t)) \quad (\text{D.12})$$

Finally, using this solution, the equation governing product formation (Equation D.4) was rewritten as:

$$\frac{d[P]}{dt} = k_2 \frac{k_1 [E] [S]_0}{k_2 - k_1 [E]} (\exp(-k_1 [E] t) - \exp(-k_2 t)) \quad (\text{D.13})$$

which is a separable differential equation that has the following general solution:

$$[P] = A_3 + k_2 \frac{k_1 [E] [S]_0}{k_2 - k_1 [E]} \left(-\frac{\exp(-k_1 [E] t)}{k_1 [E]} + \frac{\exp(-k_2 t)}{k_2} \right) \quad (\text{D.14})$$

By applying the initial condition defined by Equation D.7, the solution becomes:

$$[P] = \frac{k_2 [S]_0}{k_2 - k_1 [E]} (1 - \exp(-k_1 [E] t)) - \frac{k_1 [E] [S]_0}{k_2 - k_1 [E]} (1 - \exp(-k_2 t)) \quad (\text{D.15})$$

D.3.2 Reversible model

The reversible model takes into account two reactions representing the reversible binding ($k_{r,1}$) and unbinding ($k_{r,-1}$) of cellulases (E) on unoccupied cellulose binding sites (S) and a third reaction ($k_{r,2}$) involved the reaction of the bound cellulase (ES) to form an oligosaccharide product (P):



These two reactions along with the equation governing product concentration can be rewritten as:

$$\frac{d[S]}{dt} = -k_{r,1} [S] [E] + k_{r,-1} [ES] \quad (\text{D.17})$$

$$\begin{aligned} \frac{d[ES]}{dt} &= k_{r,1} [S] [E] - k_{r,-1} [ES] - k_{r,2} [ES] = \\ & k_{r,1} [S] [E] - (k_{r,-1} + k_{r,2}) [ES] \end{aligned} \quad (\text{D.18})$$

$$\frac{d[P]}{dt} = k_{r,2} [ES] \quad (\text{D.19})$$

The initial conditions are identical to those defined for the irreversible model:

$$[S]_{t=0} = [S]_0 \quad (\text{D.20})$$

$$[ES]_{t=0} = 0 \quad (\text{D.21})$$

$$[P]_{t=0} = 0 \quad (\text{D.22})$$

where $[S]_0$ is defined as an arbitrary non-zero initial surface concentration of cellulose binding sites. Once again, if $[E]$ is assumed to be a constant, as it was assumed for the irreversible model, Equations D.17 and D.18 become coupled linear differential equations which can be rewritten as (with matrix and/or vectors shown in bold):

$$\begin{pmatrix} \frac{d[S]}{dt} \\ \frac{d[ES]}{dt} \end{pmatrix} = \mathbf{X}' = \begin{pmatrix} -k_{r,1} [E] & -k_{r,-1} \\ k_{r,1} [E] & -(k_{r,-1} + k_{r,2}) \end{pmatrix} \begin{pmatrix} [S] \\ [ES] \end{pmatrix} = \mathbf{MX} \quad (\text{D.23})$$

The solution of this system of differential equations ($\mathbf{X}' = \mathbf{MX}$) is [309]:

$$\mathbf{X} = \sum_i A_i h_i \exp(\lambda_i t) \quad (\text{D.24})$$

where h_i is the i th eigenvector of the matrix M corresponding to the i th eigenvalue λ_i , and A_i is the i th integration constant. The eigenvalues of M can be found by solving the system:

$$\mathbf{M} - \lambda \mathbf{I} = \begin{pmatrix} -k_{r,1} [E] - \lambda & -k_{r,-1} \\ k_{r,1} [E] & -(k_{r,-1} + -k_{r,2}) - \lambda \end{pmatrix} = 0 \quad (\text{D.25})$$

where I is the identity matrix. The two solutions for the set of eigenvalues λ are:

$$\lambda_1 = \frac{-k_{r,1} [E] - k_{r,-1} - k_{r,2} + \sqrt{k_{r,1}^2 [E]^2 + k_{r,-1}^2 + k_{r,2}^2 + 2k_{r,1} [E] k_{r,-1} - 2k_{r,1} [E] k_{r,2} + 2k_{r,-1} k_{r,2}}}{2} \quad (\text{D.26})$$

$$\lambda_2 = \frac{-k_{r,1} [E] - k_{r,-1} - k_{r,2} - \sqrt{k_{r,1}^2 [E]^2 + k_{r,-1}^2 + k_{r,2}^2 + 2k_{r,1} [E] k_{r,-1} - 2k_{r,1} [E] k_{r,2} + 2k_{r,-1} k_{r,2}}}{2} \quad (\text{D.27})$$

The corresponding eigenvectors are:

$$n_1 = \begin{pmatrix} 1 \\ \frac{-k_{r,1} [E] - k_{r,-1} - k_{r,2} + \sqrt{k_{r,1}^2 [E]^2 + k_{r,-1}^2 + k_{r,2}^2 + 2k_{r,1} [E] k_{r,-1} - 2k_{r,1} [E] k_{r,2} + 2k_{r,-1} k_{r,2}}}{2k_{r,-1}} \end{pmatrix} \quad (\text{D.28})$$

$$n_2 = \begin{pmatrix} 1 \\ \frac{-k_{r,1} [E] - k_{r,-1} - k_{r,2} - \sqrt{k_{r,1}^2 [E]^2 + k_{r,-1}^2 + k_{r,2}^2 + 2k_{r,1} [E] k_{r,-1} - 2k_{r,1} [E] k_{r,2} + 2k_{r,-1} k_{r,2}}}{2k_{r,-1}} \end{pmatrix} \quad (\text{D.29})$$

Therefore, using Equation D.24, the solutions for [S] and [ES] can be written as:

$$[S] = A_4 \exp(\lambda_1 t) + A_5 \exp(\lambda_2 t) \quad (\text{D.30})$$

$$\begin{aligned}
[ES] = & A_4 \left(\frac{-k_{r,1}[E] - k_{r,-1} - k_{r,2} + \sqrt{k_{r,1}^2 [E]^2 + k_{r,-1}^2 + k_{r,2}^2 + 2k_{r,1} [E] k_{r,-1}}}{2k_{-1}} \right) \exp(\lambda_1 t) \\
& + A_5 \left(\frac{-k_{r,1}[E] - k_{r,-1} - k_{r,2} - \sqrt{k_{r,1}^2 [E]^2 + k_{r,-1}^2 + k_{r,2}^2 + 2k_{r,1} [E] k_{r,-1}}}{2k_{r,-1}} \right) \exp(\lambda_2 t)
\end{aligned} \tag{D.31}$$

The integration constants are solved for by applying the initial conditions given in Equations D.20, D.21 and D.22. The results are:

$$A_4 = [S]_0 \left(\frac{-k_{r,1} [E] + k_{r,-1} + k_{r,2} + \sqrt{k_{r,1}^2 [E]^2 + k_{r,-1}^2 + k_{r,2}^2 + 2k_{r,1} [E] k_{r,-1}}}{2 \sqrt{k_{r,1}^2 [E]^2 + k_{r,-1}^2 + k_{r,2}^2 + 2k_{r,1} [E] k_{r,-1}}} \right) \tag{D.32}$$

$$A_5 = [S]_0 \left(\frac{-k_{r,1} [E] + k_{r,-1} + k_{r,2} - \sqrt{k_{r,1}^2 [E]^2 + k_{r,-1}^2 + k_{r,2}^2 + 2k_{r,1} [E] k_{r,-1}}}{2 \sqrt{k_{r,1}^2 [E]^2 + k_{r,-1}^2 + k_{r,2}^2 + 2k_{r,1} [E] k_{r,-1}}} \right) \tag{D.33}$$

By combining the Equations D.32 and D.33 with the solutions given by D.30 and D.31, the results become:

$$[S] = \frac{[S]_0}{\sqrt{k_{r,1}^2 [E]^2 + k_{r,-1}^2 + k_{r,2}^2 + 2k_{r,1} [E] k_{r,-1}}} \times \left[\begin{aligned} & \left(\frac{-k_{r,1} [E] + k_{r,-1} + k_{r,2} + \sqrt{k_{r,1}^2 [E]^2 + k_{r,-1}^2 + k_{r,2}^2 + 2k_{r,1} [E] k_{r,-1}}}{2 \sqrt{k_{r,1}^2 [E]^2 + k_{r,-1}^2 + k_{r,2}^2 + 2k_{r,1} [E] k_{r,-1}}} \right) \exp(\lambda_1 t) - \\ & \left(\frac{-k_{r,1} [E] + k_{r,-1} + k_{r,2} - \sqrt{k_{r,1}^2 [E]^2 + k_{r,-1}^2 + k_{r,2}^2 + 2k_{r,1} [E] k_{r,-1}}}{2 \sqrt{k_{r,1}^2 [E]^2 + k_{r,-1}^2 + k_{r,2}^2 + 2k_{r,1} [E] k_{r,-1}}} \right) \exp(\lambda_2 t) \end{aligned} \right] \tag{D.34}$$

$$[ES] = \frac{k_{r,1} [E] [S]_0}{\sqrt{\begin{matrix} k_{r,1}^2 [E]^2 + k_{r,-1}^2 + k_{r,2}^2 + 2k_{r,1} [E] k_{r,-1} \\ -2k_{r,1} [E] k_{r,2} + 2k_{r,-1} k_{r,2} \end{matrix}}} [\exp(\lambda_1 t) - \exp(\lambda_2 t)] \quad (\text{D.35})$$

Finally, using this solution, the equation governing product formation (Equation D.4) can be rewritten as:

$$\frac{d[P]}{dt} = k_2 \frac{k_{r,1} [E] [S]_0}{\sqrt{\begin{matrix} k_{r,1}^2 [E]^2 + k_{r,-1}^2 + k_{r,2}^2 + 2k_{r,1} [E] k_{r,-1} \\ -2k_{r,1} [E] k_{r,2} + 2k_{r,-1} k_{r,2} \end{matrix}}} [\exp(\lambda_1 t) - \exp(\lambda_2 t)] \quad (\text{D.36})$$

This is a separable differential equation that has the following general solution:

$$[P] = A_6 + \frac{k_{r,1} [E] [S]_0}{\sqrt{\begin{matrix} k_{r,1}^2 [E]^2 + k_{r,-1}^2 + k_{r,2}^2 + 2k_{r,1} [E] k_{r,-1} \\ -2k_{r,1} [E] k_{r,2} + 2k_{r,-1} k_{r,2} \end{matrix}}} \left[\frac{\exp(\lambda_1 t)}{\lambda_1} - \frac{\exp(\lambda_2 t)}{\lambda_2} \right] \quad (\text{D.37})$$

By applying the initial condition defined by Equation D.22, the solution becomes:

$$[P] = \frac{k_{r,1} [E] [S]_0}{\sqrt{\begin{matrix} k_{r,1}^2 [E]^2 + k_{r,-1}^2 + k_{r,2}^2 + 2k_{r,1} [E] k_{r,-1} \\ -2k_{r,1} [E] k_{r,2} + 2k_{r,-1} k_{r,2} \end{matrix}}} \left[\frac{(1 - \exp(\lambda_1 t))}{\lambda_1} - \frac{(1 - \exp(\lambda_2 t))}{\lambda_2} \right] \quad (\text{D.38})$$

D.3.3 Instantaneous binding model

If a fraction of the total number of sites is assumed to be inaccessible at the start of the reaction, a reaction catalyzed by enzymes (E) can be assumed to create exposed sites (S) from inner sites (S_i). If binding is again assumed to be irreversible, the same reaction as that defined in Equation D.1 follows:



If one assumes that the binding reaction is instantaneous compared to the other processes, this reaction sequence can be rewritten as a sequence that is similar to that described in Equation D.1:



These two reactions along with the equation governing product concentration could be rewritten as the following differential equations:

$$\frac{d[S_i]}{dt} = -k_i [S_i] [E] \quad (\text{D.41})$$

$$\frac{d[ES]}{dt} = k_i [S_i] [E] - k_{i,2} [ES] \quad (\text{D.42})$$

$$\frac{d[P]}{dt} = k_{i,2} [ES] \quad (\text{D.43})$$

with initial conditions defined as:

$$[S_i]_{t=0} = [S_i]_0 \quad (\text{D.44})$$

$$[ES]_{t=0} = [ES]_0 \quad (\text{D.45})$$

$$[P]_{t=0} = 0 \quad (\text{D.46})$$

where $[S_i]_0$ was defined as a non-zero initial concentration of inaccessible cellulose binding sites and $[ES]_0$ as a non-zero initial concentration of available (and instantly occupied) sites. A fraction of initially available binding sites (ψ) can be defined such that:

$$\psi = \frac{[S_{tot}]_0 - [S_i]_0}{[S_{tot}]_0} = \frac{[ES]_0}{[S_{tot}]_0} \quad (\text{D.47})$$

$$[ES]_0 = [S_{tot}]_0 \psi \quad (\text{D.48})$$

$$[S_i]_0 = [S_{tot}]_0 (1 - \psi) \quad (\text{D.49})$$

where $[S_{tot}]$ is the initial total concentration of exposed and unexposed inner binding sites.

Once again, since the volume of the solution used was much greater than the volume of the substrate, one can assume that binding onto the substrate does not significantly affect the bulk enzyme concentration ($[E]$), which was thus assumed to stay constant. Equation D.41 has the same form as Equation D.2 and by analogy, the solution is:

$$[S_i] = [S_i]_0 \exp(-k_i [E] t) = [S_{tot}]_0 (1 - \psi) \exp(-k_i [E] t) \quad (\text{D.50})$$

Equation D.42 has the same form as Equation D.3 but has a different initial condition. Nevertheless, its general solution remains identical to Equation D.11:

$$[ES] = A_6 \exp(-k_{i,2} t) + \frac{k_i [E] [S_i]_0}{k_{i,2} - k_i [E]} \exp(-k_i [E] t) \quad (\text{D.51})$$

where A_6 is a constant. By applying the initial condition as defined in Equation D.45, Equation D.50 can be rewritten as:

$$[ES] = [ES]_0 \exp(-k_{i,2} t) + \frac{k_i [E] [S_i]_0}{k_{i,2} - k_i [E]} (\exp(-k_i [E] t) - \exp(-k_{i,2} t)) = [S_{tot}]_0 \left(\psi \exp(-k_{i,2} t) + \frac{(1 - \psi) k_i [E]}{k_{i,2} - k_i [E]} (\exp(-k_i [E] t) - \exp(-k_{i,2} t)) \right) \quad (\text{D.52})$$

Using this solution, the equation governing product formation (Equation D.43) can be rewritten as:

$$\frac{d[P]}{dt} = k_{i,2} [S_{tot}]_0 \left(\psi \exp(-k_{i,2} t) + \frac{(1 - \psi) k_i [E]}{k_{i,2} - k_i [E]} (\exp(-k_i [E] t) - \exp(-k_{i,2} t)) \right) \quad (\text{D.53})$$

which is a separable differential equation that has the following general solution:

$$[P] = A_7 + k_{i,2} [S_{tot}]_0 \left(-\psi \frac{\exp(-k_{i,2} t)}{k_{i,2}} + \frac{(1 - \psi) k_i [E]}{k_{i,2} - k_i [E]} \left(-\frac{\exp(-k_i [E] t)}{k_i} + \frac{\exp(-k_{i,2} t)}{k_{i,2}} \right) \right) \quad (\text{D.54})$$

By applying the initial condition defined by Equation D.46, the solution becomes:

$$[P] = [S_{tot}]_0 \left(\psi - (1 - \psi) \frac{k_i [E]}{k_{i,2} - k_i [E]} \right) (1 - \exp(-k_{i,2} t)) + (1 - \psi) \frac{k_{i,2} [S_{tot}]_0}{k_{i,2} - k_i [E]} (1 - \exp(-k_i [E] t)) \quad (\text{D.55})$$

D.4 Parameter estimation

Normalized fluorescence intensity data were fitted to the three models as defined by Equations 7.13 and 7.14 (irreversible model), 7.17 and 7.18 (reversible model) and 7.23 and 7.24 (instantaneous binding model) from Chapter 7 using the *lsqnonlin* function in Matlab (Mathworks, Natick, Ma) with the Levenburg-Marquadt algorithm. Parameters were estimated as they appear in these equations. The fitting range for all parameters was set between 0 and 1, while the range for α/β was 0 to 10. The ratio α/β is, by definition, positive. Setting its upper range to 10 was done to improve convergence time. Setting the upper range to 100 had no statistically significant effect on the estimated value of α/β . Parameter estimates along with their estimated standard deviation were calculated using a weighted average and standard deviation resulting from the fits for 10 observed areas that were recorded over the course of 3 independent experimental runs. Weighting was done using the size of the confidence interval for each parameter calculated for each fit using the *nlparci* Matlab function. Weighting by the size of the confidence intervals is equivalent to standard deviation weighting if a normal distribution is assumed around the fitted parameter values; this can be used as a first approximation [310]. Product concentrations and their standard deviations predicted from each model (using Equations 7.15,

7.19 or 7.25 from Chapter 7) were obtained by a non-weighted average of the set of predicted product concentrations, which were themselves obtained from the set of parameters from each of the 10 fits.

D.5 Effect of substrate preparation

The effects of substrate labeling were explored in a previous study [116]. DTAF labeling showed no statistically significant effect on the activity Cel6B, a slight hindrance of the activity of Cel9A (i.e. a 16% decrease) and a doubling of the activity of Cel5A. Therefore, although labeled BMCC can enhance the activity of some labeled enzymes as compared to native BMCC, its structure and degradability remains largely unchanged. The effect of labeling should be considered when comparing the data obtained here directly to that of native BMCC but it does not affect the general conclusions of this work.

In addition to the effect of labeling, the effect of the use of BSA and of drying was explored through experiments comparing the amount of sugars released in the presence of BMCC that had been dried and after the use of BSA blocking buffer (as detailed in Chapter 7) with experiments without any BMCC drying or which did not include the use of BSA. These experiments were run in Mattek glass bottom dishes according to the protocol detailed in Chapter 7. Their supernatant was sampled after 2, 4 and 8 hr and sugars were measured by HPLC as detailed in Chapter 7. Results are shown in Figure D.4.

As shown in Figure D.4, the amounts of sugars released after 2, 4 or 8 hr are within each other's standard deviations regardless of BMCC drying or the use of BSA blocking buffer.

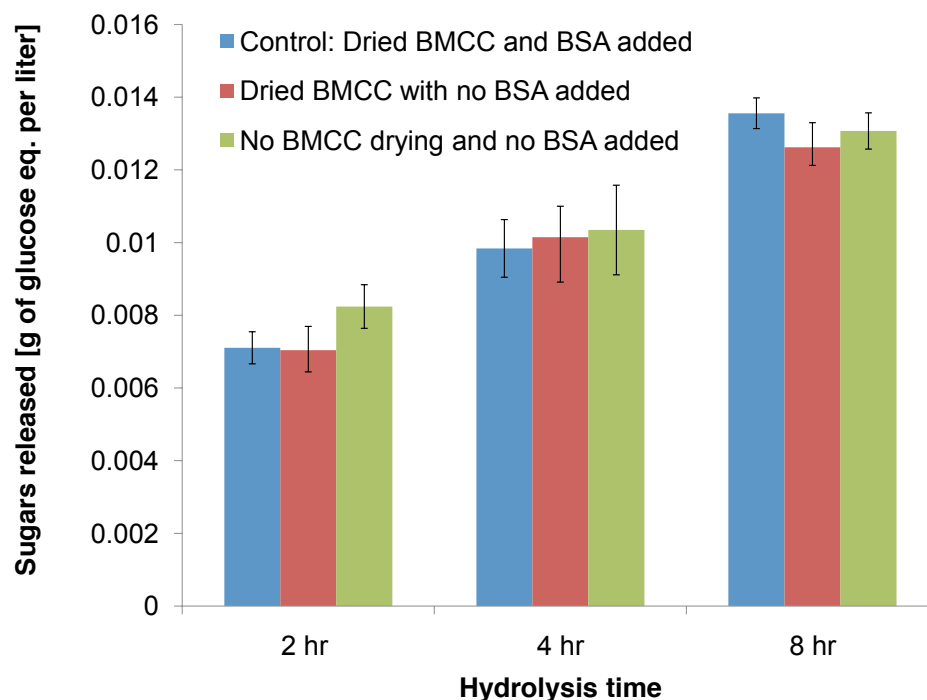


Fig. D.4: Effect of BMCC drying and using BSA blocking buffer on the production of sugars as a function of hydrolysis time. Error bars represent standard deviation based on triplicate sampling.

D.6 Imaging at high enzyme concentrations

Initially, enzyme concentrations comparable to those usually used for pretreated biomass were chosen (i.e. 0.15 FPU/ml from Selig et al., 2008). However, this led to full degradation of BMCC within 5-10 min (see Figure D.5).

As shown in Figure D.5, BMCC or bound enzyme is barely visible after 7 min demonstrating that most of the BMCC has degraded at that point.

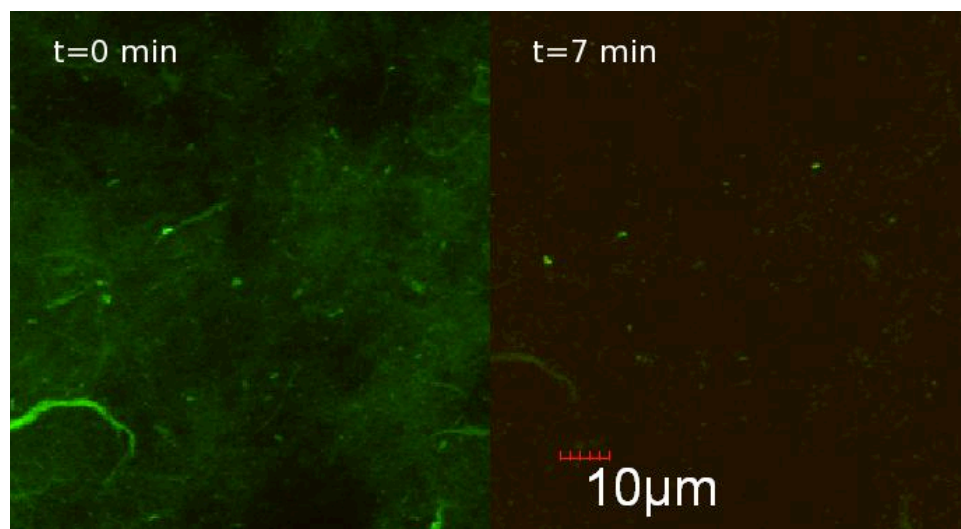


Fig. D.5: BMCC degradation imaging at high enzyme concentration (0.15 FPU/ml): overlays of green (DTAF labeled BMCC) and red (AF647 labeled Cel7A) channels before enzyme injection ($t=0$ min) and 7 min after enzyme injection.

D.7 Variations of enzyme concentration within the supernatant

To verify the assumption of constant bulk enzyme concentration control experiments were run in Mattek glass bottom dishes according to the protocol detailed in Chapter 7 and the supernatant was sampled over time. The absorbance of these samples at 280 nm was immediately measured using a DU720 Spectrophotometer (Beckman-Coulter, Indianapolis, IN). A baseline absorbance taken for an identical reaction system where water was added instead of enzyme. This baseline absorbance was subtracted to all absorbance measurements. An initial absorbance was taken with a system to which enzyme was added but to where no BMCC was present. The fraction of initial absorbance is given as a function of reaction time in Figure D.6.

As shown in Figure D.6, the fraction of initial absorbance remains within

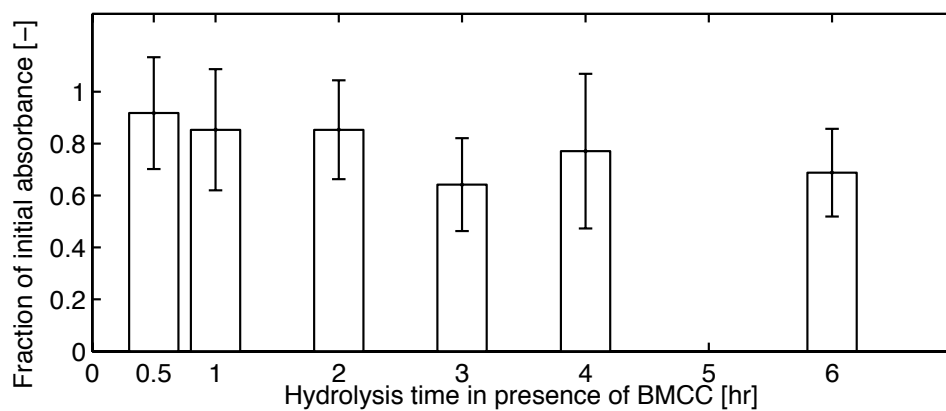


Fig. D.6: Fraction of initial absorbance at 280 nm as a function of reaction time in the presence of BMCC. Error bars represent each sample's standard deviation based on triplicate sampling.

one standard deviation of 1 throughout degradation. Therefore, assuming that the bulk enzyme concentration remains constant appears to be a reasonable assumption. Though a slight decrease in absorbance seems to have occurred after 4 to 6 hours, this cannot be due to binding to BMCC since almost all of the substrate has degraded by that point.

APPENDIX E
APPENDIX FOR CHAPTER 8

E.1 Dataset

All the data used in this study were obtained from a study by Grethlein [118] and are re-transcribed in Table E.1. Most data in Table E.1 were directly reported in Grethlein's study. However, some of the data were obtained by interpolation on figures and are listed in italics in Table E.1. Lignin was calculated as the remaining fraction of biomass other than cellulose and hemicellulose in order to close the mass balance. This assumption does not have an effect on the modeling results given that it is assumed that lignin does not react or bind cellulases.

E.2 Particle geometry and lignin binding assumptions

Figure E.1 shows two-temperature stage biphasic CO₂-H₂O pretreated hardwood (210°C, 16min, 160°C60 min) imaged during enzymatic hydrolysis (0.15 FPU/ml, 50°C) by fluorescence confocal microscopy. Pretreatment and confocal imaging techniques have been previously described (Luterbacher et al., 2012; Zhu et al., 2011). Particle auto-fluorescence is shown in green while the bound enzyme is visible in red.

Though clusters of particles are shown in Figure E.1, each individual particle approximately resembles a cylinder, which was the geometry that was chosen for the proposed model. It was determined by measuring carbohydrate concentration in the solution that, after 8 hr, 40 to 50% of the particle weight had

Table E.1: Dataset used in Chapter 8, which was obtained from Grethlein [118]. Data in italics were obtained through figure interpolation while all other data were reported numerically in the Grethleins study. Lignin composition was calculated as the remaining fraction of biomass once cellulose and hemicellulose are accounted for.

	Volume available [ml/gr]									
Molecule size [Å]	Data set 1	Data set 2	Data set 3	Data set 4	Data set 5	Data set 6	Data set 7	Data set 8	Data set 9	Data set 10
0	1.05	0.92	0.775	0.695	0.51	0.87	0.53	0.705	0.49	0.621
8	<i>1.001</i>	<i>0.965</i>	<i>0.724</i>	<i>0.561</i>	<i>0.464</i>	<i>0.855</i>	-	-	-	<i>0.572</i>
12	<i>0.941</i>	<i>0.886</i>	<i>0.639</i>	<i>0.507</i>	<i>0.241</i>	<i>0.747</i>	-	<i>0.649</i>	-	<i>0.542</i>
36	<i>0.784</i>	<i>0.633</i>	<i>0.35</i>	<i>0.295</i>	<i>0.078</i>	-	-	-	-	<i>0.351</i>
51	0.685	0.51	0.215	0.19	0.06	0.45	0.03	0.375	0.095	0.264
90	0.353	0.26	0.125	0.105	0.03	0.23	0.02	0.16	0.067	0.118
110	0.235	0.17	0.09	0.075	0.03	0.16	0.01	0.11	0.045	0.076
270	<i>0.048</i>	<i>0.06</i>	<i>0.048</i>	<i>0.024</i>	<i>0.018</i>	<i>0.025</i>	-	<i>0.045</i>	-	<i>0.013</i>
560	0	0	0	0	0	0	0	0	0	0
	Composition [wt %]									
Lignin	33.1	33.1	33.1	33.1	33.1	34	34	35.3	35.3	40.1
Hemicellulose	24.9	24.9	24.9	24.9	24.9	21	21	22.7	22.7	10.2
Cellulose	42	42	42	42	42	45	45	42	42	49.7
	Species									
	Mixed Hard-wood	Mixed Hard-wood	Mixed Hard-wood	Mixed Hard-wood	Mixed Hard-wood	Poplar	Poplar	White pine	White pine	Steam extracted pine
	Pretreatment									
	220°C, 1% H ₂ SO ₄ , 7.8 sec	200°C, 1% H ₂ SO ₄ , 7.8 sec	180°C, 1% H ₂ SO ₄ , 7.8 sec	100°C, 1% H ₂ SO ₄ , 5 hr	Un-treated	200°C, 0.41% H ₂ SO ₄ , 6 sec	Un-treated	200°C, 1% H ₂ SO ₄ , 7 sec	Un-treated	200°C, 1% H ₂ SO ₄ , 7 sec

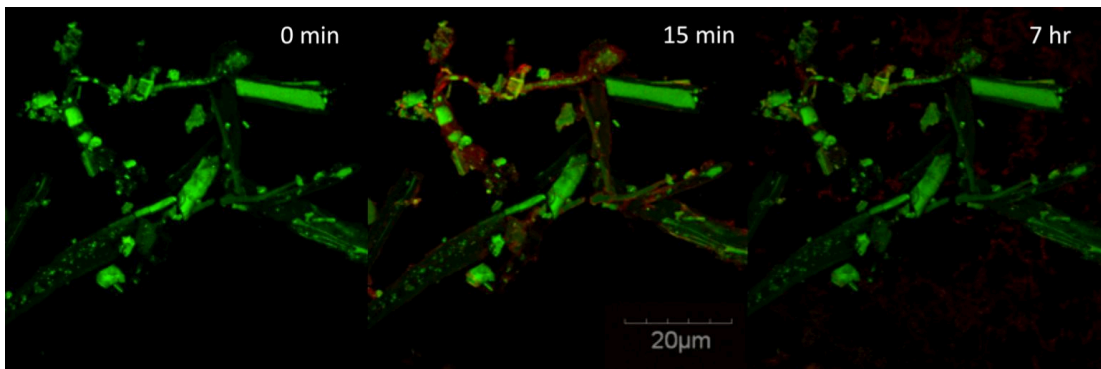


Fig. E.1: Two-temperature stage biphasic $\text{CO}_2\text{-H}_2\text{O}$ pretreated hardwood (210°C , 16min, 160°C 60 min) imaged during enzymatic hydrolysis (0.15 FPU/ml, 50°C) by fluorescence confocal microscopy. The green channel shows biomass auto-fluorescence while the bound enzyme is shown in red.

been degraded. However, the particle shape, though dimmer, appears virtually unchanged throughout the experiment. Therefore, a cylinder that becomes gradually less dense as the reaction progresses rather than a shrinking particle was chosen as the assumed geometry for the proposed model.

If a close-up is taken of the image of one of these clusters (see Figure E.2), the bound enzyme appears very brightly after 15 min but is difficult to detect after 12 hr. However, what is assumed to be unconverted cellulose debris has appeared outside of the particle in the last image of Figure E.2. This demonstrates that, though some non-specific binding may occur on non-cellulose surfaces within the particle, it is nowhere near as significant as the binding to reactive cellulose, which will have disappeared along with bound enzyme after 12 hr. At high-solids concentration non-reactive binding to the debris observed in the last image could have an effect by depleting the solution of enzyme. However, in the dilute conditions assumed for the proposed model, bulk enzyme concentrations are assumed to be constant. Furthermore, as discussed in this study, given that all sites are bound after 15 min, this phenomenon should not play a

significant role as it occurs over a much longer timescale.

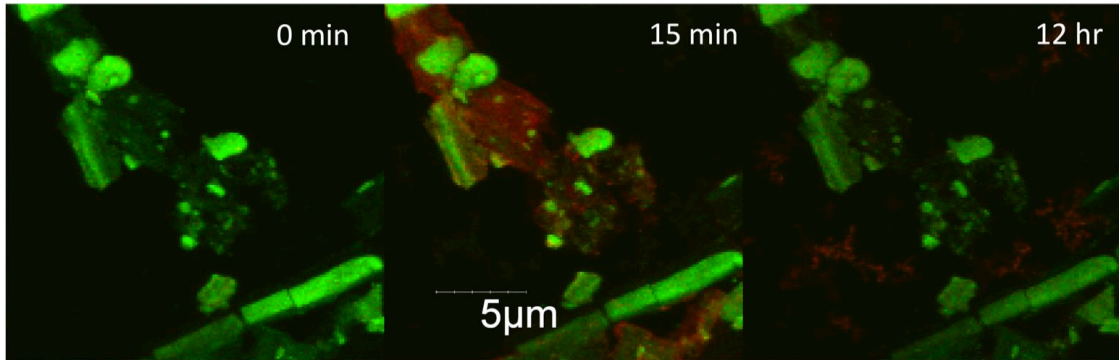


Fig. E.2: Close-up of two-temperature stage biphasic $\text{CO}_2\text{-H}_2\text{O}$ pretreated hardwood (210°C , 16min, 160°C 60 min) imaged during enzymatic hydrolysis (0.15 FPU/ml, 50°C) by fluorescence confocal microscopy. The green channel shows biomass autofluorescence while the bound enzyme is shown in red.

E.3 Computational methods

E.3.1 Numerical solver

The system of three partial differential equations described by Equations 8.6, 8.12 and 8.13 in Chapter 7 cannot be solved analytically, but can be solved numerically using the method of lines [311]. In this method, the radial portion of the problem is discretized using finite differences; splitting the radius into n sections of length h . This results in a system of ordinary differential equations with time being the only remaining independent variable. Equations 8.6, 8.12 and 8.13 from Chapter 7 can be rewritten as (symbols used below and throughout

this document are defined in Table 8.1 of Chapter 7):

$$\begin{aligned} \frac{dE_i(t)}{dt} = D_E \left(\frac{E_{i+1}(t) - 2E_i(t) + E_{i-1}(t)}{h^2} + \frac{1}{r_i} \frac{E_{i+1}(t) - E_{i-1}(t)}{2h} \right) \\ - S(1 - \eta)\sigma(1 - \vartheta_i(t))k_1E_i(t) + S(1 - \eta)\sigma\vartheta_i(t)k_2 \end{aligned} \quad (\text{E.1})$$

$$\frac{d\vartheta_i(t)}{dt} = (1 - \vartheta_i(t))E_i(t)k_1 - \vartheta_i k_2 \quad (\text{E.2})$$

$$\frac{d\rho_{A,i}(t)}{dt} = -\varepsilon_{A,0}M_pS_0(1 - \eta)\sigma\vartheta_i(t)k_2 \quad (\text{E.3})$$

Boundary conditions (Equations 8.14 and 8.15) modify the equations describing the segments at both ends of the radius ($r=0, i=1$ and $r=R, i=n$) [311]:

$$\begin{aligned} \frac{dE_1(t)}{dt} = D_E 2 \left(\frac{2E_2(t) - 2E_1(t)}{h^2} \right) - S(1 - \eta)\sigma(1 - \vartheta_1(t))k_1E_1(t) + \\ S(1 - \eta)\sigma\vartheta_1(t)k_2 \end{aligned} \quad (\text{E.4})$$

$$\begin{aligned} \frac{dE_n(t)}{dt} = D_E \left(\frac{[E]_{bulk} - 2E_n(t) + E_{n-1}(t)}{h^2} + \frac{1}{R} \frac{[E]_{bulk} - E_{n-1}(t)}{2h} \right) - \\ S(1 - \eta)\sigma(1 - \vartheta_n(t))k_1E_n(t) + S(1 - \eta)\sigma\vartheta_n(t)k_2 \end{aligned} \quad (\text{E.5})$$

This system of n ordinary differential equation can be solved with the *ode15s* function in Matlab[®] version R2008B (Mathworks, Natick, Ma).

E.3.2 Parameter estimation

Two parameters (τ and M_p) were estimated by minimizing the difference between the predicted and experimental cellulose conversion yield after 2 hr with only one of those parameters being allowed to vary by more than one order of magnitude. The fitting bounds, starting values, estimated values and confidence intervals are given in Table II of the main article. Fitting to this function is

done using the *lsqnonlin* function in Matlab® version R2008B (Mathworks, Natick, Ma) with the Trust-region-reflective algorithm. To improve convergence the minimum finite difference step size in the gradient estimation subroutine is set to a value of 0.1 using the *DiffMinChange* option. The complete dataset used for calculations, parameter estimation and comparison to data was obtained from the study by Grethlein [118] and is given in Section E.1.

E.4 Neglecting diffusion

Neglecting the effect of diffusion and assuming binding is instantaneous, Equation 8.13 can be modified to obtain:

$$\frac{d\rho_A(t)}{dt} = -\varepsilon_{A,0}M_pS_0(1 - \eta)\sigma k_2 = -\varepsilon_{A,0}M_pS_0 \left(1 - \eta_0 \frac{\rho_{A,0}}{\rho_A(t)}\right) \sigma k_2 \quad (\text{E.6})$$

Integrating this equation yields an expression explicit in time (t):

$$t = \frac{\rho_{A,0}}{\varepsilon_{A,0}M_pS_0\sigma k_2} \left[1 - \frac{\rho_A}{\rho_{A,0}} + \eta_0 \ln \left(\frac{1 - \eta_0}{\frac{\rho_A}{\rho_{A,0}} - \eta_0} \right) \right] \quad (\text{E.7})$$

Equation E.7 can be used to calculate cellulose conversion yields as a function of time similar to the predictions made from the non-simplified model in Figure 4 of the main article (see Figure E.3 below).

By comparing Figure E.3 and Figure 8.4 in the main article, it appears that these results are almost indistinguishable from the ones predicted with the unsimplified model, which accounts for diffusion. The yields after 2 hr of hydrolysis are only slightly higher (by a few percentage points) when diffusion is neglected.

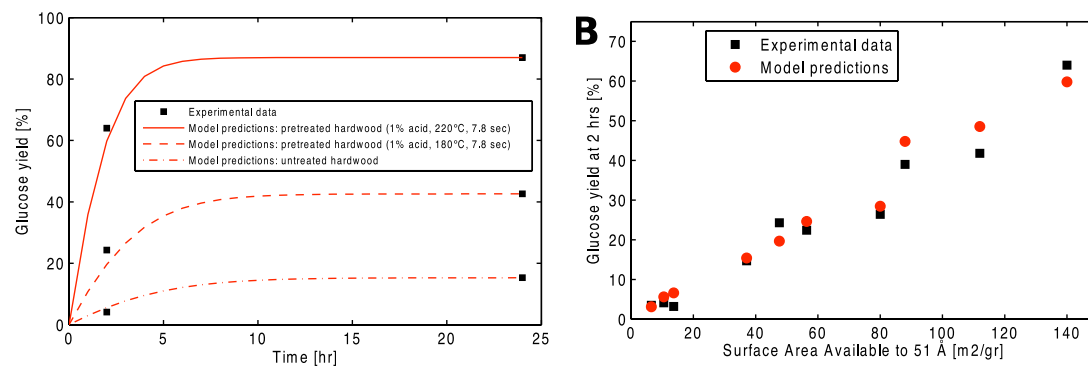


Fig. E.3: Comparison between experimental results and those predicted by the simplified model (neglecting diffusion). Part A shows cellulose to glucose conversion yields vs. time for three types of pretreated and untreated hardwood. Part B shows the cellulose to glucose conversion yields after 2 hr of hydrolysis for all the substrates vs. the surface area available to a cellulase (or a 51 Å molecule).

BIBLIOGRAPHY

- [1] J. W. Tester, *Sustainable energy*. MIT Press, 2005.
- [2] H. Lieth and R. H. Whittaker, *Primary Productivity of the Biosphere*. New York: Springer Verlag, 1975.
- [3] "BP statistical review of world energy 2009," tech. rep., BP, London, 2009.
- [4] M. D. Webster, M. Babiker, M. Mayer, J. M. Reilly, J. Harnisch, R. Hyman, M. C. Sarofim, and C. Wang, "Uncertainty in emissions projections for climate models," *Atmospheric Environment*, vol. 36, no. 22, pp. 3659–3670, 2002.
- [5] J. Sheehan, A. Aden, K. Paustian, K. Killian, J. Brenner, M. Walsh, and R. Nelson, "Energy and environmental aspects of using corn stover for fuel ethanol," *Journal of Industrial Ecology*, vol. 7, no. 3, pp. 117–146, 2003.
- [6] Melillo, J.M., D. Kicklighter, and T. Cronin, "Deforestation: an ongoing threat to the climate system," (28th MIT Global Change forum, Cambridge, Mass), 2008.
- [7] Melillo, J.M., A. Gurgel, J. Reilly, T. Cronin, B. Felzer, S. Paltsev, C. Schlosser, A. Sokolov, and X. Wang, "Unintended environmental consequences of a global biofuels program," Tech. Rep. 168, MIT, Global Change forum, Cambridge, Mass, 2009.
- [8] P. McKendry, "Energy production from biomass (part 3): gasification technologies," *Bioresource Technology*, vol. 83, no. 1, pp. 55–63, 2002.
- [9] B. Digman, H. S. Joo, and D. Kim, "Recent progress in gasification/pyrolysis technologies for biomass conversion to energy," *Environmental Progress & Sustainable Energy*, vol. 28, no. 1, pp. 47–51, 2009.
- [10] A. Duret, C. Friedli, and F. Marechal, "Process design of synthetic natural gas (SNG) production using wood gasification," *Journal Of Cleaner Production*, vol. 13, no. 15, pp. 1434–1446, 2005.
- [11] D. C. Elliott, "Catalytic hydrothermal gasification of biomass," *Biofuels, Bioproducts and Biorefining*, vol. 2, no. 3, pp. 254–265, 2008.

- [12] A. Kruse, "Hydrothermal biomass gasification," *The Journal of Supercritical Fluids*, vol. 47, no. 3, pp. 391–399, 2009.
- [13] A. A. Peterson, F. Vogel, R. P. Lachance, M. Froling, M. J. Antal, Jr., and J. W. Tester, "Thermochemical biofuel production in hydrothermal media: A review of sub- and supercritical water technologies," *Energy & Environmental Science*, vol. 1, no. 1, pp. 32–65, 2008.
- [14] F. Fischer and H. Tropsch, "Über die direkte synthese von Erdöl-Kohlenwasserstoffen bei gewöhnlichem druck. (Zweite mitteilung)," *Berichte der deutschen chemischen Gesellschaft (A and B Series)*, vol. 59, no. 4, pp. 832–836, 1926.
- [15] F. Fischer and H. Tropsch, "Über die direkte synthese von Erdöl-Kohlenwasserstoffen bei gewöhnlichem druck. (Erste mitteilung)," *Berichte der deutschen chemischen Gesellschaft (A and B Series)*, vol. 59, no. 4, pp. 830–831, 1926.
- [16] R. P. Datar, R. M. Shenkman, B. G. Cateni, R. L. Huhnke, and R. S. Lewis, "Fermentation of biomass-generated producer gas to ethanol," *Biotechnology and bioengineering*, vol. 86, no. 5, pp. 587–594, 2004.
- [17] E. D. Larson, "Technology for electricity and fuels from biomass," *Annual Review of Energy and the Environment*, vol. 18, no. 1, pp. 567–630, 1993.
- [18] A. V. Bridgwater, D. Meier, and D. Radlein, "An overview of fast pyrolysis of biomass," *Organic Geochemistry*, vol. 30, no. 12, pp. 1479–1493, 1999.
- [19] F. Goudriaan, B. Van de Beld, F. R. Boerefijn, G. M. Bos, J. E. Naber, S. Van der Wal, and J. A. Zevalkink, "Thermal efficiency of the HTU® process for biomass liquefaction," *Progress in Thermochemical Biomass Conversion*, pp. 1312–1325, 2001.
- [20] F. Ma and M. A. Hanna, "Biodiesel production: a review," *Bioresource Technology*, vol. 70, no. 1, pp. 1–15, 1999.
- [21] Y. Chisti, "Biodiesel from microalgae," *Biotechnology Advances*, vol. 25, no. 3, pp. 294–306, 2007.
- [22] T. M. Brown, P. Duan, and P. E. Savage, "Hydrothermal liquefaction and gasification of nannochloropsis sp.," *Energy & Fuels*, vol. 24, no. 6, pp. 3639–3646, 2010.

- [23] K. Weyer, D. Bush, A. Darzins, and B. Willson, "Theoretical maximum algal oil production," *BioEnergy Research*, vol. 3, no. 2, pp. 204–213, 2010.
- [24] R. Davda, J. Shabaker, G. Huber, R. Cortright, and J. Dumesic, "A review of catalytic issues and process conditions for renewable hydrogen and alkanes by aqueous-phase reforming of oxygenated hydrocarbons over supported metal catalysts," *Applied Catalysis B-Environmental*, vol. 56, no. 1-2, pp. 171–186, 2005.
- [25] G. Huber, J. Chheda, C. Barrett, and J. Dumesic, "Production of liquid alkanes by aqueous-phase processing of biomass-derived carbohydrates," *Science*, vol. 308, no. 5727, pp. 1446–1450, 2005.
- [26] E. L. Kunkes, D. A. Simonetti, R. M. West, J. C. Serrano-Ruiz, C. A. Gartner, and J. A. Dumesic, "Catalytic conversion of biomass to monofunctional hydrocarbons and targeted liquid-fuel classes," *Science*, vol. 322, no. 5900, p. 417, 2008.
- [27] G. W. Huber, J. W. Shabaker, and J. A. Dumesic, "Raney Ni-Sn catalyst for h₂ production from biomass-derived hydrocarbons," *Science*, vol. 300, no. 5628, p. 2075, 2003.
- [28] Y. Roman-Leshkov, C. J. Barrett, Z. Y. Liu, and J. A. Dumesic, "Production of dimethylfuran for liquid fuels from biomass-derived carbohydrates," *Nature*, vol. 447, no. 7147, pp. 982–985, 2007.
- [29] L. Lynd, M. Laser, D. Brandsby, B. Dale, B. Davison, R. Hamilton, M. Himmel, M. Keller, J. McMillan, J. Sheehan, and C. Wyman, "How biotech can transform biofuels," *Nature Biotechnology*, vol. 26, no. 2, pp. 169–172, 2008.
- [30] J. Houghton, "Breaking the biological barriers to cellulosic ethanol: A joint research agenda," Tech. Rep. DOE/SC-0095, US Department of Energy, Rockville, Maryland, 2005.
- [31] O. Bobleter, "Hydrothermal degradation of polymers derived from plants," *Progress In Polymer Science*, vol. 19, no. 5, pp. 797–841, 1994.
- [32] P. Béguin and J. Aubert, "The biological degradation of cellulose," *FEMS Microbiology Reviews*, vol. 13, no. 1, pp. 25–58, 1994.
- [33] G. Bonn, R. Concin, and O. Bobleter, "Hydrothermolysis - a new process

- for the utilization of biomass," *Wood Science And Technology*, vol. 17, no. 3, pp. 195–202, 1983.
- [34] O. Bobleter and G. Bonn, "The hydrothermolysis of cellobiose and its Reaction-Product D-Glucose," *Carbohydrate Research*, vol. 124, no. 2, pp. 185–193, 1983.
- [35] A. V. Bandura and S. N. Lvov, "The ionization constant of water over wide ranges of temperature and density," *Journal of Physical and Chemical Reference Data*, vol. 35, no. 1, pp. 15–30, 2006.
- [36] W. Schwald and O. Bobleter, "Hydrothermolysis of cellulose under static and dynamic conditions at high-temperatures," *Journal of Carbohydrate Chemistry*, vol. 8, no. 4, pp. 565–578, 1989.
- [37] G. Bonn and O. Bobleter, "Determination of the hydrothermal degradation products of D-(U-14C) glucose and D-(U-14C) fructose by TLC," *Journal of Radioanalytical and Nuclear Chemistry*, vol. 79, no. 2, pp. 171–177, 1983.
- [38] J. S. Luterbacher, J. W. Tester, and L. P. Walker, "High-solids biphasic CO₂-H₂O pretreatment of lignocellulosic biomass," *Biotechnology and Bioengineering*, vol. 107, no. 3, pp. 451–460, 2010.
- [39] W. S. Mok, M. J. Antal, and G. Varhegyi, "Productive and parasitic pathways in dilute acid-catalyzed hydrolysis of cellulose," *Industrial & Engineering Chemistry Research*, vol. 31, no. 1, pp. 94–100, 1992.
- [40] M. J. Antal Jr, W. S. Mok, and G. N. Richards, "Mechanism of formation of 5-(hydroxymethyl)-2-furaldehyde from d-fructose an sucrose.," *Carbohydrate research*, vol. 199, no. 1, p. 91, 1990.
- [41] B. M. Kabyemela, T. Adschiri, R. M. Malaluan, and K. Arai, "Kinetics of glucose epimerization and decomposition in subcritical and supercritical water," *Industrial & Engineering Chemistry Research*, vol. 36, no. 5, pp. 1552–1558, 1997.
- [42] Q. Xiang, Y. Y. Lee, and R. W. Torget, "Kinetics of glucose decomposition during dilute-acid hydrolysis of lignocellulosic biomass," *Applied biochemistry and biotechnology*, vol. 115, no. 1, pp. 1127–1138, 2004.
- [43] H. R. Holgate, J. C. Meyer, and J. W. Tester, "Glucose hydrolysis and ox-

- idation in supercritical water," *AIChE Journal*, vol. 41, no. 3, pp. 637–648, 1995.
- [44] Z. Srokol, A. G. Bouche, A. van Estrik, R. C. Strik, T. Maschmeyer, and J. A. Peters, "Hydrothermal upgrading of biomass to biofuel; studies on some monosaccharide model compounds," *Carbohydrate research*, vol. 339, no. 10, pp. 1717–1726, 2004.
- [45] S. Deguchi, K. Tsujii, and K. Horikoshi, "Cooking cellulose in hot and compressed water," *Chemical Communications*, vol. 2006, no. 31, pp. 3293–3295, 2006.
- [46] S. Takenouchi and G. Kennedy, "Binary system H₂O-CO₂ at high temperatures and pressures," *American Journal of Science*, vol. 262, no. 9, pp. 1055–1074, 1964.
- [47] T. Miyazawa and T. Funazukuri, "Polysaccharide hydrolysis accelerated by adding carbon dioxide under hydrothermal conditions," *Biotechnology Progress*, vol. 21, no. 6, pp. 1782–1785, 2005.
- [48] G. van Walsum and H. Shi, "Carbonic acid enhancement of hydrolysis in aqueous pretreatment of corn stover," *Bioresource Technology*, vol. 93, no. 3, pp. 217–226, 2004.
- [49] T. Adschiri, S. Hirose, R. Malaluan, and K. Arai, "Noncatalytic conversion of cellulose in supercritical and subcritical water," *Journal of Chemical Engineering of Japan*, vol. 26, no. 6, pp. 676–680, 1993.
- [50] K. Mochidzuki, A. Sakoda, and M. Suzuki, "Measurement of the hydrothermal reaction rate of cellulose using novel liquid-phase thermogravimetry," *Thermochimica Acta*, vol. 348, no. 1-2, pp. 69–76, 2000.
- [51] M. Sasaki, Z. Fang, Y. Fukushima, T. Adschiri, and K. Arai, "Dissolution and hydrolysis of cellulose in subcritical and supercritical water," *Industrial & Engineering Chemistry Research*, vol. 39, no. 8, pp. 2883–2890, 2000.
- [52] O. Bobleter and G. Pape, "Hydrothermal degradation of glucose," *Monatshfte fur Chemie*, vol. 99, no. 4, p. 1560, 1968.
- [53] S. Amin, R. C. Reid, and M. Modell, "Reforming and decomposition of glucose in an aqueous phase," in *ASME, SAE, AIAA, ASMA, and AIChE, Intersociety Conference on Environmental Systems, San Francisco, Calif*, 1975.

- [54] Y. Matsumura, S. Yanachi, and T. Yoshida, "Glucose decomposition kinetics in water at 25 MPa in the temperature range of 448–673 K," *Industrial & Engineering Chemistry Research*, vol. 45, no. 6, pp. 1875–1879, 2006.
- [55] M. L. Wolfrom and L. W. Georges, "A study of cellulose hydrolysis by means of ethyl mercaptan," *Journal of the American Chemical Society*, vol. 59, no. 2, pp. 282–286, 1937.
- [56] F. Bergius, "Conversion of wood to carbohydrates," *Industrial & Engineering Chemistry*, vol. 29, no. 3, pp. 247–253, 1937.
- [57] S. Zhang, F. Maréchal, M. Gassner, Z. Périn-Levasseur, W. Qi, Z. Ren, Y. Yan, and D. Favrat, "Process modeling and integration of fuel ethanol production from lignocellulosic biomass based on double acid hydrolysis," *Energy & Fuels*, vol. 23, no. 3, pp. 1759–1765, 2009.
- [58] A. Sluiter, B. Hames, R. Ruiz, C. Scarlata, J. Sluiter, D. Templeton, and D. Crocker, "Determination of structural carbohydrates and lignin in biomass," Tech. Rep. TP-510-42623, National Renewable Energy Laboratory, Golden, CO, 2004.
- [59] Y. P. Zhang, S. Ding, J. R. Mielenz, J. Cui, R. T. Elander, M. Laser, M. E. Himmel, J. R. McMillan, and L. R. Lynd, "Fractionating recalcitrant lignocellulose at modest reaction conditions," *Biotechnology and Bioengineering*, vol. 97, no. 2, pp. 214–223, 2007.
- [60] Z. Zhu, N. Sathitsuksanoh, T. Vinzant, D. J. Schell, J. D. McMillan, and Y. P. Zhang, "Comparative study of corn stover pretreated by dilute acid and cellulose solvent-based lignocellulose fractionation: Enzymatic hydrolysis, supramolecular structure, and substrate accessibility," *Biotechnology and Bioengineering*, vol. 103, no. 4, pp. 715–724, 2009.
- [61] R. Fagan, H. Grethlein, A. Converse, and A. Porteous, "Kinetics of the acid hydrolysis of cellulose found in paper refuse," *Environmental Science & Technology*, vol. 5, no. 6, pp. 545–547, 1971.
- [62] J. Saeman, "Kinetics of wood saccharification - hydrolysis of cellulose and decomposition of sugars in dilute acid at high temperature," *Industrial & Engineering Chemistry*, vol. 37, no. 1, pp. 43–52, 1945.
- [63] D. R. Thompson and H. E. Grethlein, "Design and evaluation of a plug flow reactor for acid hydrolysis of cellulose," *Industrial & Engineering*

Chemistry Product Research and Development, vol. 18, no. 3, pp. 166–169, 1979.

- [64] A. H. Conner, B. F. Wood, C. G. Hill, and J. F. Harris, “Kinetic model for the dilute sulfuric acid saccharification of lignocellulose,” *Journal of Wood Chemistry and Technology*, vol. 5, no. 4, pp. 461–489, 1985.
- [65] N. Abatzoglou, J. Bouchard, E. Chornet, and R. P. Overend, “Dilute acid depolymerization of cellulose in aqueous phase: Experimental evidence of the significant presence of soluble oligomeric intermediates,” *The Canadian Journal of Chemical Engineering*, vol. 64, no. 5, pp. 781–786, 1986.
- [66] Y. Zhao, W. Lu, H. Wang, and D. Li, “Combined supercritical and subcritical process for cellulose hydrolysis to fermentable hexoses,” *Environmental Science & Technology*, vol. 43, no. 5, pp. 1565–1570, 2009.
- [67] G. Bonn, H. Binder, H. Leonhard, and O. Bobleter, “The alkaline degradation of cellobiose to glucose and fructose,” *Monatshefte fur Chemie / Chemical Monthly*, vol. 116, no. 8, pp. 961–971, 1985.
- [68] F. J. Kolpak, M. Weih, and J. Blackwell, “Mercerization of cellulose: 1. determination of the structure of mercerized cotton,” *Polymer*, vol. 19, no. 2, pp. 123–131, 1978.
- [69] D. C. Dan, V. Jacopian, U. Kasulke, and B. Philipp, “Zum einfluss von quellung und mercerisierung auf den enzymatischen abbau von lintercellulose,” *Acta Polymerica*, vol. 31, no. 6, pp. 388–393, 1980.
- [70] D. B. Wilson, “Three microbial strategies for plant cell wall degradation,” *Annals of the New York Academy of Sciences*, vol. 1125, no. Incredible Anaerobes From Physiology to Genomics to Fuels, pp. 289–297, 2008.
- [71] J. A. Breznak, “Intestinal microbiota of termites and other xylophagous insects,” *Annual Review of Microbiology*, vol. 36, no. 1, pp. 323–323, 1982.
- [72] M. Ohkuma, “Termite symbiotic systems: efficient bio-recycling of lignocellulose,” *Applied Microbiology and Biotechnology*, vol. 61, no. 1, pp. 1–9, 2003.
- [73] M. Desvaux, “Unravelling carbon metabolism in anaerobic cellulolytic bacteria,” *Biotechnology Progress*, vol. 22, no. 5, pp. 1229–1238, 2006.

- [74] N. Shinzato, M. Muramatsu, Y. Watanabe, and T. Matsui, "Termite-regulated fungal monoculture in fungus combs of a macrotermitine termite *Odontotermes formosanus*," *Zoological Science*, vol. 22, no. 8, pp. 917–922, 2005.
- [75] H. Watanabe and G. Tokuda, "Animal cellulases," *Cellular and Molecular Life Sciences*, vol. 58, no. 9, pp. 1167–1178, 2001.
- [76] T. Kunieda, T. Fujiyuki, R. Kucharski, S. Foret, S. A. Ament, A. L. Toth, K. Ohashi, H. Takeuchi, A. Kamikouchi, E. Kage, M. Morioka, M. Beye, T. Kubo, G. E. Robinson, and R. Maleszka, "Carbohydrate metabolism genes and pathways in insects: insights from the honey bee genome," *Insect Molecular Biology*, vol. 15, no. 5, pp. 563–576, 2006.
- [77] L. Lynd, P. Weimer, W. van Zyl, and I. Pretorius, "Microbial cellulose utilization: Fundamentals and biotechnology," *Microbiology and molecular biology reviews*, vol. 66, no. 3, p. 506, 2002.
- [78] E. A. Bayer, H. Chanzy, R. Lamed, and Y. Shoham, "Cellulose, cellulases and cellulosomes," *Current Opinion in Structural Biology*, vol. 8, no. 5, pp. 548–557, 1998.
- [79] E. A. Bayer, J. Belaich, Y. Shoham, and R. Lamed, "The cellulosomes: Multienzyme machines for degradation of plant cell wall polysaccharides," *Annual Review of Microbiology*, vol. 58, no. 1, pp. 521–554, 2004.
- [80] J. Caspi, D. Irwin, R. Lamed, Y. Shoham, H. P. Fierobe, D. B. Wilson, and E. A. Bayer, "Thermobifida fusca family-6 cellulases as potential designer cellulosome components," *Biocatalysis and Biotransformation*, vol. 24, no. 1, pp. 3–12, 2006.
- [81] F. Mingardon, A. Chanal, C. Tardif, E. A. Bayer, and H. P. Fierobe, "Exploration of new geometries in cellulosome-like chimeras," *Applied and environmental microbiology*, vol. 73, no. 22, p. 7138, 2007.
- [82] R. E. Nordon, S. J. Craig, and F. C. Foong, "Molecular engineering of the cellulosome complex for affinity and bioenergy applications," *Biotechnology letters*, vol. 31, no. 4, pp. 465–476, 2009.
- [83] J. Caspi, D. Irwin, R. Lamed, Y. Li, H. P. Fierobe, D. B. Wilson, and E. A. Bayer, "Conversion of thermobifida fusca free exoglucanases into cellulosomal components: comparative impact on cellulose-degrading activity," *Journal of biotechnology*, vol. 135, no. 4, pp. 351–357, 2008.

- [84] D. B. Wilson, "Cellulases and biofuels," *Current opinion in biotechnology*, vol. 20, no. 3, pp. 295–299, 2009.
- [85] J. Rouvinen, T. Bergfors, T. Teeri, J. K. C. Knowles, and T. A. Jones, "Three-Dimensional structure of cellobiohydrolase II from *Trichoderma reesei*," *Science*, vol. 249, no. 4967, pp. 380–386, 1990.
- [86] C. Divne, J. Stahlberg, T. Reinikainen, L. Ruohonen, G. Pettersson, J. K. C. Knowles, T. T. Teeri, and T. A. Jones, "The Three-Dimensional crystal structure of the catalytic core of Cellobiohydrolase I from *Trichoderma reesei*," *Science*, vol. 265, no. 5171, pp. 524–528, 1994.
- [87] Z. Xiao, P. Gao, Y. Qu, and T. Wang, "Cellulose-binding domain of endoglucanase III from trichoderma reesei disrupting the structure of cellulose," *Biotechnology Letters*, vol. 23, no. 9, pp. 711–715, 2001.
- [88] N. Din, N. R. Gilkes, B. Tekant, R. C. Miller, R. A. J. Warren, and D. G. Kilburn, "Non-Hydrolytic disruption of cellulose fibres by the binding domain of a bacterial cellulase," *Nature Biotechnology*, vol. 9, no. 11, pp. 1096–1099, 1991.
- [89] G. A. Ji, C. G. Jun, W. T. Hong, Z. Y. Shu, and L. I. U. Jie, "Non-hydrolytic disruption of crystalline structure of cellulose by cellulose binding domain and linker sequence of cellobiohydrolase I from *Penicillium janthinellum*," *Acta Biochimica et Biophysica Sinica*, vol. 1, 2001.
- [90] L. Wang, Y. Zhang, and P. Gao, "A novel function for the cellulose binding module of Cellobiohydrolase I," *Science in China Series C: Life Sciences*, vol. 51, no. 7, pp. 620–629, 2008.
- [91] A. Esteghlalian, V. Srivastava, N. Gilkes, D. Kilburn, R. Warren, and J. Sadtler, "Do cellulose binding domains increase substrate accessibility?," *Applied Biochemistry and Biotechnology*, vol. 91-93, no. 1, pp. 575–592, 2001.
- [92] J. Stahlberg, G. Johansson, and G. Pettersson, "A new model for enzymatic hydrolysis of cellulose based on the two-domain structure of Cellobiohydrolase I," *Nature Biotechnology*, vol. 9, no. 3, pp. 286–290, 1991.
- [93] G. J. Davies, G. G. Dodson, R. E. Hubbard, S. P. Tolley, Z. Dauter, K. S. Wilson, C. Hjort, J. M. Mikkelsen, G. Rasmussen, and M. Schülein, "Structure and function of Endoglucanase V," *Nature*, vol. 365, no. 6444, pp. 362–364, 1993.

- [94] M. Juy, A. G. Amrt, P. M. Alzari, R. J. Poljak, M. Claeysens, P. Beguin, and J. Aubert, "Three-dimensional structure of a thermostable bacterial cellulase," *Nature*, vol. 357, no. 6373, pp. 89–91, 1992.
- [95] L. Thygesen, B. J. Hidayat, K. S. Johansen, and C. Felby, "The significance of supramolecular structures of cellulose for the enzymatic hydrolysis of plant cell walls," in *Proceedings of the 32nd Symposium on Biotechnology for fuels and chemicals*, (Clearwater beach, FL), 2010.
- [96] D. C. Irwin, M. Spezio, L. P. Walker, and D. B. Wilson, "Activity studies of eight purified cellulases: Specificity, synergism, and binding domain effects," *Biotechnology and Bioengineering*, vol. 42, no. 8, pp. 1002–1013, 1993.
- [97] D. Irwin, D. Shin, S. Zhang, B. K. Barr, J. Sakon, P. A. Karplus, and D. B. Wilson, "Roles of the catalytic domain and two cellulose binding domains of thermomonospora fusca e4 in cellulose hydrolysis," *Journal of Bacteriology*, vol. 180, no. 7, pp. 1709–1714, 1998.
- [98] J. Sakon, D. Irwin, D. B. Wilson, and P. A. Karplus, "Structure and mechanism of endo/exocellulase E4 from *Thermomonospora fusca*," *Nature Structural & Molecular Biology*, vol. 4, no. 10, pp. 810–818, 1997.
- [99] M. Holtzapple, M. Cognata, Y. Shu, and C. Hendrickson, "Inhibition of trichoderma reesei cellulase by sugars and solvents," *Biotechnology and Bioengineering*, vol. 36, no. 3, pp. 275–287, 1990.
- [100] J. Medve, J. Karlsson, D. Lee, and F. Tjerneld, "Hydrolysis of microcrystalline cellulose by Cellobiohydrolase I and Endoglucanase II from *Trichoderma reesei*: Adsorption, sugar production pattern, and synergism of the enzymes," *Biotechnology and Bioengineering*, vol. 59, no. 5, pp. 621–634, 1998.
- [101] R. Messner, K. Hagspiel, and C. P. Kubicek, "Isolation of a beta-glucosidase binding and activating polysaccharide from cell walls of *Trichoderma reesei*," *Archives of Microbiology*, vol. 154, no. 2, pp. 150–155, 1990.
- [102] C. Wyman, B. Dale, R. Elander, M. Holtzapple, M. Ladisch, and Y. Lee, "Coordinated development of leading biomass pretreatment technologies," *Bioresource Technology*, vol. 96, no. 18, pp. 1959–1966, 2005.
- [103] E. T. Reese, R. G. Siu, and H. S. Levinson, "The biological degradation of soluble cellulose derivatives and its relationship to the mechanism of cellulose hydrolysis," *Journal of Bacteriology*, vol. 59, no. 4, p. 485, 1950.

- [104] L. Walker and D. Wilson, "Enzymatic-Hydrolysis of cellulose - an overview," *Bioresource Technology*, vol. 36, no. 1, pp. 3–14, 1991.
- [105] T. M. Wood and S. I. McCrae, "Synergism between enzymes involved in the solubilization of native cellulose," *Advances in Chemistry Series*, vol. 181, pp. 181–209, 1979.
- [106] B. Nidetzky, W. Steiner, M. Hayn, and M. Claeysens, "Cellulose hydrolysis by the cellulases from *Trichoderma reesei*: a new model for synergistic interaction.," *Biochemical Journal*, vol. 298, no. Pt 3, pp. 705–710, 1994.
- [107] R. E. Carey and D. J. Cosgrove, "Portrait of the expansin superfamily in *Physcomitrella patens*: comparisons with angiosperm expansins," *Annals of Botany*, 2007.
- [108] E. S. Kim, H. J. Lee, W. G. Bang, I. G. Choi, and K. H. Kim, "Functional characterization of a bacterial expansin from bacillus subtilis for enhanced enzymatic hydrolysis of cellulose," *Biotechnology and bioengineering*, vol. 102, no. 5, pp. 1342–1353, 2008.
- [109] Q. Yao, T. T. Sun, W. F. Liu, and G. J. Chen, "Gene cloning and heterologous expression of a novel Endoglucanase, swollenin, from *Trichoderma pseudokoningii* S38," *Bioscience, biotechnology, and biochemistry*, vol. 11, no. 72, pp. 2799–2805, 2008.
- [110] S. Karkehabadi, H. Hansson, S. Kim, K. Piens, C. Mitchinson, and M. Sandgren, "The first structure of a glycoside hydrolase family 61 member, Cel61B from *Hypocrea jecorina*, at 1.6 Å resolution," *Journal of molecular biology*, vol. 383, no. 1, pp. 144–154, 2008.
- [111] L. Rosgaard, S. Pedersen, J. R. Cherry, P. Harris, and A. S. Meyer, "Efficiency of new fungal cellulase systems in boosting enzymatic degradation of barley straw lignocellulose," *Biotechnology progress*, vol. 22, no. 2, pp. 493–498, 2008.
- [112] S. Zhang, D. E. Wolfgang, and D. B. Wilson, "Substrate heterogeneity causes the nonlinear kinetics of insoluble cellulose hydrolysis," *Biotechnology and Bioengineering*, vol. 66, no. 1, pp. 35–41, 1999.
- [113] C. Schou, G. Rasmussen, M. Kalltoft, B. Henrissat, and M. Schülein, "Stereochemistry, specificity and kinetics of the hydrolysis of reduced cellooligosaccharides by nine cellulases," *European Journal of Biochemistry*, vol. 217, no. 3, pp. 947–953, 1993.

- [114] P. Biely, M. Vrsanska, and M. Claeysens, Marc, "The endo-1,4-beta-glucanase I from *Trichoderma reesei*," *European Journal of Biochemistry*, vol. 200, no. 1, pp. 157–163, 1991.
- [115] T. Jeoh, C. I. Ishizawa, M. F. Davis, M. E. Himmel, W. S. Adney, and D. K. Johnson, "Cellulase digestibility of pretreated biomass is limited by cellulose accessibility," *Biotechnology and Bioengineering*, vol. 98, no. 1, pp. 112–122, 2007.
- [116] J. Moran-Mirabal, N. Santhanam, S. Corgie, H. Craighead, and L. Walker, "Immobilization of cellulose fibrils on solid substrates for cellulase-binding studies through quantitative fluorescence microscopy," *Biotechnology and bioengineering*, vol. 101, no. 6, pp. 1129–1141, 2008.
- [117] P. Zhu, J. M. Moran-Mirabal, J. S. Luterbacher, L. P. Walker, and H. G. Craighead, "Observing thermobifida fusca cellulase binding to pretreated wood particles using time-lapse confocal laser scanning microscopy," *Cellulose*, vol. 18, no. 3, pp. 749–758, 2011.
- [118] H. Grethlein, "The effect of Pore-Size distribution on the rate of Enzymatic-Hydrolysis of cellulosic substrates," *Nature Biotechnology*, vol. 3, no. 2, pp. 155–160, 1985.
- [119] P. Bansal, M. Hall, M. J. Realff, J. H. Lee, and A. S. Bommarius, "Modeling cellulase kinetics on lignocellulosic substrates," *Biotechnology Advances*, vol. 27, no. 6, pp. 833–848, 2009.
- [120] M. M. Gharpuray, Y. Lee, and L. T. Fan, "Structural modification of lignocellulosics by pretreatments to enhance enzymatic hydrolysis," *Biotechnology and Bioengineering*, vol. 25, no. 1, pp. 157–172, 1983.
- [121] J. P. O'Dwyer, L. Zhu, C. B. Granda, and M. T. Holtzapple, "Enzymatic hydrolysis of lime-pretreated corn stover and investigation of the HCH-1 model: Inhibition pattern, degree of inhibition, validity of simplified HCH-1 model," *Bioresource Technology*, vol. 98, no. 16, pp. 2969–2977, 2007.
- [122] L. Laureano-Perez, F. Teymour, H. Alizadeh, and B. E. Dale, "Understanding factors that limit enzymatic hydrolysis of biomass," in *Twenty-Sixth Symposium on Biotechnology for Fuels and Chemicals* (B. H. Davison, B. R. Evans, M. Finkelstein, and J. D. McMillan, eds.), ABAB Symposium, pp. 1081–1099, Humana Press, 2005.

- [123] G. Banerjee, S. Car, J. S. Scott-Craig, M. S. Borrusch, N. Aslam, and J. D. Walton, "Synthetic enzyme mixtures for biomass deconstruction: production and optimization of a core set," *Biotechnology And Bioengineering*, vol. 106, no. 5, pp. 707–720, 2010.
- [124] G. Banerjee, S. Car, J. S. Scott-Craig, M. S. Borrusch, and J. D. Walton, "Rapid optimization of enzyme mixtures for deconstruction of diverse pretreatment/biomass feedstock combinations," *Biotechnology for Biofuels*, vol. 3, no. 1, pp. 1–15, 2010.
- [125] M. K. Bothwell, *Binding Kinetics of Thermomonospora Fusca E3 and E5 and Trichoderma Reesei CBHI*. Ph.D., Cornell University, Ithaca, NY, 1994.
- [126] M. K. Bothwell, S. D. Daughhetee, G. Y. Chaua, D. B. Wilson, and L. P. Walker, "Binding capacities for *Thermomonospora fusca* E3, E4 and E5, the E3 binding domain, and *Trichoderma reesei* CBHI on avicel and bacterial microcrystalline cellulose," *Bioresource technology*, vol. 60, no. 2, pp. 169–178, 1997.
- [127] K. L. Kadam, E. C. Rydholm, and J. D. McMillan, "Development and validation of a kinetic model for enzymatic saccharification of lignocellulosic biomass," *Biotechnology Progress*, vol. 20, no. 3, pp. 698–705, 2004.
- [128] J. M. Fox, S. E. Levine, D. S. Clark, and H. W. Blanch, "Initial- and Processive-Cut products reveal cellobiohydrolase rate limitations and the role of companion enzymes," *Biochemistry*, vol. 51, no. 1, pp. 442–452, 2011.
- [129] J. Luo, L. Xia, J. Lin, and P. Cen, "Kinetics of simultaneous saccharification and lactic acid fermentation processes," *Biotechnology Progress*, vol. 13, no. 6, pp. 762–767, 1997.
- [130] W. Liao, Y. Liu, Z. Wen, C. Frear, and S. Chen, "Kinetic modeling of enzymatic hydrolysis of cellulose in differently pretreated fibers from dairy manure," *Biotechnology and Bioengineering*, vol. 101, no. 3, pp. 441–451, 2008.
- [131] W. Steiner, W. Sattler, and H. Esterbauer, "Adsorption of trichoderma reesei cellulase on cellulose: Experimental data and their analysis by different equations," *Biotechnology and Bioengineering*, vol. 32, no. 7, pp. 853–865, 1988.

- [132] S. E. Levine, J. M. Fox, D. S. Clark, and H. W. Blanch, "A mechanistic model for rational design of optimal cellulase mixtures," *Biotechnology and Bioengineering*, vol. 108, no. 11, pp. 2561–2570, 2011. DOI: 10.1002/bit.23249.
- [133] S. E. Levine, J. M. Fox, H. W. Blanch, and D. S. Clark, "A mechanistic model of the enzymatic hydrolysis of cellulose," *Biotechnology and bioengineering*, vol. 107, no. 1, pp. 37–51, 2010.
- [134] Q. Gan, S. Allen, and G. Taylor, "Kinetic dynamics in heterogeneous enzymatic hydrolysis of cellulose: an overview, an experimental study and mathematical modelling," *Process Biochemistry*, vol. 38, no. 7, pp. 1003–1018, 2003.
- [135] O. Chaikumpollert, P. Methacanon, and K. Suchiva, "Structural elucidation of hemicelluloses from vetiver grass," *Carbohydrate Polymers*, vol. 57, no. 2, pp. 191–196, 2004.
- [136] M. Nimlos, H. Pilath, X. Qian, M. Himmel, and D. Johnson, "Xylose production and degradation during acid pretreatment of biomass," in *Proceedings of the 32nd Symposium on Biotechnology for fuels and chemicals*, (Clearwater beach, FL), 2010.
- [137] C. Liu and C. Wyman, "The effect of flow rate of compressed hot water on xylan, lignin, and total mass removal from corn stover," *Industrial & Engineering Chemistry Research*, vol. 42, no. 21, pp. 5409–5416, 2003.
- [138] A. P. Dunlop, "Furfural formation and behavior," *Industrial & Engineering Chemistry*, vol. 40, no. 2, pp. 204–209, 1948.
- [139] M. J. Antal, T. Leesomboon, W. S. Mok, and G. N. Richards, "Mechanism of formation of 2-furaldehyde from D-xylose," *Carbohydrate research*, vol. 217, pp. 71–85, 1991.
- [140] A. Ragauskas, Y. Pu, S. Jung, M. Foston, A. Ziebell, M. Davis, C. Fang, R. Dixon, B. Davison, M. Studer, and C. Wyman, "A perspective on pretreatment chemistry: What we know and need to know," in *Proceedings of the 32nd Symposium on Biotechnology for fuels and chemicals*, (Clearwater beach, FL), 2010.
- [141] Q. Jing and X. Lü, "Kinetics of non-catalyzed decomposition of d-xylose in high temperature liquid water," *Chinese Journal of Chemical Engineering*, vol. 15, no. 5, pp. 666–669, 2007.

- [142] M. S. Feather, "Reductic acid-14C derived from D-xylose-1-14C and 2-furaldehyde- α -14C," *The Journal of Organic Chemistry*, vol. 34, no. 6, pp. 1998–1999, 1969.
- [143] F. A. H. Rice and L. Fishbein, "Effect of aqueous sulfuric acid on sugars. II. spectrophotometric studies on the hexoses; identification of the ether-soluble products formed," *Journal of the American Chemical Society*, vol. 78, no. 15, pp. 3731–3734, 1956.
- [144] F. A. H. Rice and L. Fishbein, "Spectrophotometric studies on the action of sulfuric acid on reducing sugars and the isolation and identification of the ether-soluble substances produced from pentoses under acid conditions," *Journal of the American Chemical Society*, vol. 78, no. 5, pp. 1005–1009, 1956.
- [145] G. Garrote, H. Dominguez, and J. C. Parajo, "Mild autohydrolysis: an environmentally friendly technology for xylooligosaccharide production from wood," *Journal of Chemical Technology & Biotechnology*, vol. 74, no. 11, pp. 1101–1109, 1999.
- [146] G. Garrote and J. C. Parajo, "Non-isothermal autohydrolysis of eucalyptus wood," *Wood Science and Technology*, vol. 36, no. 2, pp. 111–123, 2002.
- [147] G. Garrote, H. Dominguez, and J. C. Parajo, "Autohydrolysis of corncob: study of non-isothermal operation for xylooligosaccharide production," *Journal of food engineering*, vol. 52, no. 3, pp. 211–218, 2002.
- [148] S. Jacobsen and C. Wyman, "Xylose monomer and oligomer yields for uncatalyzed hydrolysis of sugarcane bagasse hemicellulose at varying solids concentration," *Industrial & Engineering Chemistry Research*, vol. 41, no. 6, pp. 1454–1461, 2002.
- [149] A. Mittal, S. G. Chatterjee, G. M. Scott, and T. E. Amidon, "Modeling xylan solubilization during autohydrolysis of sugar maple wood meal: Reaction kinetics," *Holzforschung*, vol. 63, no. 3, pp. 307–314, 2009.
- [150] A. Mittal, S. G. Chatterjee, G. M. Scott, and T. E. Amidon, "Modeling xylan solubilization during autohydrolysis of sugar maple and aspen wood chips: Reaction kinetics and mass transfer," *Chemical Engineering Science*, vol. 64, no. 13, pp. 3031–3041, 2009.
- [151] C. Liu and C. Wyman, "The effect of flow rate of very dilute sulfuric acid on xylan, lignin, and total mass removal from corn stover," *Industrial & Engineering Chemistry Research*, vol. 43, no. 11, pp. 2781–2788, 2004.

- [152] S. C. Yat, A. Berger, and D. R. Shonnard, "Kinetic characterization for dilute sulfuric acid hydrolysis of timber varieties and switchgrass," *Biore-source technology*, vol. 99, no. 9, pp. 3855–3863, 2008.
- [153] I. A. Malester, M. Green, and G. Shelef, "Kinetics of dilute acid hydrolysis of cellulose originating from municipal solid wastes," *Industrial & Engineering Chemistry Research*, vol. 31, no. 8, pp. 1998–2003, 1992.
- [154] A. Esteghlalian, A. G. Hashimoto, J. J. Fenske, and M. H. Penner, "Modeling and optimization of the dilute-sulfuric-acid pretreatment of corn stover, poplar and switchgrass," *Biore-source technology*, vol. 59, no. 2-3, pp. 129–136, 1997.
- [155] S. Ranganathan, D. G. Macdonald, and N. N. Bakhshi, "Kinetic studies of wheat straw hydrolysis using sulphuric acid," *The Canadian Journal of Chemical Engineering*, vol. 63, no. 5, pp. 840–844, 1985.
- [156] J. Jensen, J. Morinelly, A. Aglan, A. Mix, and D. R. Shonnard, "Kinetic characterization of biomass dilute sulfuric acid hydrolysis: Mixtures of hardwoods, softwood, and switchgrass," *AIChE Journal*, vol. 54, no. 6, pp. 1637–1645, 2008.
- [157] T. Kobayashi and Y. Sakai, "Hydrolysis rate of pentosan of hardwood in dilute sulfuric acid," *Bulletin of the Agricultural Chemical Society of Japan*, vol. 20, no. 1, pp. 1–7, 1956.
- [158] M. T. Maloney, T. W. Chapman, and A. J. Baker, "Dilute acid hydrolysis of paper birch: Kinetics studies of xylan and acetyl-group hydrolysis," *Biotechnology and Bioengineering*, vol. 27, no. 3, pp. 355–361, 1985.
- [159] S. B. Kim and Y. Y. Lee, "Kinetics in Acid-Catalyzed hydrolysis of hardwood hemicellulose," in *Eighth Symposium on Biotechnology for Fuels and Chemicals: proceedings of the Eighth Symposium on Biotechnology for Fuels and Chemicals*, (Gatlinburg, Tennessee), p. 71, 1986.
- [160] D. Sills and J. Gossett, "Assessment of commercial hemicellulases for saccharification of alkaline pretreated perennial biomass," *Biore-source Technology*, vol. 102, no. 2, pp. 1389–1398, 2011.
- [161] J. Xu, J. J. Cheng, R. R. Sharma-Shivappa, and J. C. Burns, "Sodium hydroxide pretreatment of switchgrass for ethanol production," *Energy & Fuels*, vol. 24, no. 3, pp. 2113–2119, 2010.

- [162] Z. Wang, D. R. Keshwani, A. P. Redding, and J. J. Cheng, "Sodium hydroxide pretreatment and enzymatic hydrolysis of coastal bermuda grass," *Bioresource Technology*, vol. 101, no. 10, pp. 3583–3585, 2010.
- [163] Q. K. Beg, M. Kapoor, L. Mahajan, and G. S. Hoondal, "Microbial xylanases and their industrial applications: a review," *Applied Microbiology and Biotechnology*, vol. 56, no. 3, pp. 326–338, 2001.
- [164] P. F. I. Javier, G. Óscar, J. Sanz-Aparicio, and P. Díaz, "Xylanases: Molecular properties and applications," in *Industrial Enzymes*, pp. 65–82, 2007.
- [165] B. K. Kubata, K. Takamizawa, K. Kawai, T. Suzuki, and H. Horitsu, "Xylanase IV, an exoxylanase of *Aeromonas caviae* ME-1 which produces xylo-tetraose as the only low-molecular-weight oligosaccharide from xylan," *Applied Microbiology and Biotechnology*, vol. 61, no. 4, p. 1666, 1995.
- [166] R. P. de Vries and J. Visser, "*Aspergillus* enzymes involved in degradation of plant cell wall polysaccharides," *Microbiology and Molecular Biology Reviews*, vol. 65, no. 4, pp. 497–522, 2001.
- [167] R. P. de Vries, H. Kester, C. H. Poulsen, J. A. Benen, and J. Visser, "Synergy between enzymes from *Aspergillus* involved in the degradation of plant cell wall polysaccharides," *Carbohydrate research*, vol. 327, no. 4, pp. 401–410, 2000.
- [168] F. J. M. Kormelink and A. G. J. Voragen, "Degradation of different [(glucurono) arabino] xylans by a combination of purified xylan-degrading enzymes," *Applied Microbiology and Biotechnology*, vol. 38, no. 5, pp. 688–695, 1993.
- [169] C. Zhong, M. W. Lau, V. Balan, B. E. Dale, and Y. J. Yuan, "Optimization of enzymatic hydrolysis and ethanol fermentation from AFEX-treated rice straw," *Applied microbiology and biotechnology*, vol. 84, no. 4, pp. 667–676, 2009.
- [170] A. Berlin, V. Maximenko, N. Gilkes, and J. Saddler, "Optimization of enzyme complexes for lignocellulose hydrolysis," *Biotechnology and Bioengineering*, vol. 97, no. 2, pp. 287–296, 2007.
- [171] R. Kumar and C. E. Wyman, "Effect of xylanase supplementation of cellulase on digestion of corn stover solids prepared by leading pretreatment technologies," *Bioresource technology*, vol. 100, no. 18, pp. 4203–4213, 2009.

- [172] R. Kumar and C. E. Wyman, "Effect of enzyme supplementation at moderate cellulase loadings on initial glucose and xylose release from corn stover solids pretreated by leading technologies," *Biotechnology and Bioengineering*, vol. 102, no. 2, pp. 457–467, 2008.
- [173] H. K. Murnen, V. Balan, S. P. S. Chundawat, B. Bals, L. d. C. Sousa, and B. E. Dale, "Optimization of ammonia fiber expansion (AFEX) pretreatment and enzymatic hydrolysis of miscanthus X giganteus to fermentable sugars," *Biotechnology Progress*, vol. 23, no. 4, pp. 846–850, 2007.
- [174] R. Bura, R. Chandra, and J. Saddler, "Influence of xylan on the enzymatic hydrolysis of Steam-Pretreated corn stover and hybrid poplar," *Biotechnology Progress*, vol. 25, no. 2, pp. 315–322, 2009.
- [175] K. Ohgren, R. Bura, J. Saddler, and G. Zacchi, "Effect of hemicellulose and lignin removal on enzymatic hydrolysis of steam pretreated corn stover," *Bioresource Technology*, vol. 98, no. 13, pp. 2503–2510, 2007.
- [176] H. Nimz, "Beech lignin - proposal of a constitutional scheme," *Angewandte Chemie International Edition in English*, vol. 13, no. 5, pp. 313–321, 1974.
- [177] P. Sannigrahi, A. Ragauskas, and S. Miller, "Effects of Two-Stage dilute acid pretreatment on the structure and composition of lignin and cellulose in loblolly pine," *BioEnergy Research*, vol. 1, no. 3, pp. 205–214, 2008.
- [178] M. J. Selig, S. Viamajala, S. R. Decker, M. P. Tucker, M. E. Himmel, and T. B. Vinzant, "Deposition of lignin droplets produced during dilute acid pretreatment of maize stems retards enzymatic hydrolysis of cellulose," *Biotechnology Progress*, vol. 23, no. 6, pp. 1333–1339, 2007.
- [179] B. Yang and C. Wyman, "Effect of xylan and lignin removal by batch and flowthrough pretreatment on the enzymatic digestibility of corn stover cellulose," *Biotechnology And Bioengineering*, vol. 86, no. 1, pp. 88–95, 2004.
- [180] K. Okuda, X. Man, M. Umetsu, S. Takami, and T. Adschiri, "Efficient conversion of lignin into single chemical species by solvothermal reaction in water-p-cresol solvent," *Journal of Physics: Condensed Matter*, vol. 16, no. 14, pp. S1325–S1330, 2004.
- [181] T. Voitl and P. R. v. Rohr, "Demonstration of a process for the conversion of kraft lignin into vanillin and methyl vanillate by acidic oxidation in

- aqueous methanol," *Industrial & Engineering Chemistry Research*, vol. 49, no. 2, pp. 520–525, 2010.
- [182] T. Voithl and P. R. von Rohr, "Oxidation of lignin using aqueous polyoxometalates in the presence of alcohols," *ChemSusChem*, vol. 1, no. 8-9, pp. 763–769, 2008.
- [183] G. Wu, M. Heitz, and E. Chornet, "Improved alkaline oxidation process for the production of aldehydes (vanillin and syringaldehyde) from steam-explosion hardwood lignin," *Industrial & Engineering Chemistry Research*, vol. 33, no. 3, pp. 718–723, 1994.
- [184] Q. Xiang and Y. Y. Lee, "Production of oxychemicals from precipitated hardwood lignin," *Applied biochemistry and biotechnology*, vol. 91, no. 1, pp. 71–80, 2001.
- [185] A. T. Quitain, N. Sato, H. Daimon, and K. Fujie, "Qualitative investigation on hydrothermal treatment of hinoki *Chamaecyparis obtusa* bark for production of useful chemicals.," *Journal of agricultural and food chemistry*, vol. 51, no. 27, p. 7926, 2003.
- [186] S. Masselter, A. Zemmann, and O. Bobleter, "Analysis of lignin degradation products by capillary electrophoresis," *Chromatographia*, vol. 40, no. 1, pp. 51–57, 1995.
- [187] S. Ando, I. Arai, K. Kiyoto, and S. Hanai, "Identification of aromatic monomers in steam-exploded poplar and their influences on ethanol fermentation by *saccharomyces cerevisiae*," *Journal of Fermentation Technology*, vol. 64, no. 6, pp. 567–570, 1986.
- [188] N. K. Nishikawa, R. Sutcliffe, and J. N. Saddler, "The influence of lignin degradation products on xylose fermentation by *klebsiella pneumoniae*," *Applied Microbiology and Biotechnology*, vol. 27, no. 5, pp. 549–552, 1988.
- [189] A. Kruse and A. Gawlik, "Biomass conversion in water at 330-410 C and 30-50 MPa. identification of key compounds for indicating different chemical reaction pathways," *Industrial & Engineering Chemistry Research*, vol. 42, no. 2, pp. 267–279, 2003.
- [190] M. Waldner and F. Vogel, "Renewable production of methane from woody biomass by catalytic hydrothermal gasification," *Industrial & Engineering Chemistry Research*, vol. 44, no. 13, pp. 4543–4551, 2005.

- [191] E. Adler, "Lignin chemistry—past, present and future," *Wood Science and Technology*, vol. 11, no. 3, pp. 169–218, 1977.
- [192] V. G., A. G., G. J., F. S., and L. S., "Acetosolv pulping of pine wood. kinetic modelling of lignin solubilization and condensation," *Bioresource Technology*, vol. 59, pp. 121–127, 1997.
- [193] J. Gierer, "Chemical aspects of kraft pulping," *Wood Science and Technology*, vol. 14, no. 4, pp. 241–266, 1980.
- [194] J. Gierer, "Chemistry of delignification," *Wood Science and Technology*, vol. 19, no. 4, pp. 289–312, 1985.
- [195] J. Gierer, "Chemistry of delignification," *Wood Science and Technology*, vol. 20, no. 1, pp. 1–33, 1986.
- [196] S. Pavlostathis and J. Gossett, "Alkaline treatment of wheat straw for increasing anaerobic biodegradability," *Biotechnology And Bioengineering*, vol. 27, no. 3, pp. 334–344, 1985.
- [197] S. Pavlostathis and J. Gossett, "Modeling alkali consumption and digestibility improvement from alkaline treatment of wheat straw," *Biotechnology And Bioengineering*, vol. 27, no. 3, pp. 345–354, 1985.
- [198] S. Kim and M. T. Holtzapple, "Delignification kinetics of corn stover in lime pretreatment," *Bioresource technology*, vol. 97, no. 5, pp. 778–785, 2006.
- [199] S. Kim and M. T. Holtzapple, "Effect of structural features on enzyme digestibility of corn stover," *Bioresource technology*, vol. 97, no. 4, pp. 583–591, 2006.
- [200] S. Kim and M. Holtzapple, "Lime pretreatment and enzymatic hydrolysis of corn stover," *Bioresource Technology*, vol. 96, no. 18, pp. 1994–2006, 2005.
- [201] H. Alizadeh, F. Teymouri, T. Gilbert, and B. Dale, "Pretreatment of switchgrass by ammonia fiber explosion (AFEX)," *Applied Biochemistry and Biotechnology*, vol. 124, no. 1, pp. 1133–1141, 2005.
- [202] V. Balan, L. Sousa, S. Chundawat, D. Marshall, L. Sharma, C. Chambliss, and B. Dale, "Enzymatic digestibility and pretreatment degradation products of AFEX-Treated hardwoods (*Populus nigra*)," *Biotechnology Progress*, vol. 25, no. 2, pp. 365–375, 2009.

- [203] L. Gollapalli, B. Dale, and D. Rivers, "Predicting digestibility of ammonia fiber explosion (AFEX)-treated rice straw," *Applied Biochemistry And Biotechnology*, vol. 98, pp. 23–35, 2002.
- [204] F. Teymouri, L. Laureano-Perez, H. Alizadeh, and B. Dale, "Optimization of the ammonia fiber explosion (AFEX) treatment parameters for enzymatic hydrolysis of corn stover," *Bioresource Technology*, vol. 96, no. 18, pp. 2014–2018, 2005.
- [205] A. Hatakka, "Lignin-modifying enzymes from selected white-rot fungi: production and role from in lignin degradation," *FEMS Microbiology Reviews*, vol. 13, no. 2-3, pp. 125–135, 1994.
- [206] T. K. Kirk and R. L. Farrell, "Enzymatic "Combustion": the microbial degradation of lignin," *Annual Review of Microbiology*, vol. 41, no. 1, pp. 465–501, 1987.
- [207] T. R. Green, "Significance of glucose oxidase in lignin degradation," *Nature*, vol. 268, no. 5615, pp. 78–80, 1977.
- [208] J. W. Lee, K. S. Gwak, J. Y. Park, M. J. Park, D. H. Choi, M. Kwon, and I. G. Choi, "Biological pretreatment of softwood pinus densiflora by three white rot fungi," *Journal of microbiology (Seoul, Korea)*, vol. 45, no. 6, p. 485, 2007.
- [209] P. Harriott, *Chemical reactor design*. CRC Press, 2003.
- [210] R. Neuman and L. Walker, "Solute exclusion from cellulose in Packed-Columns - experimental investigation and pore volume measurements," *Biotechnology And Bioengineering*, vol. 40, no. 2, pp. 218–225, 1992.
- [211] C. Wyman, B. Dale, R. Elander, M. Holtzapple, M. Ladisch, and Y. Lee, "Comparative sugar recovery data from laboratory scale application of leading pretreatment technologies to corn stover," *Bioresource Technology*, vol. 96, no. 18, pp. 2026–2032, 2005.
- [212] C. Wyman, B. Dale, R. Elander, M. Holtzapple, M. Ladisch, Y. Lee, C. Mitchinson, and J. Saddler, "Comparative sugar recovery and fermentation data following pretreatment of poplar wood by leading technologies," *Biotechnology Progress*, vol. 25, no. 2, pp. 333–339, 2009.
- [213] N. Mosier, C. Wyman, B. Dale, R. Elander, Y. Lee, M. Holtzapple, and

- M. Ladisch, "Features of promising technologies for pretreatment of lignocellulosic biomass," *Bioresource Technology*, vol. 96, no. 6, pp. 673–686, 2005.
- [214] J. A. Rollin, Z. Zhu, N. Sathitsuksanoh, and Y. H. Zhang, "Increasing cellulose accessibility is more important than removing lignin: A comparison of cellulose solvent-based lignocellulose fractionation and soaking in aqueous ammonia," *Biotechnology and bioengineering*, vol. 108, no. 1, pp. 22–30, 2011.
- [215] S. Spatari, D. M. Bagley, and H. L. MacLean, "Life cycle evaluation of emerging lignocellulosic ethanol conversion technologies," *Bioresource Technology*, vol. 101, no. 2, pp. 654–667, 2010.
- [216] A. Cuvilliez, *Thermo-economic model of a lignocellulosic bioethanol process*. M.Sc. thesis, Ecole Polytechnique Federale, Lausanne, Switzerland, 2009.
- [217] S. Larsson, P. Cassland, and L. J. Jonsson, "Development of a *saccharomyces cerevisiae* strain with enhanced resistance to phenolic fermentation inhibitors in lignocellulose hydrolysates by heterologous expression of laccase," *Applied and environmental microbiology*, vol. 67, no. 3, p. 1163, 2001.
- [218] S. Larsson, E. Palmqvist, B. Hahn-Hagerdal, C. Tengborg, K. Stenberg, G. Zacchi, and N. O. Nilvebrant, "The generation of fermentation inhibitors during dilute acid hydrolysis of softwood," *Enzyme and Microbial Technology*, vol. 24, no. 3-4, pp. 151–159, 1999.
- [219] B. Sanchez and J. Bautista, "Effects of furfural and 5-hydroxymethylfurfural on the fermentation of *saccharomyces cerevisiae* and biomass production from *Candida guilliermondii*," *Enzyme and Microbial Technology*, vol. 10, no. 5, pp. 315–318, 1988.
- [220] H. L. MacLean and S. Spatari, "The contribution of enzymes and process chemicals to the life cycle of ethanol," *Environmental Research Letters*, vol. 4, p. 014001, 2009.
- [221] T. Groode, *Biomass to ethanol : potential production and environmental impacts*. PhD thesis, Massachusetts Institute of Technology, 2008.
- [222] J. S. Luterbacher, M. Fröling, F. Vogel, F. Maréchal, and J. W. Tester, "Hydrothermal gasification of waste biomass: Process design and life cycle

- assessment," *Environmental Science & Technology*, vol. 43, no. 5, pp. 1578–1583, 2009.
- [223] A. Wingren, M. Galbe, and G. Zacchi, "Techno-economic evaluation of producing ethanol from softwood: Comparison of SSF and SHF and identification of bottlenecks," *Biotechnology progress*, vol. 19, no. 4, pp. 1109–1117, 2003.
- [224] M. A. Collura and W. L. Luyben, "Energy-saving distillation designs in ethanol production," *Industrial & Engineering Chemistry Research*, vol. 27, no. 9, pp. 1686–1696, 1988.
- [225] D. P. Bayrock and W. Michael Ingledew, "Application of multistage continuous fermentation for production of fuel alcohol by very-high-gravity fermentation technology," *Journal of Industrial Microbiology and Biotechnology*, vol. 27, no. 2, pp. 87–93, 2001.
- [226] T. Lloyd and C. Wyman, "Combined sugar yields for dilute sulfuric acid pretreatment of corn stover followed by enzymatic hydrolysis of the remaining solids," *Bioresource Technology*, vol. 96, no. 18, pp. 1967–1977, 2005.
- [227] J. B. Kristensen, C. Felby, and H. Jorgensen, "Yield-determining factors in high-solids enzymatic hydrolysis of lignocellulose," *Biotechnology for Biofuels*, vol. 2, no. 1, p. 11, 2009.
- [228] X. Pan, "Role of functional groups in lignin inhibition of enzymatic hydrolysis of cellulose to glucose," *Journal of Biobased Materials and Bioenergy*, vol. 2, no. 1, pp. 25–32, 2008.
- [229] G. Panagiotou and L. Olsson, "Effect of compounds released during pretreatment of wheat straw on microbial growth and enzymatic hydrolysis rates," *Biotechnology and bioengineering*, vol. 96, no. 2, pp. 250–258, 2006.
- [230] B. E. Dale, "Editorial: Consortium for applied fundamentals and innovation (CAFI)," *Biotechnology Progress*, vol. 25, no. 2, p. 301, 2009.
- [231] R. Elander, B. Dale, M. Holtzapple, M. Ladisch, Y. Lee, C. Mitchinson, J. Saddler, and C. Wyman, "Summary of findings from the biomass refining consortium for applied fundamentals and innovation (CAFI): corn stover pretreatment," *Cellulose*, vol. 16, no. 4, pp. 649–659, 2009.

- [232] N. Mosier, R. Hendrickson, N. Ho, M. Sedlak, and M. R. Ladisch, "Optimization of pH controlled liquid hot water pretreatment of corn stover," *Bioresource Technology*, vol. 96, no. 18, pp. 1986–1993, 2005.
- [233] T. H. Kim and Y. Y. Lee, "Pretreatment and fractionation of corn stover by ammonia recycle percolation process," *Bioresource technology*, vol. 96, no. 18, pp. 2007–2013, 2005.
- [234] Y. Kim, N. S. Mosier, and M. R. Ladisch, "Enzymatic digestion of liquid hot water pretreated hybrid poplar," *Biotechnology Progress*, vol. 25, no. 2, pp. 340–348, 2009.
- [235] R. Gupta and Y. Y. Lee, "Pretreatment of hybrid poplar by aqueous ammonia," *Biotechnology Progress*, vol. 25, no. 2, pp. 357–364, 2009.
- [236] R. Sierra, C. Granda, and M. T. Holtzapple, "Short-term lime pretreatment of poplar wood," *Biotechnology Progress*, vol. 25, no. 2, pp. 323–332, 2009.
- [237] X. Li, A. Converse, and C. Wyman, "Characterization of molecular weight distribution of oligomers from autocatalyzed batch hydrolysis of xylan," *Applied Biochemistry And Biotechnology*, vol. 105, pp. 515–522, 2003.
- [238] G. Garrote, H. Dominguez, and J. C. Parajo, "Hydrothermal processing of lignocellulosic materials," *European Journal of Wood and Wood Products*, vol. 57, no. 3, pp. 191–202, 1999.
- [239] M. Heitz, E. Capek-Ménard, P. G. Koeberle, J. Gagne, E. Chornet, R. P. Overend, J. D. Taylor, and E. Yu, "Fractionation of populus tremuloides at the pilot plant scale: Optimization of steam pretreatment conditions using the STAKE II technology," *Bioresource Technology*, vol. 35, no. 1, pp. 23–32, 1991.
- [240] Y. Kim, R. Hendrickson, N. S. Mosier, and M. R. Ladisch, "Liquid hot water pretreatment of cellulosic biomass.," *Methods in molecular biology (Clifton, NJ)*, vol. 581, p. 93, 2009.
- [241] M. Zeng, N. S. Mosier, C. P. Huang, D. M. Sherman, and M. R. Ladisch, "Microscopic examination of changes of plant cell structure in corn stover due to hot water pretreatment and enzymatic hydrolysis," *Biotechnology and bioengineering*, vol. 97, no. 2, pp. 265–278, 2006.
- [242] N. S. Mosier, R. Hendrickson, M. Brewer, N. Ho, M. Sedlak, R. Dreshel,

- G. Welch, B. S. Dien, A. Aden, and M. R. Ladisch, "Industrial scale-up of pH-controlled liquid hot water pretreatment of corn fiber for fuel ethanol production," *Applied Biochemistry and Biotechnology*, vol. 125, no. 2, pp. 77–97, 2005.
- [243] C. Liu and C. Wyman, "Partial flow of compressed-hot water through corn stover to enhance hemicellulose sugar recovery and enzymatic digestibility of cellulose," *Bioresource Technology*, vol. 96, no. 18, pp. 1978–1985, 2005.
- [244] H. Jorgensen, J. Vibe-Pedersen, J. Larsen, and C. Felby, "Liquefaction of lignocellulose at high-solids concentrations," *Biotechnology and Bioengineering*, vol. 96, no. 5, pp. 862–870, 2007.
- [245] D. Schell, J. Farmer, M. Newman, and J. McMillan, "Dilute-sulfuric acid pretreatment of corn stover in pilot-scale reactor," *Applied Biochemistry and Biotechnology*, vol. 105, no. 1, pp. 69–85, 2003.
- [246] J. McMillan, M. Newman, D. Templeton, and A. Mohagheghi, "Simultaneous saccharification and cofermentation of dilute-acid pretreated yellow poplar hardwood to ethanol using xylose-fermenting *Zymomonas mobilis*," *Applied biochemistry and biotechnology*, vol. 79, no. 1, pp. 649–665, 1999.
- [247] D. Gao, S. P. Chundawat, C. Krishnan, V. Balan, and B. E. Dale, "Mixture optimization of six core glycosyl hydrolases for maximizing saccharification of ammonia fiber expansion (AFEX) pretreated corn stover," *Bioresource Technology*, 2009.
- [248] V. S. Chang, M. Nagwani, C. H. Kim, and M. T. Holtzapple, "Oxidative lime pretreatment of high-lignin biomass," *Applied biochemistry and biotechnology*, vol. 94, no. 1, pp. 1–28, 2001.
- [249] K. Kim and J. Hong, "Supercritical CO₂ pretreatment of lignocellulose enhances enzymatic cellulose hydrolysis," *Bioresource Technology*, vol. 77, no. 2, pp. 139–144, 2001.
- [250] R. McWilliams and G. van Walsum, "Comparison of aspen wood hydrolysates produced by pretreatment with liquid hot water and carbonic acid," *Applied Biochemistry and Biotechnology*, vol. 98, pp. 109–121, 2002.
- [251] A. P. Dadi, S. Varanasi, and C. A. Schall, "Enhancement of cellulose sac-

- charification kinetics using an ionic liquid pretreatment step," *Biotechnology and Bioengineering*, vol. 95, no. 5, pp. 904–910, 2006.
- [252] C. Li and Z. K. Zhao, "Efficient Acid-Catalyzed hydrolysis of cellulose in ionic liquid," *Advanced Synthesis & Catalysis*, vol. 349, no. 11-12, pp. 1847–1850, 2007.
- [253] Q. Li, Y. C. He, M. Xian, G. Jun, X. Xu, J. M. Yang, and L. Z. Li, "Improving enzymatic hydrolysis of wheat straw using ionic liquid 1-ethyl-3-methyl imidazolium diethyl phosphate pretreatment," *Bioresource technology*, vol. 100, no. 14, pp. 3570–3575, 2009.
- [254] H. Zhao, C. L. Jones, G. A. Baker, S. Xia, O. Olubajo, and V. N. Person, "Regenerating cellulose from ionic liquids for an accelerated enzymatic hydrolysis," *Journal of Biotechnology*, vol. 139, no. 1, pp. 47–54, 2009.
- [255] D. Tilman, J. Hill, and C. Lehman, "Carbon-Negative biofuels from Low-Input High-Diversity grassland biomass," *Science*, vol. 314, no. 5805, pp. 1598–1600, 2006.
- [256] A. Farrell, R. Plevin, B. Turner, A. Jones, M. O'Hare, and D. Kammen, "Ethanol can contribute to energy and environmental goals," *Science*, vol. 311, no. 5760, pp. 506–508, 2006.
- [257] S. Spatari, Y. Zhang, and H. MacLean, "Life cycle assessment of switchgrass- and corn stover-derived ethanol-fueled automobiles," *Environmental Science & Technology*, vol. 39, no. 24, pp. 9750–9758, 2005.
- [258] Z. Duan and R. Sun, "An improved model calculating CO₂ solubility in pure water and aqueous NaCl solutions from 273 to 533 K and from 0 to 2000 bar," *Chemical Geology*, vol. 193, no. 3-4, pp. 257–271, 2003.
- [259] M. Stamenic, I. Zizovic, R. Eggers, P. Jaeger, H. Heinrich, E. Rój, J. Ivanovic, and D. Skala, "Swelling of plant material in supercritical carbon dioxide," *The Journal of Supercritical Fluids*, vol. 52, no. 1, pp. 125–133, 2010.
- [260] P. J. Van Soest, J. B. Robertson, and B. A. Lewis, "Methods for dietary fiber, neutral detergent fiber, and nonstarch polysaccharides in relation to animal nutrition," *Journal of Dairy Science*, vol. 74, no. 10, pp. 3583–3597, 1991.

- [261] M. J. Serapiglia, K. D. Cameron, A. J. Stipanovic, and L. B. Smart, "Analysis of biomass composition using High-Resolution thermogravimetric analysis and percent bark content for the selection of shrub willow bioenergy crop varieties," *BioEnergy Research*, vol. 2, no. 1, pp. 1–9, 2009.
- [262] Y. C. Chung, A. Bakalinsky, and M. H. Penner, "Enzymatic saccharification and fermentation of xylose-optimized dilute acid-treated lignocellulosics," *Applied biochemistry and biotechnology*, vol. 124, no. 1, pp. 947–961, 2005.
- [263] J. S. Luterbacher, J. W. Tester, and L. P. Walker, "Two-temperature stage biphasic CO₂-H₂O pretreatment of lignocellulosic biomass at high solid loadings," *Biotechnology and Bioengineering*, vol. 109, no. 6, pp. 1499–1507, 2012.
- [264] R. Alinia, S. Zabihi, F. Esmailzadeh, and J. F. Kalajahi, "Pretreatment of wheat straw by supercritical CO₂ and its enzymatic hydrolysis for sugar production," *Biosystems Engineering*, vol. 107, no. 1, pp. 61–66, 2010.
- [265] N. Srinivasan and L. Ju, "Pretreatment of guayule biomass using supercritical carbon dioxide-based method," *Bioresource Technology*, vol. 101, no. 24, pp. 9785–9791, 2010.
- [266] K. H. Kim, M. P. Tucker, and Q. A. Nguyen, "Effects of pressing lignocellulosic biomass on sugar yield in Two-Stage Dilute-Acid hydrolysis process," *Biotechnology progress*, vol. 18, no. 3, pp. 489–494, 2002.
- [267] Q. Nguyen, M. Tucker, F. Keller, and F. Eddy, "Two-stage dilute-acid pretreatment of softwoods," *Applied Biochemistry and Biotechnology*, vol. 84-6, pp. 561–576, 2000.
- [268] J. Soderstrom, L. Pilcher, M. Galbe, and G. Zacchi, "Two-step steam pretreatment of softwood by dilute H₂SO₄ impregnation for ethanol production," *Biomass and Bioenergy*, vol. 24, no. 6, pp. 475–486, 2003.
- [269] A. Sluiter, B. Hames, R. Ruiz, C. Scarlata, J. Sluiter, and D. Templeton, "Determination of sugars, byproducts, and degradation products in liquid fraction process samples," Tech. Rep. TP-510-42623, National Renewable Energy Laboratory, Golden, CO, 2004.
- [270] M. J. Selig, N. Weiss, and Y. Ji, "Enzymatic saccharification of lignocellulosic biomass," Tech. Rep. TP-510-42629, National Renewable Energy Laboratory, Golden, CO, 2008.

- [271] B. Hahn-Hagerdal, K. Karhumaa, C. Fonseca, I. Spencer-Martins, and M. F. Gorwa-Grauslund, "Towards industrial pentose-fermenting yeast strains," *Applied Microbiology and Biotechnology*, vol. 74, no. 5, pp. 937–953, 2007.
- [272] J. S. Luterbacher, Q. Chew, Y. Li, J. W. Tester, and L. P. Walker, "Producing concentrated solutions of monosaccharides using biphasic CO₂-H₂O mixtures," *Energy & Environmental Science*, vol. 5, no. 5, pp. 6990–7000, 2012.
- [273] G. Dragone, D. P. Silva, J. B. de Almeida e Silva, and U. de Almeida Lima, "Improvement of the ethanol productivity in a high gravity brewing at pilot plant scale," *Biotechnology Letters*, vol. 25, no. 14, pp. 1171–1174, 2003.
- [274] E. L. Krause, M. J. Villa-García, S. A. Henry, and L. P. Walker, "Determining the effects of inositol supplementation and the *opi1* mutation on ethanol tolerance of *saccharomyces cerevisiae*," *Industrial Biotechnology*, vol. 3, no. 3, pp. 260–268, 2007.
- [275] H. Tadesse and R. Luque, "Advances on biomass pretreatment using ionic liquids: An overview," *Energy & Environmental Science*, vol. 4, no. 10, pp. 3913–3929, 2011.
- [276] E. Ximenes, Y. Kim, N. Mosier, B. Dien, and M. Ladisch, "Deactivation of cellulases by phenols," *Enzyme and microbial technology*, vol. 48, no. 1, pp. 54–60, 2011.
- [277] L. P. Ramos, C. Breuil, and J. N. Saddler, "The use of enzyme recycling and the influence of sugar accumulation on cellulose hydrolysis by *trichoderma* cellulases," *Enzyme and microbial technology*, vol. 15, no. 1, pp. 19–25, 1993.
- [278] D. B. Hodge, M. N. Karim, D. J. Schell, and J. D. McMillan, "Soluble and insoluble solids contributions to high-solids enzymatic hydrolysis of lignocellulose," *Bioresource Technology*, vol. 99, no. 18, pp. 8940–8948, 2008.
- [279] J. Soderstrom, M. Galbe, and G. Zacchi, "Effect of washing on yield in one- and two-step steam pretreatment of softwood for production of ethanol," *Biotechnology progress*, vol. 20, no. 3, pp. 744–749, 2004.
- [280] A. Wingren, J. Soderstrom, M. Galbe, and G. Zacchi, "Process considerations and economic evaluation of Two-Step steam pretreatment for pro-

- duction of fuel ethanol from softwood," *Biotechnology progress*, vol. 20, no. 5, pp. 1421–1429, 2004.
- [281] C. Cara, M. Moya, I. Ballesteros, M. J. Negro, A. González, and E. Ruiz, "Influence of solid loading on enzymatic hydrolysis of steam exploded or liquid hot water pretreated olive tree biomass," *Process Biochemistry*, vol. 42, no. 6, pp. 1003–1009, 2007.
- [282] R. Kumar and C. E. Wyman, "Effects of cellulase and xylanase enzymes on the deconstruction of solids from pretreatment of poplar by leading technologies," *Biotechnology Progress*, vol. 25, no. 2, pp. 302–314, 2009.
- [283] A. Berlin, M. Balakshin, N. Gilkes, J. Kadla, V. Maximenko, S. Kubo, and J. Saddler, "Inhibition of cellulase, xylanase and beta-glucosidase activities by softwood lignin preparations," *Journal of biotechnology*, vol. 125, no. 2, pp. 198–209, 2006.
- [284] R. Span and W. Wagner, "A new equation of state for carbon dioxide covering the fluid region from the Triple-Point temperature to 1100 k at pressures up to 800 MPa," *Journal of Physical and Chemical Reference Data*, vol. 25, no. 6, p. 1509, 1996.
- [285] C. Wyman, B. Dale, R. Elander, M. Holtzapple, M. Ladisch, and Y. Lee, "Comparative sugar recovery data from laboratory scale application of leading pretreatment technologies to corn stover," *Bioresource Technology*, vol. 96, no. 18, pp. 2026–2032, 2005.
- [286] J. S. Luterbacher, L. P. Walker, and J. M. Moran-Mirabal, "Observing and modeling BMCC depolymerization by commercial enzyme cocktails using confocal fluorescence microscopy," *Biotechnology and Bioengineering*, in press, 2012.
- [287] S. Singh, B. A. Simmons, and K. P. Vogel, "Visualization of biomass solubilization and cellulose regeneration during ionic liquid pretreatment of switchgrass," *Biotechnology And Bioengineering*, vol. 104, no. 1, pp. 68–75, 2009.
- [288] E. Husson, S. Buchoux, C. Avondo, D. Cailleu, K. Djellab, I. Gosselin, O. Wattraint, and C. Sarazin, "Enzymatic hydrolysis of ionic liquid-pretreated celluloses: Contribution of CP-MAS ^{13}C NMR and SEM," *Bioresource Technology*, vol. 102, no. 15, pp. 7335–7342, 2011.

- [289] K. Igarashi, T. Uchihashi, A. Koivula, M. Wada, S. Kimura, T. Okamoto, M. Penttilä, T. Ando, and M. Samejima, "Traffic jams reduce hydrolytic efficiency of cellulase on cellulose surface," *Science*, vol. 333, no. 6047, pp. 1279–1282, 2011.
- [290] K. Igarashi, A. Koivula, M. Wada, S. Kimura, M. Penttilä, and M. Samejima, "High speed atomic force microscopy visualizes processive movement of trichoderma reesei Cellobiohydrolase I on crystalline cellulose," *Journal of Biological Chemistry*, vol. 284, no. 52, p. 36186, 2009.
- [291] C. Wyman, B. Dale, R. Elander, M. Holtzapple, M. Ladisch, and Y. Lee, "Coordinated development of leading biomass pretreatment technologies," *Bioresource Technology*, vol. 96, no. 18, pp. 1959–1966, 2005.
- [292] J. M. Moran-Mirabal, S. C. Corgie, J. C. Bolewski, H. M. Smith, B. R. Cipriany, H. G. Craighead, and L. P. Walker, "Labeling and purification of Cellulose-Binding proteins for high resolution fluorescence applications," *Analytical chemistry*, vol. 81, no. 19, pp. 7981–7987, 2009.
- [293] W. Helbert, H. Chanzy, T. L. Husum, M. Schülein, and S. Ernst, "Fluorescent cellulose microfibrils as substrate for the detection of cellulase activity," *Biomacromolecules*, vol. 4, no. 3, pp. 481–487, 2003.
- [294] P. Thevenaz, U. Ruttimann, and M. Unser, "A pyramid approach to sub-pixel registration based on intensity," *Image Processing, IEEE Transactions on*, vol. 7, no. 1, pp. 27–41, 1998.
- [295] M. M. Bradford, "A rapid and sensitive method for the quantitation of microgram quantities of protein utilizing the principle of protein-dye binding," *Analytical Biochemistry*, vol. 72, pp. 248–254, 1976.
- [296] R. Pinto, A. L. Amaral, J. Carvalho, E. C. Ferreira, M. Mota, and M. Gama, "Development of a method using image analysis for the measurement of cellulose-binding domains adsorbed onto cellulose fibers," *Biotechnology progress*, vol. 23, no. 6, pp. 1492–1497, 2007.
- [297] J. S. Luterbacher and L. P. Parlangue, Jean-Yves Walker, "A pore-hindered diffusion and reaction model can help explain the importance of pore size distribution in enzymatic hydrolysis of biomass," *Biotechnology and Bioengineering*, submitted, 2012.
- [298] S. P. Chundawat, V. Balan, and B. E. Dale, "High-throughput microplate

- technique for enzymatic hydrolysis of lignocellulosic biomass," *Biotechnology and bioengineering*, vol. 99, no. 6, pp. 1281–1294, 2008.
- [299] S. R. Decker, R. Brunecky, M. P. Tucker, M. E. Himmel, and M. J. Selig, "High-throughput screening techniques for biomass conversion," *BioEnergy Research*, vol. 2, no. 4, pp. 179–192, 2009.
- [300] M. H. Studer, J. D. DeMartini, S. Brethauer, H. L. McKenzie, and C. E. Wyman, "Engineering of a high-throughput screening system to identify cellulosic biomass, pretreatments, and enzyme formulations that enhance sugar release," *Biotechnology and Bioengineering*, vol. 105, no. 2, pp. 231–238, 2010.
- [301] M. Zavrel, D. Bross, M. Funke, J. Buchs, and A. C. Spiess, "High-throughput screening for ionic liquids dissolving (ligno-) cellulose," *Biore-source technology*, vol. 100, no. 9, pp. 2580–2587, 2009.
- [302] B. C. King, M. K. Donnelly, G. C. Bergstrom, L. P. Walker, and D. M. Gibson, "An optimized microplate assay system for quantitative evaluation of plant cell wall-degrading enzyme activity of fungal culture extracts," *Biotechnology and Bioengineering*, vol. 102, no. 4, pp. 1033–1044, 2009.
- [303] B. C. King, K. D. Waxman, N. V. Nenni, L. P. Walker, G. C. Bergstrom, D. M. Gibson, *et al.*, "Arsenal of plant cell wall degrading enzymes reflects host preference among plant pathogenic fungi," *Biotechnology for Biofuels*, vol. 4, no. 1, p. 4, 2011.
- [304] M. Young, P. Carroad, and R. Bell, "Estimation of diffusion coefficients of proteins," *Biotechnology and Bioengineering*, vol. 22, no. 5, pp. 947–955, 1980.
- [305] E. Ehrnrooth, "Change in pulp fibre density with acid-chlorite delignification," *Journal of wood chemistry and technology*, vol. 4, no. 1, pp. 91–109, 1984.
- [306] K. Kipper, P. Valjamae, and G. Johansson, "Processive action of cellobiohydrolase Cel7A from *Trichoderma reesei* is revealed as 'burst' kinetics on fluorescent polymeric model substrates," *Biochemical Journal*, vol. 385, no. Pt 2, pp. 527–535, 2005.
- [307] G. W. Huber, S. Iborra, and A. Corma, "Synthesis of transportation fuels from biomass: chemistry, catalysts, and engineering," *Chemical Reviews*, vol. 106, no. 9, p. 4044, 2006.

- [308] F. Henry, *Optimization of an Integrated Lignocellulosic Biomass to Ethanol Conversion System*. M.Sc. thesis, Ecole Polytechnique Federale, Lausanne, Switzerland, 2012.
- [309] E. Kreyszig, *Advanced Engineering Mathematics*. John Wiley & Sons, 1972.
- [310] P. Bevington and D. Robinson, *Data Reduction and Error Analysis for the Physical Sciences*. Boston, MA: McGraw Hill, 2nd edition ed., 1992.
- [311] W. Schiesser and G. Griffiths, *A compendium of partial differential equation models: method of lines analysis with MATLAB*. Cambridge University Press, 2009.